UNIVERSITY OF OKLAHOMA

GRADUATE COLLEGE

DYNAMIC BEHAVIOR OF BRIDGE STRUCTURES UNDER MOVING LOADS AND MASSES USING DIFFERENTIAL QUADRATURE METHOD

A DISSERTATION

SUBMITTED TO THE GRADUATE FACULTY

in partial fulfillment of the requirements for the

Degree of

DOCTOR OF PHILOSOPHY

By

GOPINATH VENKATESAN
Norman, Oklahoma
2009

DYNAMIC BEHAVIOR OF BRIDGE STRUCTURES UNDER MOVING LOADS AND MASSES USING DIFFERENTIAL QUADRATURE METHOD

A DISSERTATION APPROVED FOR THE
SCHOOL OF AEROSPACE AND MECHANICAL ENGINEERING

BY

_____

Dr. David Baldwin, Chair

_____

Dr. Alfred Striz

_____

Dr. Kuang-Hua Chang

_____

Dr. Zahed Siddique

_____

Dr. Shivakumar Raman

Acknowledgments

I sincerely thank the *School of Aerospace and Mechanical Engineering,* OU for supporting me during my masters and doctorate programs, and the AME faculty members for their friendly advice and guidance that I received during my stay. This work was partially supported by the *Dynamic Structures Sensing and Control* (DySSC) center, and I thank all the DySSC members for their friendly interesting discussions.

I am happy to have *Dr. David Baldwin* as my thesis adviser, and I sincerely thank him for supporting and encouraging me in the hardest times. I gained good knowledge on fatigue and fracture mechanics, vibrations and structural dynamics and I owe him for shaping my career toward these rewarding and interesting areas.

I am pleased to have *Dr. Alfred G. Striz, Dr. Kuang-Hua Chang, Dr. Zahed Siddique* and *Dr. Shivakumar Raman* on my thesis committee. I enjoyed learning a variety of topics from the courses I took from them during my stay at OU. I would like to thank them for accepting to sit on my thesis committee.

My special thanks are due to *Mr. David Park, Dr. Major Bob* (forum nickname) and *Mr. Oliver Ruebenko* for their valuable hints on my coding issues in *Mathematica* through the *Mathematica* forum. I would like to thank *Dr. Charles W. Bert, Dr. Kyran K. Mish* and *Dr. Peter J. Attar* for showing interest in my thesis studies, and I found the discussions I had with them helpful and educating. I also thank *Dr. Seung Son* of University of Colorado at Colorado Springs for suggesting spline interpolation to me when I was using monomials of a polynomial. I appreciate the brief comments from *Dr. Malekzadeh* and

Dr. Michaltsos on their work to clear my doubts relating to the use of DQM for moving load problems. I also benefitted from the XANSYS forum discussions and my special thanks are due to *Dr. K. S. Raghavan*, *Dr. Senthil Gopinathan* and *Mr. Christopher Wright*.

I also thank *Ms. Suzi Skinner* and *Ms. Paula Gerhard* in supporting me to fulfill academic related procedures and requirements on time.

I sincerely thank *Cessna Aircraft Company*, Wichita, for giving me an opportunity to work as an engineer during which time I gained a good amount of knowledge about the aircraft industry. I am also happy that I am going back to *Textron GTC* to continue my work on *Cessna* related projects.

I thank *Mr. Mangesh Edke*, *Mr. Suyog Lokhande* and *Mr. Anand Mohan* for their timely friendly favors and the support I received.

I dedicate the accomplishments to my family members *Mr. & Mrs. Kamala Venkatesan* (my parents), *Mr. & Mrs. Sumathi Ravichandran* (my brother and sister-in-law) and their two wonderful kids – *Ms. Nithya* and *Mr. Prasanna Ravichandran*.

Gopinath Venkatesan
Norman, OK 73019.

Date: 23rd September 2009

Table of Contents

List of Tables

List of Figures

Abstract

The current study is focused on the dynamic behavior of an idealized highway bridge structure subjected to moving heavy vehicular loads using simplified representative models such as *Euler* beams and *Kirchhoff* plates. The study also successfully implemented the application of a numerical procedure called *Differential Quadrature Method* (DQM) to solve transient dynamic systems using conventional and generalized DQ schemes. A semi-analytical (modal method) DQ procedure proved computationally very effective to study the vehicle-bridge dynamic system.

Three types of models were used to represent the vehicle-bridge system i.e. moving force, moving mass and moving oscillator systems. The dynamic behavior of the vehicle-bridge system is discussed with reference to vehicle speed, damping characteristics of the bridge, vehicle to bridge frequency ratio, vehicle to bridge mass ratio for a single axle load system, including inter-load spacing for a two axle load system. The dynamic amplification factor (DAF), characterizing the dynamic behavior of a bridge structure, was found to increase with the speed of moving vehicles. The vehicle-bridge dynamic behavior is unclear in the low speed parameter range to sufficiently address the differences in the moving force, moving mass and moving oscillator models. For a single axle load system with speed parameters ranging above 0.1, the moving mass model appeared conservative with higher DAF's, the moving oscillator yielded reduced DAF's and the moving force model predicted DAF's in between the above models. However, for a two axle load system with speed parameters ranging above 0.1, a moving oscillator model predicted higher dynamic responses than a corresponding moving force model.

Chapter 1: Introduction and Background

1.1 Introduction:

Moving loads are defined as those loads that vary both in space and time. One of the most common examples for moving loads is the passage of vehicular loads such as trains/automobiles over rail/road tracks. Other interesting engineering areas where moving load problems are encountered include high speed machining tools, rotating magnetic disk drives, transportation cables, aircraft carriers, etc. A moving load amplifies the structural response that otherwise would be experienced due to a static load of the same magnitude at similar conditions. The dynamic nature of moving loads acting on structures is being investigated by researchers for its far-reaching impact on structural responses such as displacements and stresses. The present work focuses on the dynamic behavior of idealized highway bridge structures subjected to moving loads.

The moving load effects can be either due to only the moving force, or both the moving force and the inertial load associated with it, if any. The latter case is categorized as moving mass, and in general, the whole problem is referred to as ‘moving force-moving mass’ problem. In both the above cases, the vibrations of the moving vehicles themselves (i.e. bouncing actions) are neglected compared with the vibration of a bridge structure. When vehicle to bridge interactions are included in the moving force-moving mass problem, the problem is referred to as ‘moving oscillator’ problem.

This study is focused on the dynamic behavior of idealized bridge structures subjected to moving vehicular loads, with and without the inclusion of inertia effects of the vehicles.

This study is also intended to extend the application of the Differential Quadrature Method (DQM) to solve transient dynamic problems. The Vehicle to Bridge Interaction (VBI) phenomenon using a beam model is also studied as a part of this project.

The following sections discuss the significance of the moving mass problem, current design procedures and practices, and provide a brief literature survey on moving load problem and a short note on key aspects of the research tasks such as field tests and analyses of two highway bridges carried out by the Dynamic Structures Sensing & Control (DySSC) center at the University of Oklahoma (OU).

1.2 Significance of moving masses:

In the early years, due to lesser traffic loads moving at lower speeds than today, the significance of the dynamic impact of vehicular loads was not realized, and bridge design protocols developed and practiced by the American Association of State Highway and Transportation Officials (AASHTO) [1] mainly relied on static load calculations. The old bridge design procedures employed higher safety factors (via the dynamic amplification factor, to be discussed later) to substitute for the computational expenses and efforts associated with the application of numerical tools required to analyze a moving load problem.

The safety criteria of a bridge structure are assessed by evaluating the relation [2],

$$R_{structure} > P_{applied} \tag{1.1}$$

where $R_{structure}$ is the resistance of the structure and $P_{applied}$ is the applied load on the structure. The safety factor is applied to the resistance side of the above relation which then becomes $(R_{structure} / F_{safety}) > P_{applied}$ where F_{safety} is the safety factor assigned. This procedure is generally referred to as Allowable Stress Design (ASD) and assumes deterministic applied loads to evaluate the safety criteria.

Only a few decades earlier, with the increased usage of heavy truck vehicles, high speed automobiles (and high speed trains in railway infrastructure), and with the need for optimizing infrastructure costs associated with increased numbers of bridges to accommodate growing traffic, moving load problems drew our attention. Heavy truck loads add lumped mass to the location of contact with the bridge deck and, hence, are expected to change the modal properties of the bridge. Heavy truck vehicles also produce bouncing effects due to the suspension system at places of road deck unevenness resulting in a pronounced vibration response of the bridge system, and this increased response is dependent mainly on the mass and speed of the vehicles passing over, and their suspension system parameters. These issues required subsequent studies on the dynamic behavior of bridge structures with the inclusion of mass (inertia) effects of the moving load as well as its bouncing effects. One of the many reasons to call for moving mass and VBI calculations comes from the fact that the level of vibration of bridges observed due to the passage of long and heavy trucks was so phenomenal that it induces a psychological effect of fear on pedestrians and observers.

The increased dynamic response of bridge structures associated with heavy moving vehicular loads also results in increased structural stresses in the bridge structure. Not only do the vehicular loads impart stresses on the bridge components but they also introduce fatigue effects owing to the dynamic nature of the loads involved. Hence, it becomes an inevitable task to assess the dynamic response of bridge structures under moving vehicles with due consideration for the vehicles' inertia effects on bridge response. Also, prior knowledge of the magnitudes of the stresses experienced by the structural components due to moving masses helps us determine the remaining life of the structure using fatigue life estimation techniques.

Among the moving load problems, the magnitude of the structural response is expected to increase in the following representative models: 1) moving force, 2) moving mass and 3) moving oscillator. The moving oscillator model is expected to be an effective representation of a moving vehicle with a suspension system, and a system of connected multiple oscillators that includes both the translational and rotational degrees of freedom. It offers opportunities to address several aspects of the vehicle-bridge coupled system such as identification of influential parameters and their effects on the vibration response of the bridge system.

It is also worthwhile to note that by identifying the influential parameters of the moving mass problem, we can effectively reduce the detrimental impact of moving vehicles on bridge structures either by suitably adjusting vehicle and bridge parameters or by updating highway guidelines for allowable vehicular loads for a bridge, i.e., load entry

specifications, and corresponding speed limits. The vehicle and bridge parameters to be adjusted may include bridge design parameters such as geometry, material, weight, etc., and vehicle parameters such as chassis weight and suspension system parameters (stiffness of the springs and damping coefficient of the damper). Of these, the bridge design, i.e., geometry and material parameters, and the vehicle mass are fixed and, hence, the only feasible option available for control during traverse (other than the vehicle speed) are the vehicle suspension system parameters. Thus the vehicle suspension parameters could be modified in real time to suitably reduce the instantaneous vibration response of vehicles and eliminate any resulting vehicle-bridge interactions.

The issue of vehicle bouncing effects and their influence on the vibration response of bridges boosted research initiatives in modern transportation systems such as controllable hardware attachments to structures (forming a part of Structural Health Monitoring (SHM) and Control), and reliable bridge design standards and load specifications using improved design models. A study on developing coordinated control of vehicle suspension characteristics from bridge response data using a wireless network system is being pursued by the DySSC center at OU through its novel Intelligent Vehicle Bridge System (IVBS) program, thus, addressing the two-fold objectives of health monitoring and control of structural members.

1.3 Bridge design procedures and parameters – An overview:

Bridges can be broadly classified by the functional requirements (type of traffic like highway, railroad, etc), material resource types (wooden, metal, stone/concrete, etc),

design details (cantilever, simple span, multi-span, arch or truss type, skewed, etc.) and application of technology (suspension bridges, slab, girder, etc) but any given bridge structure is always associated with a mix of the above factors such as multi-span slab-girder bridge, single span simply supported slab-girder bridge, etc.

This thesis is limited to the discussion of the development of numerical models for analyzing the dynamic behavior of beam and slab type bridges only. Also, it is interesting to note that the present design codes are based on beam models and work well, because in spite of ignoring the vehicle mass and vehicle-bridge interaction effects, most of the bridges designed and built as per this design code are in healthy operating conditions (probably due to higher safety factors). However, a better estimate of the dynamic behavior of bridge structures including vehicle mass and vehicle-bridge interaction effects allows bridge designers to assign appropriate safety factors. The safety factor specified applies only to the structural resistance parameter as discussed in the previous section (refer to *Equation 1.1*), i.e., the Allowable Stress Design (ASD) approach. Bridge design codes were updated recently by the AASHTO that replaced the traditional Allowable Stress Design (ASD) concept with the Load and Resistance Factor Design (LRFD) procedure [2]. The LRFD procedure applies multiplication factors on both sides of the *Equation 1.1*, i.e., for both the structural resistance and applied loads.

Bridge loads are typically classified into permanent and transient loads. Permanent loads include those that stay with the bridge structure for its lifetime (mostly) such as self-weight of the deck, girders, curbs, and other attachments. Transient loads includes all

types of time varying loads such as vehicle loads, pedestrian loads, loads due to winds, earthquakes, temperature variations, etc.

The recent version of the AASHTO standard specifications classifies the vehicular design loads into design truck, design tandem and design lane loads, and requires that the load effects of the design truck and design tandem be superimposed with the load effects of design lane loads unlike in the previous AASHTO standard specifications where the loads were considered separately. The design truck is a typical semi-trailer truck and has the configuration of HS20-44, one of the standard specifications that AASHTO used since 1944. Here, '20' in HS20-44 stands for the total weight of the first two axle loads in US customary units, i.e., 20 *tons*. The total weight of HS20-44 including the trailer is 36 *tons* approx. with 4 *tons* in the front axle, and 16 *tons* each at the remaining two axles (here, second and third axle load actually mean a vector sum of two consecutive axle loads). The design tandem is a two axle load specification with each axle weighing 12.36 *tons* (110 *kN*) approx. The design tandem closely resembles another AASHTO standard configuration H20-44 whose total weight is 20 *tons*. However, in the H20-44 the loads are distributed as 4 *tons* in the front and 16 *tons* in the rear axle. The design lane load is a uniformly distributed load of 9.3 *N/mm*.

The AASHTO assesses the dynamic load effects due to moving loads using a dynamic load allowance factor (DLA) given by

$$DLA = \frac{D_{dyn}}{D_{st(\max)}} \tag{1.2}$$

where $D_{st(\max)}$ is the maximum static deflection and D_{dyn} is the additional deflection due to dynamic effects, i.e. $D_{dyn} = D_{dyn(\max)} - D_{st(\max)}$ where $D_{dyn(\max)}$ is the maximum dynamic deflection at the point of maximum static response. The DLA factor varies for the same load with different load positions but is usually measured at the mid-span location. Another way to express the dynamic load effects is to define the dynamic increment factor (DI) as

$$DI = \frac{\{D_{dyn}\}_{\max} - D_{st\max}}{D_{st\max}} \tag{1.3}$$

The basic difference is that the point of measure of maximum dynamic deflection may be different from the point of occurrence of maximum static deflection but both these definitions yield similar values. In this study, the dynamic effects are measured using the dynamic amplification factor (DAF) which is simply the ratio of maximum dynamic deflection to the corresponding static deflection of the bridge, i.e.,

$$DAF = \frac{\{D_{dyn}\}_{\max}}{D_{st}} \tag{1.4}$$

and is measured usually at the center of the beam.

1.4 Literature Review:

The problem of moving loads is believed to have been identified early in the nineteenth century concurrent to the design and construction of railway bridges. In those days, the dynamic nature of moving loads and its consequences on foundation structures as the

loads passed by were not fully understood owing to limited engineering resources available for experimental observations. The collapse of the Chester Railway Bridge in 1849 and the subsequent efforts by *Willis* [3] and *Stokes* [4] drew the engineers' attention to note the impact of moving loads on the underlying structures.

In the initial stages of development of the theory and practice of moving load problems, a few assumptions were considered to simplify the original moving load problem to simple cases such as massless beam carrying moving mass, or a beam carrying massless load (force), etc. Several of the studies (conducted in the late nineteenth century and early twentieth century) based on these assumptions promoted our understanding of the dynamic nature of moving loads and contributed further research related to the moving load problem. Early investigations on highway bridge vibrations resulting from moving vehicles with and without the effect of vehicle bridge interactions, and/or those in the presence of wind and seismic activity were reviewed by *Wright and Green* [5] in 1959, *Ting et al.* [6] in 1975, *Huang* [7] in 1976, and *Venancio Filho* [8] in 1978.

Very few monographs exist on this special subject of moving loads, the earliest being a collection of case studies on vibrations of railway bridges by *Inglis* [9] published in 1934. Another popularly referred monograph is due to *Fryba* [10], first published in 1972 (3rd edition, 1999), which briefly reviews the research carried out from the late nineteenth century until recently, with concise discussions including several case studies on various aspects of moving loads. Another popular monograph on the moving load problem published in 2004, also targeted at the application to railways, was written by *Yang* et al.

[11]. In this book, the authors treated the vehicle-bridge interaction using a new method called dynamic condensation technique.

1.4.1 Literature Survey Classifications:

One of the criteria to classify moving load and VBI studies could be the representative model, i.e., whether the model used to represent the system is a continuous/distributed system (infinite degrees of freedom) or a discrete/lumped system (finite degrees of freedom). Another representative model classification in case of VBI problems could be quarter-car (single oscillator), half-car (two oscillators) and full-car (four oscillators) models, with and without the trailers, and their defined degrees of freedom, etc.

Based on the type of governing equations of motion for the bridge vehicle system, we have two forms, namely, a coupled and an uncoupled form of the equations. The advantage of the uncoupled form is that we can solve the equations separately for the bridge and the vehicle starting with some valid initial assumptions. The solution for the vehicle system is independent of the bridge system, and it is easy to solve and takes less time. The equations, although said to be uncoupled, are in fact coupled by the interaction forces. The interaction forces govern the equations of motion of the bridge and vehicle system, and since they are defined explicitly in the equations of motion, they offer more information on bouncing of the vehicle, and any possible loss of contact between bridge and vehicle wheels.

On the other hand, the coupled equation system takes a longer time to solve since the responses of vehicle and bridge are directly coupled. In the coupled equations, we have

no explicit term to define the interaction forces that govern the equations of motion for vehicle and bridge system. Thus, the coupled equations may not yield a solution (the solution will diverge if a direct time integration procedure is employed) when there is a loss of contact between bridge and vehicle wheels. This can be avoided in the case of the uncoupled set of equations by allowing only a non-zero positive value for the interaction forces acting from vehicle to bridge. In other words, the uncoupled set of equations offers control over the solution during solution processing whereas the coupled set of equations allows control of the solution procedure (like time step values, etc) only at the beginning of the solution process.

Based on the formulation of governing equations of motion for the vehicle and bridge system, we observe that the following classification is possible: 1) *Lagrange multiplier* scheme – yields equations of motion with multipliers (interaction force terms) that can be eliminated (coupled) or solved as is (uncoupled), 2) *Equilibrium of forces – Euler Bernoulli* or *Timoshenko* equations for beam, and corresponding *Kirchhoff* or *Mindlin* equations for plate structures, 3) *Weak form generation* for FEM using governing differential equations obtained from Equilibrium or Energy methods through a variational formulation.

We can also classify the nature of the work based on the solution method such as the use of 1) *Modal decomposition* methods – assumed modes or generalized mode decomposition, 2) *Laplace* or *Fourier Transform* techniques, 3) *Direct time integration* of the differential system (and this includes vastly different schemes such as the

Newmark's scheme [12, 121], the *Houbolt's* [12] scheme, *Precise integration* methods [122], *Wilson-θ* [12], *Runge-Kutta-Nyström* [10], *Finite Difference* schemes, the *Differential Quadrature* method), 4) *Perturbation* methods (multiple scales method [123]), and 5) the *Finite Strip* method [45], and 6) *Finite Element* methods.

Recently, *Nassif* and *Liu* [72] nicely summarized some of the past key research work carried out in moving load analysis using a tabular representation. The following section presents the literature survey on the moving load problem in chronological order. The references on research contributions by some of the non-English authors were taken from *Fryba*'s [10] monograph citations. References on some of the methods and concepts used in the study of the dynamical behavior of structures can be seen in *Humar* [12] and other texts on structural dynamics.

1.4.2 Chronological Survey:

The first known attempts at solving a moving load problem were made in the year 1849 by *Willis* [3] and *Stokes* [4]. *Willis* published a case study on the collapse of the Chester Railway Bridge in which he formulated a differential equation to study the vibration involved, and in the same year, *Stokes* provided a closed form solution of that differential equation using a power series method.

Zimmermann [13] also solved the *Willis* differential equation [3] independently and proposed a similar closed form solution. It is interesting to note that they assumed a massless beam traversed by a point mass. The opposite case wherein the load mass is

neglected when compared to the beam mass, was examined for a simply supported beam under the action of a constant concentrated force by *Kryloff* [14] in 1905, and later by *Timoshenko* [15] in 1908 who also studied the effects of moving harmonic forces due to counterweights on the locomotive driving wheels driven at constant speed.

The analysis of moving loads becomes more complicated when both the beam mass and the moving mass are taken into consideration. This case was first analyzed by *Saller* [16] in 1921 and by many researchers since then. A satisfactory solution method was worked out in 1937 by *Schallenkamp* [17] who used *Fourier* series with unknown coefficients to analyze the effects of a constant point load moving over a beam. In all of the above mentioned investigations, the transit mass (vehicle) was designated as a point mass to simplify the calculations.

Jeffcott [18] used the method of approximations to solve the moving load problem. According to this method, initially, the vertical displacement of the beam due to the moving load is calculated by ignoring any inertia effects of the beam, i.e., a massless beam as shown in *Equation 1.5*.

$$EI\frac{\partial^4 \overline{W}}{\partial x^4} = \delta(x - ct)P \tag{1.5}$$

where $\overline{W}$, E, and I represent lateral (or vertical) deflection at location (*x*, *t*), *Young's* modulus and area moment of inertia of the beam, respectively, and $\delta(\cdot)$ is the *Dirac Delta* function; *ct* denotes the distance traveled by the load *P* in time *t*. Then, the

displacement solution is substituted back into *Equation 1.6* that includes the inertia effects of the beam and moving load, and a new displacement solution is found.

$$\mu \frac{\partial^2 \overline{W}}{\partial t^2} + EI \frac{\partial^4 \overline{W}}{\partial x^4} = \delta(x - ct)(P - M \frac{\partial^2 \overline{W}}{\partial t^2}) \tag{1.6}$$

where μ is the linear density (mass per unit length) of the beam and M is the representative mass of the load *P*. This iteration is continued until the solution converges. *Jeffcott's* solution was the first successful numerical attempt to solving the moving load problem with mass effects of both the beam and load included. The sprung and unsprung mass effects were not considered in his approach.

In 1934, *Inglis* [9] published a treatise on the dynamic analysis of railway bridges and included most of the important cases of moving load problems using harmonic analysis. He used the term, 'crawl deflection' to denote the moving force problem, and used a *Fourier* sine series to approximate the effect of a moving point load, i.e., replaced the hard to handle *Dirac Delta* function with a *Fourier* sine series. Thus, according to his treatment, the governing equation of a beam subjected to a moving force is given by

$$\mu \frac{\partial^2 \overline{W}}{\partial t^2} + EI \frac{\partial^4 \overline{W}}{\partial x^4} = \frac{2P}{L} \sum_{k=1}^{\infty} Sin \frac{k\pi x}{L} Sin \frac{k\pi ct}{L} \tag{1.7}$$

The above equation can then be solved as a regular partial differential equation without requiring integral transformation techniques. *Inglis* showed that the maximum contribution to the dynamic displacement solution comes from the first mode only, and

that the error introduced in the displacement solution is less than 0.5 % if higher modes are neglected in the calculations. *Inglis* included “hammer-blows” due to balance weights attached to locomotive driving-wheels with a moving harmonic force model (similar to *Timoshenko* [15]), and obtained the same solution as *Timoshenko* but with less difficulty.

Inglis also extended this study by considering the combined effects of the harmonic force and the associated inertia of a moving mass. Here, he assumed the mass to be concentrated at a fixed point (preferably at the center of the beam) which would result in an upper bound of the displacement solution for the moving mass problem and produce conservative stress results. This idea of assuming a lumped mass centered at the beam is covered later in the third chapter, section 3.2. He also treated the bouncing effects of the locomotive body using a simplified 2 *DOF* sprung and unsprung mass system. He accounted for the effect of damping using a viscous damper model, i.e., the resistance to motion due to damping is proportional to the velocity of the moving load.

In 1951, *Hillerborg* [19] studied the motion of sprung masses on a simply supported beam using *Fourier*’s method and the method of numerical differences. *Hillerborg* assumed that the dynamic deflection of the beam due to a moving load at any given time is proportional to its instantaneous static deflection due to the moving load. *Biggs* et al. [20] using *Inglis’s* method, and *Tung* et al. [21] using *Hillerborg’s* approach solved the problem on digital computers, and applied this traditional railway bridge problem to highway bridges. Other notable contributors of the 1950s and 1960s, in the study of the

dynamic response of a structure due to a moving load, include *Bolotin* [22], *Kolousek* [23], *Filippov* [24], and *Bondar* [25].

Wen [26] investigated the dynamic response of beams traversed by a two-axle load system with an assumption that the dynamic deflection is proportional to the static deflection caused by the beam weight and loads. This assumption is based on *Hillerborg's* assumption but also takes into account the weight of the beam to express the dynamic deflection. *Wen* also considered the surface waviness using a sinusoidal function for the initial beam profile.

In 1966, *Walker and Veletsos* [27] studied the differences in dynamic behavior of beams subjected individually to a moving constant force and to a moving sprung mass. They observed that the vehicle-bridge interaction phenomenon is dependent on frequency ratio (ratio of natural frequency of vehicle to natural frequency of bridge vibration), and concluded that bridge-vehicle interaction can safely be neglected for frequency ratios less than 0.3.

Fryba [28] also studied the dynamic behavior of a uniform beam under a moving two-axle load system containing sprung and unsprung masses. Both, *Wen* [26] and *Fryba* included the effect of rotary inertia of the vehicle (sprung mass) in their studies. *Wen* obtained the differential equations governing the dynamic behavior of a beam from an energy formulation (using *Lagrange's* equations [12]) while *Fryba* obtained them using force equilibrium conditions. *Wen* used *Newmark's* [12] method to numerically integrate

the system of equations. *Fryba* used the finite *Fourier* sine integral transformation method for the analytical solution, and a *Runge-Kutta-Nyström* scheme for the numerical solution. *Fryba's* solution also included damping effects and the surface waviness of the beam in the dynamical behavior due to moving loads.

In 1968, *Fryba* [28] extended the study to include the loss of contact between the load system and the beam due to non-uniform surfaces. Thus, the governing equations of motion for the beam and mass system are written separately but are coupled together by contact forces at the points of contact. The inclusion of *Hertz* contact forces into the moving load problem makes it a nonlinear problem. However, in order to simplify the analysis, *Fryba* introduced linear springs to represent the contact forces between tires and bridge, i.e., he linearized the otherwise non-linear *Hertz* contact forces.

Stanisic et al. [1968, 29] studied the undamped vibration response of a simply supported plate structure under moving multiple masses using a modified *Fourier* transform technique and presented the solution in the form of a convergent series. They used a sine series approximation to replace the *Dirac Delta* term, and neglected the convective terms in the governing differential equation of the moving mass problem. They also found that the resonance conditions are met earlier for the case of a moving mass system than for the moving force system, with the other conditions remaining the same, indicating the significance of the mass of the moving load.

Steele [30] obtained a series solution for the case of a concentrated load moving over a simply supported *Euler-Bernoulli* beam with and without elastic foundation.

In 1970, *Veletsos and Huang* [31] discretized the bridge as a linearly elastic beam of multiple degrees of freedom (DOF) having lumped point masses and distributed flexibility, and analyzed the dynamic response of a vehicle modeled as a three axle system having sprung masses. They uncoupled the equations of motion for vehicle and bridge (similar to *Fryba* [10]) and solved the system of equations separately at each lumped mass point (node) of the beam using *Newmark's* time integration method. They used influence coefficients (denoting reaction induced due to unit concentrated force and unit deflection) to scale the interaction forces and deflection at each node of the beam. They analyzed the dynamic response of three-span cantilever-type continuous bridges and compared it to the results obtained from previous research conducted on simple span bridges by *Walker and Veletsos* [27]. *Veletsos* and *Huang* concluded that the peak variation in interaction forces computed for cantilever type bridges was thrice greater than that for simple span bridges under similar combinations of weight ratio, frequency ratio and speed parameter.

Nelson and *Conover* [32] studied the dynamic response of a simply supported beam loaded by a continuous series of equally spaced moving mass particles. They used both *Galerkin*'s method and the modal expansion technique to solve for the dynamic response of the beam carrying a moving load, and also discussed the stability regions for the same.

In 1972, *Csagoly et al*. [33] used the finite element code ICES STRUDL II to compute natural frequencies and the dynamic response of continuous bridges up to 100 *ft* in length with two to five spans. They suggested that the proportioning of bridge span length so that the fundamental frequency is greater than 5 *cps* could reduce resonance with modern vehicles. They also carried out field tests on continuous pre-stressed concrete deck bridges with a test vehicle of 90,000 lb and observed that the impact factor was dependent on the matching frequencies of bridge and vehicle, and the state of excitation before the entry of the vehicle.

Shepherd and *Aves* [34] carried out analytical and experimental investigations on the dynamic response of simply supported bridges. They modeled the bridge as a simply supported beam and the vehicle as a single sprung mass. By comparing the results obtained from field tests on bridges and the analytical results, they found that the dynamic impact allowance factor prescribed then was insufficient and it underestimated the dynamic effects due to a moving load. The design code for the dynamic impact allowance factor was an empirical relation based only on the bridge span length. *Shepherd* and *Aves* suggested a correction in the impact allowance factor, and included the speed parameter and an experimental parameter J such that the corrected impact allowance factor is given by the following relation,

$$I = \left(J + \frac{\alpha}{1-\alpha} \right) \times 100\% \tag{1.8}$$

In 1974, *Ting* et al. [35] introduced a structural impedance approach to solve for the dynamic response of a finite elastic beam under a moving mass. They used influence

functions (*Green*'s functions) to express the equations of motion for a point mass-beam coupled system in the form of integro-differential equations. The integral formulation eliminates the higher order partial derivatives, the *Dirac Delta* function and explicit boundary conditions. In 1975, *Ting* et al. [6] also reviewed some of the past research on the moving load problem.

Stanisic et al. [1974, 36] proposed as an alternative approach an asymptotic method to solve for moving mass problems where modified natural frequency due to the moving mass was used to replace the existing governing equation of motion with an equivalent free *Eigen* system, and they also presented a numerically exact solution for the same.

Blejwas et al. [37] studied the moving force-moving mass problem on a *Bernoulli-Euler* beam using *Lagrange* multipliers, and suggested that the vertical acceleration of the mass is not exactly equal to the vertical acceleration of the beam but contained additional or convective acceleration terms. The equations of motion obtained from *Lagrange*'s method were solved in uncoupled form with constraints to obtain the interaction forces, i.e., the *Lagrange* multipliers. Since the use of *Lagrange* multipliers introduced more unknowns, the solution procedure involved more computational time and effort.

In 1981, *Hamada* [38] employed a double *Laplace* transform to evaluate the response of a simply supported damped *Euler-Bernoulli* beam under the action of moving forces. *Hamada* obtained the forced vibration part of the transient response in closed form *Fourier* summation series.

Mulcahy [39] discussed the dynamic response of single span multi-girder bridges due to vehicular loads using a finite strip method. *Mulcahy* used an orthotropic plate model to represent the bridge structure as simply supported on two of its opposite sides and free on the other pair of edges, and analyzed the dynamic response of a three axle tractor-trailer vehicle. He included effects of vehicle acceleration or braking, deck surface waviness effects and the effect of eccentric loading due to placement of the vehicle on one side of the plate. He used *Newmark*'s method to numerically integrate the equations of motion in time.

In 1985, *Olsson* [40] used the finite element method to analyze the effect of moving forces traversing a simply supported beam at uniform speed. The beam was assumed to have a harmonically varying surface profile and the generalized modal coordinate method was applied to simplify the solution procedure and *Newmark*'s method was used to time integrate the equations of motion.

Palamas et al. [41] studied the effects of surface waviness on the dynamic response of bridges subjected to moving loads using the *Rayleigh-Ritz* method and demonstrated the need for inclusion of dynamic effects into bridge design codes. *Hino* et al. [42] used a *Galerkin* finite element formulation to calculate beam deflections under the action of a moving load. They included the geometric non-linearity associated with the stretching of the middle surface due to axial loads.

In 1987, *Sadiku* and *Leipholz* [43] used *Green*'s functions to present a series solution for the dynamic response involving moving masses. They compared the solutions for the moving-mass and their corresponding approximated moving force models, and concluded that the moving-force solution was not always an upper-bound solution as suggested by *Timoshenko* et al. [15] earlier.

Wu et al. [44] analyzed the dynamic response of a continuous flat plate under various moving loads using the finite element method and discussed the effects of eccentricity, acceleration, and initial velocity of the moving load, and the plate span length on the dynamic response of the system. They claimed that the dynamic behavior of plate structures depends on the eccentricity of the applied load on the plate. They also concluded that, if the initial velocity of the moving load is kept constant, a larger acceleration yielded smaller fluctuations in the dynamic response and, for specified system parameters, increased acceleration values resulted in an increased maximum central displacement up to a certain initial velocity ($V_0^{'}$) but produced a decreased displacement after the initial velocity exceeded $V_0^{'}$. They also showed that, for a single-span plate, a larger span length resulted in higher fluctuations of the maximum central displacement corresponding to changes in velocity of the moving load.

In 1990, *Geannakakes and Wang* [45] applied a finite strip method to analyze moving load problems involving arbitrarily shaped plates. They used B_3-splines (for the long direction) in combination with *Hermitian* polynomials (for the short direction) to interpolate the displacement function. Further, the governing equation of motion was

numerically integrated using *Houbolt*'s [12] and *Zienkiewicz* et al. [126] time integration methods. The plate was assumed to be simply supported on all sides, with the load traveling along the plate's center-line, and hence, by the use of symmetry, only half the plate was included in the analysis. This work is one of the few studies based on finite strip techniques to perform moving load analysis.

In 1990, *Mackertich* [46] studied the dynamic response of a simply supported *Timoshenko* beam subjected to moving force. He used the modal superposition method to compute the deflections of the *Timoshenko* beam under a moving constant force and compared the solutions with those for *Euler-Bernoulli* beams. A couple of years later, *Mackertich* [47] also studied the *Timoshenko* beam under the action of a moving mass wherein he approximated the total time derivative of the vertical displacement of the mass using its partial time derivative so as to remove the mixed derivatives in the acceleration expression.

In 1992, *Ahmed H. Kashif* [48] in his studies discussed the formulation of bridge design procedures using the relationships between the major parameters affecting the bridge response for both single and two-axle vehicle models. *Kashif* investigated the response of a bridge structure modeled as a rectangular plate (both isotropic and orthotropic) under the action of multiple moving bodies, each of them represented by a single sprung mass. *Kashif* also studied the forced vibration response of a box girder bridge under the action of moving vehicle loads, and found that the dynamic response of the bridge is dependent on the frequency ratio (ϕ), the mass ratio (κ), the speed parameter (α), the aspect ratio,

and the flexural and torsional rigidity distribution of the bridge. In all the cases above, *Kashif* ignored the effect of damping in the bridge and the vehicle.

In 1993, *Nassif* [1993, 49] and his group experimentally investigated the static and dynamic responses of slab bridges due to truck loads with weigh-in-motion (WIM) and a dynamic data acquisition system. A couple of years later, *Nassif and Nowak* [1995, 50] and their group conducted field tests to experimentally determine the dynamic load factor (DLF) of slab-on-girder bridges.

Green and Cebon [1994, 51] evaluated the dynamic response of a bridge system with a convolution integral expressed in terms of modal responses and then solved it in the frequency domain using a discrete *Fourier* transform. They also treated the vehicle-bridge interaction with an iterative scheme in which the initial set of vehicle wheel loads calculated from the vehicle response is used for deducing the displacement response of the bridge, and the bridge response is added to modify the vehicle response (so that new wheel loads can be predicted) for further iteration. They also carried out experimental investigations on two highway bridges in the UK (one being a four span pre-stressed concrete box-girder bridge and the other a three-span slab-on-girder pre-stressed concrete bridge) and validated the measured bridge response data with those predicted from the convolution integral formulation. The mode shapes recorded during the experimental procedure were used in the validation model.

In 1995, *Yang and Lin* [53] applied a sub-structuring procedure (based on the modified condensation technique proposed by *Paz* [52]) to divide the vehicle and bridge system such that the model consists of vehicle-bridge interaction elements at places of contact between vehicle and bridge, and only bridge elements at the rest of the points. The vehicle-bridge interaction element is a condensed form of the vehicle suspension unit and the bridge element. The equations of motion for the suspension unit and the bridge element at the point of contact were coupled through the contact force that varies in time and space (position along bridge). Also, constraint conditions were developed such that there is no loss of contact between the vehicle and the bridge. The substitution of the contact force from the suspension unit governing equation (in terms of the constraint conditions) into the bridge element modifies the bridge element at the points of contact. They also treated the bridge deck road roughness in the VBI studies using a power spectral density (PSD) function.

In 1996, *Michaltsos* et al. [54] used a similar approximation as *Mackertich* and obtained a series solution for the beam deflection in terms of normal modes. They used an *Eigen* solution to reduce the governing differential equation to contain only modal coordinates and found the first approximate solution to the reduced modal equation by neglecting the additional term due to inertia of the moving load. By iterating the solution in the reduced modal equation, they obtained an exact solution that addresses the mass effects of the load.

Ali Al-Sowaidi [55] studied the vehicle-truck interaction using the finite element method. *Al-Sowaidi* included viscous damping in the bridge and vehicle, and used beam elements to model the bridge. He found that increased axle weight, stiffness coefficient of the wheel, bridge span length, and wheel damping coefficient resulted in increased transverse displacement of the bridge as well as a higher interaction force between vehicle and bridge.

Lee [56] presented a numerical solution based on the *Runge-Kutta-Nyström* method for a clamped-clamped beam acted upon by a moving mass using the assumed mode method. *Lee* also showed, using calculations, the possibility for the mass separating from the beam for certain slow speed and low mass combinations. The study also agreed with *Sadiku* and *Leipholz* [43] that the approximation using a moving force model is not always conservative.

Yang and Fonder [1996, 57] studied bridge-vehicle systems by uncoupling the bridge and vehicle equations of motion, and solving them separately using an iterative procedure based on the *Newmark* time integration method. They included a specific relaxation coefficient for the iterative scheme and claimed that their iterative scheme coincides with the *Green and Cebon* [1994, 51] procedures for a relaxation coefficient of 0.5. They also pointed out that a relaxation coefficient close to 0.85 is needed for a good iterative scheme, i.e., for a better convergence rate. They also applied *Aitken's* acceleration method [127] to this iterative scheme as an alternative to the relaxation procedure. Both, the relaxation coefficient and the *Aitken* acceleration procedures were used to control

(increase) the convergence of the iteration process. Both these methods can be applied instead of direct time integration methods to solve for the dynamic response of bridge and vehicle systems. They also concluded that *Aitken*'s acceleration method works better than the relaxation coefficient method.

In 1997, *Green and Cebon* [58] conducted parametric studies on the effects of several bridge-vehicle parameters on the dynamic response of bridges to assess the importance of vehicle to bridge interaction, and showed the maximum error in the dynamic response, when vehicle interaction is ignored, to be around 11 % and 22 % for speed parameters $\alpha = 0.1$ and 0.2, respectively. They concluded that vehicle interaction can be safely ignored in bridge response calculations either if both $\alpha < 0.1$ and vehicle to bridge mass ratio $\kappa \leq 0.3$ are valid, or if the vehicle to bridge frequency ratio is $\gamma < 0.5$.

In 1997, *Xu* et al. [59] formulated coupled equations of motion governing the transverse and longitudinal displacements of a finite beam subjected to a moving mass using Hamilton's principle and then solved the resulting boundary value problem using the finite difference method combined with perturbation techniques. They found that, within the elastic limits, the coupling between the longitudinal and transverse motion doesn't differ significantly from that of pure bending with no friction and that the friction factor influences the longitudinal motion.

Yang and Yau [60] improved the dynamic condensation method introduced by *Yang and Lin* [53], and proposed a vehicle-bridge interaction element formed by condensing the

sprung mass element discretized in *Newmark*'s finite difference scheme to the bridge elements at contact points.

Pesterev and *Bergman* [61] presented a series solution for the response of a conservative 1D elastic continuum carrying a moving oscillator by reducing the governing equation of the system to a *Volterra* equation of the second kind.

In 1998, *Foda* and *Abduljabbar* [62] improved the application of *Green*'s function proposed by *Ting* et al. [35] to evaluate the dynamic response of a simply-supported beam under the effects of a moving mass. They presented a dynamic *Green*'s method which reduced the complexity involved in computing the deflection using the original *Green*'s function.

Henchi et al. [63] treated the dynamic interaction between bridge and vehicle using a coupled finite element formulation which was then solved by a central difference scheme. The coupled system consists of modal components of the bridge and physical components of the vehicle. They also treated the bridge surface waviness using a power spectral density function.

Kai Deng [64] discussed the dynamic response of a vehicle moving over skew slab bridges, skew slab-on-girder bridges and multi-span continuous and cantilever bridges using the finite element method. The vehicle was modeled as a single axle sprung mass, the skew slab was modeled by plate elements and the girders by beam elements, and

damping in both the bridge and the vehicle was neglected. *Deng* concluded that skew bridges with different aspect ratios yield similar responses if they have the same frequency ratio (ϕ), speed parameter (α), skew angle (θ), and mass ratio (κ). Deng also showed that the first and second frequencies of the skew bridges get close to each other as the skew angle is increased.

Tan et al. [65] used 2D grillage to model the bridge structure and analyzed the vehicle bridge interaction with a full car model of seven DOF (one vertical displacement motion each for the four wheels, and roll, pitch and vertical motions for the vehicle chassis), and concluded that the vehicle response reaches steady state along its traverse after an initial excitation and is unaffected for a wide range of speeds but the bridge response is highly influenced by the vehicle speed.

Marchesiello et al. [66] studied the moving load problem by modeling the bridge as a continuous multi-span isotropic plate and obtained the response using the mode superposition principle. The study included both the flexural and torsional mode shapes, and used the *Rayleigh-Ritz* method to compute the modes.

In 2000, *Huan Zeng* [67] proposed a semi-analytical method using the mode superposition principle to study the vibration of bridges under moving vehicles, where the bridges were modeled as orthogonally stiffened skewed plates and a three-axle vehicle model was chosen to represent the moving load. *Zeng* used a pb-2 *Rayleigh-Ritz* function to solve for the mode shapes and natural frequencies.

Yang et al. [68] discussed the asymptotic behavior due to a change in stiffness of the suspension spring in an undamped 1-DOF oscillator traversing a 1D elastic continuum, and showed that, as the stiffness approaches infinity, the moving oscillator model reduces to a moving mass model. They also provided an exact integral formulation for the response solution of the coupled system which required integration only in the time domain, and proposed a direct integration approach to solve for the response. They also demonstrated their direct integration procedure by solving for the displacement response of a taut uniform string and a simply supported beam subjected to moving loads.

Zhu [69] analyzed the dynamic behavior of a continuous bridge deck under moving loads and included influence factors such as road surface waviness of the bridge and presence of multiple vehicles and their relative positions on the track, braking (deceleration) and acceleration effects, using computational simulations and laboratory tests. *Zhu* also addressed two new methods based on a regularization technique to identify the time varying loads from moving vehicles.

Yang Lee [70] proposed a method using complex eigenfunction expansion to evaluate coupled dynamic vehicle-bridge interaction problems. *Lee* based his technique on *Galerkin*'s method of *Eigenvalue* estimation using complex *Eigenfunctions* and concluded that this method is effective when large numbers of trial functions are used.

Nassif et al. [2003, 71] developed a computational model based on the *Newmark* algorithm to evaluate the DLF's of the bridge system. They validated their computational

procedure using experimental data obtained previously [1993 49 and 1995 50]. They also compared their computed and experimental DLF values to the DLF data suggested in the AASHTO-LRFD (1998) specifications. Recently, *Nassif and Liu* [2004, 72] discussed the effect of road waviness using a randomly (*Gaussian*) generated profile as well as measured actual road waviness profile data. In their three dimensional vehicle bridge interaction system, they used a grillage model loaded with a five axle vehicle system having eleven degrees of freedom to analyze the dynamic behavior of a slab-on-girder bridge under a moving semi-tractor-trailer. They also included a brief summary of research performed on slab-on-girder bridges. One interesting feature is the summary of selected research in table form with associated key aspects.

Recently, *Bilello* et al. [73] presented their experimental observations on a small-scale bridge model under a moving mass. They determined a set of static and dynamic similitude conditions using a selected prototype bridge structure and studied the bridge response using a similitude-maintained small-scale model (especially mass similitude). They confirmed the experimental results using an analytical series expansion method with *Eigenfunctions*.

Other literature references related to the moving load problem but not included in the survey are in the area of vehicle axle load identification from bridge responses [*Law* et al. 2004, 74, *Pinkaew* 2006, 75], extraction of bridge frequencies from the vehicle response [*Yang* et al. 2004, 76], damage detection of bridge structures under moving loads [*Zhu* and *Law* 2007, 77], etc.

1.4.3 Selected Works – A short note on the research program at OU:

The studies related to bridge life enhancement at the *University of Oklahoma* were initiated by *Patten* and associates/coworkers [1996 [78], 1999 [79]] at the *Center for Structural Control*, Norman Campus. Other studies on the dynamic response of bridge structures under moving loads carried out at OU include *Taheri et al*. [80, 81], who used structural impedance and the finite element method, and *Bert and Zeng* [82], who used pb-2 *Rayleigh-Ritz* functions.

The application and installation of structural vibration mitigation mechanisms on highway bridge structures was suggested earlier by *Abdel-Rohman* et al. [83] and *Lin* and *Trethewey* [84] but their models were based on an active structural control system. *Patten* et al. [1996 [78], 1999 [79]] proposed a semi-active mechanism to reduce the vibration response of bridge structures subjected to vehicular loads through their Intelligent Stiffeners for Bridge (ISB) concept, i.e., through the use of intelligent stiffeners retrofitted to an existing bridge, allowing varying the stiffness appropriately as traffic loads over the bridge vary. The stiffness regulation is possible through an adjustable semi-active vibration absorber (SAVA) system energized by a 12 *volt* automobile battery supply. The SAVA offers a good trade-off between a fully passive or fully active controller, i.e., the semi-active controller uses only little power (battery supplied) but behaves adaptively and provides control for stiffness regulation.

As a preliminary step to install and test the ISB at an existing bridge, *Patten* et al. [1999, 79] performed drop hammer tests on the I-35 north bound *Walnut Creek* bridge located at

Purcell, Oklahoma, to get modal properties of the bridge, and also to validate their finite element model built using *I-deas*.

Figure 1.1: Intelligent Stiffener for Bridge (ISB) attached to *Walnut Creek* Bridge

The *Walnut Creek* bridge is a four span skewed bridge supported by three concrete piers at intervals of 30.5 *m*. The bridge has four lanes, two each for north and south bound traffic, with the north bound side measuring approximately 10.4 *m* in width. The bridge superstructure consists of a reinforced 0.19 *m* thick concrete deck resting on five continuous steel girders weighing 196.5 *kg/m* (mass per unit length or linear density) with an external attachment of a set of 12 piezo-resistive accelerometers each along the girders at two ends and center such that three accelerometers are available to record the acceleration data per girder per span. The other attachments includes a string potentiometer at the center point of each span (along the center girder) for measuring

absolute displacement of the superstructure, and strain gages for measuring mid-span strain of the girders.

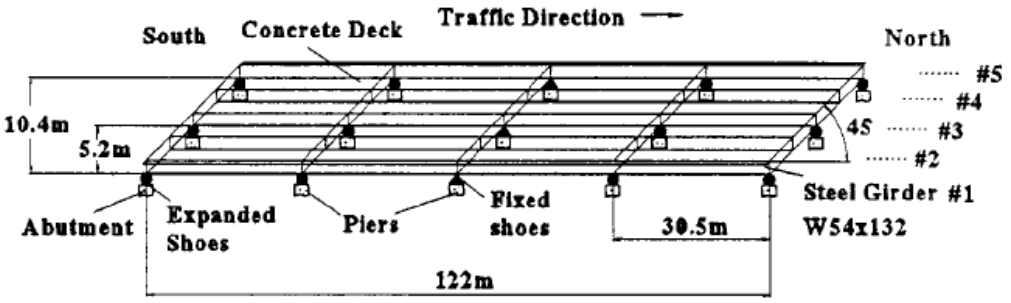

Figure 1.2: Walnut Creek Bridge details (Courtesy: Patten et al. [79])

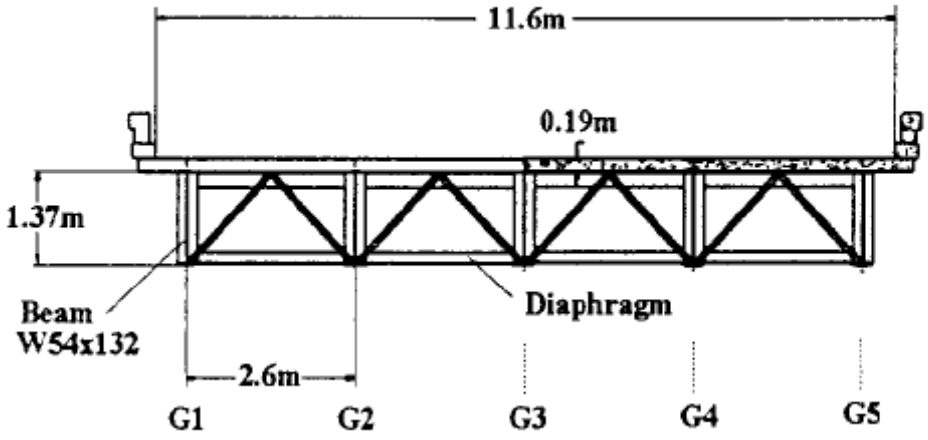

Figure 1.3: Front view (Cross-section) of Walnut Creek Bridge (Courtesy: Patten et al. [79])

Two types of trucks were considered for the bridge tests, of which the heavier type carried rocks and gravel and weighed about 36,320 *kg* (or 40.036 *tons* force ≡ 80.1 *kips* in US units), and had five axles with a 9.8 *m* wheel base. The other truck type was a tandem

load type (steering and tandem axle only) vehicle with a permissible load of 25,880 *kg* (or 28.5 *tons* force ≡ 57.1 *kips*) and a 4.3 *m* wheel base.

Patten et al. [1999, 79] concluded that their proposed ISB model could reduce the peak stresses by over 50%, and extend the service life of bridge structures by 50 years. Some of the key findings of this research work included 1) the extraction of modal frequencies of the bridge from drop hammer tests, 2) a successful finite element validation model matching closely with the experimentally recorded modal frequencies, 3) recorded data showing the presence of a dynamic coupling phenomenon between heavy trucks and bridge response, and 4) an experimentally observed substantial reduction in the vibration response of the bridge system with a passive ISB (open SAVA control valves) immediately after the passage of a heavy truck compared to that of a bridge system without ISB, and a similar reduction in bridge response even during the passage of heavy trucks at high speeds with active ISB (closed SAVA control valves).

They also confirmed that the dominant responses of the bridge were limited to modal frequencies below 10 *Hz* which indicated the optimum range for the required bandwidth of the controller hardware. Because the natural frequencies of heavy truck-trailer systems also lie in the above frequency range (first natural frequency of the truck may likely be in the range 3-5 *Hz*), more dynamic effects due to vehicle-bridge interaction were observed. The SAVA implementation is complete but not included in standard bridge design practice probably due to concerns that the SAVA is an external attachment to the bridge.

The patented work is now owned by the firm *Scrub Oak Technologies Inc.*, Norman, Oklahoma.

Baldwin and *DeBrunner* along with their coworkers [2005, 85], continued the research initiatives of *Patten* et al. [1999, 79] but later shifted their focus from stiffness regulation of bridge structures to developing an intelligent vehicle bridge system (IVBS). The IVBS consists of two main functional modules, namely, the intelligent bridge system (IBS) and smart shock absorbers (SSA). The IBS enables continuous monitoring of the vibration response and integrity (health status) of the bridge structure remotely to a central monitoring station. The SSA installed on the vehicle reduces the structural damage imparted to the bridge structures by the intelligent control of dampers in real time.

Thus, the IVBS objectives are twofold in that it is aimed to reduce the vibration response of bridge structures, enhancing their service life, and to improve the riding comfort of passengers by the use of smart shock absorbers to be installed at several locations of the vehicle. This also eliminates the concern of bridge structural design engineers, who don't want to install additional mechanical vibration controller components on bridge structures that interfere with the dynamical response of the bridge structure and that are not recommended in current bridge design practice, i.e., in the AASHTO standard specifications. However, although external vibration controller mechanisms are avoided in the IVBS project, still, some monitoring attachments such as accelerometers and strain gages need to be installed on the bridge structures.

Smart shock absorbers were designed so as to adjust their stiffness according to the vibration response of the bridge structure (data supplied remotely from the bridge) during their traverse over the bridge. They use a definite scheme of damper properties at other times, i.e., during their traverse over roads before and after passing the bridge. The IVBS project is progressing toward the final phase of testing and validation of the IBS and SSA.

This thesis is limited to the application of numerical methods to analyze the dynamic response of idealized bridge structures under moving loads using simple models. The following sections serve as a brief introductory text to the *Differential Quadrature Method* (DQM), and also summarize the organization of this thesis.

1.5 Introduction to Differential Quadrature Method (DQM):

The *Differential Quadrature Method* (DQM) was introduced by *Bellman* and *Casti* [87] in the early 1970s as a numerical technique to approximate the partial derivatives of a function in terms of function values. The DQM is primarily used to solve initial and/or boundary value problems encountered in several engineering topics. *Bert* and *Malik* [88] published a review article on the DQ method, demonstrated its capabilities through a variety of sample problems and discussed the contributions of several researchers to this method since its introduction (in 1971) through 1996. Probably the only monograph available to date on this special technique is due to *Shu* [89] which also discusses the historical developments of the method with some demonstrations on the application of the method to solve different problems. A brief literature survey on the DQM is included

in the next chapter to outline the development and application of DQM over the last 35 years.

The DQM numerically approximates the partial derivative of a function with respect to a space (or time) variable at a given discrete point as a weighted linear sum of function values at all discrete points in the domain of that variable. Mathematically, this can be explained [88] as follows: -

"If $\psi(x, y)$ is a function defined using space variables (x, y) such that $0 \le x \le a$, $0 \le y \le b$, and let the domain be divided into N_x and N_y points along x and y, respectively, then a r^{th}-order x-partial derivative of the function $\psi(x, y)$ at a point $x = x_i$ along any line $y = y_j$ parallel to the x-axis may be written as

$$\left.\frac{\partial^r \psi}{\partial x^r}\right|_{x=x_i} = \sum_{k=1}^{N_x} A_{ik}^{(r)} \psi_{kj} \text{ , for i = 1, 2, 3, …, } N_x \tag{1.9}$$

and a s^{th} order y-partial derivative at a discrete point $y = y_j$ along any line $x = x_i$ parallel to the y-axis may be written as

$$\left.\frac{\partial^s \psi}{\partial y^s}\right|_{y=y_j} = \sum_{l=1}^{N_y} B_{jl}^{(s)} \psi_{il} \text{ , for j = 1, 2, 3, …, } N_y \tag{1.10}$$

where $A_{ik}^{(r)}$ and $B_{jl}^{(s)}$ are the respective weighting coefficients, and $\psi_{ij} = \psi(x_i, y_j)$". (The above definition is a quote from *Bert and Malik* [88])

The principal attractive features of the DQM are its simple procedure and straightforward implementation in any solver, solution accuracy versus grid density (or number of nodes used in 1D), ability to represent mixed derivatives, flexibility to use different test functions, one time determination of weighting coefficients, etc. Some of the disadvantages include its limited applications to simple geometries such as beams and plates, and restrictions on the choice of nodal points.

This study applies DQM to solve the transient dynamic problem involving beams and plates subjected to moving loads and masses, and *Mathematica 5.2/6.0,* is used to implement the DQM procedure. The implementation procedure involves choosing test functions, determining weighting coefficients, and converting the existing governing differential equations, boundary and initial conditions into linear algebraic equations that can be solved by any standard method such as the *Gauss-Seidel* method.

1.6 Moving load analysis using DQM – Scope of present study:

In the past, the DQM has been primarily used to solve either initial value or boundary value problems. *Wu* et al. [90] applied DQM to solve the forced vibration of an *Euler-Bernoulli* beam, an initial boundary value problem with the forcing function sinusoidal in time. This thesis study followed their work and applied the DQM to solve moving load problems. The methodology was also extended to study vehicle-bridge interactions (VBI) phenomenon.

One of the difficulties associated with the moving load problem is that the forcing function varies in space and time. The versatility of the DQM to simultaneously express spatial and temporal derivatives in a partial differential equation (PDE) is utilized to solve moving load problems without much difficulty. On the other hand, the application of finite element method involves the use of time integration methods such as Newmark's or *Houbolt's* scheme in addition to spatial interpolation functions to solve for moving load problems. Since the FEM has emerged as a well established procedure to analyze irregular/complex geometries, it seems to offer various attractive features like graphical interface and matrix reduction techniques. All these features can also be integrated into DQM to obtain a similar package as FEM is, and some of the foundation works were seen in the *Generalized* and *Extended Differential Quadrature Element Methods* (GDQEM and EDQEM).

In a moving force model, the forcing function is assumed to be a constant force representative of the weight of the moving load, and any contribution to the forcing function due to inertia effects of the moving load is neglected. However in a moving mass representation, the contribution of inertia effects to the forcing function is included, and a solution to such a problem requires the use of an iterative method. A first approximate displacement solution is obtained with a moving force model which is then used to compute the contribution of inertia terms to the moving mass system, and the resultant system with the updated forcing function is solved further to improve the previous solution. This process is iterated until the solution converges.

The vehicular interactions in the vibration of bridge structures are studied in a similar manner. In this case, the vibration responses of the bridge structure and the vehicles are coupled, and a moving oscillator model is used to study the VBI. The moving oscillator consists of a sprung mass (representing the vehicle chassis load), and an unsprung mass (representing the wheel and axle load) which are connected via spring and dashpot system. The displacement solution for moving force problem is obtained neglecting the inertia effects of both the masses, and is substituted in the governing equation of sprung mass to compute the vertical displacement of the sprung mass. Again the above system of equations is iterated until the solution converges.

The DQM can be applied either directly to express the spatial and temporal derivatives together, or after separating the spatial terms from temporal terms (assumed or generalized mode decomposition principle). The latter method is very effective and reduces the overall computational time involved. The *Lagrange* and *Spline* interpolating polynomials can be used for spatial domain, and *Lagrange*, *Spline*, and *Hermite-Fejér* interpolating polynomials can be used for temporal domain.

The scope of present study is limited to simple beam and plate structures representative of fundamental bridge structures. Thus several design parameters of an actual bridge structure are left out, and only those vital parameters such as span length, cross-section area, density, etc are taken into account. The effect of multiple moving loads is addressed with a two point load system, and then extended to a two axle load system.

A simple *Euler-Bernoulli* beam model is used to represent 1D beam structures. A *Kirchhoff-Love* model representing a uniform isotropic rectangular plate structure is used to study the dynamic behavior of 2D structures subjected to moving loads. The effect of concentrated moving load is approximated using Fourier sine series representation. The use of approximate series representation for a concentrated load eliminates the need for application of external time integration (direct integration) methods such as *Newmark* method.

1.7 Overview of dissertation manuscript:

Since this thesis focuses on the application of DQM to solve moving load problems, a brief introduction to the DQM with a sample application of the DQM to solve free vibration problems in beams and plates is provided in the second chapter. In the third chapter, moving force and moving mass models for beam geometries are discussed with a point force and a point mass, respectively. The fourth chapter extends the moving constant point force analysis to study the moving two point load scenario. The vehicle bridge interaction (VBI) effects using a moving single oscillator model is presented in the fifth chapter which is then extended in the sixth chapter to study the two axle moving load oscillator system. The last chapter covers the application of DQM to solve moving point force problems in 2D structures using *Kirchhoff-Love* plate model.

Chapter 2: Differential Quadrature Method

2.1 Introduction:

The Differential Quadrature Method (DQM) is used to numerically approximate a partial derivative of a function at any point in a domain with a weighted linear sum of function values at all points in the respective domain. If $\psi(x, y)$ is the function distributed in *x*-*y* domain and the whole domain is discretized into $M \times N$ grids, i.e., with *M* points along *x*-axis and *N* points along *y*-axis, then the function's r^{th} order *x*-partial derivative value at a point $x = x_i$ along any line $y = y_j$ parallel to *x*-axis is written in DQ form as,

$$\left.\frac{\partial^r \psi}{\partial x^r}\right|_{x_i, y_j} = \sum_{k=1}^{M} A_{ik}^{(x,r)} \psi_{kj} \tag{2.1}$$

where ψ_{ij} represents $\psi(x_i, y_j)$, $A_{ik}^{(x,r)}$ is the *x*-axis weighting coefficient at $x = x_k$ for the r^{th} order. For simplicity, while specifying the weighting coefficients, only the variable of differentiation is denoted in the superscript, and the order is identified by alphabetical manner, i.e., *A, B, C, D* represents 1^{st}, 2^{nd}, 3^{rd}, and 4^{th} order coefficients, respectively. The weighting coefficients are computed usually by assuming generic polynomials or *Lagrange* polynomials as test functions.

Since the introduction of DQM, a high volume of research papers were published, and the following survey on DQM briefs here only a selected few important developments in the DQ technique in chronological order.

2.2 A brief literature survey on DQM:

The concept of differential quadrature method appeared in the form of exercise problems in a text book by *Hamming* [86]. The credit for extending this text book example into a standard methodology goes to *Bellman and Casti* [87] who in 1971 proposed the differential quadrature method to solve initial value problems. They discussed differential quadrature as an alternative to long term integration for providing 1) numerical stability against accumulation of error at each time steps, 2) number of time steps required for acceptable solution accuracy, and 3) reasonably accurate solution at fewer grid points as opposed to highly accurate determination of the entire set of values in the function domain.

In 1972, *Bellman et al.* [91] demonstrated the applicability of differential quadrature method in solving partial differential equations governing fluid flow and turbulence criterion, and were able to obtain high accuracy in lieu of fewer grid points used. The grid points used in this study corresponded to zeros of shifted *Legendre* polynomials.

In 1977, *Mingle* [92] studied nonlinear transient heat conduction phenomenon in one dimension using differential quadrature, and presented an efficient method to treat the boundary conditions, according to which, the governing equation is applied to all the inner grid points leaving out the end points of the domain exclusively to represent boundary conditions. The differential analogs of boundary conditions are written in a similar manner as that of governing equation, and both the governing and boundary conditions are assembled together for the whole domain.

In the next few years, *Civan* [93], and *Civan* with *Sliepcevich* [94] extended the application of differential quadrature to transport phenomena problems. They generalized the DQM to consider initial boundary value and boundary value problems defined in three dimensions, and successfully applied DQM to solve three dimensional transient and steady state problems. They also utilized the concept of domain decomposition to add flexibility in the application of differential quadrature to split large domains (that would require higher number of grid points and hence computational resources) into smaller sub-domains for computational efficiency. Also it is worth mentioning here that *Civan* [] later developed a novel technique called Differential Cubature Method (DCM) intended for three-dimensional analyses.

In the year 1987, *Jang* [95] contributed structural mechanics studies with his successful implementation of DQM in static analysis of structural components. *Jang* et al. [96] demonstrated the application of DQM to solve free vibration of structural components, and bending of beams and plates. In their work, they used classic power polynomial test functions and derived weighting coefficients for 1^{st}, 2^{nd}, 3^{rd}, and 4^{th} derivatives using 3, 4 and 5 equally spaced nodal points. They defined grid points very close to end points of the grid to handle multiple boundary value problems. For example, in case of a beam under bending which is a fourth order boundary value problem requiring two boundary conditions to be satisfied at each end. This method of implementation of multiple boundary conditions by introducing fictitious grid points near the ends is referred as δ-technique.

In 1989, *Quan and Chang* [97, 98] showed that the general collocation method [*Finlayson* 1972 review] and differential quadrature method are equivalent procedures. In their work, they also derived explicit formulae for weighting coefficients considering *Lagrange* and *Jacobi* polynomial test functions. They also indicated the computational comfort achieved when the grid points are symmetrically distributed (for symmetric analyses). However one of the advantages of explicit formulae for weighting coefficients is that there is no restriction whatsoever on the distribution of grid points. Their work demonstrated the advantages of using explicit formulae for determining DQ weighting coefficients over the inversion of *Vandermonde* matrices which was widely followed then.

It should be noted that the *Vandermonde* matrix becomes ill-conditioned and leads to erroneous determination of weighting coefficients when the number of grid points is increased beyond a certain number. The problem can be alleviated if a special algorithm is used to invert the *Vandermonde* matrices, and one such algorithm by *Björck and Pereyra* [99] is cited in the review paper by *Bert and Malik* [88] who argued that the use of algorithm produced weighting coefficients as good as other procedures.

In 1992, *Shu and Richards* [100] published similar procedure of determining explicit formulae for weighting coefficients, and in that they derived weighting coefficients of higher order coefficients using a recurrence relationship, and introduced the method as Generalized Differential Quadrature Method (GDQM). It is worth to note that *Quan and Chang* [97, 98] has already expressed a recurrence relationship for 2^{nd} order weighting

coefficients in terms of the 1st order weighting coefficients. *Shu and Richards* also claimed that the DQM is equivalent to the highest order Finite Difference Method (FDM) which is verified to be true. However DQM is now recognized as a unique method for its simplified methodology and easiness in software implementation of the scheme.

In 1994, *Striz et al.* [101] applied domain decomposition principle and solved truss and frame problems using DQM, and called the procedure Quadrature Element Method (QEM). *Wang et al.* [102] and *Bert and Malik* [103] modified the weighting coefficient matrices to implement part of the boundary conditions in a multiple boundary problem, and reported improved solution accuracy for specific beam and plate problems. In 1996, *Bert and Malik* [88] reviewed the historical and technical aspects of DQM, and discussed the advantages and limitations of DQM as a numerical approximation technique.

In the years 1996 and 1997, *Wang et al.* [104] and *Wang and Gu* [105] defined additional degrees of freedom to end points for tackling multiple boundary conditions. *Wang et al.* [] called this technique, the Differential Quadrature Element Method (DQEM) as it is an extended version of QEM.

In 1999, *Chang-New Chen* [106] introduced *Extended Differential Quadrature* (EDQ) method that allows to define partial derivatives of function at discrete points which can be different from nodes i.e. approximation of function derivatives is possible at any point as a weighted linear sum of function values at all nodes. He also applied EDQ based GDQ to add flexibility in treating boundary conditions at element interfaces.

Chang-New Chen [107] and *Wu and Liu* [108] independently proposed an improved version of DQM and named it Generalized Differential Quadrature (GDQ) and Generalized Differential Quadrature Rule (GDQR), respectively. The essence of the GDQ and GDQR is derived from the concept of DQEM i.e. inclusion of additional degrees of freedom. Thus according to GDQ(R), partial derivatives of a function at any point is written as a weighted linear sum of the values of function and/or its possible derivatives at all nodes in that domain. The main difference between the DQEM and the GDQR is that the GDQR is applicable to any higher order of differential equations while the DQEM is developed mainly to solve a fourth order differential equation (which has two boundary conditions at each end points) i.e. if an higher ($> 4^{th}$) order differential equation require satisfying more than two boundary conditions at a point.

In 2000, *Chen et al.* [109] introduced DQ scheme built on a *Galerkin* weak formulation that increased the convergence rate with only a few grid points, and also discussed the influence of collocation points on the solution accuracy.

In 2002-03, *Wu et al.* [110] and *Shu et al.* [111] independently showed that DQM can be employed to spatial and temporal domains simultaneously. *Shu et al.* [111] used the *Lagrange* interpolation scheme for determining weighting coefficients, and called the method, 'Block marching technique' since solution is obtained progressively from the initial conditions. *Wu et al.* [110] showed that GDQR can be applied to define both the spatial and temporal derivatives simultaneously, and demonstrated the application by solving forced vibration of *Euler* and *Timoshenko* beam which is a fourth order in space

and second order in time domain initial boundary value problem. They used *Hermite-Fejér* interpolation functions to interpolate the deflection function of beam in spatial and temporal dimensions. Their work fascinated the authors of this paper to explore the application of DQM to solve for moving load problems. Before *Shu et al.* [111] and *Wu et al.* [110], the methodology to tackle space-time differential equations was to reduce them to one variable (time) using DQM and apply time step integration methods [Newmark] on the resultant equation to solve for the system.

Karami and Malekzadeh [112] combined the principles of DQEM and GDQ in their built-in method and devised a DQ scheme incorporating boundary conditions. They considered the displacements as the only DOF within the spatial domain (excluding the boundaries), and added additional degrees of freedom specifically second derivatives of displacement as independent variables along the boundaries.

2.3 Methodology of DQM:

The application of DQM to solve any differential equation requires predetermination of weighting coefficients and appropriate treatment of boundary and initial conditions. Further the determination of weighting coefficients depends on the choice of test functions. The DQM can be classified into several categories based on the type of test functions/interpolation polynomials are used for finding weighting coefficients, how the solution variable is expressed – use of function values (Classic DQM) or both the function values and its differentials (Generalized DQM), how the boundary or initial conditions are applied, and choice of grid points (equally or unequally spaced grid

points). *Shu and Richards* [100] pre-pended the term “Generalized” to DQM to differentiate their approach of using different test functions. Later the term “Generalized” also stood for defining additional degrees of freedom and to accommodate a variety of boundary conditions (e.g. GDQEM and GDQR) otherwise difficult through traditional practices. In the following sub-sections, the power polynomial and *Legendre* polynomial test functions are included as classic DQM, and the *Lagrange* and *Hermite* interpolation type polynomials are listed as generalized DQM.

2.3.1 Choice of test functions and Classic DQM:

The test functions for computing DQ weighting coefficients should comply with the completeness requirement [88] as per which the chosen test functions should be differentiable up to the highest order of differential equation to be solved.

These test functions are used to interpolate the function values in the grid domain, and a popular choice is a power polynomial. *Bellman et al.* [91] used monomial basis polynomials and *Legendre* polynomials as test functions in DQM. In the latter case i.e. the *Legendre* polynomial test functions, grid points are roots of shifted N^{th} order *Legendre* polynomials, and once N is chosen, the distribution of grid points is fixed. The former case i.e. monomial basis power polynomial offers some flexibility in the distribution of grid points, and the procedure for determining the weighting coefficients is discussed here briefly for monomial basis polynomial test functions. The minimum number of grid points (nodes) in any variable coordinate direction is one plus the highest

order of derivative of function with respect to that variable appearing in the differential equation.

For example, assume that the differential equation to be solved contains differentials of $F(\xi)$ with respect to normalized space variable ξ. In this case, a test function $F(\xi) = \xi^{\gamma-1}$ is chosen such that $\gamma = 1, 2, 3, ..., M$ where M is the number of grid points along ξ-axis. If there are three grid points in the domain i.e. $M = 3$, then we have monomials of polynomial, $F(\xi) = \{1, \xi, \xi^2\}$. The 1st and 2nd order derivatives of $F(\xi)$ are approximated as,

$$\left.\frac{dF}{d\xi}\right|_{\xi_i} = \sum_{k=1}^{M} A_{ik}^{(\xi,1)} F(\xi_k) = \frac{d}{d\xi}(\xi^{\gamma-1})\Big|_{\xi_i} = (\gamma-1)\xi_i^{\gamma-2} \tag{2.2}$$

$$\left.\frac{d^2F}{d\xi^2}\right|_{\xi_i} = \sum_{k=1}^{M} B_{ik}^{(\xi,2)} F(\xi_k) = \frac{d^2}{d\xi^2}(\xi^{\gamma-1})\Big|_{\xi_i} = (\gamma-1)(\gamma-2)\xi_i^{\gamma-3} \tag{2.3}$$

where $\gamma = 1, 2, \text{and } 3\ (M = 3)$.

The superscripts 1 and 2 in terms $A_{ik}^{(\xi,1)}$ and $B_{ik}^{(\xi,2)}$ denote the 1st and 2nd order differential, respectively. Each of the above equations results in a system of $M \times M$ linear equations with $M \times M$ unknowns in *A* or *B* when supplied with grid point values, and are solved for weighting coefficients, *A* or *B*, respectively. Here the weighting coefficients for 3rd order derivatives are zero since 3rd order differential of $\xi^{\gamma-1}$ is zero. In general, the weighting coefficients of M^{th} and higher order derivatives are zero, and so

the number of grid points (*M*) is chosen to be one plus the highest order of derivative (with respect to grid variable) appearing in the differential equation.

Similarly for a multi-variable function (say, two variable function dependent on space ξ and time τ variables) such that $W(\xi,\tau) = F(\xi)G(\tau)$. For relevance to our application, let us assume that the two variable field function $W(\xi,\tau)$ denotes the lateral deflection of a beam which is the solution to governing differential equation *Equation 2.2* containing partial derivatives with respect to both ξ and τ, and also let $F(\xi) = \xi^{\gamma-1}$ and $G(\tau) = \tau^{\lambda-1}$ be two test functions introduced in spatial and temporal domains, respectively. Then the lateral deflection $W(\xi,\tau)$ is expressed as,

$$W(\xi,\tau) = F(\xi)G(\tau) = \xi^{\gamma-1}\tau^{\lambda-1} \tag{2.4}$$

where $\gamma = 1,2,3...,M$ and $\lambda = 1,2,3...,N$.

The DQ analogs of spatial and temporal second derivatives of the function are given by,

$$\left.\frac{\partial^2 W}{\partial \xi^2}\right|_{\xi=\xi_i} = \sum_{k=1}^{M} B_{ik}^{(\xi)} W_{kj} = (\gamma-1)(\gamma-2)\xi_i^{\gamma-3}\tau_j^{\lambda-1} \tag{2.5}$$

$$\left.\frac{\partial^2 W}{\partial \tau^2}\right|_{\tau=\tau_j} = \sum_{k=1}^{N} B_{jk}^{(\tau)} W_{ik} = (\lambda-1)(\lambda-2)\xi_i^{\gamma-1}\tau_j^{\lambda-3} \tag{2.6}$$

where $W_{ij} \equiv W(\xi_i,\tau_j)$.

Since these weighting coefficients are determined from normalized variables, they can be used for any system parameters. However the weighting coefficients are solely dependent on the number and distribution of node points, and hence should be used appropriately i.e. coefficients determined from equal interval node points should be used only for equally spaced distribution. The set of linear equations resulting from *Equations 2.5* and *2.6* forms *Vandermonde* equations. The *Vandermonde* equations become ill-conditioned for dense grid, and the accuracy of solution is highly dependent on the number of grid points and type of solvers used to handle these *Vandermonde* matrices (authors of [*88*] reported accurate solutions when *Bjorck-Pereyra* [99] algorithm is used).

2.3.2 Lagrange and Hermite interpolation polynomials and GDQM:

The *Lagrange* polynomial based interpolation shape (or test) function is given by

$$l_j(\xi) = \frac{\phi(\xi)}{(\xi - \xi_j)\phi^{(1)}(\xi_j)}; \qquad j = 1, 2, ..., M \tag{2.7}$$

where $\phi(\xi) = \prod_{k=1}^{M} (\xi - \xi_k)$ and $\phi^{(1)}(\xi_j) = \left.\frac{d\phi(\xi)}{d\xi}\right|_{\xi=\xi_j} = \prod_{\substack{k=1; \\ k\neq j}}^{M} (\xi_j - \xi_k)$.

The *Lagrange* polynomial test function is characterized by an identity matrix because

$$l_j(V_i) = \begin{cases} 1 & \text{if } i = j \\ 0 & \text{otherwise} \end{cases} \tag{2.8}$$

where V stands for spatial (ξ) or temporal (τ) field variables. The field function $W(\xi,\tau)$ is expressed as a double summation of *Lagrange* interpolation polynomial operating on function values available at grid points.

$$W(\xi_i,\tau_j)=\sum_{q=1}^{N} l_q(\tau_j)\sum_{p=1}^{M} l_p(\xi_i)W_{pq} \tag{2.9}$$

Since the *Lagrange* polynomial function of space and time domain shown above are independent of each other, the above relation can also be written as

$$W(\xi_i,\tau_j)=\sum_{q=1}^{N}\sum_{p=1}^{M} l_q(\tau_j)l_p(\xi_i)W_{pq} \tag{2.10}$$

The weighting coefficients for higher order derivatives are then obtained from the recursive formulae [97 and 100] given by,

$$a_{ij}^{(1)}=l_j^{(1)}(\xi_i)=\frac{\phi^{(1)}(\xi_i)}{(\xi_i-\xi_j)\phi^{(1)}(\xi_j)}; \qquad i,j=1,2,...,M;\ \ i\neq j \tag{2.11}$$

$$a_{ij}^{(r)}=l_j^{(r)}(\xi_i)=r(a_{ii}^{(r-1)}\,a_{ij}^{(1)}-\frac{a_{ij}^{(r-1)}}{(\xi_i-\xi_j)}); \qquad i,j=1,2,...,M;\ \ i\neq j;\ \ r\geq 2 \tag{2.12}$$

$$a_{ii}^{(r)}=l_i^{(r)}(\xi_i)=-\sum_{\substack{j=1;\\ j\neq i}}^{M} a_{ij}^{(r)}; \qquad i=1,2,...,M;\ r\geq 1 \tag{2.13}$$

Because the above is a recursive relation involving weighting coefficients, small lettered alphabet a is used here to avoid any confusion over the order of weighting coefficients i.e. $a_{ij}^{(1)} = A_{ij}, a_{ij}^{(2)} = B_{ij}$ and so on. Since the use of *Legendre* polynomials restricted the distribution of grid points, and power polynomials resulted in ill-conditioned *Vandermonde* matrices for increased grid points, *Shu and Richards* [100] proposed the use of *Lagrange* polynomials as generalized DQM as it addressed these limitations. The above weighting coefficients based on the Lagrange interpolation polynomials can be used for both the spatial and temporal domains, and such an application is demonstrated by *Shu et al.* [111] with their block marching technique.

Another version of generalized DQM called the GDQR, proposed by *Wu and Liu* [113], uses *Hermite-Fejér* interpolation polynomials for finding weighting coefficients. The GDQR considers both the function values and their appropriate derivatives (of possible lowest order) as independent variables. According to this method, each nodal point is associated with its function values and derivatives up to one less than the number of equations defined on that point. This approach handles the multiple boundary conditions or multiple initial conditions or both. *Wu et al.* [110] applied this approach to both the spatial and temporal domains.

For example, if we consider a two variable field function $W(\xi, \tau)$, and assuming second order initial value problem having two equations (initial conditions) associated with the start point, i.e., $n_1 = 2$ for τ_1, and one equation (governing equation of motion) associated with the inner nodal points and the end point, i.e., $n_k = 1$ for all $\tau_k, k = 2, 3, ..., N$. Hence

the independent variables associated with the start point are function values and their first derivatives (of time), i.e. W_{j1} and $W_{j1}^{'}$; $j = 1, 2, ..., M$ and the independent variables associated with the rest of the domain are function values themselves, i.e., W_{jk}; $k = 2, 3, ..., N$.

Now two different schemes are possible namely, 1) *Lagrange* interpolation in spatial, and *Hermite-Fejér* interpolation in temporal domain, and 2) *Hermite-Fejér* in spatial and temporal domains. In the first case, the field function $W(\xi, \tau)$ is given by,

$$W(\xi, \tau) = \sum_{k=1}^{N} \sum_{j=1}^{M} p_{k0}(\tau) l_j(\xi) W_{jk} + \sum_{j=1}^{M} l_j(\xi) p_{11}(\tau) W_{j1}^{'} \tag{2.14}$$

Here $W_{j1}^{'} = T \left. \frac{\partial W}{\partial t} \right|_{t=t_1} = \left. \frac{\partial W}{\partial \tau} \right|_{\xi_j, \tau_1}$ where T is the time factor used to normalize time variable noting that if the normalized variable is expressed as the ratio $\tau = t/T$ where t is the un-scaled or actual time, then $\partial(.)/\partial\tau = T\,\partial(.)/\partial t$. The *Hermite-Fejér* shape functions, $p_{k0}(\tau)$ and $p_{11}(\tau)$, are derived assuming a linear function on time, i.e., $p_k(\tau) = (m\tau + c) l_k(\tau)$ where $l_k(\tau)$ is the *Lagrange* interpolation polynomial, m and c are constants found using the relations,

$$p_{k0}(\tau_k) = 1; \quad p_{k0}^{(1)}(\tau_j) = 0; \quad p_{k0}(\tau_j) = 0; \quad p_{11}(\tau_j) = 0; \quad p_{11}^{(1)}(\tau_1) = 1;$$

with $k = 1, 2, ..., N; \quad j = 1, 2, ..., N; \quad j \neq k$

The *Hermite-Fejér* shape functions satisfying the above properties are then given by,

$$p_{10}(\tau) = \{1 + (\tau_1 - \tau) l_1^{(1)}(\tau_1)\} l_1(\tau) \tag{2.15}$$

$$p_{k0}(\tau) = \frac{\tau - \tau_1}{\tau_k - \tau_1} l_k(\tau); \qquad k = 2, 3, ..., N \tag{2.16}$$

$$p_{11}(\tau) = (\tau - \tau_1) l_1(\tau) \tag{2.17}$$

The differential operation is directly applied to the interpolation function based on the respective variable of differentiation to yield appropriate derivatives of field function. For example, the second derivative of $W(\xi, \tau)$ w.r.t ξ is given by

$$\frac{\partial^2 W}{\partial \xi^2} = \sum_{k=1}^{N} \sum_{j=1}^{M} p_{k0}(\tau) l_j^{(2)}(\xi) W_{jk} + \sum_{j=1}^{M} l_j^{(2)}(\xi) p_{11}(\tau) W_{j1}^{'} \tag{2.18}$$

Since *Lagrange* interpolation is used for spatial domain, the weighting coefficients of r-th order spatial derivatives are given by $l_j^{(r)}(\xi_i)$ whose explicit formulae are shown in Eq. 16 and 17. The weighting coefficients of r-th order temporal derivatives are obtained in the same manner as [108], and are given by $p_k^{(r)}(\tau_j);\ k = 0, 1, 2, ..., N$, where $p_0(\tau) \equiv p_{11}(\tau)$ and $p_k(\tau) \equiv p_{k0}(\tau)$. For example, if $p_k(\tau) = (a\tau + b) l_k(\tau)$, then $p_k^{(r)}(\tau) = (a\tau + b) l_k^{(r)}(\tau) + ra l_k^{(r-1)}(\tau)$.

Similarly in an initial boundary value problem (second order in time and fourth order in space), we have 2 equations (boundary conditions) at each ends of spatial domain, and 2

equations at the start point (initial conditions) of temporal domain, and using *Hermite-Fejér* interpolation polynomial, the field function is given by,

$$W(\xi,\tau) = \sum_{k=1}^{N}\sum_{j=1}^{M} p_{k0}(\tau)h_{j0}(\xi)W_{jk} + \sum_{j=1}^{M} l_j(\xi)p_{11}(\tau)\left.\frac{\partial W}{\partial \tau}\right|_{\xi,\tau_1} + \sum_{k=1}^{N} l_k(\tau)\{h_{11}(\xi)\left.\frac{\partial W}{\partial \xi}\right|_{\xi_1,\tau} + h_{M1}(\xi)\left.\frac{\partial W}{\partial \xi}\right|_{\xi_1,\tau}\} \tag{2.19}$$

The *Hermite-Fejér* shape functions for spatial domain, $h_{j0}(\xi)$, $h_{11}(\xi)$ and $h_{M1}(\xi)$, are defined on the same basis as those for temporal domain.

2.3.3 Treatment of boundary conditions:

Another crucial step in the application of DQM to structural mechanics problems is the implementation of various boundary conditions. A variety of new concepts in handling boundary and initial conditions have been introduced ever since the introduction of DQM to structural mechanics applications, and these approaches were comprehensively reviewed by *Wang et al.* [114] very recently. The boundary conditions for GDQM based solution procedures are easily implemented because of the introduction of additional degrees of freedom.

In the δ-technique, a dummy grid point is chosen very near a boundary point for enforcing multiple boundary conditions at a point. In an initial boundary value problem (of fourth order in spatial and second order in temporal distribution), two dummy points one each at each boundary point in spatial domain, and one dummy point near the start

point in temporal domain are inserted. Thus in a normalized spatial distribution of $\{\xi_1, \xi_2, \xi_3, ..., \xi_{M-2}, \xi_{M-1}, \xi_M\}$ where $\xi_1 = 0$ and $\xi_M = 1$, the points are chosen such that $\xi_2 = \delta$ and $\xi_{M-1} = 1 - \delta$ where δ is a very small positive number close to zero.

In the replaced equations approach, we simply replace the DQ analogs of governing differential equations at and closest boundary points with the DQ analogs of boundary conditions. This is the easiest yet effective method of implementation of boundary conditions in case of classic DQ test functions.

In case of GDQR or DQEM, the additional degrees of freedom are introduced and hence the number of weighting coefficients is increased by the number of additional degrees of freedom i.e. for M grid points in a variable domain, and considering two boundary conditions at two end points, the weighting coefficient matrix is of order $M \times (M + 2)$. The DQ analogs are written from governing equation from all the points except the end points where the multiple degrees of freedom defined. The DQ analogs of boundary conditions at those end points are also written, and the resultant system of equation is solved.

2.4 Application of DQM to free vibration problems:

This section briefly covers the aspects involved in the application of DQM to solve free vibration problems. In the first case, the bridge is modeled as an *Euler* beam with uniform cross-section, and in the second case the bridge is modeled as an isotropic *Kirchhoff* plate. The modal properties of bridge (natural frequencies and mode shapes)

obtained from free vibration analysis are helpful in assessing the structures response when subjected to general forcing conditions. Hence a free vibration analysis is carried out early in the bridge dynamic analysis to determine the possibility of resonance phenomenon due to matching bridge and vehicle frequencies.

2.4.1 Free vibration of simply supported *Bernoulli-Euler* beams:

The equations of motion governing undamped and damped free vibration of *Euler* beams are given by,

$$\mu \frac{\partial^2 \overline{W}}{\partial t^2} + EI \frac{\partial^4 \overline{W}}{\partial x^4} = 0 \tag{2.20}$$

$$\mu \frac{\partial^2 \overline{W}}{\partial t^2} + 2\mu\omega_b \frac{\partial \overline{W}}{\partial t} + EI \frac{\partial^4 \overline{W}}{\partial x^4} = 0 \tag{2.21}$$

where $\mu, E, I,$ and ω_b are the mass per unit length (linear density), *Young's* modulus, area moment of inertia, and circular frequency of damping for the beam, respectively and $\overline{W}$ is the vertical displacement of the beam. The beam is assumed to be simply supported at both the ends, and the respective boundary conditions are then given by,

$$\overline{W}(0,t) = \overline{W}(L,t) = 0 \tag{2.22}$$

$$\left.\frac{\partial^2 \overline{W}(x,t)}{\partial x^2}\right|_{x=0} = \left.\frac{\partial^2 \overline{W}(x,t)}{\partial x^2}\right|_{x=L} = 0 \tag{2.23}$$

where L is the length of beam. The initial conditions are given by $\overline{W}(x,0) = \left.\frac{\partial \overline{W}}{\partial t}\right|_{t=0} = 0.$

The following properties are assumed for demonstrating the application of DQM for solving this free vibration problem.

Length of beam (L) = 25 m, (984.25 in or 82 ft)

Linear density of the beam (μ) = 2303 kg/m, (129 lb/in)

Elasticity modulus of the beam (E) = 2.87 x 10^9 N/m^2, (416.26 ksi)

Area moment of Inertia of the beam (I) = $bh^3/12$ = 2.9 m^4, (6967222 in^4)

The lateral deflection $\overline{W}(x,t)$, if assumed to be of the form $\overline{W}(x,t) = \overline{w}(x)T(t)$ or its equivalent normalized form $W(\xi,t) = w(\xi)T(t)$, where $T(t)$ is harmonic in time such as $Sin\,\omega t$ or $Cos\,\omega t$, reduces the governing equation to

$$-\mu\omega^2 w(\xi) + \frac{EI}{L^4}\frac{d^4 w(\xi)}{d\xi^4} = 0 \tag{2.24}$$

where $\xi = x/L$ is the normalized spatial coordinate, $w(\xi)$ or simply w is the normalized mode shape and ω is the natural frequency of vibrating beam. The DQ analog for the above equation is then given by,

$$-\mu\omega^2 w_i + \frac{EI}{L^4}\sum_{k=1}^{M} D_{ik} w_k = 0 \tag{2.25}$$

Thus the spatial and temporal terms are decoupled in the case of undamped free vibration. Since the above formulation is free of temporal terms, only boundary conditions are needed in addition to governing equation of motion.

If the *x*-domain is discretized into *M* nodes, the boundary conditions are applied at the boundary nodes $\xi_i = 0$ and 1 corresponding to $i = 1$ and M, respectively, and the respective DQ analogs are written as,

$$w_i = 0 \quad \text{and} \quad \sum_{k=1}^{M} B_{ik} w_k = 0, \qquad i = 1 \tag{2.26}$$

$$w_i = 0 \quad \text{and} \quad \sum_{k=1}^{M} B_{ik} w_k = 0, \qquad i = M \tag{2.27}$$

The governing equations at the boundary points were trimmed to accommodate the boundary DQ analogs i.e.

$$-\mu\omega^2 w_i + \frac{EI}{L^4} \sum_{k=1}^{M} D_{ik} w_k = 0, \qquad i = 3, 4, ..., M-2 \tag{2.28}$$

However, the above assumption does not decouple the spatial and temporal terms in case of damped free vibration. In such cases, the lateral deflection is expressed in assumed modes so that the spatial terms are decoupled from the mode coordinates.

The modal frequency of vibration for a simply supported *Euler* beam is given by,

$$\omega_{(j)} = \frac{j^2 \pi^2}{L^2}\sqrt{\frac{E I}{\mu}} \tag{2.29}$$

Table 1.1: First three mode frequencies of SS beam

Frequency mode	Frequency (Analytical solution), in rad/sec	Frequency (DQM), in rad/sec
1	30.0174	30.0174
2	120.072	120.069
3	270.278	270.156

2.4.2 Free vibration of SS-F-SS-F *Kirchhoff-Love* plates:

This section considers the free vibration problem in plates with two opposite edges simply supported and the other pair of opposite edges kept free, in short denoted as *SS-F-SS-F*. The present DQ model used *Karami and Malekzadeh* [112] scheme that applied two boundary conditions on a boundary node to study the free vibration of a *SS-F-SS-F* plate. The lateral deflection of the plate is a function of spatial and temporal variables i.e. $\overline{W} = \overline{W}(X,Y,t)$. The differential equation governing free undamped vibration of an isotropic *Kirchhoff* plate is given by,

$$\mu \frac{\partial^2 \overline{W}(X,Y,t)}{\partial t^2} + D\left[\frac{\partial^4 \overline{W}(X,Y,t)}{\partial X^4} + 2\frac{\partial^4 \overline{W}(X,Y,t)}{\partial X^2 \partial Y^2} + \frac{\partial^4 \overline{W}(X,Y,t)}{\partial Y^4}\right] = 0 \tag{2.30}$$

where $D = Eh^3/12(1-\nu^2)$ is the bending or flexural rigidity of the plate, and $\mu = \rho h$ is the mass per unit area of plate. The above governing equation is decoupled from temporal domain using variable separation and is expressed in normalized form as

$$\frac{-\mu a^4 \omega^2}{D} W(x,y) + \frac{\partial^4 W(x,y)}{\partial x^4} + 2\lambda^2 \frac{\partial^4 W(x,y)}{\partial x^2 \partial y^2} + \lambda^4 \frac{\partial^4 W(x,y)}{\partial y^4} = 0 \qquad (2.31)$$

where $x = X/a$ and $y = Y/b$, $\lambda = a/b$ is the aspect ratio of the plate and ω is its dimensional frequency of vibration.

Karami and Malekzadeh [112] suggested treating the second derivative of displacement κ (factor of bending moment) along the boundary as a DOF in addition to the displacement DOF for implementing various boundary conditions of plate vibration problems. The procedure is similar to that of DQEM or GDQR in that an additional DOF is introduced, however the additional DOF is not a first derivative as in GDQR but rather a second derivative of the deflection function i.e. $\kappa^{(x)} = \frac{\partial^2 W}{\partial x^2}$ and $\kappa^{(y)} = \frac{\partial^2 W}{\partial y^2}$, and it is also essential to note that these κ terms were treated as variables only along the boundary i.e.

$$\kappa_{ij}^{(x)} = \begin{cases} \kappa_{ij}^{(x)} & \text{for boundary grid points} \\ & \text{with } i = 1 \text{ or } M, \text{ and } j = 2,3,...N-1 \\ \dfrac{\partial^2 W}{\partial x^2} = \sum_{p=1}^{M} B_{ip}^{(x)} W_{pj} & \text{for inner domain grid points} \\ & \text{with } i = 2,3,...M-1, \text{ and } j = 2,3,...N-1 \end{cases} \tag{2.32}$$

$$\kappa_{ij}^{(y)} = \begin{cases} \kappa_{ij}^{(y)} & \text{for boundary grid points} \\ & \text{with } j = 1 \text{ or } N, \text{ and } i = 2,3,...M-1 \\ \dfrac{\partial^2 W}{\partial y^2} = \sum_{q=1}^{N} B_{jq}^{(y)} W_{iq} & \text{for inner domain grid points} \\ & \text{with } i = 2,3,...M-1, \text{ and } j = 2,3,...N-1 \end{cases} \tag{2.33}$$

The governing differential equation of motion for the plate in DQ analog is given by,

$$\sum_{m=1}^{M} B_{im}^{(x)} \kappa_{mj}^{(x)} + \lambda^2 \sum_{n=1}^{N} B_{jn}^{(y)} \kappa_{in}^{(x)} + \lambda^4 \sum_{n=1}^{N} B_{jn}^{(y)} \kappa_{in}^{(y)}$$

$$+\lambda^2 \sum_{m=1}^{M} B_{im}^{(x)} \kappa_{mj}^{(y)} - \Omega^2 W(x,y) = 0 \tag{2.34}$$

$$\text{for } \; i = 2,3,...,M-1 \; \text{ and } \; j = 2,3,...,N-1$$

where $\Omega = \omega a^2 \sqrt{\mu / D}$ is the dimensionless frequency. The governing equation is further expanded for κ terms in the inner domain (using *Equations* 2.32 and 2.33) as given below

$$\sum_{m=2}^{M-1}\sum_{n=1}^{M} B_{im}^{(x)} B_{mn}^{(x)} W_{nj} + 2\lambda^2 \sum_{n=1}^{N}\sum_{m=1}^{M} B_{im}^{(x)} B_{jn}^{(y)} W_{mn} + \lambda^4 \sum_{m=2}^{N-1}\sum_{n=1}^{N} B_{jm}^{(y)} B_{mn}^{(y)} W_{in}$$

$$+ B_{i1}^{(x)} \kappa_{1j}^{(x)} + B_{iM}^{(x)} \kappa_{Mj}^{(x)} + \lambda^4 B_{j1}^{(y)} \kappa_{i1}^{(y)} + \lambda^4 B_{jN}^{(y)} \kappa_{iN}^{(y)} - \Omega^2 W_{ij} = 0 \qquad (2.35)$$

$$\text{for } i = 2,3,...,M-1 \text{ and } j = 2,3,...,N-1$$

For the *SS-F-SS-F* boundary condition, 1) the displacements and normal bending moments at the *x*-boundaries are zero, and 2) the normal bending moments and effective shear force resultants at the *y*-boundaries are zero, and thus transform in DQ analog to

$$W_{1j} = \kappa_{1j}^{(x)} = W_{Mj} = \kappa_{Mj}^{(x)} = 0 \qquad \text{for } j = 2,3,...,N-1 \qquad (2.36)$$

$$\lambda^2 \kappa_{i1}^{(y)} + \nu \sum_{m=1}^{M} B_{im}^{(x)} W_{m1} = \lambda^2 \kappa_{iN}^{(y)} + \nu \sum_{m=1}^{M} B_{im}^{(x)} W_{mN} = 0 \qquad (2.37)$$

$$\text{for } i = 1,2,...,M-1$$

$$\lambda^2 \sum_{m=1}^{N} A_{1m}^{(y)} \kappa_{im}^{(y)} + (2-\nu) \sum_{m=1}^{M}\sum_{n=1}^{N} A_{1n}^{(y)} B_{im}^{(x)} W_{mn}$$

$$= \lambda^2 \sum_{m=1}^{N} A_{Nm}^{(y)} \kappa_{im}^{(y)} + (2-\nu) \sum_{m=1}^{M}\sum_{n=1}^{N} A_{Nn}^{(y)} B_{im}^{(x)} W_{mn} = 0 \qquad (2.38)$$

$$\text{for } i = 2,3,...,M-1$$

The above Equation 2.38 is rewritten as,

$$\lambda^2 \sum_{m=2}^{N-1}\sum_{n=1}^{N} A_{1m}^{(y)} B_{mn}^{(y)} W_{in} + (2-\nu)\sum_{m=1}^{M}\sum_{n=1}^{N} A_{1n}^{(y)} B_{im}^{(x)} W_{mn}$$

$$+ \lambda^2 A_{11}^{(y)} \kappa_{i1}^{(y)} + \lambda^2 A_{1N}^{(y)} \kappa_{iN}^{(y)}$$

$$= \lambda^2 \sum_{m=2}^{N-1}\sum_{n=1}^{N} A_{Nm}^{(y)} B_{mn}^{(y)} W_{in} + (2-\nu)\sum_{m=1}^{M}\sum_{n=1}^{N} A_{Nn}^{(y)} B_{im}^{(x)} W_{mn} \tag{2.39}$$

$$+ \lambda^2 A_{N1}^{(y)} \kappa_{i1}^{(y)} + \lambda^2 A_{NN}^{(y)} \kappa_{iN}^{(y)} = 0$$

$$\text{for } i = 2, 3, ..., M-1$$

The above model is in the normalized form, and applies to plates of any configuration of appropriate aspect ratio. The dimensionless fundamental frequency Ω obtained from the present DQ scheme, *Bert and Malik* [103] DQ model, and *Leissa* [115] for different aspect ratios were listed in the *Table* 1.2:

Table 1.2: Natural frequency of the SS-F-SS-F plate from DQM compared with literature results

Model / Literature	Aspect Ratio				
	$\lambda = \frac{2}{5}$	$\lambda = \frac{2}{3}$	$\lambda = 1$	$\lambda = \frac{3}{2}$	$\lambda = \frac{5}{2}$
Present DQ model	9.77007	9.6996	9.63005	9.55622	9.4821
Bert & *Malik*	9.76013	9.69832	9.63138	9.55818	9.48414
Leissa	9.76	9.6983	9.6314	9.5582	9.4841

The first five modes of dimensionless frequencies at different plate aspect ratios were listed in the *Table* 1.3:

Table 1.3: First 5 mode frequencies of a SS-F-SS-F plate for different aspect ratios

Frequency mode	Aspect Ratio				
	$\lambda = \frac{2}{5}$	$\lambda = \frac{2}{3}$	$\lambda = 1$	$\lambda = \frac{3}{2}$	$\lambda = \frac{5}{2}$
1	9.77007	9.6996	9.63005	9.55622	9.4821
2	11.1086	13.0482	16.1913	21.6621	33.6491
3	15.5858	23.6726	37.6451	40.8791	40.4946
4	18.7089	33.881	41.1339	57.3943	78.0328
5	21.5749	41.3356	49.2301	67.1215	88.0572

The present DQ model used 5x5 and 7x7 grid nodes for the spatial domain. The data shown in the Table 1 and 2 were obtained from a grid distribution of 7x7 and were in excellent agreement with the published results of *Bert and Malik* [103] and *Leissa* [115]. However it is also to be noted here that it took abnormal computational time which could probably arise from the efficiency of the algorithm included within *Mathematica* for solving *Eigen* value problems. The nominal time of computation using a 5x5 grid was about 30 seconds while it took an hour for 7x7 grid.

The results also included mode coordinates at each grid point with corresponding aspect ratio which can be used to plot the appropriate mode shapes which is not discussed here. The mode coordinates at grid points were expressed as a fraction of another grid point (and usually a common grid point), and mode coordinate at the common grid point is assumed a value so that a scaled mode coordinate distribution (and thus a mode shape) is obtained.

Chapter 3: Moving Force – Moving Mass Problem in Beams

Introduction:

In this chapter, the dynamic behavior of bridge structures is studied with a simple 1D *Euler-Bernoulli* beam representation using the DQM. The geometric entities of an *Euler-Bernoulli* beam can be suitably modified to approximately represent bridge geometric and modal properties, and this treatment is expected to give us an approximate estimate on the vibration behavior of real bridge structures. This chapter covers the dynamic behavior of beam structures subjected to moving forces and masses, i.e., with and without inertia effects of moving loads, respectively. Although the 'moving force-moving mass' model can successfully be used to predict the dynamic behavior of bridges, this representation ignores any vibrations of vehicle relative to bridge, and hence it is not applicable to vehicle-bridge interactions studies.

The first half of this chapter is focused on the dynamic behavior of an *Euler-Bernoulli* beam subjected to a moving constant point force, and the second half extends to the case of an *Euler-Bernoulli* beam carrying a moving concentrated mass. Analytical solutions obtained from previous researches are used to benchmark the solutions obtained using the DQM. Several parameters influence the dynamic behavior of bridges (beams) under moving vehicles (loads), and the primary candidates among them are speed parameter (α), mass ratio (κ), and damping parameter (β). The effect of these variables on dynamic behavior of bridges is assessed by plotting the dynamic impact factor for different combinations of influence parameters.

3.1 *Euler-Bernoulli* beam subjected to moving constant point force:

The governing equation of motion/bending for an *Euler-Bernoulli* beam subjected to a point load P (refer *Figure 3.1*) moving at a constant speed c is given by

$$\mu \frac{\partial^2 W}{\partial t^2} + 2\mu\omega_b \frac{\partial W}{\partial t} + EI \frac{\partial^4 W}{\partial x^4} = \delta(x - ct)P \tag{3.1}$$

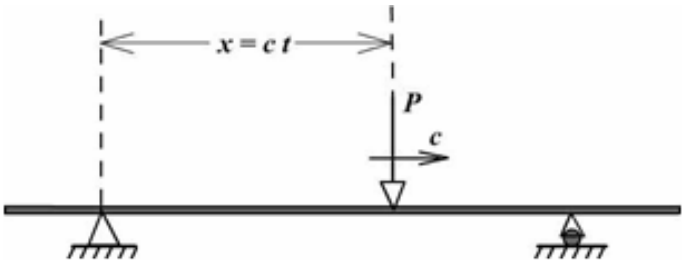

Figure 3.1: Beam subjected to moving constant point force

where W, μ, ω_b, E, and I represent lateral (or vertical) deflection, linear density (mass per unit length), circular frequency of damping, *Young's* modulus and area moment of inertia of the beam, respectively. Here $\delta(\cdot)$ is the *Dirac* delta function; ct denotes the distance traveled by the load in time t. The *Dirac* delta function $\delta(\cdot)$ takes values according to $\delta(x - ct) = \begin{cases} 1 & \text{when } x = ct \\ 0 & \text{elsewhere} \end{cases}$. The above given differential equation falls in the category of fourth order (spatial) hyperbolic partial differential equations.

The beam is assumed to be simply supported at both the ends so that the displacement and bending moment at either ends are zero. Also initially the beam is supposed to be

undeformed, and hence has zero initial vertical displacement and slope (initial vertical velocity). Accordingly, boundary and initial conditions for the beam are given below: -

Boundary conditions:

$$W(0,t) = W(L,t) = 0$$

$$\left.\frac{\partial^2 W(x,t)}{\partial x^2}\right|_{x=0} = \left.\frac{\partial^2 W(x,t)}{\partial x^2}\right|_{x=L} = 0 \tag{3.1A}$$

where L is the length of the beam.

Initial conditions:

$$W(x,0) = \left.\frac{\partial W(x,t)}{\partial t}\right|_{t=0} = 0 \tag{3.1B}$$

The deflection of the beam $W = W(x,t)$ is then determined by solving the governing differential equation, subject to the boundary and initial conditions as shown in Equations 3.1A and 3.1B, respectively. The above set of equations constitutes an initial boundary value problem (or a two point boundary value problem – because of boundary conditions involving two end points) and the displacement solution obtained is called the transient dynamic response of the beam.

3.1.1 Analytical solution for moving force problem:

A free vibration analysis (solution to homogenous differential equation counterpart of Equation 3.1, i.e., with $P = 0$) is carried out to determine the modal parameters of beam prior to solving the forced vibration problem involving moving load, and if we denote

$\omega_{(j)}$ for the j^{th} mode circular natural frequency of vibration of the beam, then we have $\omega_{(j)}^2 = \frac{j^4 \pi^4}{L^4} \frac{EI}{\mu}$. The circular frequency of damped vibration is then given by $\omega'^2_{(j)} = \left| \omega_{(j)}^2 - \omega_b^2 \right|$, where ω_b is the circular frequency of damping of the beam.

Then a 'closed-form' solution in the form of *Fourier* sine series [10] is obtained by *Fourier* integral transformation method for the forced vibration problem with a moving constant point force *P*, i.e., Equation 3.1. The *Fourier* integral transformation method is carried out in a two-fold procedure, first by applying the *Fourier* finite sine integral transformation to the Equation 3.1 followed by the *Laplace-Carson* integral transformation on the resultant equation, and then by applying *Fourier* inverse transformation to obtain the displacement solution.

Two dimensionless parameters – speed parameter (α) and damping parameter (β) – as shown in Equations 3.2 and 3.3 are used to express the analytical solution in a simple form.

$$\alpha = \frac{\omega}{\omega_{(1)}} = \frac{c}{2 f_{(1)} L} = \frac{T_{(1)}}{2T} = \frac{c}{c_{cr}} \tag{3.2}$$

$$\beta = \frac{\omega_b}{\omega_{(1)}} = \frac{\omega_b L^2}{\pi^2} \left(\frac{\mu}{EI} \right)^{1/2} = \frac{\vartheta}{2\pi} \tag{3.3}$$

where $\omega = \pi c / L$ is the frequency of vibration, $f_{(j)}$ is the natural frequency of j^{th} mode, $T_{(1)} = 1/ f_{(1)}$ is the time period of the first free vibration, $T = L/c$ is the total time of traverse of moving force over beam, $c_{cr} = \dfrac{2 f_{(j)} L}{j} \approx \dfrac{\pi}{L}\left(\dfrac{EI}{L}\right)^{1/2}$ is the critical speed, and $\vartheta = \dfrac{\omega_b}{f_{(1)}}$ is the logarithmic decrement of damping of the beam.

The analytical solution for transverse beam displacement obtained from the *Fourier* integral transformation method [10] is given by,

$$W(x,t) = \Delta_s \sum_{j=1}^{\infty} \left\{ \frac{1}{j^2\left[j^2(j^2-\alpha^2)^2 + 4\alpha^2\beta^2\right]} \left[j^2(j^2-\alpha^2) Sin\, j\omega t \right.\right.$$

$$- \frac{j\alpha\left[j^2(j^2-\alpha^2) - 2\beta^2\right]}{\left(j^4-\beta^2\right)^{1/2}} e^{-\omega_b t} Sin\, \omega'_{(j)} t \qquad (3.4)$$

$$\left.\left. - 2j\alpha\beta(Cos\, j\omega t - e^{-\omega_b t} Cos\, \omega'_{(j)} t) \right] Sin \frac{j\pi x}{L} \right\}$$

where Δ_s is the mid-span static deflection of a centrally loaded simply supported beam (with a load value same as P) given by

$$\Delta_s = \frac{PL^3}{48EI} \approx \frac{2P}{\mu L \omega_{(1)}^2} = \frac{2PL^3}{\pi^4 EI} \qquad (3.5)$$

The total beam deflection is expressed as a summation series containing a product of decoupled time coordinate and sinusoidal mode shape terms. The dynamic deflection is usually expressed in dimensionless form as a fraction of mid-span static deflection, i.e., $W(\xi,\tau) = W(x,t)/\Delta_s$ where $W(\xi,\tau)$ is the dimensionless deflection of the beam.

The bending moment and shear force values are found from the displacement solution, and are given by,

$$M(x,t) = -EI\frac{\partial^2 W(x,t)}{\partial x^2} \tag{3.6}$$

$$Q(x,t) = -EI\frac{\partial^3 W(x,t)}{\partial x^3} \tag{3.7}$$

where *M*, *Q*, *E* and *I* represent the bending moment, shear force, elasticity modulus and area moment of inertia, respectively.

3.1.2 Application of assumed modes method:

The analytical solution in Equation 3.4 contains separated spatial and temporal functions, and suggests that the same solution could be obtained by using mode superposition principle (or variable separation in general) to separate the mode shapes ($Sin\ j\pi x/L$ here or orthogonal shape functions in general) and solving only time dependent displacement function. This way, the original initial boundary value problem is reduced to an initial value problem only, and saves computational time. The mode shape factor is obtained by enforcing the boundary conditions on spatial function. Since the beam is simply supported (SS) at both the ends, and since one end point of the beam aligns with the origin of the coordinate system, the mode shape function is simply $Sin\ j\pi\ x/L$.

Hence, by using mode superposition principle, lateral deflection of SS beam is expressed as,

$$W(x,t) = \sum_{j=1}^{\infty} w(j,t)\, Sin\frac{j\pi x}{L} \tag{3.8}$$

Although the spatial terms are separated from temporal terms, it is not yet removed from the governing equation and the set of equations still remain as an initial boundary value problem. In order to get rid of the spatial function from the governing equation, the load on the right hand side of the Equation 3.1 can be approximated using *Fourier* series representation [9], i.e.,

$$\delta(x-ct)P = \frac{2P}{L}\sum_{j=1}^{\infty} Sin\frac{j\pi x}{L} Sin\frac{j\pi ct}{L} \tag{3.9}$$

By using mode superposition principle and *Fourier* series representation for point load together, i.e., Equations 3.8 and 3.9, the governing equation of motion (Equation 3.1) becomes

$$\begin{aligned} \sum_{j=1}^{\infty}\left(\mu\frac{d^2 w_j(t)}{dt^2} + 2\mu\omega_b\frac{dw_j(t)}{dt} + EI\frac{j^4\pi^4}{L^4}w_j(t)\right)Sin\frac{j\pi x}{L} \\ = \delta(x-ct)P = \sum_{j=1}^{\infty}\left(\frac{2P}{L}Sin\frac{j\pi ct}{L}\right)Sin\frac{j\pi x}{L} \end{aligned} \tag{3.10}$$

or simply,

$$\mu\frac{d^2 w_j(t)}{dt^2} + 2\mu\omega_b\frac{dw_j(t)}{dt} + EI\frac{j^4\pi^4}{L^4}w_j(t) - \frac{2P}{L}Sin\frac{j\pi ct}{L} = 0 \tag{3.11}$$

where $w_j(t) \equiv w(j,t)$. The above equation is simply an initial value problem which is relatively easier to solve than an initial boundary value problem.

By normalizing the time variable t using the total time of traverse ($T = L/c$), i.e., $\tau = t/T$, the first and second derivatives of displacement function $w_j(t)$ are given by

$$\frac{dw_j(t)}{dt} = \frac{1}{T}\frac{dw_j(\tau)}{d\tau} \tag{3.12}$$

$$\frac{d^2w_j(t)}{dt^2} = \frac{1}{T^2}\frac{d^2w_j(\tau)}{d\tau^2} \tag{3.13}$$

The above equation is re-written in a non-dimensional form using the parameters α, β, and Δ_s, defined in Equation 3.2, 3.3 and 3.5, as given below:

$$\frac{\alpha^2}{\pi^2}\frac{d^2w_j(\tau)}{d\tau^2} + \frac{2\alpha\beta}{\pi}\frac{dw_j(\tau)}{d\tau} + j^4 w_j(\tau) - Sin\, j\pi\tau \;=\; 0 \tag{3.14}$$

The above equation is free of spatial terms (and hence no boundary conditions), and is solved along with the initial conditions stated in Equation 3.1B. The solution to Equation 3.14 is then combined with the respective mode shapes to yield the resultant lateral displacement of beam at any point of space and time.

Past researches [9, 10] indicated that the first mode solution dominates over other modes, and without appreciable loss in solution accuracy, we can obtain the displacement

response considering only the first mode shape. In the coming sections, displacement responses for both the single mode and multiple modes are discussed.

3.1.3 DQ approach to moving force problem:

The application of DQM to solve moving load problems can be implemented either by using generic polynomial test functions or by using special polynomial interpolation schemes such as *Lagrange* interpolation, *Spline* interpolation, and *Hermite-Fejér* interpolation schemes. In general, these interpolation or test functions can be applied to both the spatial and temporal domains. However the use of spatial interpolation functions is not required for the solution procedure involving Equation 3.14 since the spatial terms were decoupled. In the forthcoming discussions, the DQM applied to both the spatial and temporal domain simultaneously is referred as the direct or space-time DQM, and the DQM procedure based on the mode superposition principle is called the semi-analytical or modal DQM.

In this section, the use of DQM to approximate both the spatial and temporal derivatives simultaneously is demonstrated, and in order to approximate the *Dirac Delta* distribution, either the *Fourier* sine series or other general distribution functions could be used. In the event of not using either of the above approximations for *Dirac Delta* function, any direct time integration methods such as *Newmark* [121] could also be used. *Olsson* [67 1991] used the first term $Sin\frac{\pi x}{L}Sin\frac{\pi c t}{L}$ of the *Fourier* sine series to approximate the moving load, and *Inglis* [9] also pointed out earlier that less than a 0.5 percent error results due to

such approximation. The governing equation of motion of the beam, *Equation 1* is then given by

$$\mu \frac{\partial^2 W(x,t)}{\partial t^2} + 2\mu\omega_b \frac{\partial W(x,t)}{\partial t} + EI \frac{\partial^4 W(x,t)}{\partial x^4} = \frac{2P}{L} Sin \frac{\pi x}{L} Sin \frac{\pi c t}{L} \tag{3.15}$$

The independent variables in these equations, *x* and *t*, are normalized using the relation, $\xi = x/L$ and $\tau = t/T$ where L is the length of the beam and T is the total time of traverse, i.e., $T = L/c$. With the parameters α and β, and the dimensionless variables ξ and τ, the governing equation of motion Equation 3.15 becomes,

$$\pi^2 \alpha^2 \frac{\partial^2 W(\xi,\tau)}{\partial \tau^2} + 2\pi^3 \alpha\beta \frac{\partial W(\xi,\tau)}{\partial \tau} + \frac{\partial^4 W(\xi,\tau)}{\partial \xi^4} = 96\ Sin\,\pi\xi\ Sin\,\pi\tau \tag{3.16}$$

The boundary conditions for a simply supported beam are given by,

$$W(\xi,\tau) = \frac{\partial^2 W(\xi,\tau)}{\partial \xi^2} = 0 \tag{3.16A}$$

at any instant of time for both the ends of the beam, i.e., at $\xi = 0,1$ and the initial conditions are given by,

$$W(\xi,\tau) = \frac{\partial W(\xi,\tau)}{\partial \tau} = 0 \tag{3.16B}$$

at time $\tau = 0$ for any point along the beam.

Description of study parameters:

The dynamic behavior of an idealized bridge structure due to a moving force-moving mass is studied for the below given beam and load parameters to enable a comparison of DQM results with the published literature results. The set of parameters chosen for the study is the same as used by *Yang and Yau* [60] and are given below in SI units (and English units within parenthesis). The moving force solution obtained from the DQM is compared with the analytical solution available in the form of *Fourier* series. Both the forms of implementation namely, 1) the direct space-time DQM, i.e., applying spatial-temporal DQ discretization simultaneously, and 2) semi-analytical or modal DQM, i.e., applying temporal DQ scheme to Equation 3.14 and obtaining the total displacement solution by mode superposition principle, were used and the results obtained were then compared for different speed and damping parameters.

Input Data:

Length of beam (L) = 25 m, (~984.25 in or 82.02 ft)

Mass density of the concrete slab (ρ) = 151.913 kg/m^3, ($\sim 0.005488\ lb/in^3$)

Linear density of the beam (μ) = 2303 kg/m, ($\sim 0.05599\ lb/in$)

Elasticity modulus of the beam (E) = $2.87\times10^9\ N/m^2$, ($\sim 416\ ksi$)

Base or Cross section width of the beam (b) = 10 m, (~393.7 in)

Cross section height of the beam (h) = 1.516 m, (~59.685 in)

Area moment of Inertia of the beam (I) = $bh^3/12 = 2.9\ m^4$, ($\sim 6967278\ in^4$)

Weight of the moving point load (P) = 56408 N, (~12681 lbf or 6.34 *tons*)

Speed of the moving point load (c) = 27.778 *m/sec*, (~62 *miles/hr* or 91 *ft/sec*)

Total time of traverse, $T = \frac{L}{c} = \frac{25}{27.778} = 0.8999$ sec

Frequency of the forced vibration, $\omega = \frac{\pi c}{L} = \frac{\pi}{T} = 3.49068 \frac{rad}{\text{sec}}$

Fundamental circular frequency of free vibration, $\omega_{(1)} = \frac{\pi^2}{L^2}\sqrt{\frac{EI}{\mu}} = 30.02 \ \frac{rad}{\text{sec}}$

(or the fundamental frequency of vibration is $4.777 \ Hz$)

Speed parameter, $\alpha = \frac{\omega}{\omega_{(1)}} = \frac{\pi c}{L}\frac{L^2}{\pi^2}\sqrt{\frac{\mu}{EI}} = 0.1163$

Frequency of damping, ω_b = expressed in fractions of the fundamental frequency, $\omega_{(1)}$

Damping parameter, $\beta = \frac{\omega_b}{\omega_{(1)}} = 0.1$

In the above list of parameters, the material and geometry parameters of beam remain fixed, and only the load parameters *P* and speed *c* are subjected to change.

3.1.3 a) DQM applied to spatial and temporal domain

The dynamic deflection distribution is discretized using *M* nodal points along the spatial domain, and *N* nodal points along the temporal domain, and at any location and time, (ξ_i, τ_j), the deflection is denoted by W_{ij} such that $i = 1, 2, ..., M$ and $j = 1, 2, ..., N$. The DQ analog for the governing equation, Equation 3.16, is given by

$$\pi^2 \alpha^2 \sum_{k=1}^{N} B_{jk}^{(\tau)} W_{ik} + 2\pi^3 \alpha\beta \sum_{k=1}^{N} A_{jk}^{(\tau)} W_{ik} + \sum_{k=1}^{M} D_{ik}^{(\xi)} W_{kj} = 96 \, Sin \, \pi\xi \ Sin \, \pi\tau \qquad (3.17)$$

Here, the weighting coefficients for the spatial and temporal domains are indicated with their superscripts ξ and τ, respectively and *A*, *B*, and *D* represent the 1^{st}, 2^{nd} and 4^{th} order weighting coefficients, respectively. The governing equation in DQ form is independent of the choice of polynomial test functions. The governing equation in the DQ form is then solved along with the boundary and initial conditions.

The displacement solution to Equation 3.17 above is obtained by using different types of interpolating polynomials namely, 1) classic polynomial test function (for both space and time domain), 2) *Lagrange* type interpolating polynomials for spatial and temporal domains, 3) *Lagrange* and *Hermite-Fejér* type interpolating polynomials for spatial and temporal domains, respectively, and 4) Spline and *Hermite-Fejér* type interpolating polynomials for spatial and temporal domains, respectively. The working methodologies of these procedures are similar except that a different form of polynomial is used for interpolation.

The classic polynomial test functions resulted in *Vandermonde* matrix which posed difficulty in finding inverses during computation especially at higher number of nodes. The *Lagrange* type interpolating polynomials is preferred over the classic monomial basis polynomial test functions since it adds exact weights at nodal points. The solution time in case of the application of spline interpolation is larger than that of other interpolation schemes.

The *Hermite-Fejér* method uses both the function values and its derivatives of the possible lowest order to interpolate on the given data. This type of interpolation is more suitable for initial value problems where the initial conditions are usually a function value and its lowest order derivative. For example, in the free vibration study of a 1 DOF system given by $m\ddot{x}(t) + c\dot{x}(t) + kx = 0$ where x is the displacement at time t, with the initial conditions $x(t = 0) = a;\ \dot{x}(t = 0) = b$ the *Hermite-Fejér* type interpolating polynomials can be used.

The displacement solution obtained from the *Lagrange* and *Hermite-Fejér* type interpolating polynomials are almost same for most of the conditions. Both the *Lagrange* as well as the *Hermite-Fejér* type interpolating polynomials produce oscillatory behavior at higher degree (more number of nodal points) when used to interpolate on equally spaced node points. This phenomenon is called *Runge* phenomenon, and is avoided/minimized by choosing *Chebyshev-Gauss-Lobatto* nodal points for distribution. The spline interpolation technique can also be used instead (to avoid *Runge* phenomenon without the use of *Chebyshev-Gauss-Lobatto* distribution) as it is a piecewise polynomial function that increases the number of such piecewise polynomials without increasing the degree of the interpolating polynomial function.

The dynamic response of a beam with the above mentioned parameters is plotted at mid-span beam and is shown below in the *Figure 3.2*. The dimensionless deflection ratio, i.e., the ratio of dynamic vertical displacement due to moving load (P) to the mid-span static displacement due to the same load acting at the center of the beam, is plotted versus the

normalized time of traverse (ratio of instantaneous time at the point of application of load to the total time of traverse). The dimensionless deflection ratio is a very useful measure since it is valid for any geometry and material parameters as well as the loading conditions. The normalized displacement solution obtained using the direct DQM (DQM applied to both the spatial and temporal nodes simultaneously or the space-time DQM) shown in the *Figure 3.2* included only the first mode of vibration while the analytical solution included the first 5 terms of *Fourier* series, i.e., first 5 modes of vibration.

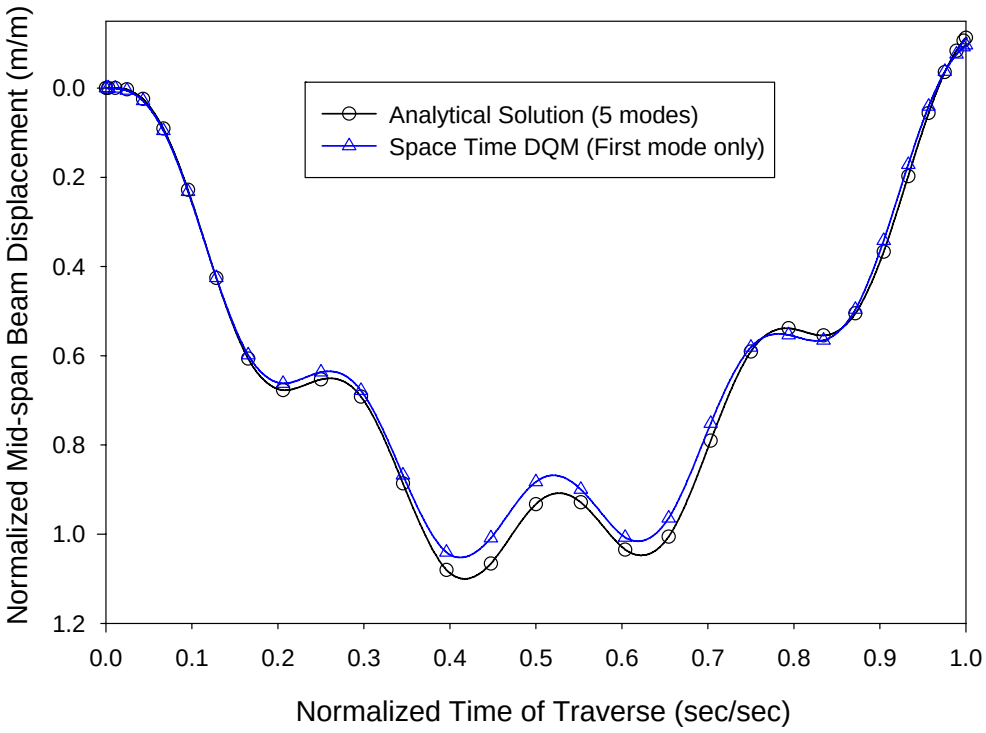

Figure 3.2: Dynamic beam response from analytical & space-time DQM

(α = 0.116, β = 0, m = 7, n = 31)

The differences in the displacement solution between the space-time DQM and analytical procedure, i.e., the error in the displacement solution obtained from the DQM are shown

in *Figure 3.3*. Assuming that the maximum range of error to occur in the mid-span of the beam, the mid-span displacements of the beam computed from analytical and DQ methods were compared.

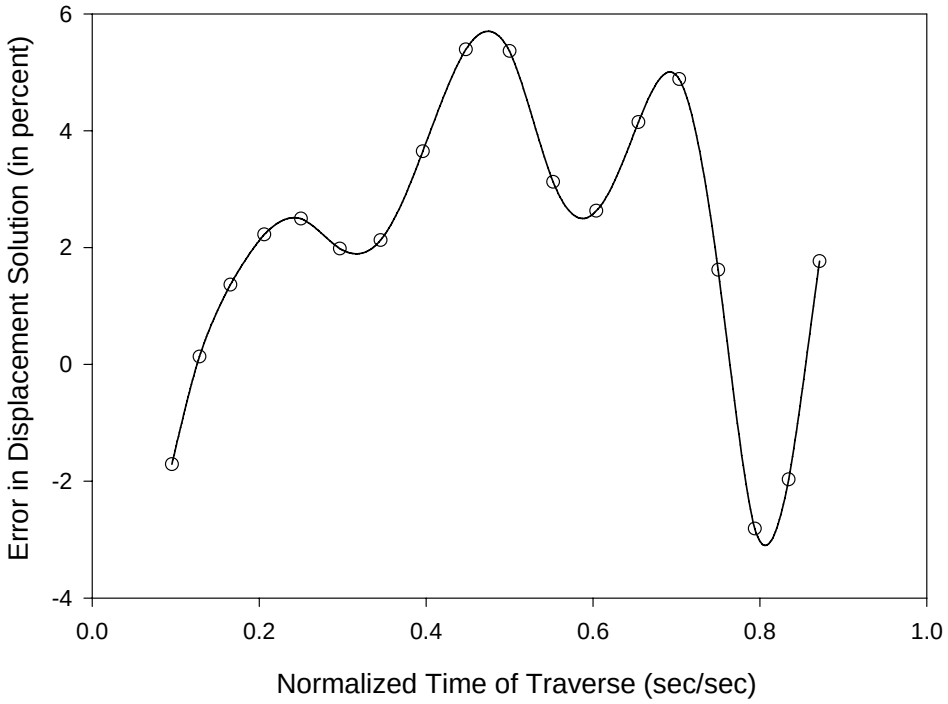

Figure 3.3: Error in displacement solution using space-time DQM

(α = 0.116, β = 0 with m = 7, n = 31)

The maximum percentage error in the displacement solution from the DQ method amounted to 5.3 % (approx.) in the time zone [0.067, 0.9] (and over 25 % in the time zone [0, 0.05] and [0.9, 1.0] which were discarded as the deflections were negligible and hence resulting in an abnormal error range). However the displacement predicted by the direct DQM in this case is not an upper bound, i.e., the displacement solution is underestimated, and hence the solution procedure needed improvements such as addition of nodes in the space and/or temporal domains or application of other techniques. The modal superposition principle produced accurate solutions and the results were promising enough (discussed in the section 3.1.3 (b)) to be used for further analyses.

Also as shown in *Figure 3.4*, the differences in the deflection values obtained from analytical methods, for the first mode and up to the first 5 modes were almost negligible, and this suggested that the direct DQM solution contained error not because of the first mode approximation, but could be due to the coarse discretization of spatial or temporal domain. By introducing more number of nodes in the spatial domain, the solution improved as shown in *Figure 3.5*. The spatial domain is discretized into 7 nodes in the former case, i.e., *Figure 3.2*, whereas 15 nodes in the latter case, i.e., *Figure 3.5*, and in both the cases 31 temporal nodes were used. The maximum error in this case dropped to less than 4 %.

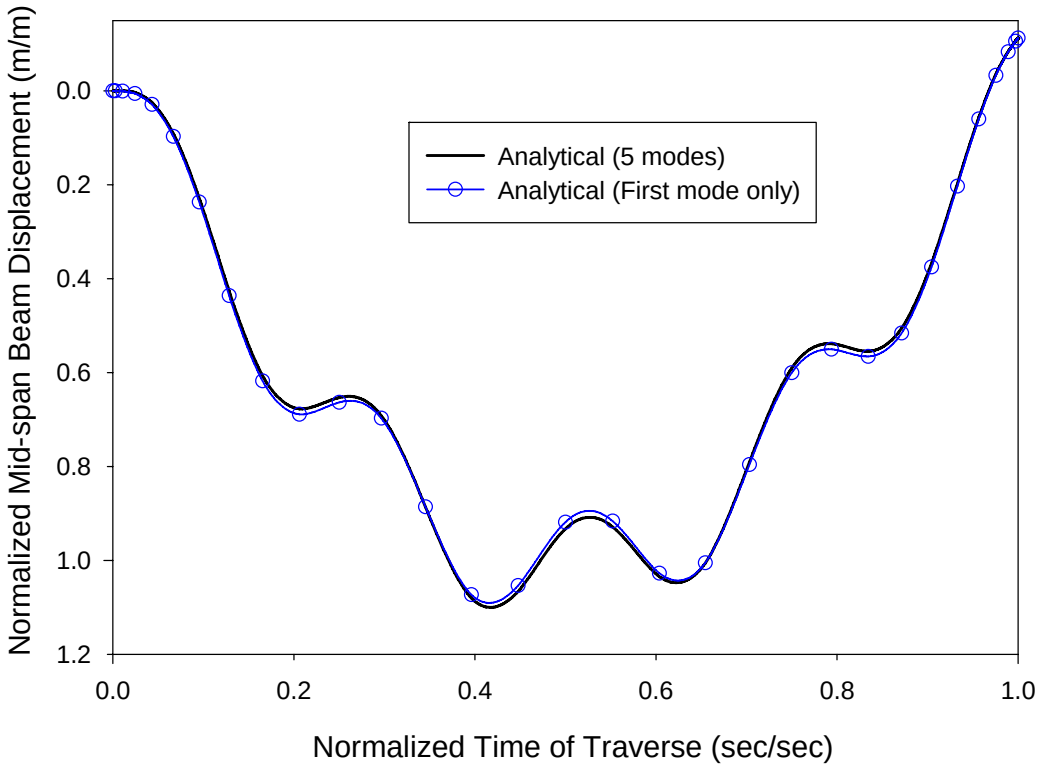

Figure 3.4: Dynamic beam response from analytical solution – Effect of number of modes of vibration ($\alpha = 0.116$, $\beta = 0$)

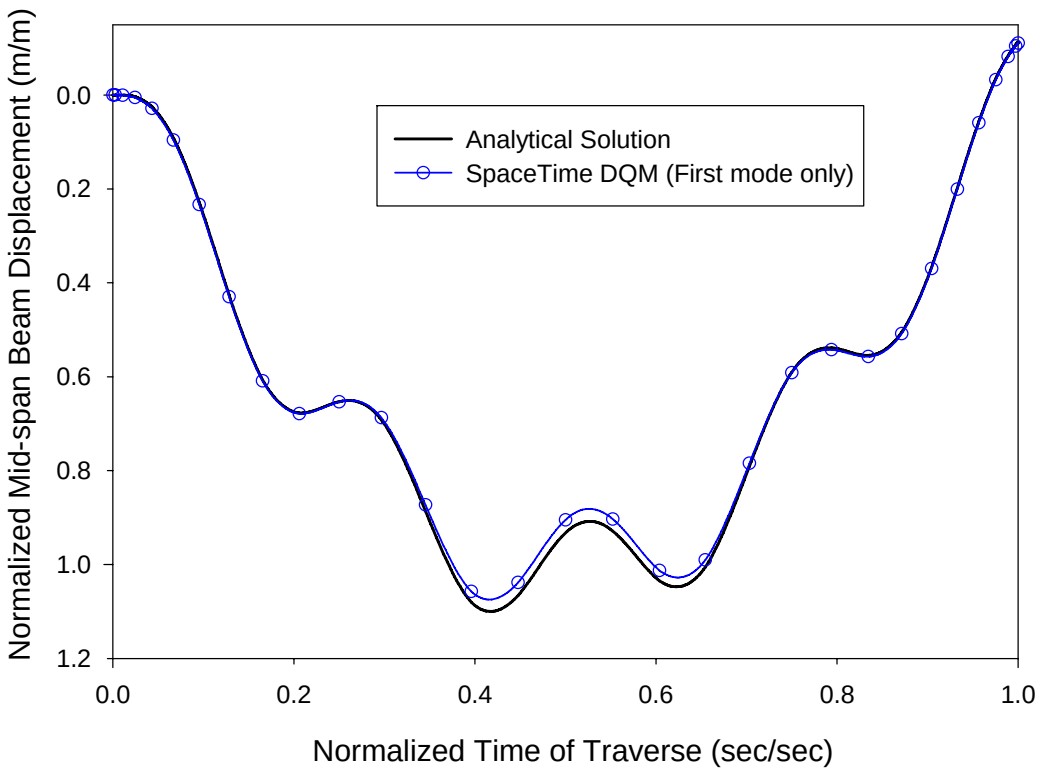

Figure 3.5: Dynamic beam response from space-time DQM and analytical solution

(α = 0.116, β = 0, m=15, n=31)

Though the solution accuracy depended on the number of nodal points used in the temporal domain, increasing beyond a certain number did not improve the solution accuracy, i.e., the displacement solution converged but differences between analytical and numerical procedures remained, say in the range 3-5 %. For example, the displacement solution obtained from the direct space-time DQM with less than 24 nodes in the temporal domain for this set of data (α = 0.116) contained considerable percentage of error (compared to the analytical solution), and the solution improved as the number of nodes is increased beyond 24 and up to 35. However increasing the number of nodes in the time domain above 35 did not improve the solution much and the displacement

solution essentially remained the same for nodes above 35, for example, the solution obtained for 61 temporal nodes is shown in the *Figure 3.6.* The number of nodes in the spatial domain was kept at 7 to spare the computational time. *Figure 3.7* shows the error in the mid-span beam displacement solution obtained from the DQM with respect to the analytical solution.

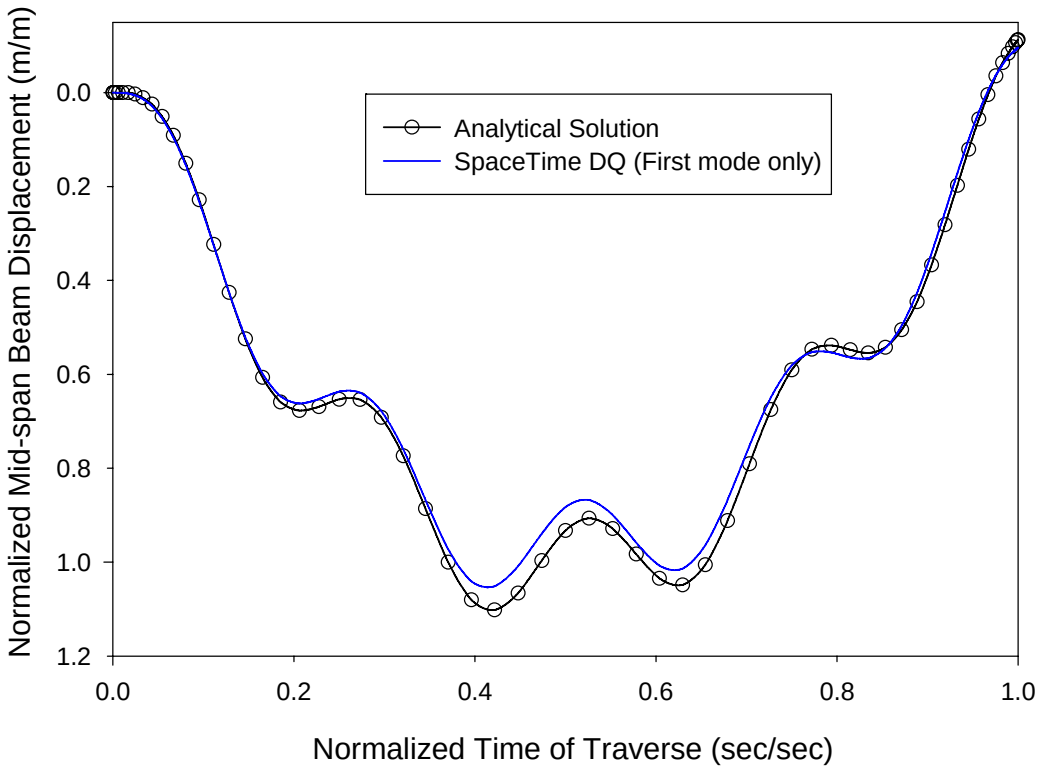

Figure 3.6: Dynamic beam response from space-time DQM and analytical solution

(α = 0.116, β = 0, m=15, n=61)

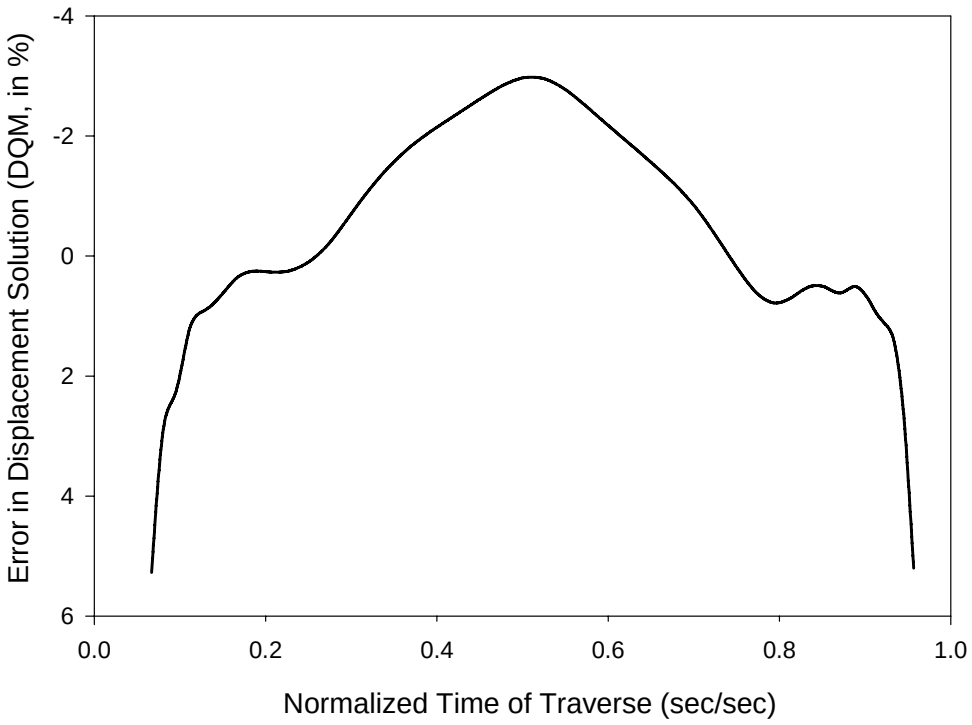

Figure 3.7: Error in mid-span displacement solution obtained from space-time DQM over analytical solution (α = 0.116, β = 0, m=15, n=61)

The *Runge* phenomenon, i.e., oscillations/error in displacement values due to equidistant nodal distribution for higher degree interpolating polynomials, is avoided by using the *Chebyshev-Gauss-Lobatto* distribution. It is also interesting to note that the minimum number of nodes in the temporal domain required for acceptable displacement solutions, say within 5 % error mark (here 31 nodes for the data set used in the *Figure 3.2* and *Figure 3.5*) decreased as the speed parameter is increased. Since the number of nodal points can be reduced for high speed parameter problems, it is also observed that there is no need for *Chebyshev-Gauss-Lobatto* node distribution at higher values of speed parameter.

3.1.3 b) DQM applied to temporal domain only (Assumed modes principle):

The application of DQM to solve moving load problem based on the modal approach is recommended since the model is computationally efficient – spatial variation is decoupled, and contribution of different modes to the displacement solution can be assessed. The application of modal approach to solve for moving load problems is outlined in the *Section 3.1.2*. The DQ analog of the governing equation of motion is solved only for temporal variables, and then combined with the mode shape factor (for spatial distribution). The normalized displacement solutions obtained from the DQM based on the mode superposition principle for the first mode only and up to first 3 modes are shown in *Figure 3.8* and *Figure 3.9*, respectively. *Figure 3.9* shows that the modal superposition results compared well with the analytical solution.

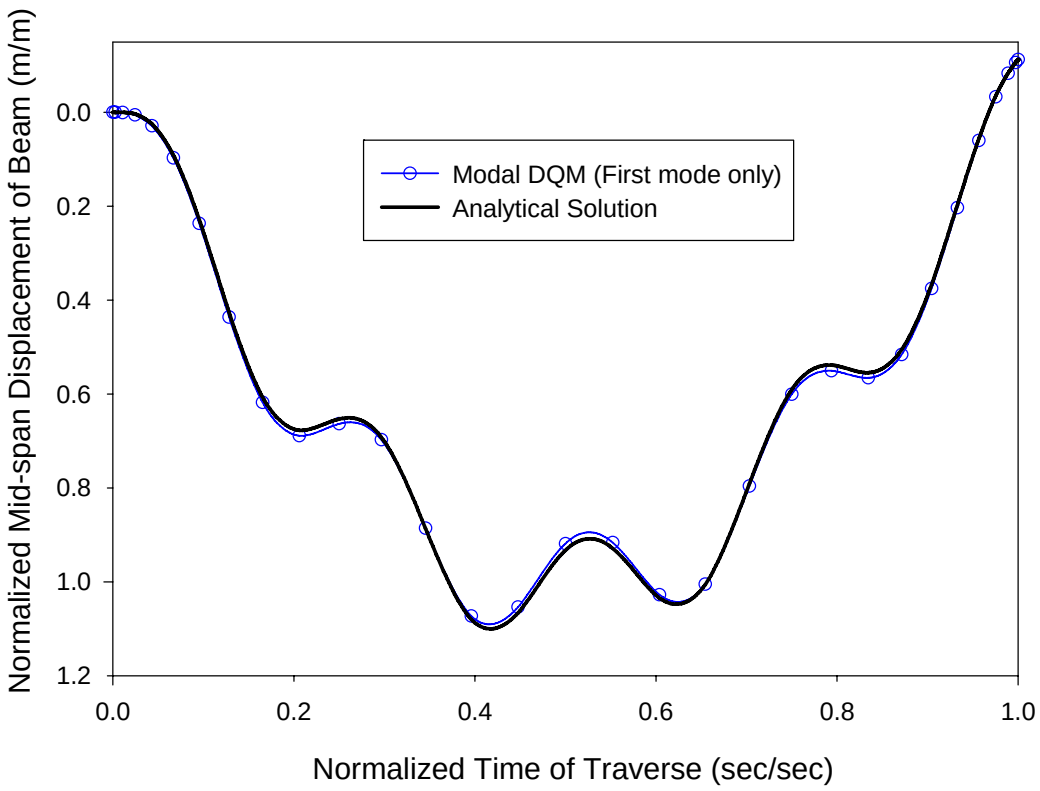

Figure 3.8: Dynamic beam response from modal DQM (1st mode only) and analytical solution (3 modes)

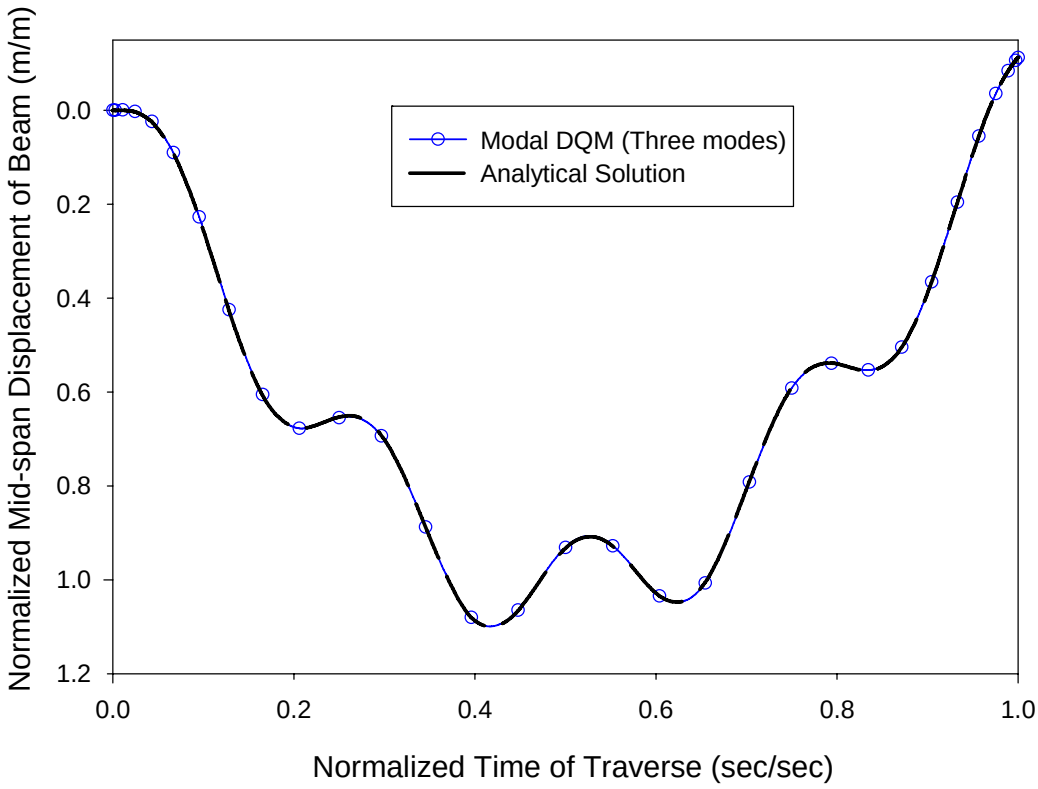

Figure 3.9: Dynamic beam response from modal DQM (3 modes) and analytical solution (3 modes)

3.1.4 Discussion on results:

The mid-span static and dynamic response of an idealized bridge structure is shown in *Figure 3.10*. The static response is considered for the static load of same magnitude as that of a moving load but that acts at the mid-span of the bridge structure. The dynamic deflection computed from solving *Equation 3.1* with appropriate boundary and initial conditions is studied for convergence in solution by increasing the number of node points in spatial/temporal domain. This is one of the difficult tasks in DQM, since there is no well established relationship between the solution accuracy and the number of node points. As a result, the DQM with only 7 nodes that produces acceptable solution for a problem *A* (say) could prove to be substandard for a different problem *B*. In another case,

confined to problem *A* or *B*, we don't know if the solution could be in acceptable limits to start with a certain number of nodes. The convergence criterion could be any of the system parameters such as energy, stress, displacement, etc., and in this study the convergence test is performed based on the displacement parameter. The DQ procedure was run for different node numbers starting from coarser grids (less node points) toward finer grids (more node points) and the results were discussed in the later section.

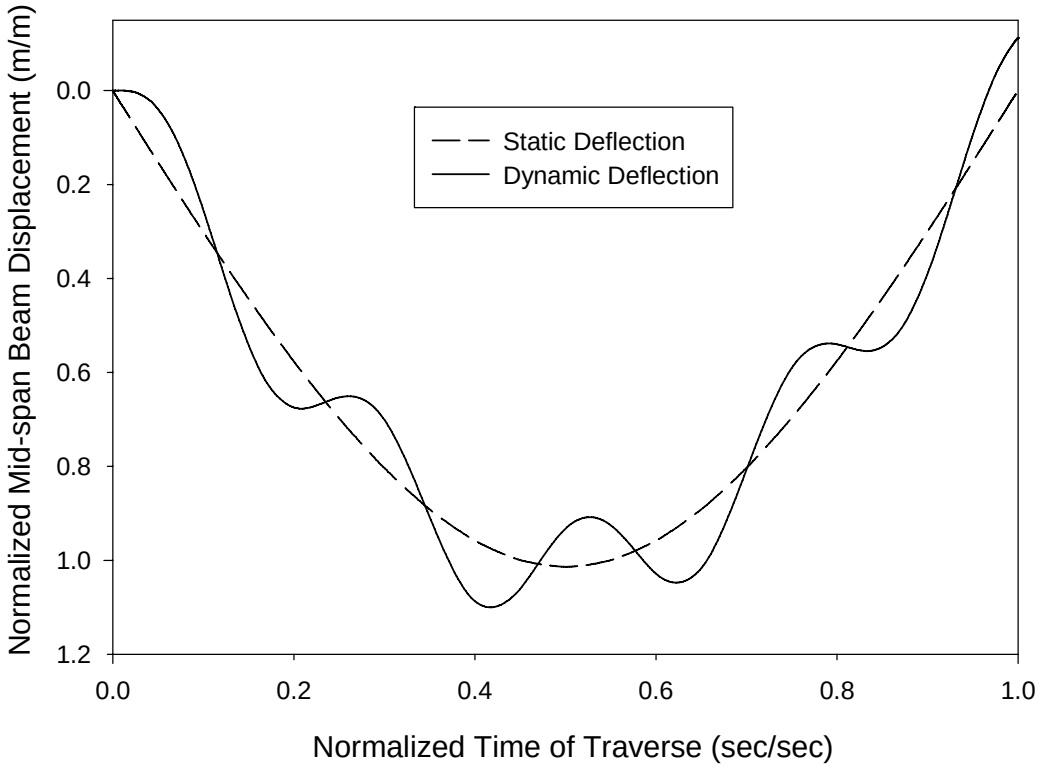

Figure 3.10: Analytical dynamic beam response due to moving force shown with static deflection

The bending moments and shear forces at any section could be calculated from the displacement values as given in Equations 3.18 and 3.19, respectively. The bending moments and shear forces could be readily obtained from the DQM since both the DQ

coefficients as well as the displacement values are known at any node point, and incase of the modal method, the bending moment is written in terms of time coordinates as

$$M = -EI\frac{\partial^2 W}{\partial x^2} = -EI\frac{\partial^2}{\partial x^2}\left(\sum_{k=1}^{\infty} w_k(t)Sin\frac{k\pi x}{L}\right)$$
$$= \frac{\pi^2 EI}{L^2}\sum_{k=1}^{\infty} k^2 w_k(t)Sin\frac{k\pi x}{L} \tag{3.18}$$

Similarly shear forces are given by,

$$Q = -EI\frac{\partial^3}{\partial x^3}\left(\sum_{k=1}^{\infty} w_k(t)Sin\frac{k\pi x}{L}\right)$$
$$= \frac{\pi^3 EI}{L^3}\sum_{k=1}^{\infty} k^3 w_k(t)Cos\frac{k\pi x}{L} \tag{3.19}$$

Like the normalized dynamic deflection, bending moments and shear forces were also expressed in dimensionless forms using the maximum bending moment $M_0 = PL/4$ due to *P* acting at mid-span, and shear force *P*, respectively. Thus the Equations 3.18 and 3.19 become

$$M_{normalized} = \frac{M}{M_0} = \frac{4\pi^2 EI}{PL^3}\sum_{k=1}^{\infty} k^2 w_k(t)Sin\frac{k\pi x}{L}$$
$$= \frac{\pi^2}{12\Delta_{st}}\sum_{k=1}^{\infty} k^2 w_k(t)Sin\frac{k\pi x}{L} \tag{3.20}$$

$$Q_{normalized} = \frac{Q}{P} = \frac{\pi^3 EI}{PL^3} \sum_{k=1}^{\infty} k^3 w_k(t) Cos \frac{k\pi x}{L}$$
$$= \frac{\pi^3}{48\Delta_{st}} \sum_{k=1}^{\infty} k^3 w_k(t) Cos \frac{k\pi x}{L} \quad (3.21)$$

where Δ_{st} is the mid-span static deflection of a centrally loaded beam.

As the bending moments are related to displacements using 2^{nd} differentials, and that the assumed mode shape is a sine function, the bending moment also distributes similar to the dynamic displacement of the beam. The absolute maximum value (for the set of parameters given above) of the bending moment due to the moving load P is 333350 *N-m*. The bending moment and shear force parameters at the mid-span of the beam as a function of time were shown in dimensionless forms in the *Figure 3.11* and *Figure 3.12*, respectively. The absolute maximum value of the shear force due to moving load *P* is 48418 *N*.

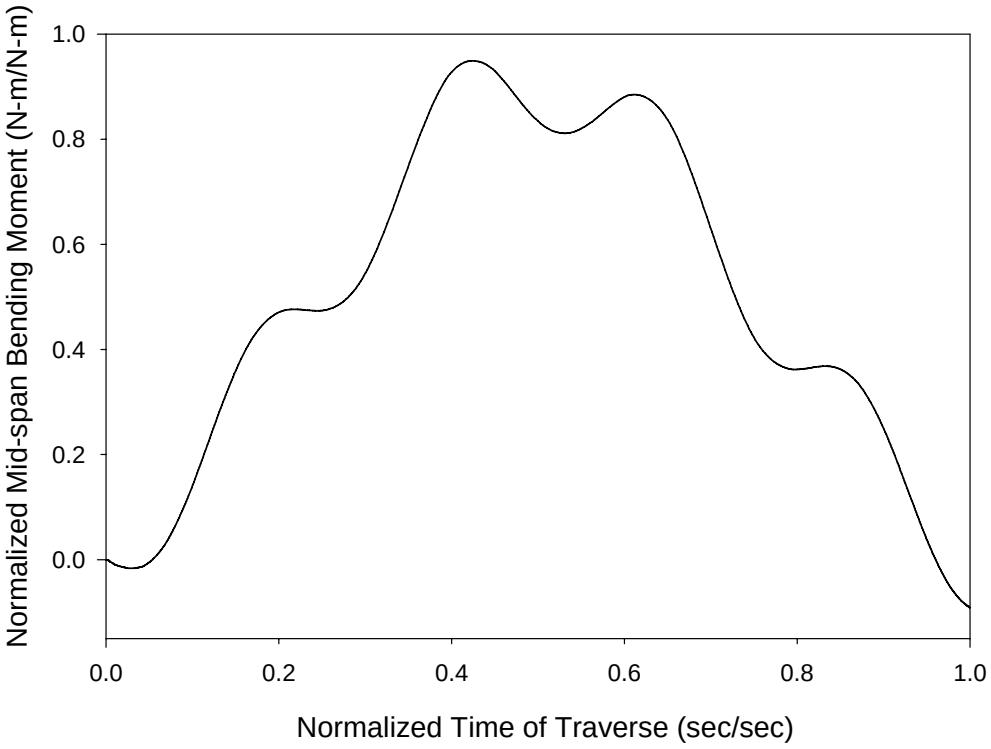

Figure 3.11: Normalized mid-span beam bending moment due to moving force

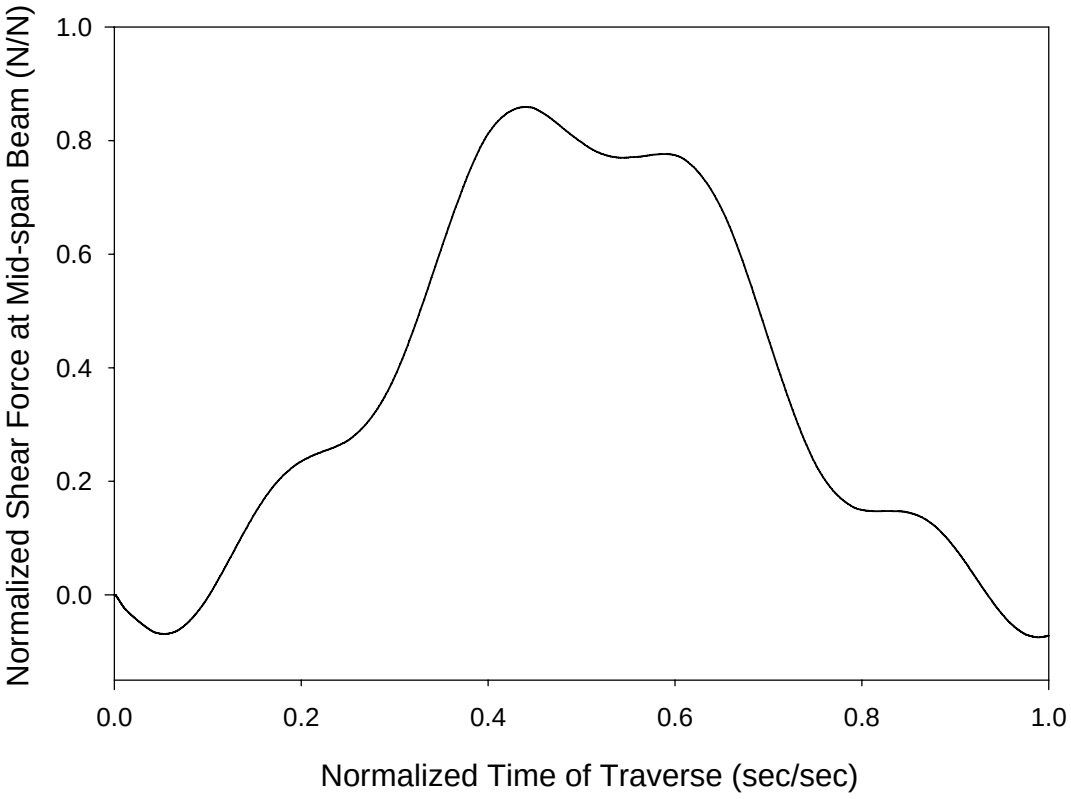

Figure 3.12: Normalized mid-span beam shear force due to moving force

Similarly the bending stress at any point across a section is calculated as $\sigma = M\ y / I$ where I is the area moment of inertia, and y is the vertical distance from the neutral axis to the point where the bending stress is measured. The maximum stress is experienced in the top and bottom of the beam and is about $120{,}700\ N/m^2$.

3.1.5 Influence of beam and load parameters on vibration response of beam:

Some of the major parameters that influence the dynamic behavior of bridge structures are the speed of the vehicle passing over the bridge, damping characteristics of bridge system, vehicle to bridge mass ratio, vehicle to bridge frequency ratio, and others. Among these, only speed and damping parameters were applicable to moving force

problems, and the influence of these parameters on the dynamic behavior of the bridge structures is studied via the dynamic impact factor.

3.1.5 a) Effect of Speed Parameter (α)

The dynamic impact factor is used as a measure of the dynamic behavior of the bridge structure and is defined with respect to the mid-span static deflection. A few variations of the definition and meaning of the term 'dynamic impact factor' exist as discussed in the first chapter section 1.3. In this section, the effect of speed and damping parameters on the dynamic response of the bridge structure is assessed by studying the changes in the dynamic amplification factor for different values of speed and damping parameters. The *Figure 3.13* shows the variations in dynamic amplification factor with respect to the speed parameter for an undamped beam, and also from *Figure 3.14* it is observed that the dynamic amplification factors obtained from modal DQM compared well with those obtained from analytical method except at very low speeds where the DQ method fails to capture the oscillating behavior as seen in the analytical solution.

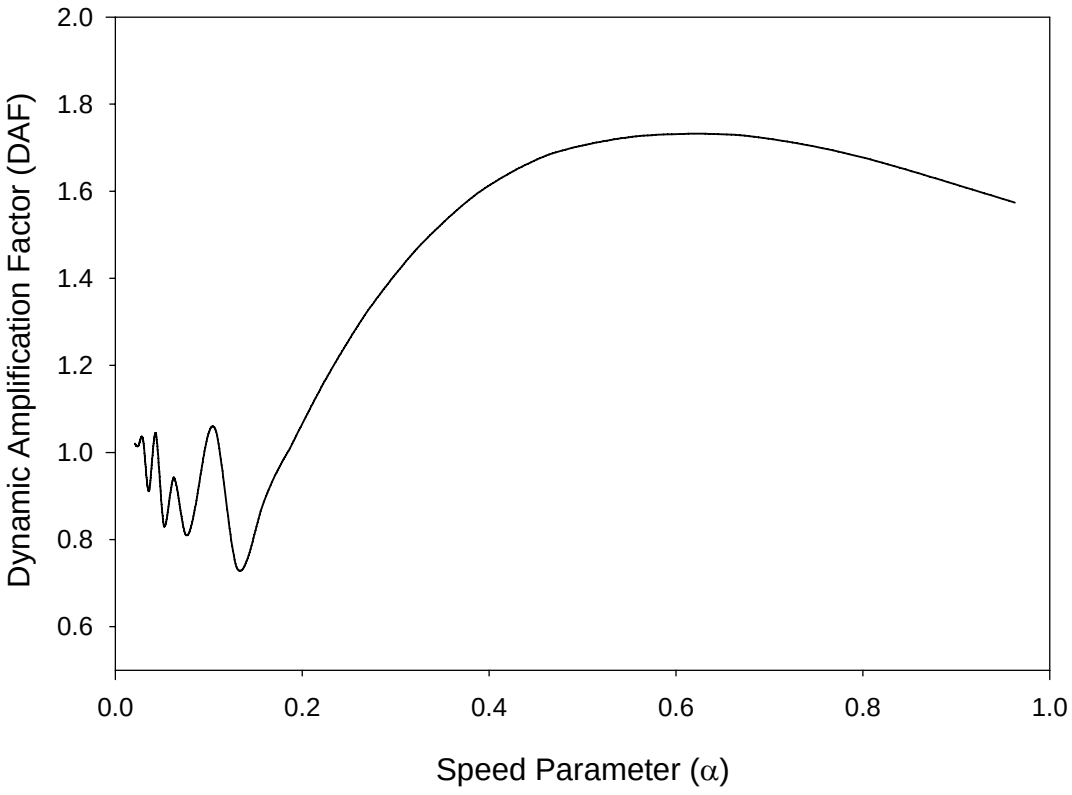

Figure 3.13: Effect of speed parameter on DAF of undamped beam due to moving force (Analytical solution)

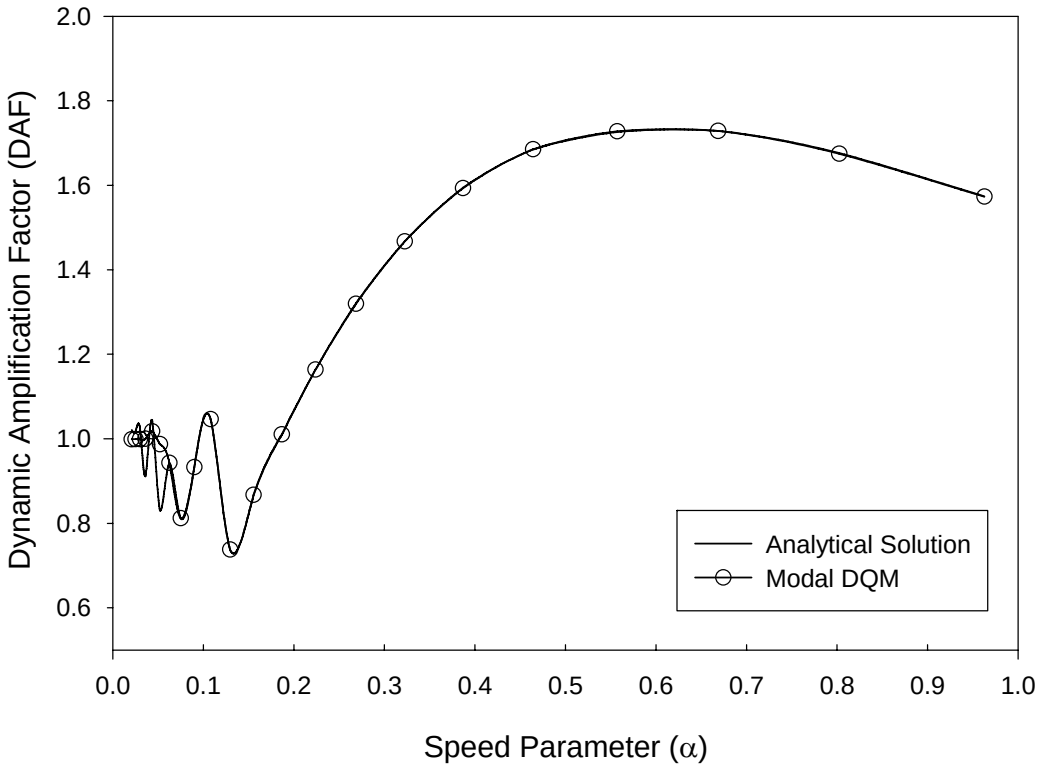

Figure 3.14: DAF vs. speed parameter from DQM and analytical solutions for moving force model

The amplification factor increases initially with the increase in the speed parameter up to a critical value which is around 0.5, and decreases thereafter. However the real life cases of transient dynamic problems involving bridge structures hardly ever reaches the critical speed parameter value so that the dynamic response of the bridge structures falls within the rising phase of the amplification factor vs. speed parameter curve, and hence it is justified to assume that the dynamic behavior is directly proportional to the speed parameter.

3.1.5 b) Damping parameter (β):

The effect of damping parameter on the dynamic response of a bridge structure modeled as beam is studied using variations in dynamic amplification factor versus speed

parameter for different damping characteristics of the beam, and is shown in the *Figure 3.15*. The *Figure 3.16* shows the same data but instead directly plots the variations of dynamic amplification factor versus damping parameters. As expected, the dynamic response of a bridge system decreases with the increase in its damping characteristics. Also to be noted is that there is no appreciable direct impact of the damping parameter on the dynamic response of the system at low speeds $\alpha < 0.1$.

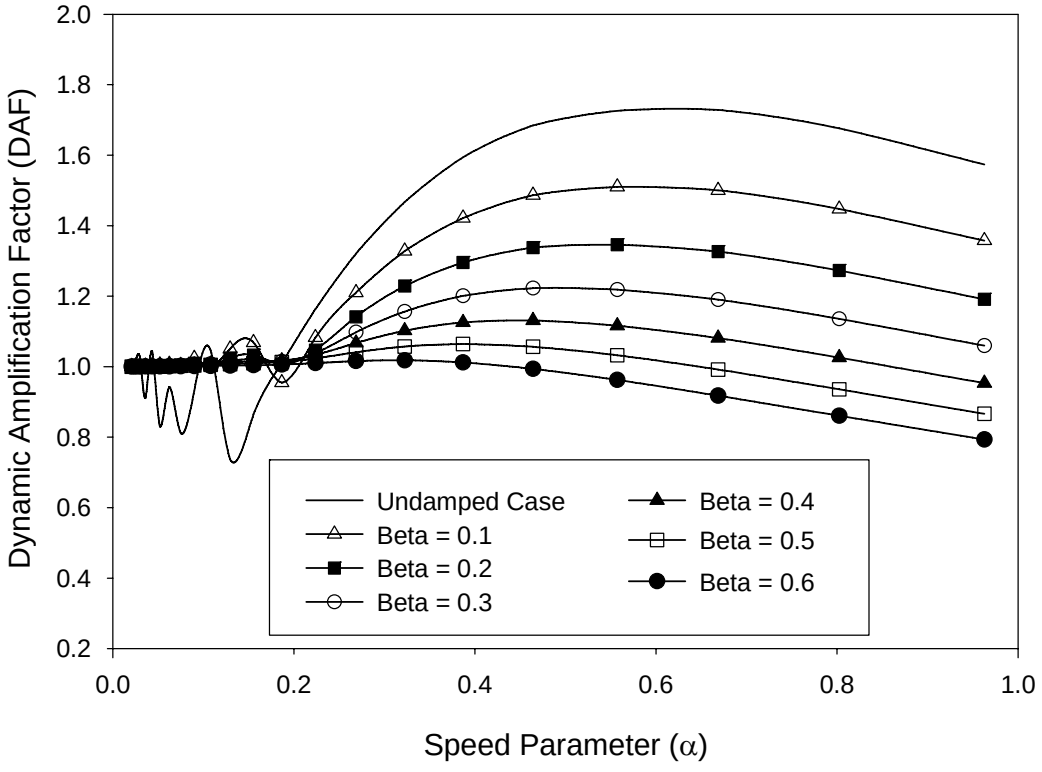

Figure 3.15: DAF vs. speed parameter at various damping levels for moving force model (Analytical solution)

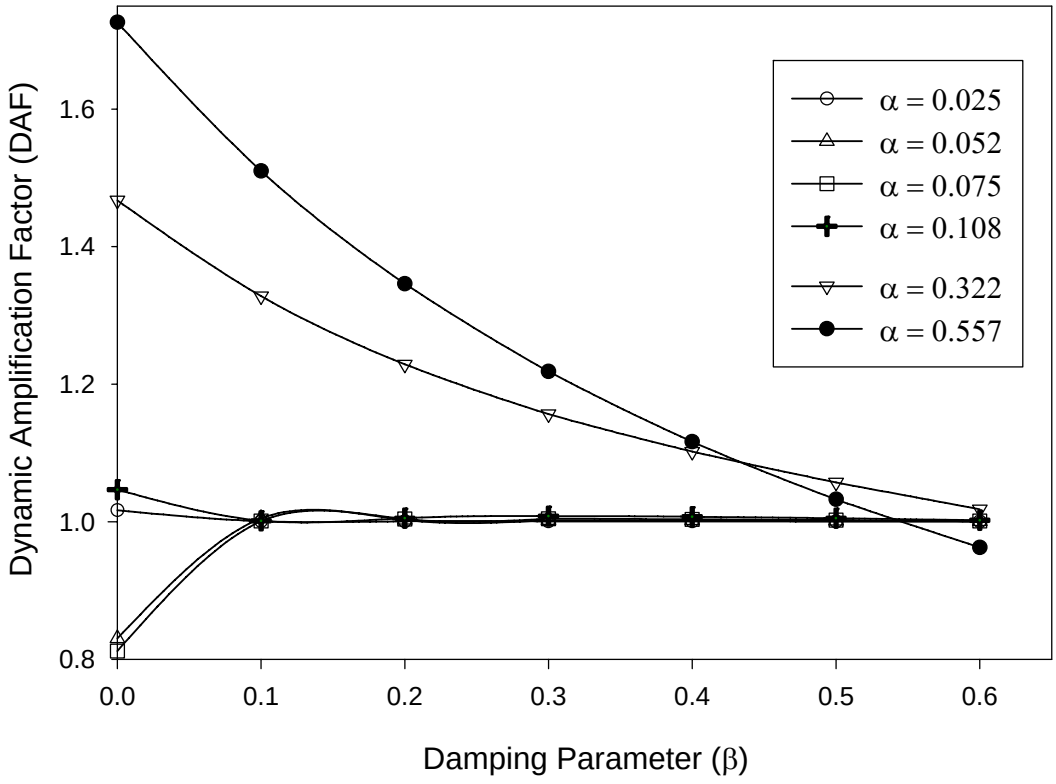

Figure 3.16: Effect of damping parameter on dynamic response

In order to validate and compare the DQ solution with the analytical solution, a convergence study was performed based on the displacement parameter, and the dynamic amplification values for different speed parameter values were plot in the *Figure 3.17* which indicated that the DQ solution obtained from temporal nodes numbering 24 and above compared well with the analytical solution for speed parameter values above 0.12.

The analytical and DQ solutions did not match well for low speed parameter values (refer to *Figure 3.18*) especially for less number of nodes. As the number of nodal points is increased to 40 and above, the DQ and analytical solutions matched well with the part of

the data belonging to low speed parameter zone. *Fryba* [10] reported a linear variation of the dynamic amplification with respect to speed parameter values up to 0.2.

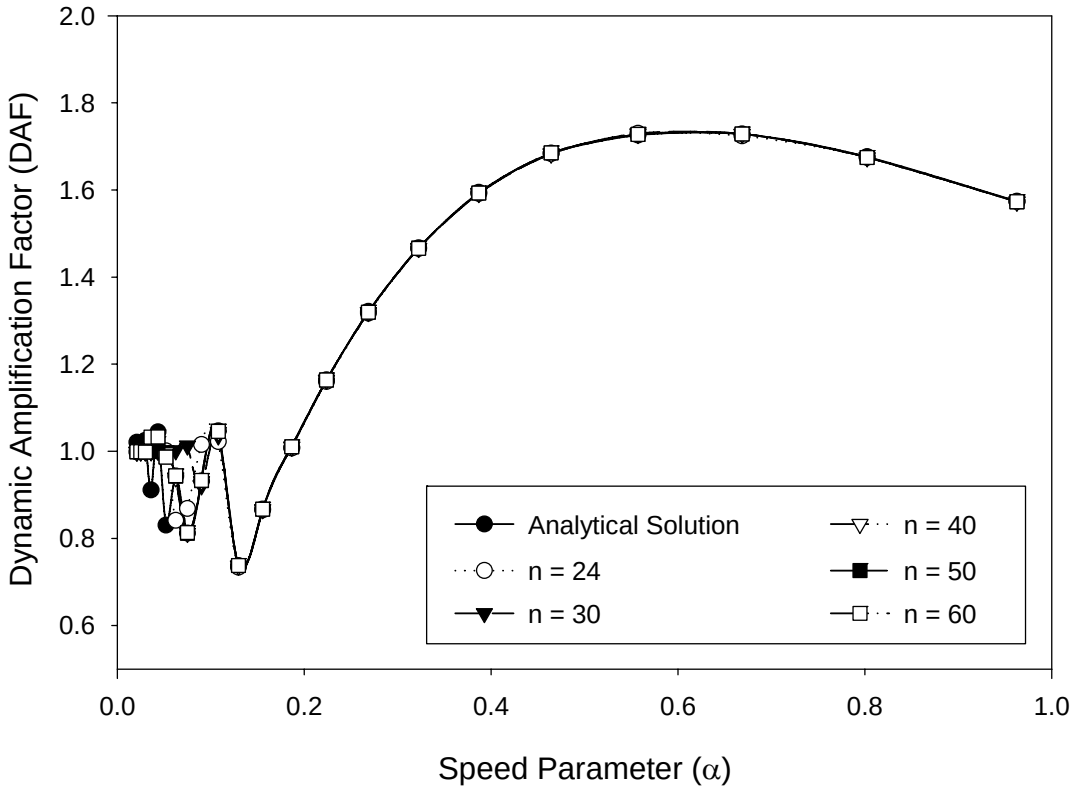

Figure 3.17: Effect of number of nodal points on solution accuracy

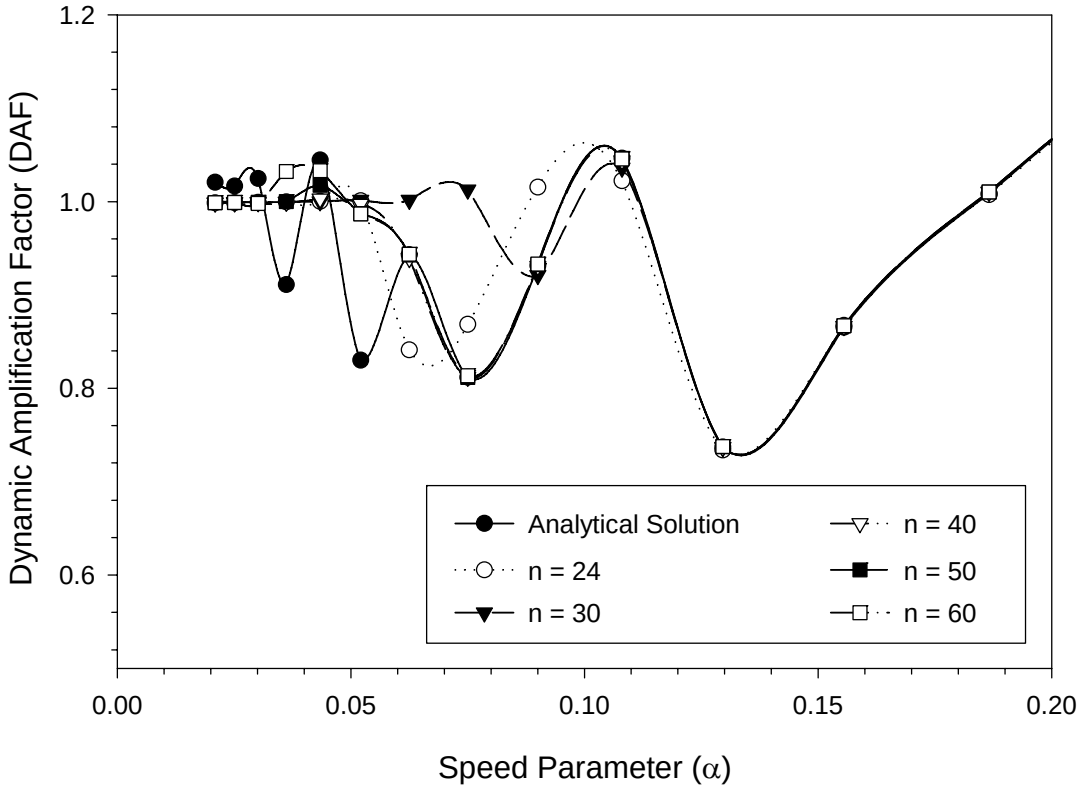

Figure 3.18: Effect of number of nodes on solution accuracy in low speed parameter range

3.2 Treatment of moving mass (*Inglis* approach):

Inglis [9] studied the effects of mass of the moving load on the dynamic response of a beam by assuming a fixed definite location to associate the point of action of the mass (as in a lumped mass model). The moving mass solution is then a combination of the response due to the moving force and the stationary mass at a certain point. The governing equation of motion for the beam in this case is expressed as

$$\mu\frac{\partial^2 W(x,t)}{\partial t^2}+2\mu\omega_b\frac{\partial W(x,t)}{\partial t}+EI\frac{\partial^4 W(x,t)}{\partial x^4}=\delta(x-ct)P - \delta(x-x_0)M\frac{\partial^2 W(x,t)}{\partial t^2}\bigg|_{x=x_0} \tag{3.22}$$

The dynamic response of the beam was found to be very similar to the analytical solution for the moving force case, i.e., *Equation* 3.4 with the parameters $\omega_{(j)}, \omega_b$ and $\omega'_{(j)}$ replaced by $\overline{\omega}_{(j)}$, $\overline{\omega}_b$ and $\overline{\omega}'_{(j)}$ such that $\overline{\omega}_{(j)}{}^2 = \omega_{(j)}{}^2 \mu / \overline{\mu}$, $\overline{\omega}_b = \omega_b \mu / \overline{\mu}$ and $\overline{\omega}'_{(j)}{}^2 = \overline{\omega}^2_{(j)} - \overline{\omega}^2_b$. Here $\overline{\mu}$ is the effective linear density given by $\overline{\mu} = \mu\left(1 + \frac{2P}{G} Sin^2 \frac{j\pi x_0}{L}\right)$ with G representing the total weight of the beam. The variation of natural frequency of the beam, i.e., the ratio $\frac{\overline{\omega}_{(1)}}{\omega_{(1)}}$ is minimal near the center of the beam especially for small values of P/G ratio. This is also the point of action of mass where the effective mass $\overline{\mu}$ assumes its maximum value, i.e., $\mu\left(1 + \frac{2P}{G}\right)$, and hence by assuming the mass to be located at the center of the beam, the dynamic response of the beam due to moving mass is better approximated.

The moving mass response using *Inglis* approach is shown in the *Figure 3.19* along with the analytical solution for the moving force problem under the same conditions. The effects of moving mass (due to simplified assumption that the mass is concentrated at the center of the beam) showed an increase in the dynamic response of the bridge structure and the maximum response at the center of the beam was observed when the load just passed the center of the beam, i.e., at time $t = 0.5L/c = 0.4499 \text{sec}$ or $\tau = 0.5$ (data: length = 25 *m* and speed = 27.778 *m/s*) which is expected however with a dynamic response magnitude that is 1.2 times higher than the dynamic response only due to moving force.

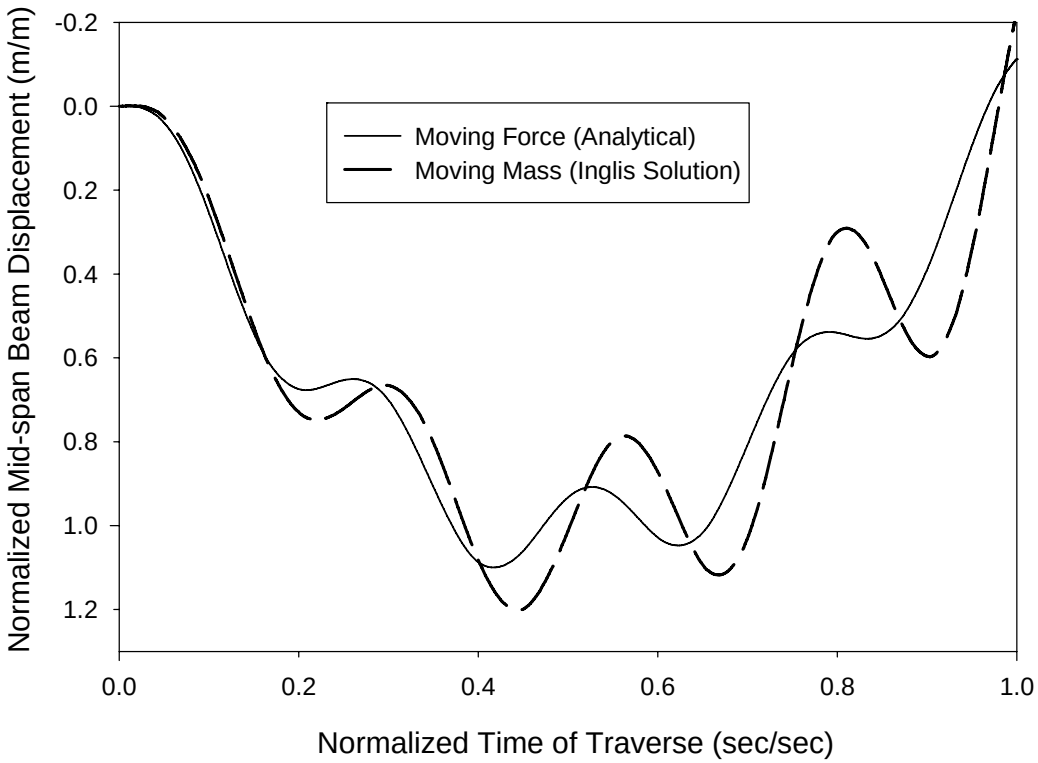

Figure 3.19: Dynamic beam response due to moving mass using *Inglis* approach

3.3 *Euler-Bernoulli* beam subjected to moving mass:

The moving mass system can either be a moving concentrated mass or an assembly of masses, i.e., a system of sprung and unsprung masses connected via a spring and dashpot system. The former case is simply termed as moving mass problem, while the latter is referred to as a moving oscillator problem.

In this section, we consider only an unsprung concentrated mass moving over an *Euler* beam at a constant speed, with an assumption that the moving mass maintains its contact with the beam during the entire traverse period. The moving mass system, just like moving force system, is mainly used to study the dynamic behavior of bridge structures, and ignores any dynamic behavior of vehicles arising from vehicle-bridge interactions.

3.3.1 Analytical solution to moving mass problem:

Following the usual notations, governing equation of motion for a beam traversed by a moving mass at a constant speed is given by,

$$\mu \frac{\partial^2 W}{\partial t^2} + 2\mu\omega_b \frac{\partial W}{\partial t} + EI \frac{\partial^4 W}{\partial x^4} = \delta(x - ct)\{Mg - M \frac{\partial^2 W}{\partial t^2}\Big|_{x=ct}\} \qquad (3.23)$$

The spatial and temporal variables are then normalized using parameters, $\xi = x/L$ and $\tau = ct/L$, as well as recognizing that $\frac{L^4}{EI} M \frac{\partial^2 W}{\partial t^2} = \frac{L^4 M}{EI T^2} \frac{\partial^2 W}{\partial \tau^2} = \pi^2 \alpha^2 \kappa L \frac{\partial^2 W}{\partial \tau^2}$, where κ is the mass ratio ($\kappa = \frac{M}{\mu L}$), the governing equation given in Equation 3.23 becomes,

$$\pi^2\alpha^2 \frac{\partial^2 W}{\partial \tau^2} + 2\pi^3 \alpha\beta \frac{\partial W}{\partial \tau} + \frac{\partial^4 W}{\partial \xi^4} = \frac{2\,Sin\pi\xi\, Sin\pi\tau}{L}\left\{\frac{Mg}{\Delta_{st}} \frac{L^4}{EI} - \pi^2\alpha^2\kappa L \frac{\partial^2 W}{\partial \tau^2}\Big|_{\xi=\tau}\right\}$$

$$= \left\{\frac{2\,Mg}{\Delta_{st} L} \frac{L^4}{EI} - 2\pi^2\alpha^2\kappa \frac{\partial^2 W}{\partial \tau^2}\Big|_{\xi=\tau}\right\} Sin\pi\xi\, Sin\pi\tau \qquad (3.24)$$

$$= \left\{96 - 2\pi^2\alpha^2\kappa \frac{\partial^2 W}{\partial \tau^2}\Big|_{\xi=\tau}\right\} Sin\pi\xi\, Sin\pi\tau$$

The above governing equation has no exact solution but an equivalent analytical solution could be obtained by using iterative schemes. For example, one such iterative scheme was used by *Michaltsos* [54] to solve the moving mass problem where the governing

equation, i.e., Equation 3.24 is solved first for moving force case (with the second term on the right hand side, i.e., $\pi^2\alpha^2\kappa L\dfrac{\partial^2 W}{\partial\tau^2}$ kept zero), and later on the second term $\pi^2\alpha^2\kappa L\dfrac{\partial^2 W}{\partial\tau^2}$ is determined from the known values of displacement, and a iterative solution procedure is used thereafter.

3.3.2 DQM implementation and solution:

The DQ analog for the above equation becomes

$$\pi^2\alpha^2\sum_{k=1}^{n}B_{jk}^{(t)}W_{ik}+2\pi^3\alpha\beta\sum_{k=1}^{n}A_{jk}^{(t)}W_{ik}+\sum_{k=1}^{m}D_{ik}^{(x)}W_{kj}= \left(96-2\pi^2\alpha^2\kappa\sum_{k=1}^{n}B_{jk}^{(t)}W_{ik}\Big|_{\xi=\tau}\right)Sin\,\pi\xi\,Sin\,\pi\tau \tag{3.25}$$

If mode superposition principle is used to express the transverse deflection, the spatial component is separated from temporal component, and the scheme is reduced to one containing only temporal components, as given below:

$$\frac{\alpha^2}{\pi^2}\frac{d^2Y_n}{d\tau^2}+\frac{2\alpha\beta}{\pi}\frac{dY_n}{d\tau}+n^4Y_n-\left(1-\frac{2\kappa\alpha^2}{\pi^2}\frac{d^2W}{d\tau^2}\Big|_{\xi=\tau}\right)Sin\,n\pi\tau=0 \tag{3.26}$$

which is further expressed in terms of modal coordinates $Y_n(\tau)$ as

$$\frac{\alpha^2}{\pi^2}\frac{d^2Y_n}{d\tau^2}+\frac{2\alpha\beta}{\pi}\frac{dY_n}{d\tau}+n^4Y_n-\left\{1-\frac{2\kappa\alpha^2}{\pi^2}\sum_{j=1}^{\infty}\left(\frac{d^2Y_j}{d\tau^2}Sin\ j\pi\tau\right)\right\}Sin\,n\pi\tau=0 \qquad (3.27)$$

where in the *Equation 1*, $W=W(x,t)=\sum_{n=1}^{\infty}Y_n(t)Sin\frac{n\pi x}{L}$ is used to decouple the spatial and temporal terms. The actual vertical acceleration of the moving mass includes the mixed partial derivatives called convective terms, and the contact force due to moving load considering the convective terms (*H. P. Lee* [moving mass 1995]) is given by,

$$F_c=Mg-M\left\{\frac{\partial^2W}{\partial x^2}+2c\frac{\partial^2W}{\partial x\partial t}+c^2\frac{\partial^2W}{\partial t^2}\right\} \qquad (3.28)$$

The DQ procedure could be easily extended for the moving mass problem with convective terms since the mixed derivatives were expressed in a similar way as were the spatial or temporal derivatives. The convective terms are significant only for very high speed parameter and were neglected in the above equations, i.e., *Equations 3.24-3.27*.

3.3.3 Discussion on results:

The moving mass problem has no exact solution but researchers in the past such as *Stanisic* [29, 36], *Mackertich* [47] and others were able to represent the solution in series form. *Michaltsos* [54] proposed an iterative scheme resulting in a series solution that is similar to the *Fourier* series solution of a moving force problem. The computational time for the solution was found to be excessively higher than the solution time required by the DQM for the same set of data. For a set of data with 24 temporal nodes and first 10 modes, analytical solution given by *Michaltsos* took about 55 minutes while the DQM

took only around 2 minutes. Also, a direct email conversation with *Michaltsos* helped the author (me) to attribute the excessive computational time to *Mathematica*'s inability to handle integration functions applied on the summation of a product of three or more sine (trigonometric) functions. *Figures 3.20* and *3.21* show the dynamic response of the beam for moving force and moving mass models using analytical and DQ methods. The moving mass solution indicated that the dynamic response of the bridge structures considering inertia effects is slightly higher than the dynamic response due to moving forces alone even at low mass ratios.

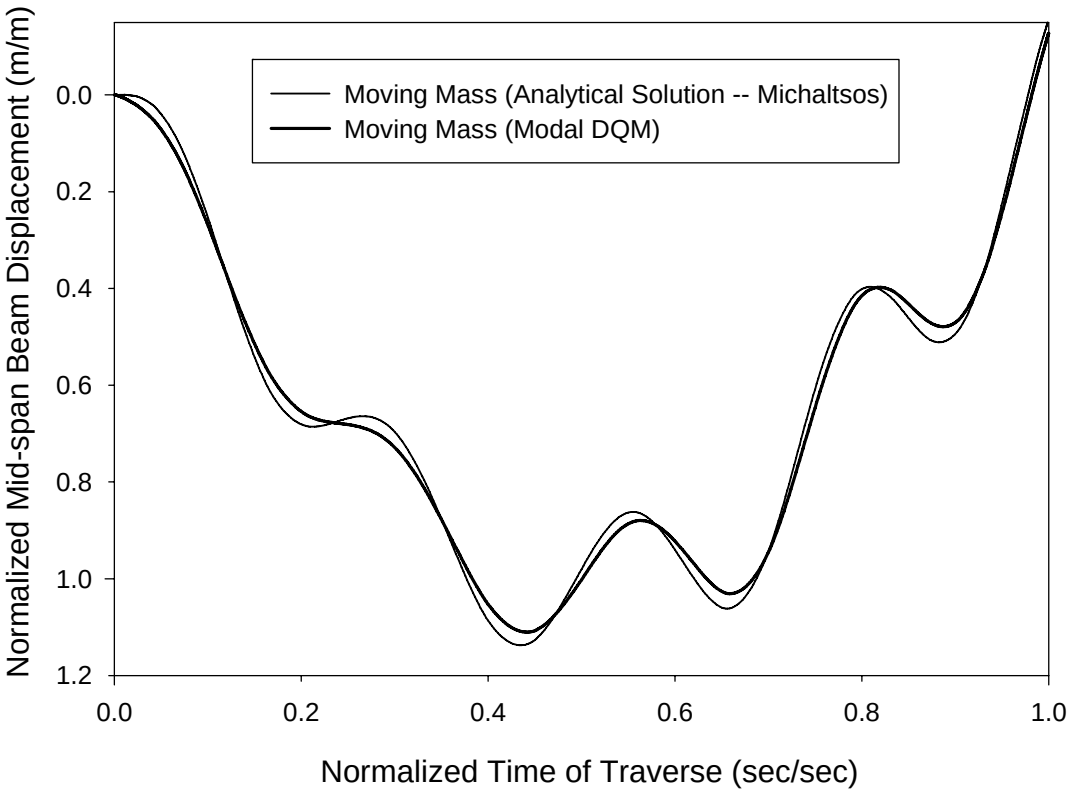

Figure 3.20: Dynamic beam response due to moving mass using DQM and analytical solution

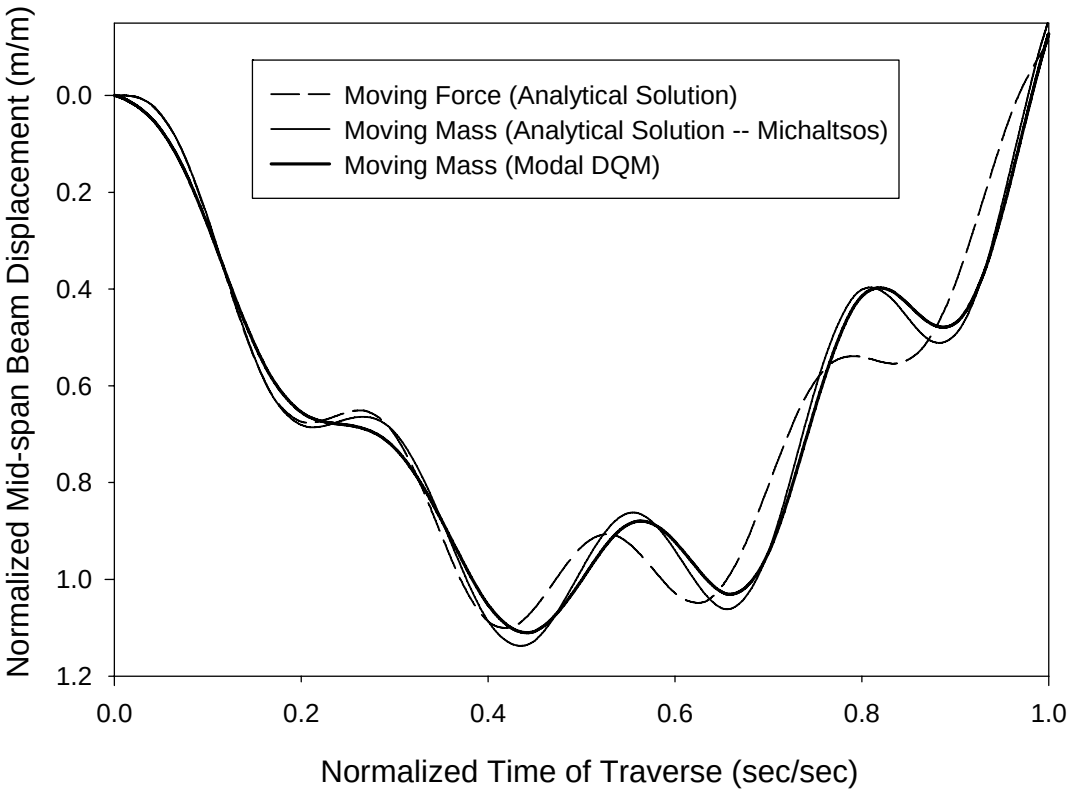

Figure 3.21: Dynamic beam response due to moving force and moving mass – comparison of analytical and DQM solutions

The *Figure 3.22* compares the dynamic response of the bridge structure using moving force and moving mass model and the *Figure 3.23* presents a closer look on the same at low speed parameter ranges. The dynamic amplification factor from a moving mass model was found to be higher than that obtained from a moving force model for speed parameter range $0.05 \le \alpha \le 0.7$.

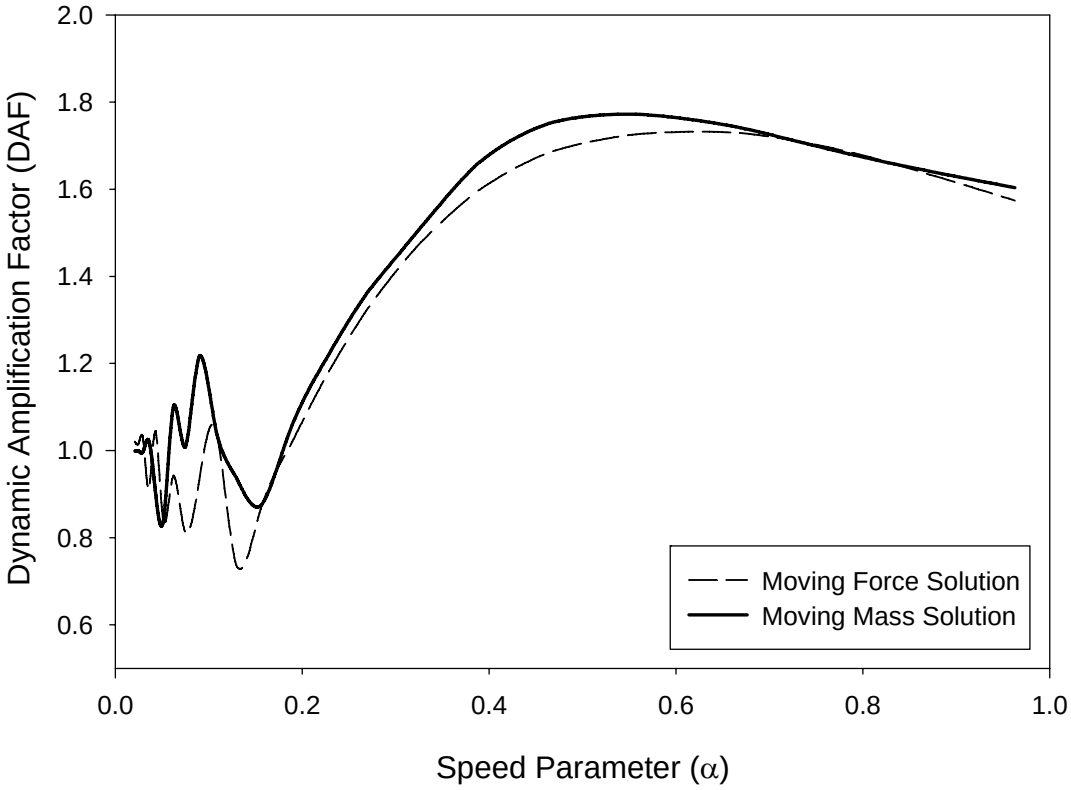

Figure 3.22: DAF vs. speed parameter for moving force and mass models

(κ = 0.098)

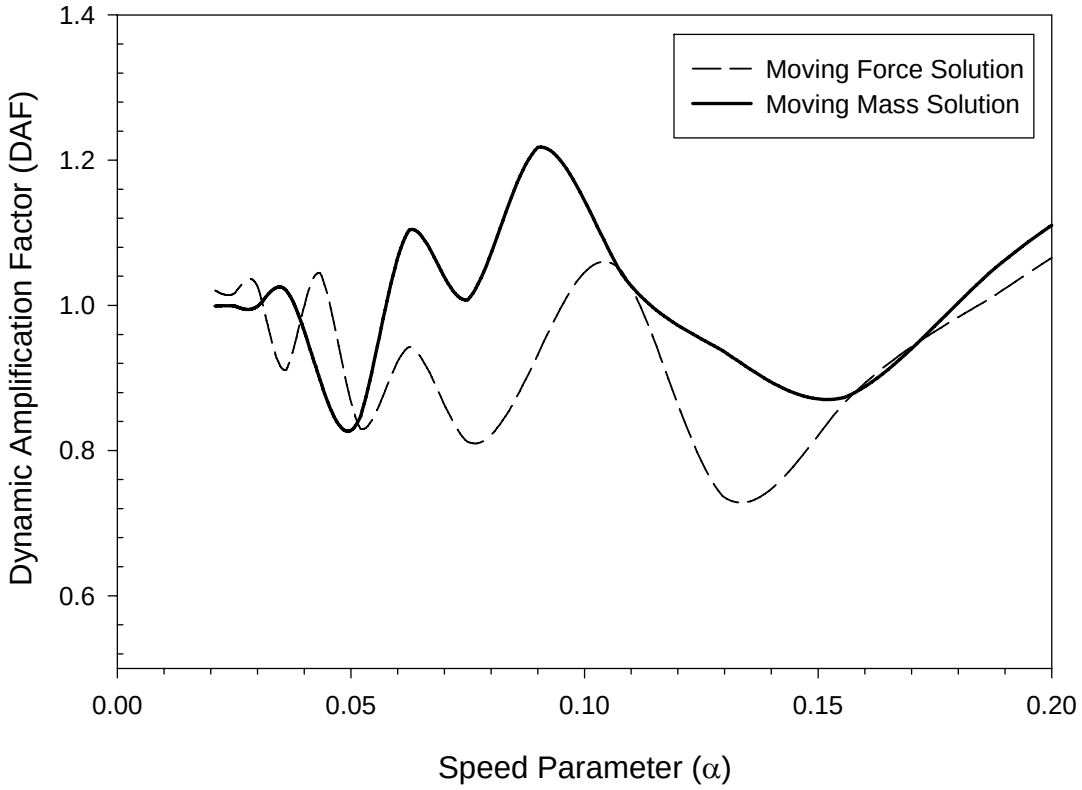

Figure 3.23: DAF vs. speed parameter for moving force and moving mass models in low speed parameter range

The dynamic response of the beam obtained using moving mass model with different mass ratios and speed parameters were plot in the *Figures 3.24 – 3.27*. The dynamic response of the beam increased with the increase in mass ratio, and specifically after the load just passed the mid-span of the beam.

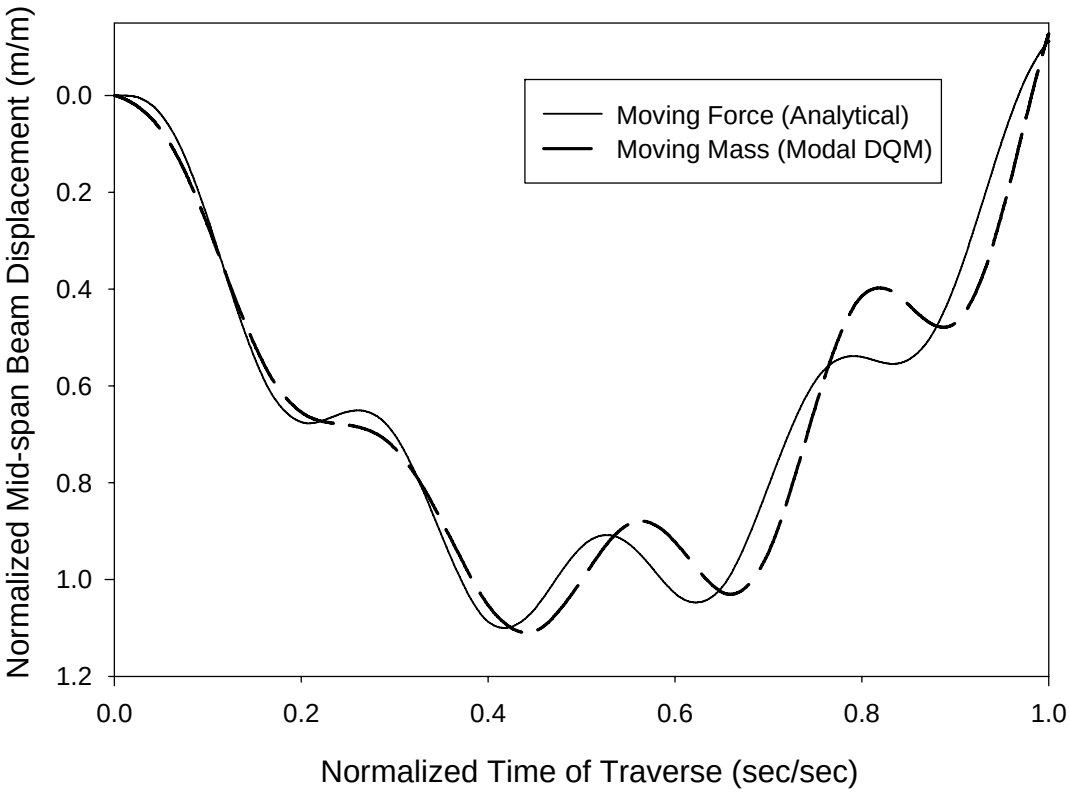

Figure 3.24: Normalized undamped mid-span beam displacement for moving force and moving mass model at $\alpha = 0.116$, $\kappa = 0.0998$

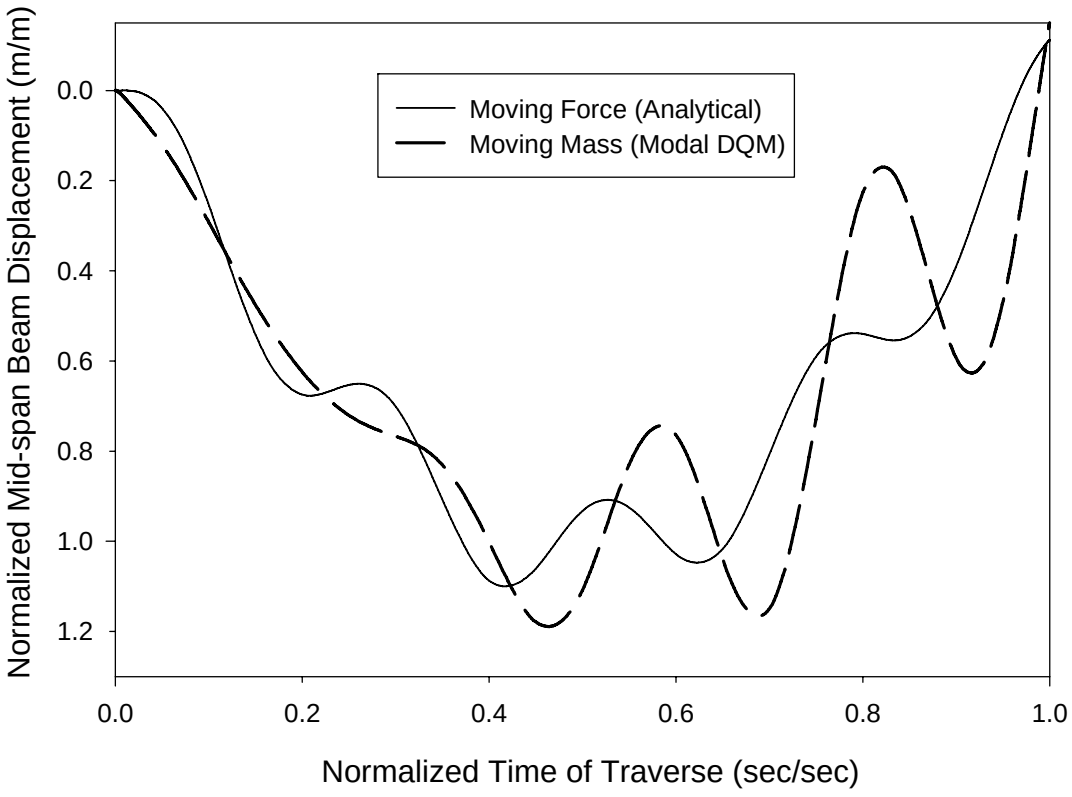

Figure 3.25: Normalized undamped mid-span beam displacement for moving force and moving mass model at $\alpha = 0.116$, $\kappa = 0.249$

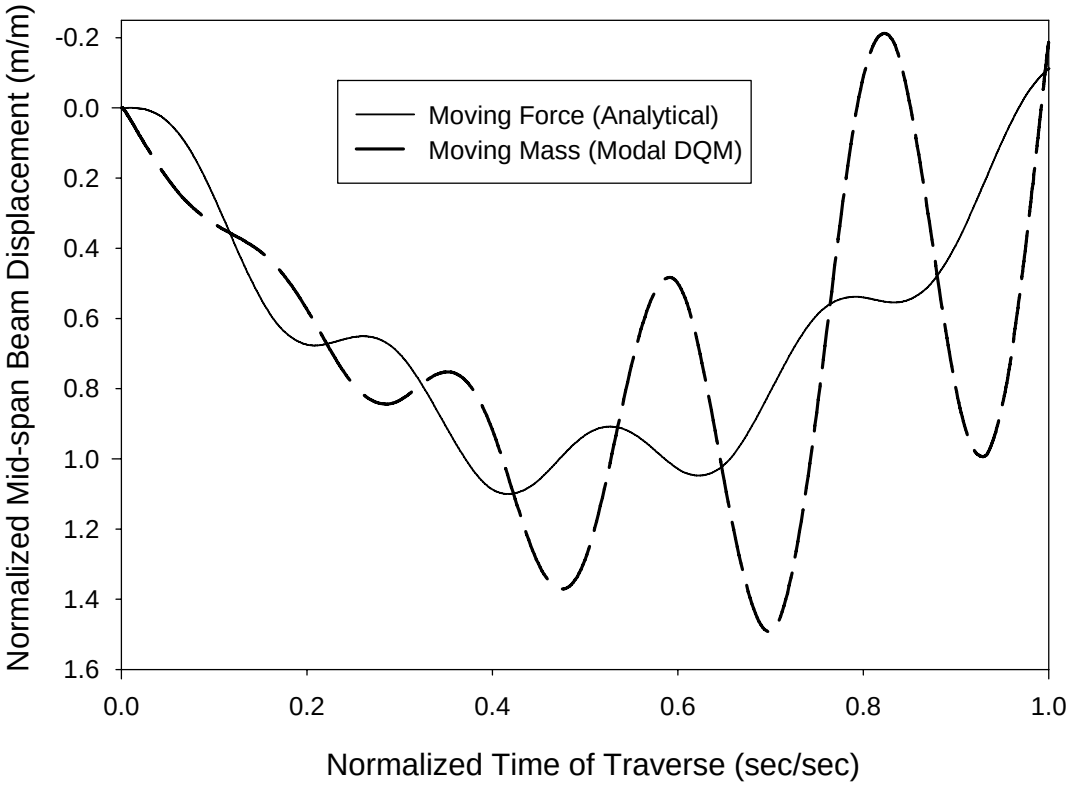

Figure 3.26: Normalized undamped mid-span beam displacement for moving force and moving mass model at $\alpha = 0.116$, $\kappa = 0.499$

The mid-span dynamic response of the beam decreased with the increase in the speed parameter at low mass ratios.

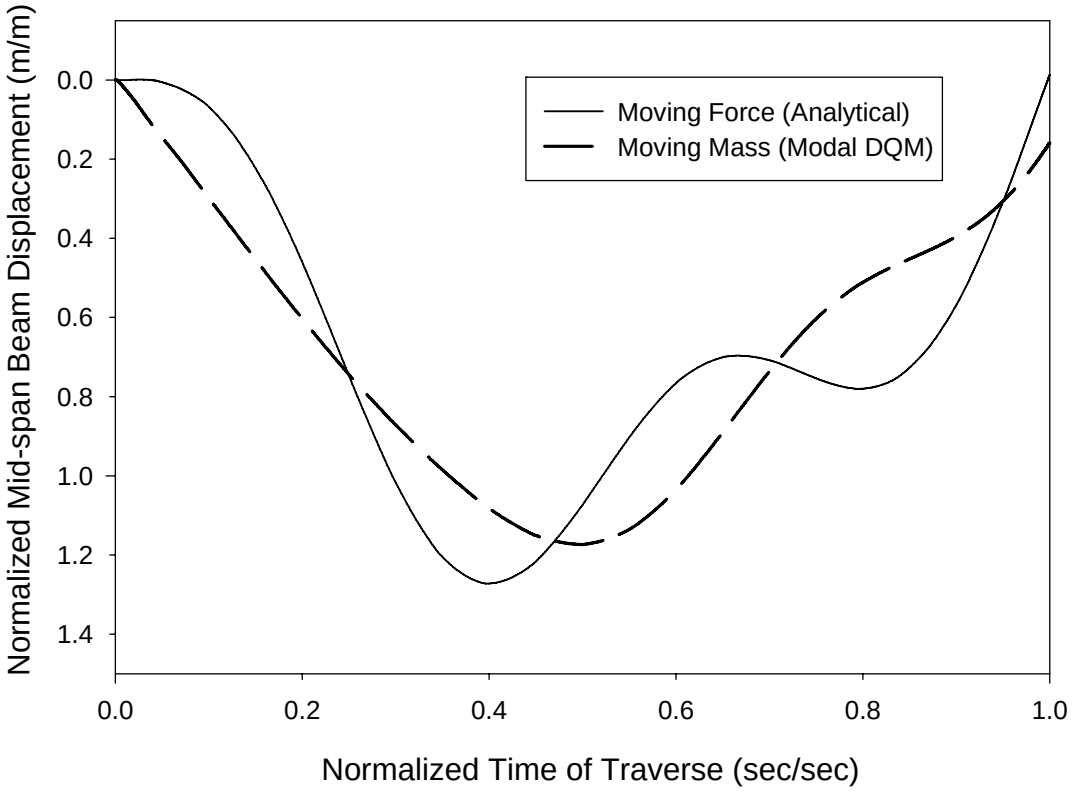

Figure 3.27: Normalized undamped mid-span beam displacement for moving force and moving mass model at $\alpha = 0.249$, $\kappa = 0.099$

The dynamic behavior due to the moving mass was studied for the parameters of influence, speed parameter, damping parameter and moving load to bridge mass ratio. The results indicated similar behavior in the dynamic response of the beam due to moving mass as observed in the case of moving force. The *Figure 3.28* shows the effect of mass ratio on the dynamic amplification factor which is noticeable in case of an undamped beam. The *Figure 3.29* shows the dynamic amplification factor obtained using moving mass model with the mass ratio $\kappa = 0.1$

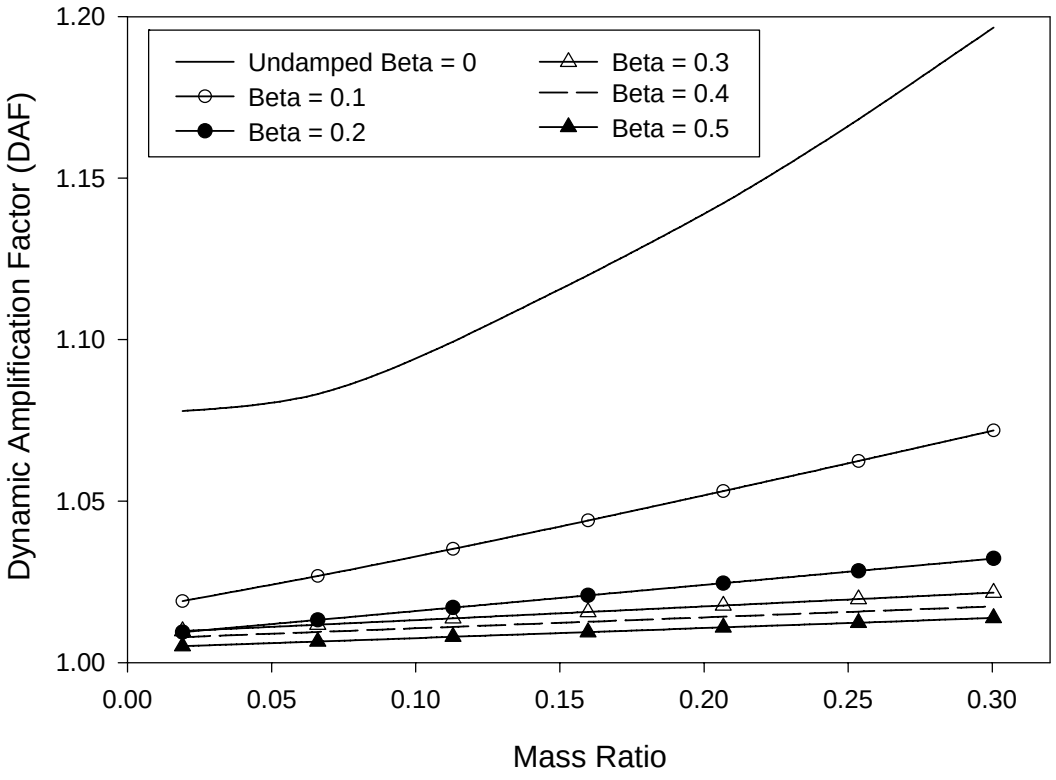

Figure 3.28: Effect of mass ratio on DAF of beam with different damping characteristics

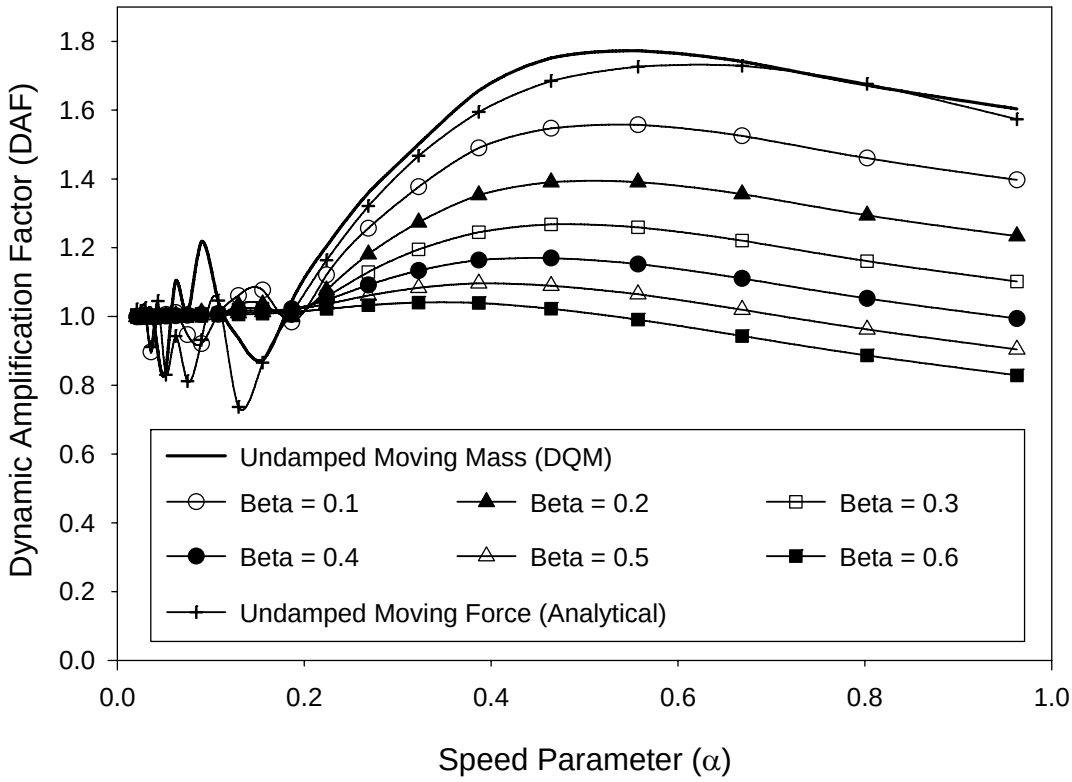

Figure 3.29: DAF vs. speed parameter for moving mass of $\kappa = 0.1$

In general, the dynamic response obtained using moving mass model appeared higher than that obtained using moving force model, and *Inglis* treatment of moving mass yielded higher dynamic response than that obtained using moving force and moving mass. Also, the application of DQM using various interpolation schemes were tested, and *Lagrange* type interpolation polynomial based DQM was chosen for further studies due to its simplicity and effectiveness.

Chapter 4: Two Point Moving Force System

Introduction:

The preceding chapter addressed the dynamic behavior of an idealized bridge structure subjected to a moving concentrated load with and without inertia effects. In this chapter, the dynamic behavior of an idealized bridge structure due to multiple moving loads is discussed using a two point moving load system. A two point moving load system could be used to represent either a two-axle moving vehicle whose total weight is considered to be distributed among its two axles (with a further simplification to a 1D model representation) or two vehicles (assumed to have each of their weights to be concentrated at a point) moving in the same direction. In the former case, both the point loads move at the same speed i.e., the separation distance between two moving loads considered is kept constant, while in the latter case they may move at same or different speeds. In this study, the dynamic effects of a two axle vehicle on a bridge structure is studied using a two point load system moving at a constant speed with a simplified beam model.

4.1 Governing equation of motion for beam and its DQ analog

The *Figure 4.1* below shows a system of two moving constant point loads P_1 and P_2 separated by a constant distance (*d*), with P_1 acting at a distance $x = ct$ at time *t* from one end of the beam, and P_2 acting at $x = ct - d$, where *c* is the speed of either of the moving loads.

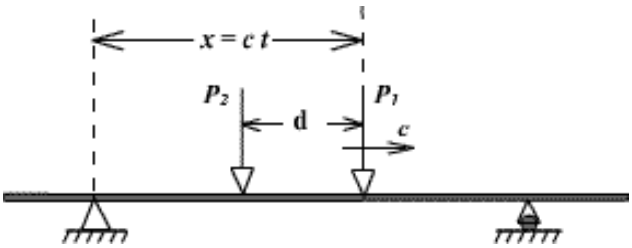

Figure 4.1: A simply supported beam traversed by a two point load at a constant speed 'c'

The governing equation of motion for the above system is given by

$$\mu \frac{\partial^2 W(x,t)}{\partial t^2} + 2\mu\omega_b \frac{\partial W(x,t)}{\partial t} + EI \frac{\partial^4 W(x,t)}{\partial x^4} = \delta(x-ct)P_1 + \delta(x-ct+d)P_2 \qquad (4.1)$$

The loading scenario for the above dynamic system involved three main phases i.e., 1) Only P_1 acts as the moving load system just entered the bridge, 2) Both the loads, P_1 and P_2, act on the bridge, and 3) Only P_2 acts as the load P_1 just passed the other end of the bridge. Another case in which no loads act on the bridge structure i.e., when both the loads were yet to enter the bridge deck or when both the loads completely passed the bridge structure, were not considered.

The above cases transform into conditions on time parameter i.e. from the case 1 above where the load P_1 acts on the beam, we have $ct \geq 0$ from P_1 and $ct - d < 0$ from P_2, or simply $0 \leq t < \frac{d}{c}$. Similarly the case 2 implies $\frac{d}{c} \leq t \leq \frac{L}{c}$ when both the loads are acting on the beam, and case 3 gives $\frac{L}{c} < t \leq \frac{L+d}{c}$ when only P_2 is acting on the beam. The

time of traverse for the first load is denoted by T (where $T = \frac{L}{c}$), and the total time of traverse (T_{tot}) for both the loads to completely cross the beam is given by $T_{tot} = T + \frac{d}{c} = \frac{L+d}{c}$.

The governing equation of motion for the beam subjected to moving two point load system defined by piecewise *Dirac Delta* forcing functions in accordance with the time zone is given by

$$\mu \frac{\partial^2 W(x,t)}{\partial t^2} + 2\mu\omega_b \frac{\partial W(x,t)}{\partial t} + EI \frac{\partial^4 W(x,t)}{\partial x^4}$$

$$= \begin{cases} \delta(x-ct)P_1 & \text{for} \quad 0 \le t < \frac{d}{c} \\ \delta(x-ct)P_1 + \delta(x-ct+d)P_2 & \text{for} \quad \frac{d}{c} \le t \le \frac{L}{c} \\ \delta(x-ct+d)P_2 & \text{for} \quad \frac{L}{c} < t \le \frac{L+d}{c} \end{cases} \tag{4.2}$$

The forcing function in the above governing equation, i.e., $\delta(x-ct)P_1 + \delta(x-ct+d)P_2$ can be expressed as shown in the *Equation 4.3* using harmonic approximation suggested by *Inglis* [11].

$$\delta(x-ct)P_1+\delta(x-ct+d)P_2 = \frac{2P_1}{L}\{Sin\frac{\pi x}{L}Sin\frac{\pi ct}{L}+Sin\frac{2\pi x}{L}Sin\frac{2\pi ct}{L}+...\}$$
$$+\frac{2P_2}{L}\{Sin\frac{\pi x}{L}Sin\frac{\pi(ct-d)}{L}+Sin\frac{2\pi x}{L}Sin\frac{2\pi(ct-d)}{L}+...\} \quad (4.3)$$

The space and time variables were normalized using $\xi = x/L$ and $\tau = t/T$, and the forcing function in terms of normalized space and time variables is given by

$$\delta(x-ct)P_1+\delta(x-ct+d)P_2 =$$
$$\frac{2P_1}{L}\{Sin\,\pi\xi\ Sin\,\pi\tau+Sin\,2\pi\xi\ Sin\,2\pi\tau+...\} \quad (4.4)$$
$$+\frac{2P_2}{L}\{Sin\,\pi\xi\ Sin\,\pi\left(\tau-\frac{d}{L}\right)+Sin\,2\pi\xi\ Sin\,2\pi\left(\tau-\frac{d}{L}\right)+...\}$$

The modal DQ procedure with the *Lagrange* interpolation scheme to generate the DQ coefficients was practiced to study the dynamic response of beam under moving two point load system. Alternatively a *Hermite-Fejér* interpolation scheme can also be used in place of *Lagrange* interpolating polynomial procedure.

The DQ analog in discretized, normalized form of the governing equation shown in the *Equation 4.2* is given by

$$\frac{\alpha^2}{\pi^2}\sum_{k=1}^{n} B_{sk} w_{jk} + \frac{2\alpha\beta}{\pi}\sum_{k=1}^{n} A_{sk} w_{jk} + j^4 w_{js}$$

$$= \begin{cases} Q_1 \, Sin \, j\pi\tau_s & \text{for } 0 \le \tau_s \le \dfrac{d}{L} \\ Q_1 \, Sin \, j\pi\tau_s + Q_2 \, Sin \, j\pi\left(\tau_s - \dfrac{d}{L}\right) & \text{for } \dfrac{d}{L} < \tau_s < 1 \\ Q_2 \, Sin \, j\pi\left(\tau_s - \dfrac{d}{L}\right) & \text{for } 1 \le \tau_s \le 1 + \dfrac{d}{L} \end{cases} \tag{4.5}$$

where $Q_1 = P_1 / P$, $Q_2 = P_2 / P$ with $P = P_1 + P_2$ and w_{js} represents time coordinate function of j^{th} mode at time $\tau = \tau_s$ such that

$$\frac{W(x_i, t_j)}{\Delta_{st}} = W(\xi_i, \tau_j) = \sum_{k=1}^{n} (w_{kj} \, Sin \, k\pi\xi_i) \tag{4.6}$$

The equivalent moving two point force model to a two axle vehicle with a sprung mass resting on two unsprung masses can be found out by assigning proportionate amount of sprung mass to each of the unsprung masses i.e. if P_s, P_{w1} and P_{w2} represent the sprung (chassis) and unsprung (wheel and axle) weights of the vehicle with an axle spacing of d, then the load parameters P_1 and P_2 used in the moving force system are expressed as $P_1 = P_{w1} + P_s \frac{d_2}{d}$ and $P_2 = P_{w2} + P_s \frac{d_1}{d}$ where d_1 and d_2 denote the distances from the

point of action of loads P_1 and P_2, respectively to the center of gravity of the sprung load P_s.

4.2 Results and Discussions:

The term $\frac{d}{L}$ in the *Equation 4.5* is sometimes referred to as the normalized inter-load spacing (*ILS*), and plays an important role in determining the dynamic behavior of the bridge due to a two-point moving load system. *Brady and O'Brien* [124] observed the effects of *ILS* on the maximum dynamic amplification factor at different speeds and concluded that vehicles with $ILS < 0.5$ moving at speeds such that $\alpha \geq 0.17$ produced maximum dynamic deflections more than 20% of the static mid-span deflection. Though *Brady and O'Brien* reported the above result for the case of two moving vehicles, the conclusion is applicable for the case of two point moving force system because the speeds of two moving vehicles were kept the same i.e. the separation distance is constant.

This study used a similar set of parameters used by *Brady and O'Brien* [124] to validate the DQ model with their findings. Some of the parameters describing bridge geometry and material properties were assumed so as to yield identical dependent (normalized) parameters used by *Brady and O'Brien*. Some of the parameters used were listed below: -

Length of the beam, $L = 25\,\text{m}$

Natural frequency of the beam, $\omega_{(1)} = 21.86\,\text{rad/sec}$

Linear density of the beam, $\mu = 2289\,\text{kg/m}$

The dynamic responses of the beam subjected to moving two point loads of same magnitude at inter-load spacing of 0.1 and 0.5 are presented in *Figures 4.2, 4.3, 4.4* and *4.5*. The two moving point loads representing the front and rear axle loads were taken as $P_1 = P_2 = 28241\ N$ such that the total load is $P = P_1 + P_2 = 56482\ N$, and since the governing equation is normalized, the magnitude of loads does not affect the behavior of the system i.e. the static mid-span deflection used to normalize the system variables is linearly proportional to the load magnitude.

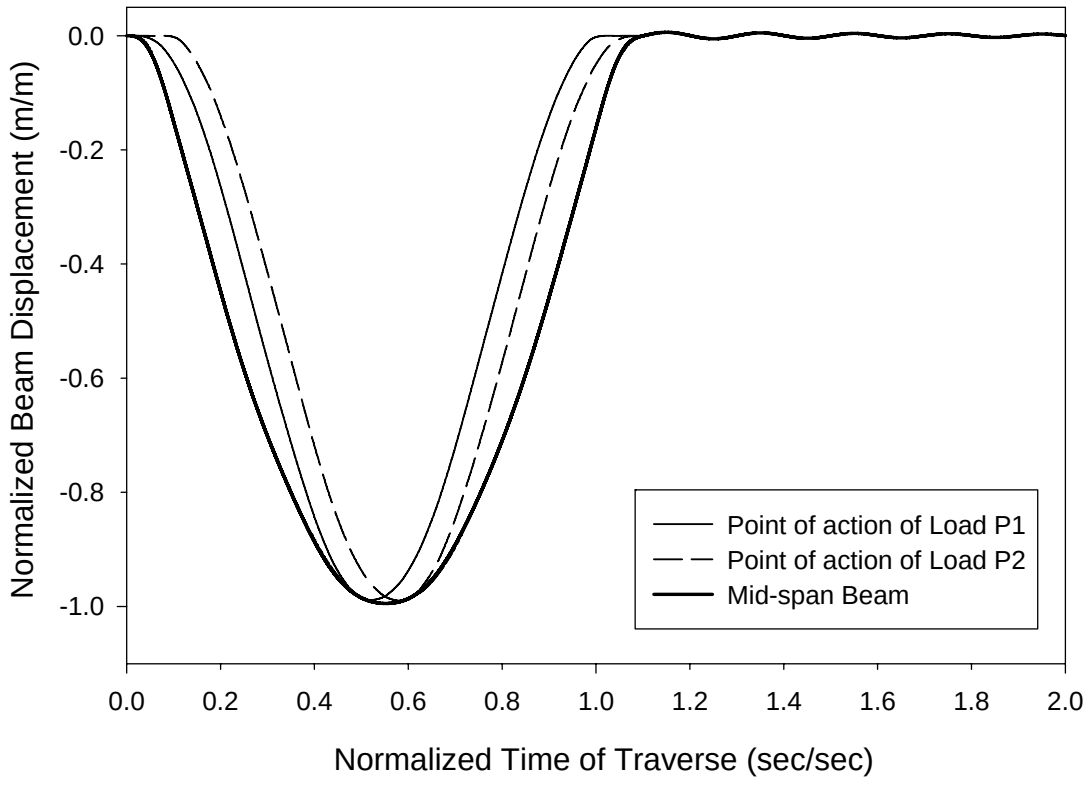

Figure 4.2: Dynamic response at the point of action of loads ($P_1 = P_2$) and at mid-span beam for α = 0.1, ILS = 0.1 and β = 0.03

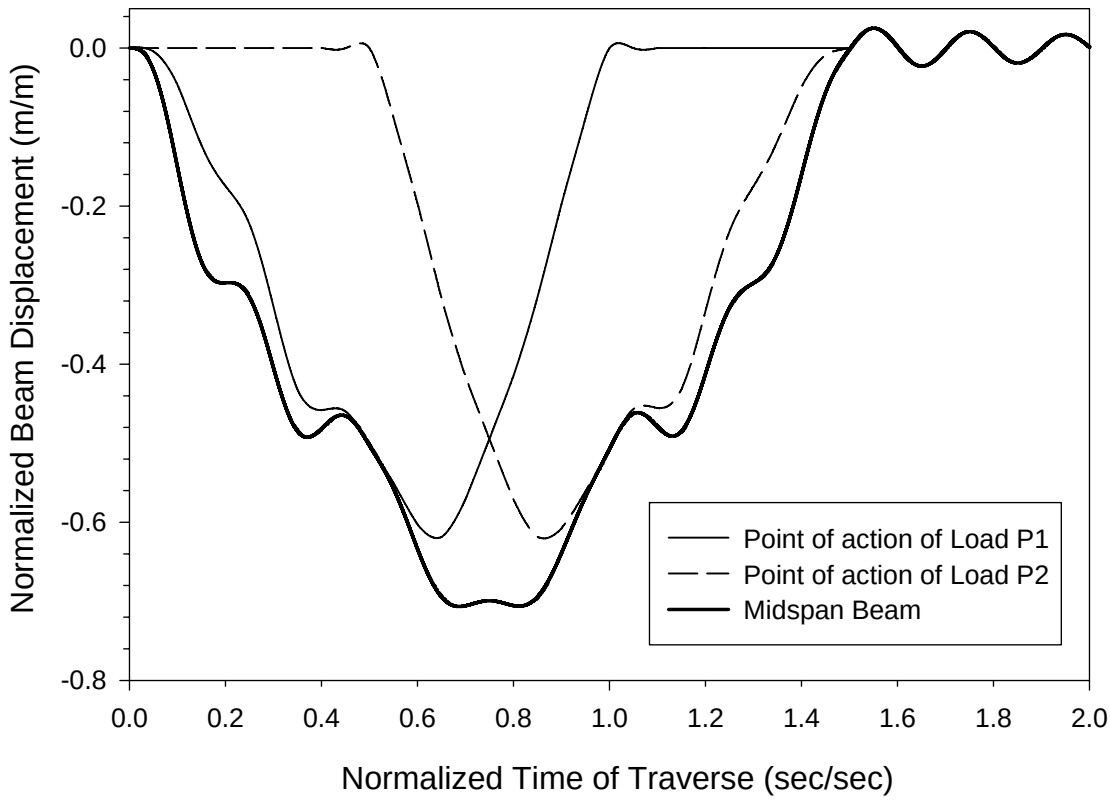

Figure 4.3: Dynamic response at the point of action of loads ($P_1 = P_2$) and at mid-span beam for α = 0.1, ILS = 0.5 and β = 0.03

The dynamic response of the bridge structure due to two equal moving point loads decreased with the increase in the ILS at speed parameter $\alpha = 0.1$. The normalized displacement dropped from approximately 1 at $ILS = 0.1$ to about 0.7 at $ILS = 0.5$ (see *Figure 4.2* and *4.3*). This behavior of reduced dynamic response for increasing ILS was also reported by *Kashif* [48].

The dynamic response increased with the increased speed parameter $\alpha = 0.2$ as shown in the *Figures 4.4* and *4.5*. This increased dynamic effect due to increasing speed parameter

can be observed by comparing the *Figure 4.2* with *Figure 4.4*, and *Figure 4.3* with *Figure 4.5*.

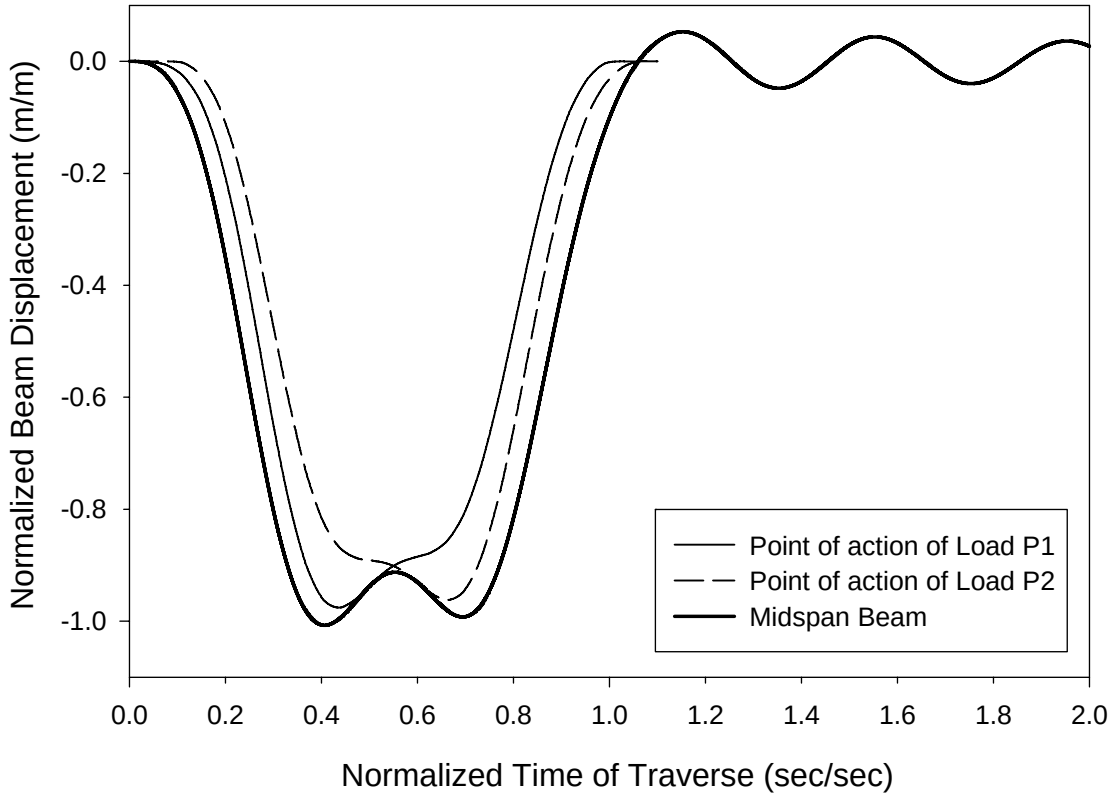

Figure 4.4: Dynamic response at the point of action of loads ($P_1 = P_2$) and at mid-span beam for α = 0.2, ILS = 0.1 and β = 0.03

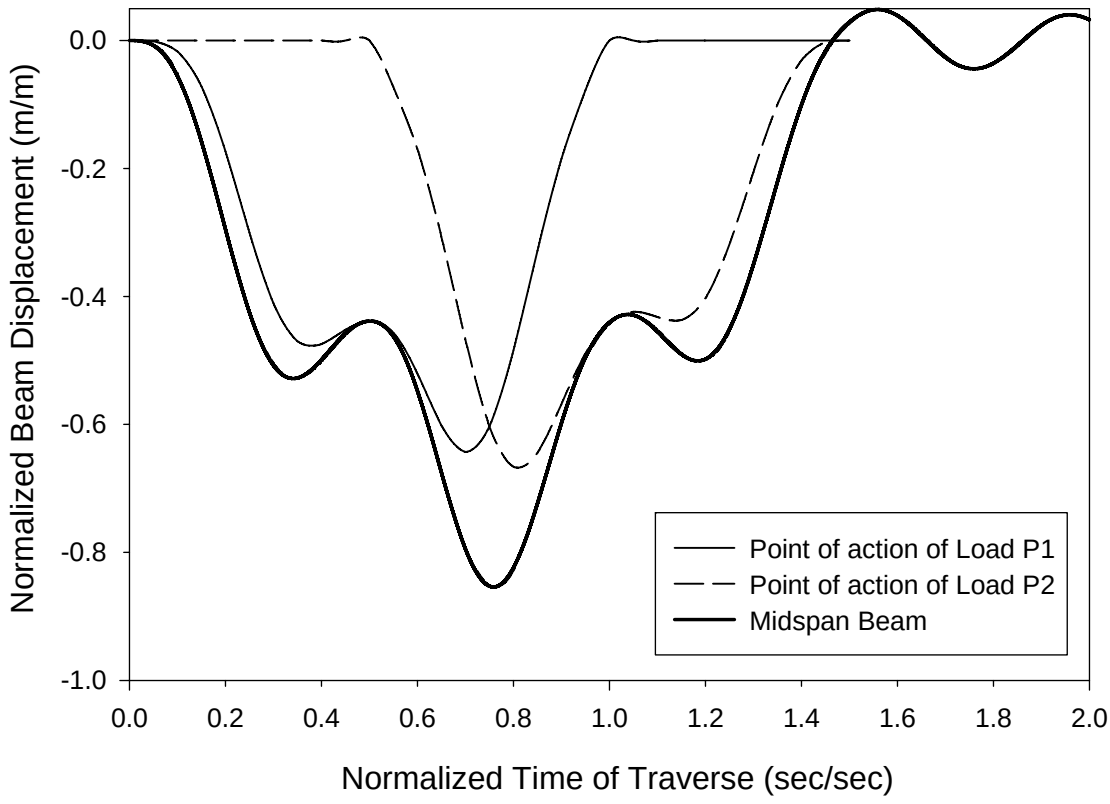

Figure 4.5: Dynamic response at the point of action of loads ($P_1 = P_2$) and at mid-span beam for α = 0.2, ILS = 0.5 and β = 0.03

The dynamic response of the beam subjected to two unequal moving point loads $P_1 = P_2 / 3$ (with $P = 37654\ N$) for $ILS = 0.1 \text{ and } 0.5$ were shown in the *Figures 4.6, 4.7, 4.8* and *4.9*. The dynamic response decreased with the increase in the *ILS* at speed parameter $\alpha = 0.1$ but the variation due to *ILS* effect seemed little. The normalized displacement dropped from approximately 1 at $ILS = 0.1$ to about 0.8 at $ILS = 0.5$. The dynamic response increased with the increased speed parameter $\alpha = 0.2$ as shown in the *Figures 4.8* and *4.9*.

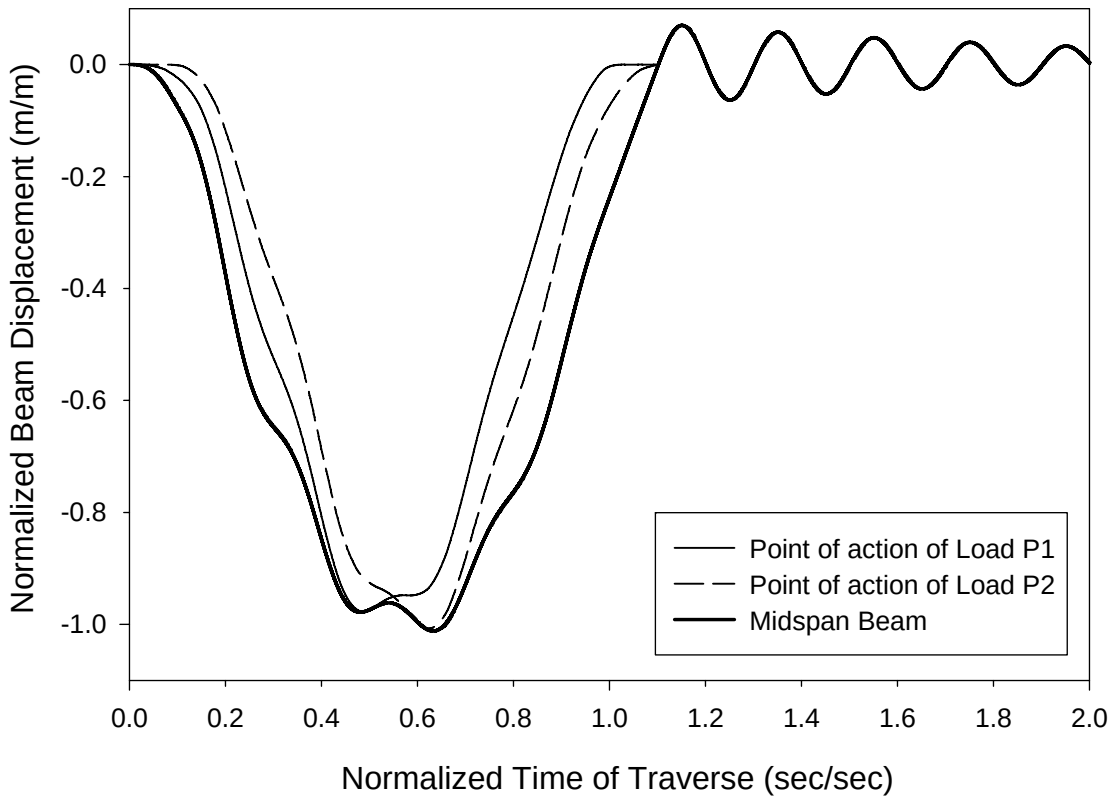

Figure 4.6: Dynamic response at the point of action of loads ($P_1 = P_2 / 3$) and at mid-span beam for α = 0.1, ILS = 0.1 and β = 0.03

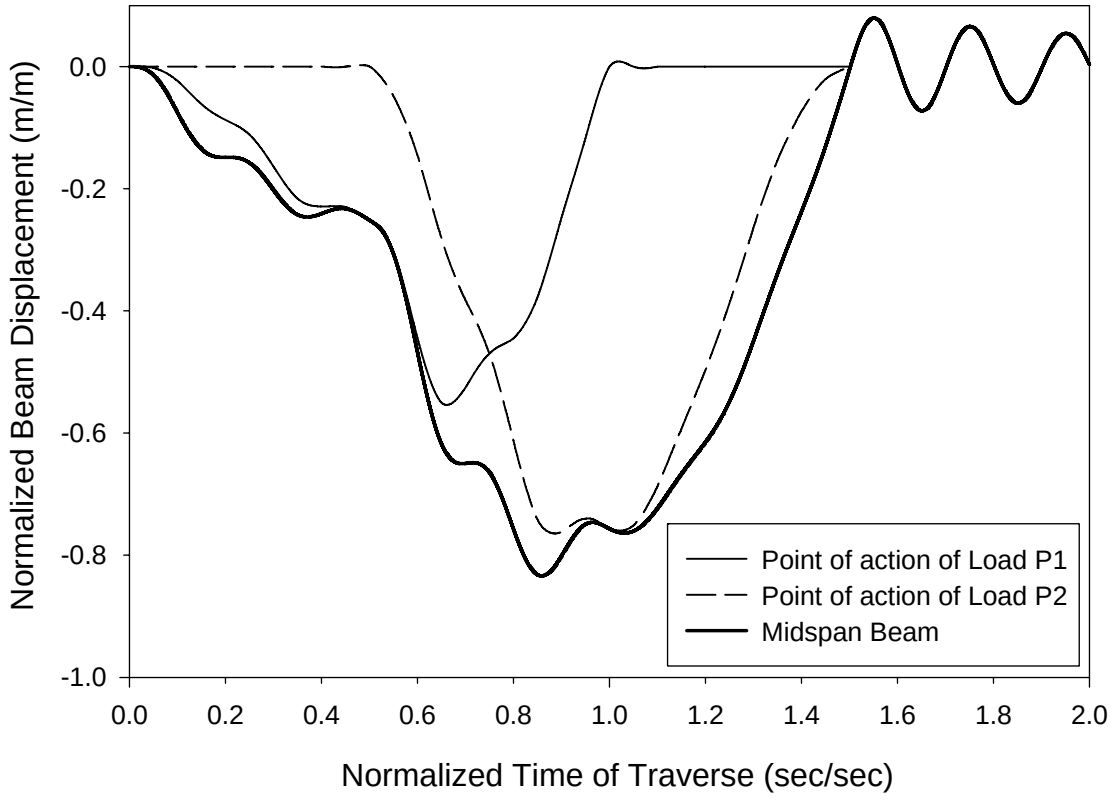

Figure 4.7: Dynamic response at the point of action of loads ($P_1 = P_2 / 3$) and at mid-span beam for α = 0.1, ILS = 0.5 and β = 0.03

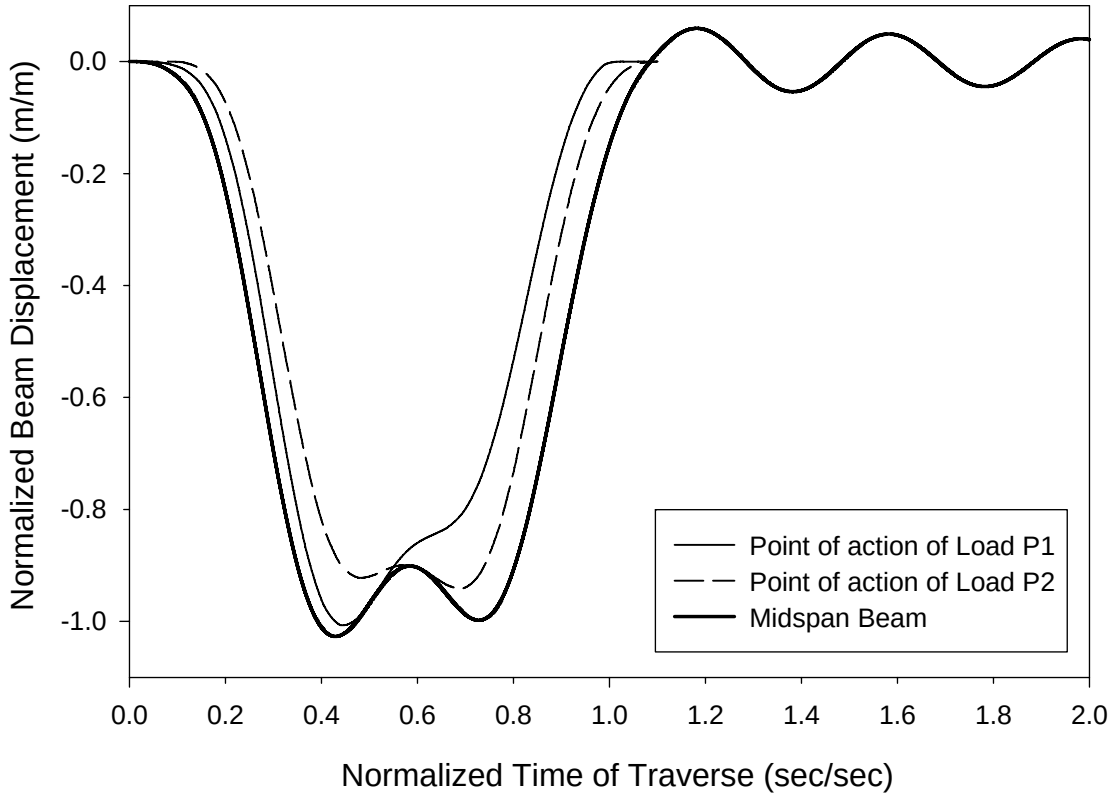

Figure 4.8: Dynamic response at the point of action of loads ($P_1 = P_2 / 3$) and at mid-span beam for α = 0.2, ILS = 0.1 and β = 0.03

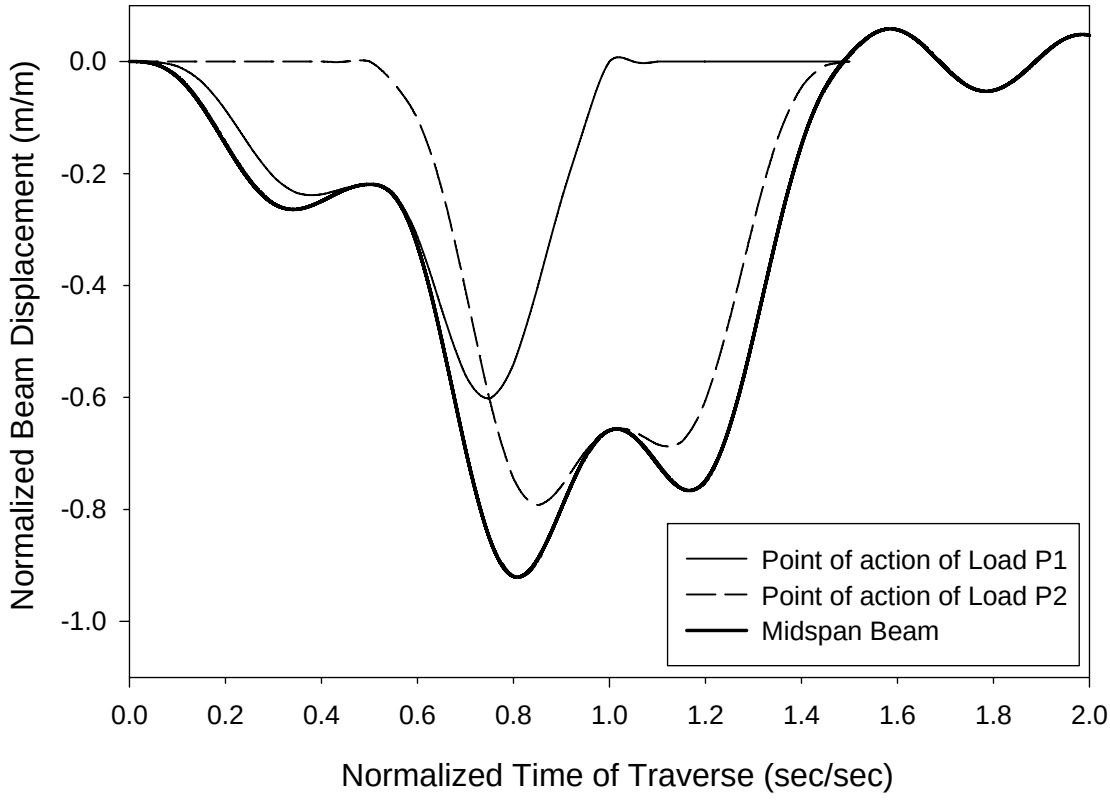

Figure 4.9: Dynamic response at the point of action of loads ($P_1 = P_2 / 3$) and at mid-span beam for α = 0.2, ILS = 0.5 and β = 0.03

The deflected beam shape at a few selected normalized time levels for a beam subjected to a two equal moving point loads with $ILS = 0.1$ were shown in the *Figure 4.10*. Similar behavior with a reduced normalized deflection value was seen for the case $ILS = 0.5$.

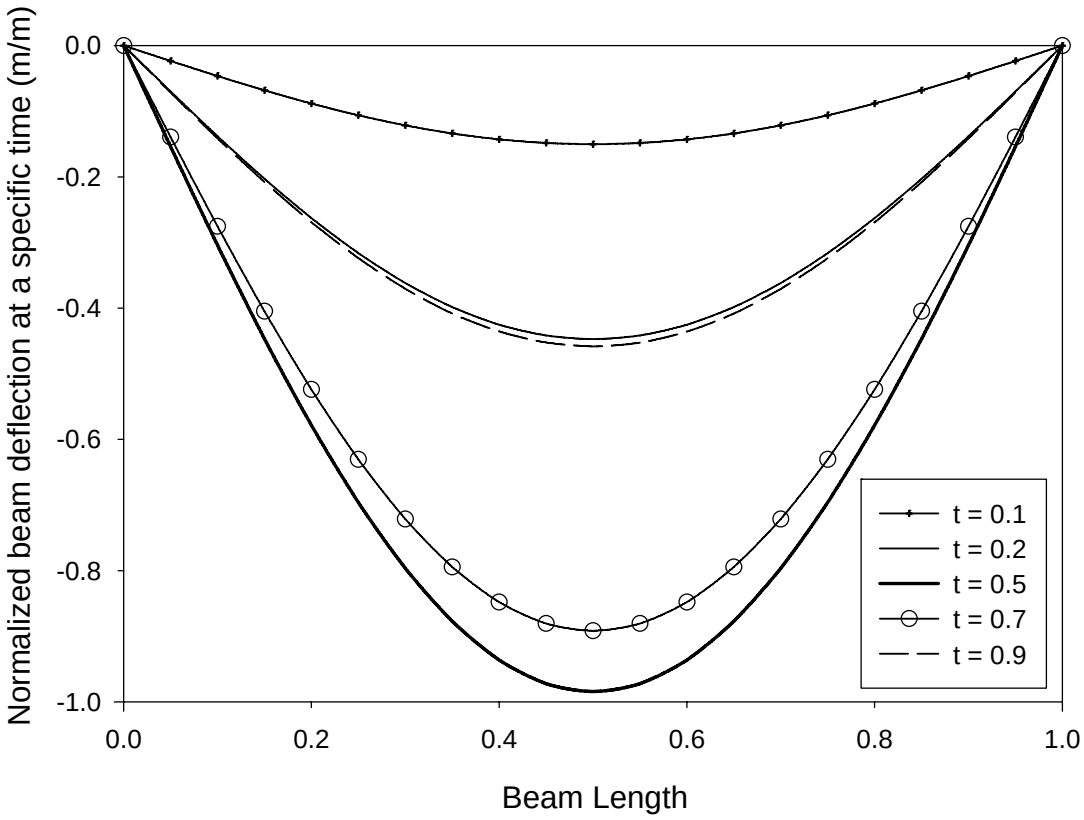

Figure 4.10: Deflected beam shape at any instant of time (normalized)

From the above presented results, it is observed that the increase in *ILS* reduced the dynamic response of the system. The present study found conforming results on the conclusions of *Brady and O'Brien* [124] on the nature of dynamic response with regard to the *ILS* but also found contradicting results on the comparison of bridge dynamic behavior due to a moving point load and two moving point load system.

It is also interesting to note that in their paper [124], *Table 1* [124] did not correlate well with the inferences from *Figure 5* [124], i.e. the *Figure 5* [124] shows that $\alpha \geq 0.27$ to yield dynamic amplification factors greater than 1.2 for $ILS < 0.5$. (seems a typo in the

Table 1 – 0.17 should be 0.27, but the discussion on *Page 251* [124] of the same paper also repeated 0.17)

The dynamic response of the bridge was found to reach its maximum in the speed parameter range [0.55-0.65] at $ILS = 0.1$. The dynamic response showed a decreasing pattern with the increased *ILS* from $ILS = 0.1$ to 0.5. For $ILS > 0.5$ also, the dynamic amplification factor decreased with increasing *ILS* due to the fact that when the second wheel is entering the span, the first wheel has already moved past the mid-span of the bridge whereas in the case of $ILS < 0.5$, the dynamic response was found to be a resultant of a varied combination of the both the loads acting on the bridge.

A likely justification for the lower dynamic amplification factor with increased *ILS* is that the dynamic amplification factor for a two point load system is defined on the basis of maximum static deflection due to equivalent total load acting at the mid-span of the beam. While this definition holds reasonable for the case $ILS < 0.5$, it raises doubts for the case $ILS > 0.5$ since the first load has already crossed the center of the bridge when the second load is entering the bridge. Additionally for the case $ILS = 1$, the two loads act in the absence of the other as if it is equivalent to the case of a moving point force system for which the normalization of the dynamic response is carried with respect to the maximum static deflection due to a point force acting at the mid-span beam.

Brady and O'Brien did not detail their basis for comparing the variation of amplification factor on speed parameter for single and two moving point loads. Since *Brady and*

O'Brien discussed the bridge response due to two moving vehicles (and compared them with the response due to a moving point load), this study assumed that the single moving vehicular load is the same as either of the two moving vehicles' loads i.e. in this study, the single moving point load equals halve the total load of the two axle system. Also it is noted that in the other case i.e. taking the single moving point load to be equal to the total load of the two axle system, the normalized bridge displacement in the latter case should be similar to that in the former since the static mid-span deflection is increased two-fold. Differences between these two cases could become noticeable either when the effects due to *VBI* phenomenon are included or when the dynamic response is expressed in absolute scale.

The dynamic amplification factor recorded at the mid-span of the beam at different speed parameters for a moving point load and two point load system were shown in the *Figure 4.11*. The present study found that the dynamic amplification factor for a two point load system (with $ILS = 0.1$) to be less than that for a moving point load at most of the speed parameters (excluding a few local minimums such as the range $\alpha = 0.2 \text{ to } 0.25$), which contradicted the conclusive remarks of *Brady and O'Brien* [124]. It is interesting to add here that *Kashif* [48] concluded earlier that the dynamic response for a two axle moving load to be lower than that due to moving single axle load.

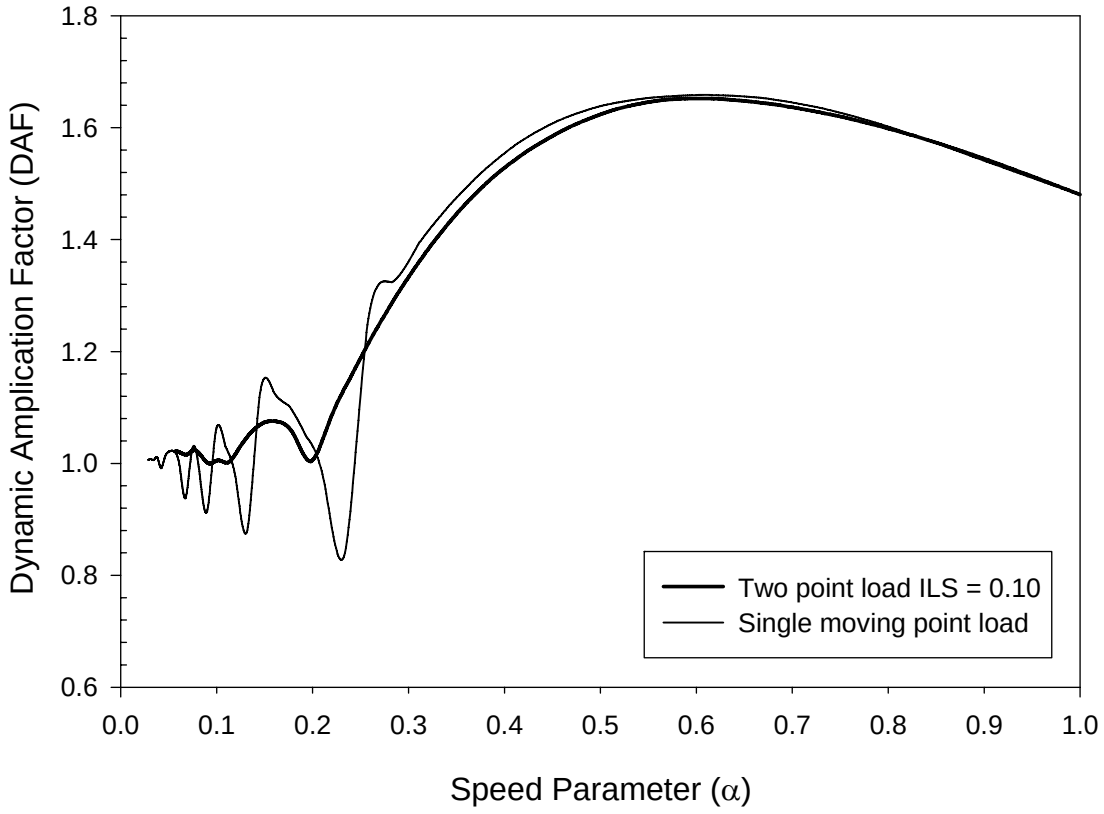

Figure 4.11: Dynamic Amplification factor vs. speed parameter for single and two point loads (ILS = 0.1)

Another way of looking at the comparison is to reduce the *ILS* to about 0.05 and notice the direction of behavior of the two point load system with respect to the single moving load system. The *Figure 4.12* shows that when the *ILS* is reduced to 0.05, the two point load system response moved toward the single moving point load system response (with the absence of local maximums and minimums presented in the single moving load system response). This characteristic hinted that the results obtained seemed satisfactory. This inference becomes stronger from the results of amplification factor vs. speed parameter provided by *Brady and O'Brien* [124] for two point load systems at different *ILS*. Because they concluded that at an ILS of 0.1, the response due to moving two point

load was higher than that due to a moving point load, and taking in to consideration their remarks on the decreasing dynamic amplification factor with increasing ILS (or increasing dynamic amplification factor with decreasing ILS), it is expected that the dynamic response due to two point load system at an ILS of 0.05 to be higher than that at an ILS of 0.1.

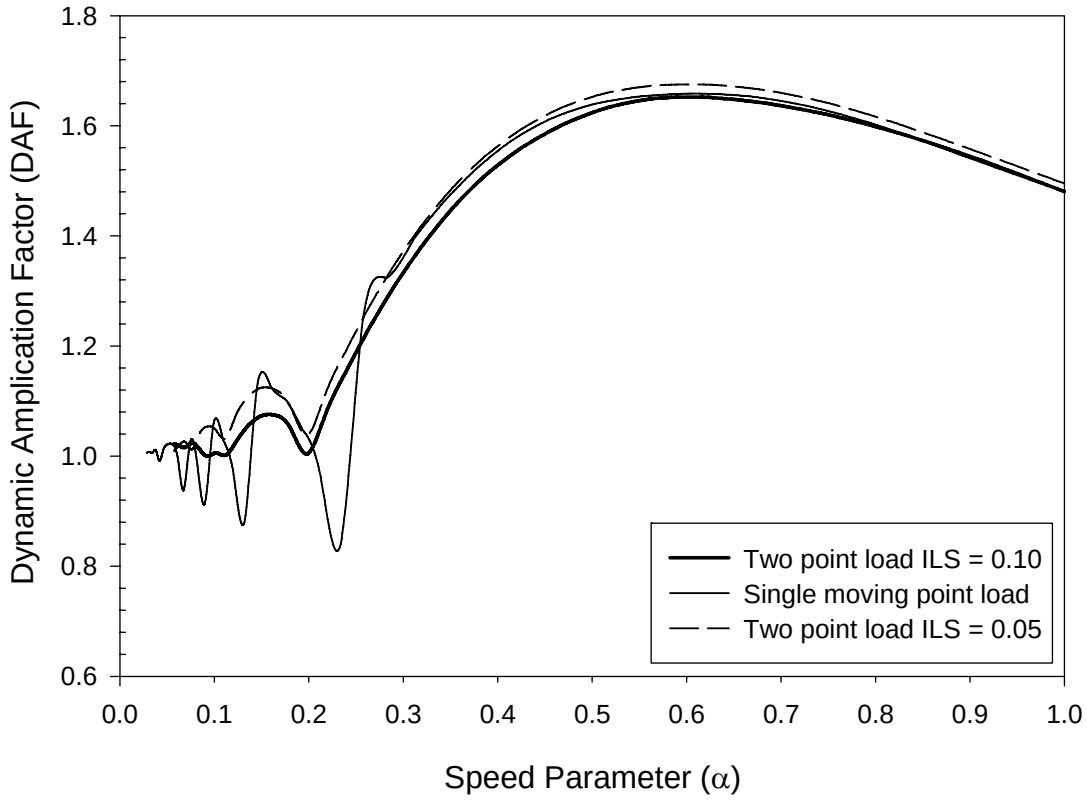

Figure 4.12: Dynamic Amplification factor vs. speed parameter for single and two point load (ILS = 0.05 and 0.1) systems

The dynamic amplification factor plotted against speed parameter (from the present study) at different *ILS* for a two point load system shown in the *Figure 13* indicated that the dynamic response decreased with the increase in the *ILS* as expected.

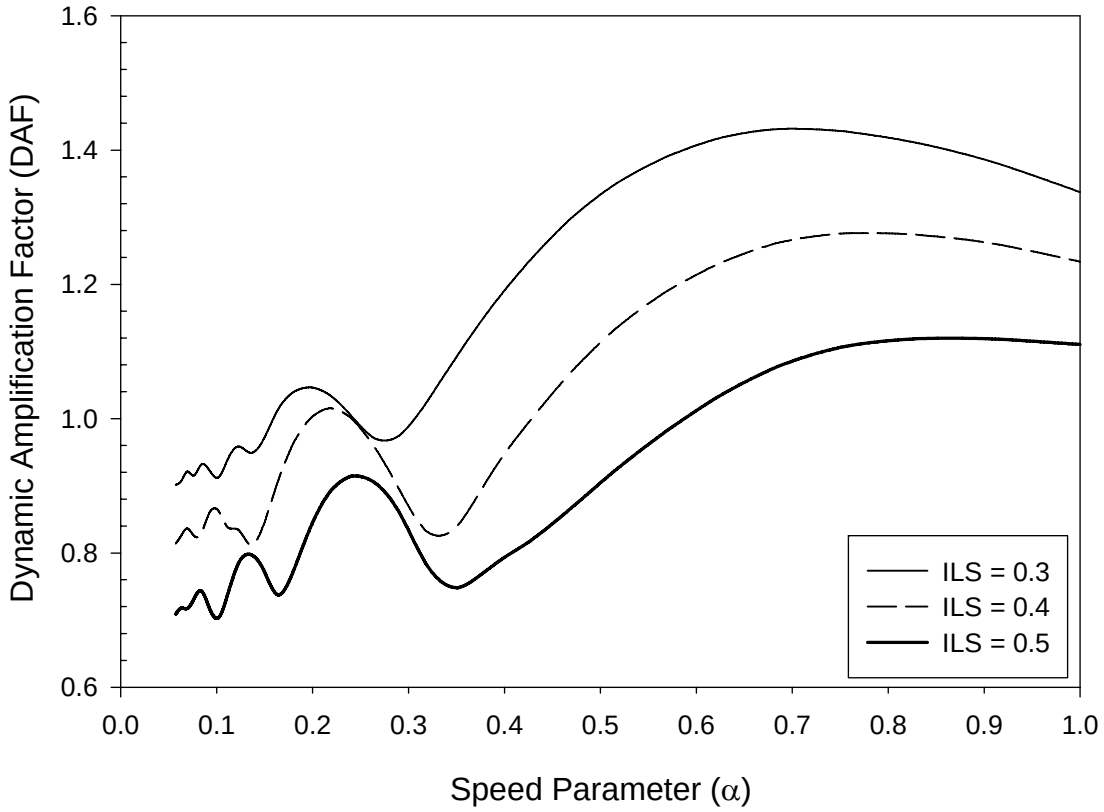

Figure 4.13: Dynamic amplification factor vs. speed parameter for two point load system at ILS = 0.3, 0.4 and 0.5

This chapter focused on the dynamic behavior of an *Euler* beam subjected to moving two point load system with no interaction effects. The study confirmed some of the findings from other past studies on comparison of dynamic responses due to single and two moving point loads, and the effect of inter-load spacing and speed parameter on the dynamic response of the system.

Chapter 5: Vehicle Bridge Interaction using Moving Oscillator

Introduction:

The moving mass problem discussed in the preceding chapter included inertia effects of a moving vehicle, and provided a satisfactory model for studying the vibration response of a bridge subjected to a light or heavy vehicular load but with no or little bouncing effects. The interaction effects of a vehicle on the bridge system are studied under a special category called Vehicle-Bridge Interaction (VBI) phenomenon. The VBI phenomenon arises due to track waviness profile, unbalanced vibration effect on wheels due to bouncing of vehicle chassis (varying reaction forces between wheels and roads), and varying elastic properties of road surface, and also due to braking effects. In this chapter, a single axle load system is studied using a moving oscillator solved using the DQM.

5.1 Moving oscillator model description:

A simple moving oscillator is shown in the *Figure 5.1*, where the sprung mass M_s represents the vehicle chassis, and the unsprung mass M_w represents the wheel and axle. The masses M_s and M_w are connected to each other through a spring and dashpot system having a spring constant C and viscous damping coefficient C_b, and a spring constant K is assumed for the tire stiffness.

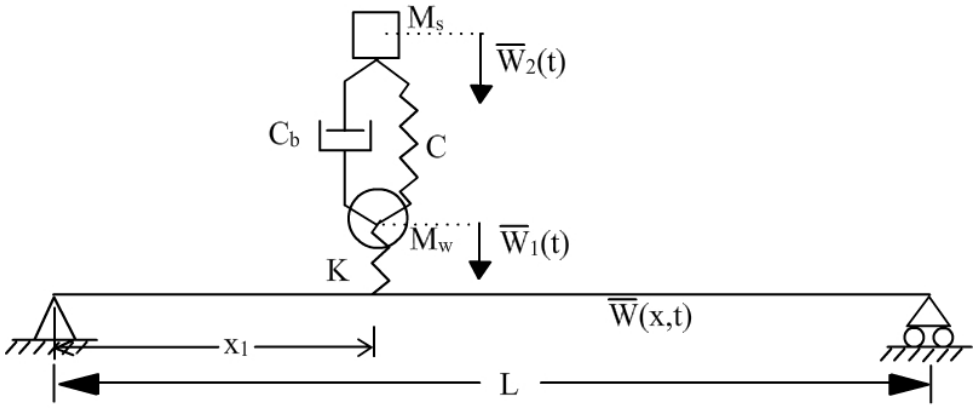

Figure 5.1: Moving oscillator system on a simply supported beam

The oscillator is assumed to move over a simply supported, uniform *Euler* beam of length L and mass per unit length μ, at a constant speed c such that its instantaneous position is given by $x_0 = ct$. The moment of inertia, elasticity modulus and the frequency of damping of the beam are denoted by I, E and ω_b, respectively.

5.2 VBI study for Euler beam carrying moving oscillator:

5.2.1 Governing equations:

The beam, the masses M_w and M_s were assumed to displace vertically $\overline{W}(t)$, $\overline{W_1}(t)$ and $\overline{W_2}(t)$, respectively. The displacement $\overline{W_2}(t)$ is measured such that the effects of the dead load due to sprung mass M_s on the spring C is included, i.e. displacement of M_s is measured from the equilibrium position. The equations of motion for the beam, the sprung and unsprung masses are given by

$$\mu \frac{\partial^2 \overline{W}(x,t)}{\partial t^2} + 2\mu\omega_b \frac{\partial \overline{W}(x,t)}{\partial t} + EI \frac{\partial^4 \overline{W}(x,t)}{\partial x^4} = \delta(x - x_0)\overline{R}(t) \tag{5.1}$$

$$-M_s \frac{d^2 \overline{W}_2(t)}{dt^2} - C\left(\overline{W}_2(t) - \overline{W}_1(t)\right) - C_b\left(\frac{d\overline{W}_2(t)}{dt} - \frac{d\overline{W}_1(t)}{dt}\right) = 0 \tag{5.2}$$

$$P - M_w \frac{d^2 \overline{W}_1(t)}{dt^2} + C\left(\overline{W}_2(t) - \overline{W}_1(t)\right) + C_b\left(\frac{d\overline{W}_2(t)}{dt} - \frac{d\overline{W}_1(t)}{dt}\right) - \overline{R}(t) = 0 \tag{5.3}$$

where $P = (M_s + M_w)g$ is the total vehicle load, and $\overline{R}(t) = K\left(\overline{W}_1(t) - W(x_0,t) - \bar{r}(x_0)\right)$ is the interaction force experienced by the beam at the point of contact between the unsprung mass and beam (here $\overline{R}(t)$ is the same as f_c with reversed sign used by *Yang and Yau* [60] for representing the reactive or contact force between the wheel mass and the bridge element). Assuming both the bridge and the wheel displace downwards, and since the stiffness K is always positive, if the vertical displacement of the wheel is larger than the sum of vertical displacement of the bridge and the bridge deck surface irregularity, then the wheel exerts a positive interactive force on the bridge through the tire.

A negative interaction force value indicates that the wheel displaces less than the bridge and hence resulting in a separation between the two. In this study, a 'no separation criteria' between the beam and the oscillator system is assumed, and hence the interaction force is always positive or non-negative i.e. $\overline{R}(t) \geq 0$, and is assumed zero when evaluated negative. Moreover, the interactive force should be sufficiently low in magnitude to avoid wheel separation.

In general, the tire stiffness K is considerably higher than the suspension stiffness C and hence prevents frequent unstable vertical oscillations between the wheels and chassis. A moving oscillator system of only a sprung mass M_s (and no or negligible unsprung mass relative to the chassis weight i.e., $M_w = 0$ or $M_w << M_s$) with very large stiffness characteristics (both the K and C assumed 10^7 kN/m) tends to approach the moving mass model.

It is worth to note that in the light of *Equations 5.2* and *5.3* above, the interaction force $\overline{R}(t)$ is expressed as,

$$\overline{R}(t) = P - M_w \frac{d^2\overline{W}_1(t)}{dt^2} - M_s \frac{d^2\overline{W}_2(t)}{dt^2} \tag{5.4}$$

Thus the dynamic behavior of a bridge structure is also influenced by the vertical accelerations of the sprung and unsprung masses i.e. the behavior of the suspension system of the vehicle.

The boundary conditions for the simply supported beam are represented by zero displacement and zero moment at the two ends and are given by

$$\overline{W}(0,t) = \left.\frac{\partial^2\overline{W}}{\partial x^2}\right|_{x=0} = 0 \tag{5.5}$$

$$\overline{W}(L,t) = \left.\frac{\partial^2 \overline{W}}{\partial x^2}\right|_{x=L} = 0 \tag{5.6}$$

The initial conditions for the above set of differential equations of motion are given by

$$\overline{W}(x,0) = \left.\frac{\partial \overline{W}(x,t)}{\partial t}\right|_{t=0} = 0 \text{ for the beam} \tag{5.7}$$

$$\overline{W_1}(0) = \overline{w}_{10} \text{ and } \left.\frac{d\overline{W_1}(t)}{dt}\right|_{t=0} = \dot{\overline{w}}_{10} \text{ for unsprung mass } M_w \tag{5.8}$$

$$\overline{W_2}(0) = \overline{w}_{20} \text{ and } \left.\frac{d\overline{W_2}(t)}{dt}\right|_{t=0} = \dot{\overline{w}}_{20} \text{ for the sprung mass } M_s \tag{5.9}$$

5.2.2 Dimensionless form of governing equations of motion:

A set of dimensionless parameters were introduced to simplify the above set of differential equations of motion with the help of a few additional parameters namely speed (α) parameter, vehicle to bridge mass ratio (κ), wheel/axle to chassis mass ratio (κ_{ws}), frequency parameters for unsprung and sprung masses (γ_w and γ_s, respectively), and logarithmic decrement for vehicle suspension and bridge damping (ϑ_s and ϑ, respectively). These parameter definitions were adopted from *Fryba* [10] and characterize the effects of sprung and unsprung masses on the vibration response of the system.

The speed parameter is defined as the ratio of the frequency of moving oscillator to the natural frequency of the beam, i.e.

$$\alpha = \frac{\omega}{\omega_{(1)}} = \frac{c}{2 f_{(1)} L} \tag{5.10}$$

where $\omega = \frac{\pi c}{L}$ is the frequency of the moving oscillator.

The vehicle-bridge mass ratio is given by $\kappa = P / G$ where $G = \mu g L$ is the total bridge weight. The wheel/axle to chassis mass ratio (κ_{ws}) is given by $\kappa_{ws} = M_w / M_s$.

The other parameters that influence the vehicle-bridge interaction phenomenon are the frequency parameters for wheel/axle and chassis masses. The frequency parameter for the wheel/axle mass is defined as the ratio of natural frequency of wheel/axle to the natural frequency of the bridge, i.e.,

$$\gamma_w = \frac{f_w}{f_{(1)}} = \frac{1}{\omega_{(1)}} \sqrt{\frac{K}{M_w}} \tag{5.11}$$

where $f_w = \frac{1}{2\pi} \sqrt{\frac{K}{M_w}}$ is the frequency of the wheel/axle. Similarly, the frequency parameter for the vehicle chassis is defined as the ratio of natural frequency of the chassis to that of the bridge, i.e.,

$$\gamma_s = \frac{f_s}{f_{(1)}} = \frac{1}{\omega_{(1)}}\sqrt{\frac{C}{M_s}} \tag{5.12}$$

where $f_s = \frac{1}{2\pi}\sqrt{\frac{C}{M_s}}$ is the frequency of the sprung mass.

The logarithmic decrement of damping for the beam and the vehicle suspension are given by $\vartheta = \omega_b / f_{(1)}$ and $\vartheta_s = C_b /(2M_s f_s)$, respectively.

The normalized space and time variables are given by $\xi = x/L$ and $\tau = t/T$ where $T = L/c$. The lateral displacements of beam, unsprung and sprung masses were also expressed in dimensionless form using the static mid-span deflection parameter Δ_{st}, i.e.,

$$W(\xi,\tau) = \frac{\overline{W}(x,t)}{\Delta_{st}} \tag{5.13}$$

$$W_1(\tau) = \frac{\overline{W_1}(t)}{\Delta_{st}} \tag{5.14}$$

$$W_2(\tau) = \frac{\overline{W_2}(t)}{\Delta_{st}} \tag{5.15}$$

The normalized governing differential equations of motion for the beam and the masses using the above defined dimensionless parameters are given by,

$$\pi^2\alpha^2\frac{\partial^2 W(\xi,\tau)}{\partial\tau^2} + 2\pi^3\alpha\beta\frac{\partial W(\xi,\tau)}{\partial\tau} + \frac{\partial^4 W(\xi,\tau)}{\partial\xi^4} = \frac{L^4}{EI}\delta(x-x_0)\frac{\overline{R}(t)}{\Delta_{st}} = 48\delta(\xi-\xi_0)R(\tau) \tag{5.16}$$

$$\frac{d^2W_2(\tau)}{d\tau^2} + \frac{\pi^2\gamma_s^2}{\alpha^2}\left(W_2(\tau)-W_1(\tau)\right) + \frac{\vartheta_s\gamma_s}{\alpha}\left(\frac{dW_2(\tau)}{d\tau}-\frac{dW_1(\tau)}{d\tau}\right) = 0 \tag{5.17}$$

$$\frac{d^2W_1(\tau)}{d\tau^2} - \frac{\pi^2}{\alpha^2}\left(\frac{1+\kappa_{ws}}{2\kappa\kappa_{ws}}\right)\left(1-R(\tau)\right) + \frac{\pi^2\gamma_s^2}{\alpha^2\kappa_{ws}}\left(W_1(\tau)-W_2(\tau)\right) + \frac{\vartheta_2\gamma_s}{\kappa_{ws}\alpha}\left(\frac{dW_1(\tau)}{d\tau}-\frac{dW_2(\tau)}{d\tau}\right) = 0 \tag{5.18}$$

where the interaction force is given by

$$R(\tau) = \frac{\overline{R}(t)}{P} = \left(\frac{2\kappa\kappa_{ws}}{1+\kappa_{ws}}\right)\gamma_w^2\left(W_1(\tau)-W(\xi_0,\tau)-r(\tau)\right) \tag{5.19}$$

Here, $r(\tau)$ is the dimensionless surface waviness computed by normalizing the assumed surface waviness profile $r(x_0)$ using static mid-span displacement Δ_{st} of the beam. The surface waviness parameter is neglected in this study to simplify the model.

The beam displacement $W(\xi,\tau)$ is then expressed in sinusoidal modal shape function i.e. $W(\xi,\tau)=\sum_{j=1}^{m} w_j(\tau) Sin\, j\pi\xi$ where $w_j(\tau)$ is the time coordinate function, and m is the mode number of significance. The governing equation of motion for the beam becomes

$$\pi^2\alpha^2\frac{d^2w_j(\tau)}{d\tau^2}+2\pi^3\alpha\beta\frac{dw_j(\tau)}{d\tau}+j^4\pi^4 w_j(\tau)=96R(\tau)Sin\, j\pi\tau \qquad \text{for } j=1,2,3,...,m \tag{5.20}$$

or further simplified with the approximation $\pi^4 \approx 96$,

$$\frac{\alpha^2}{\pi^2}\frac{d^2w_j(\tau)}{d\tau^2}+\frac{2\alpha\beta}{\pi}\frac{dw_j(\tau)}{d\tau}+j^4 w_j(\tau)=R(\tau)Sin\, j\pi\tau \qquad \text{for } j=1,2,3,...,m \tag{5.21}$$

Since the above governing equation is free of spatial terms, the boundary conditions were not required to solve the system. The initial conditions for the above set of equations, *Equation 5.21* and *Equations 5.17 and 5.18*, are given by,

$$w_j(0)=\left.\frac{dw_j(\tau)}{d\tau}\right|_{\tau=0}=0 \text{ at } j=1,2,3,...,m \text{ for the beam,} \tag{5.22}$$

$$W_1(0)=W_{10} \text{ and } \left.\frac{dW_1(\tau)}{d\tau}\right|_{\tau=0}=\dot{W}_{10} \text{ for the unsprung mass } M_w, \text{ and} \tag{5.23}$$

$$W_2(0)=W_{20} \text{ and } \left.\frac{dW_2(\tau)}{d\tau}\right|_{\tau=0}=\dot{W}_{20} \text{ for the sprung mass } M_s. \tag{5.24}$$

The initial vertical displacements of both the wheel/axle and vehicle chassis were assumed to be same and by allowing them to displace a constant value, both the wheel/axle and chassis experience zero initial vertical velocity. The bridge is assumed to be at rest initially and hence there were no inertia terms associated with it due to vehicle at the point of entrance. Thus the weight of the moving vehicle solely contributes for the interactive force i.e., $R(\tau)\big|_{\tau=0} = \left.\frac{\overline{R}(t)}{P}\right|_{t=0} = 1$.

The initial displacement values of the unsprung wheel/axle and the sprung chassis are then computed by substituting $W(\xi_0,\tau)\big|_{\tau=0} = 0$ in the Equation 5.19, i.e., $W_1(0) = W_{10} = \left(\frac{1+\kappa_{ws}}{2\kappa\kappa_{ws}}\right)\left(\frac{1}{\gamma_w^2}\right) = W_2(0) = W_{20}$. Since both the above initial displacement values are time independent quantities, the initial lateral velocity of vibration is zero for both the unsprung and sprung masses. Although the above quantity seemed to be defined on the basis of modal mass ratio and wheel/axle to chassis mass ratio terms, it could be easily verified to be dependent on only the independent parameters μ, L, $\omega_{(1)}$ and K.

5.2.3 DQ implementation and solution:

The governing equations of motion for the moving oscillator system in the DQ form were given by

$$\frac{\alpha^2}{\pi^2}\sum_{k=1}^{n} B_{sk} w_{jk} + \frac{2\alpha\beta}{\pi}\sum_{k=1}^{n} A_{sk} w_{jk} + j^4 w_{js} - \left(\frac{2\kappa\kappa_{ws}}{1+\kappa_{ws}}\right)\gamma_w^2\left(W_1(\tau_s) - W\big|_{\xi=\tau} - r(\tau_s)\right) Sin\, j\pi\tau_s = 0 \tag{5.25}$$

where w_{js} represents the modal coordinate of j^{th} mode at time τ_s, and similarly the parameters $W_1(\tau_s)$ and $r(\tau_s)$ represent the vertical displacement of the wheel and axle system and the road surface waviness, respectively. The beam displacement $W\big|_{\xi=\tau}$ is expressed in terms of modal coordinates, i.e. $W\big|_{\xi=\tau} = \sum_{j=1}^{m} w_{js} Sin\, j\pi\xi = \sum_{j=1}^{m} w_{js} Sin\, j\pi\tau_s$.

The governing equations of motion for the sprung and unsprung masses in the DQ form were given by

$$\sum_{k=1}^{n} B_{sk} W_{(2)k} + \frac{\pi^2 \gamma_s^2}{\alpha^2}(W_2 - W_1) + \frac{\vartheta_2 \gamma_s}{\alpha}\left(\sum_{k=1}^{n} A_{sk} W_{(2)k} - \sum_{k=1}^{n} A_{sk} W_{(1)k}\right) = 0 \tag{5.26}$$

$$\begin{aligned}\sum_{k=1}^{n} B_{sk} W_{(1)k} + \frac{\pi^2 \gamma_s^2}{\alpha^2 \kappa_{ws}}(W_1 - W_2) + \frac{\vartheta_2 \gamma_s}{\alpha \kappa_{ws}}\left(\sum_{k=1}^{n} A_{sk} W_{(1)k} - \sum_{k=1}^{n} A_{sk} W_{(2)k}\right) \\ - \frac{\pi^2}{\alpha^2}\left(\frac{1+\kappa_{ws}}{2\kappa\kappa_{ws}}\right)\gamma_w^2(1 - R(\tau)) = 0\end{aligned} \tag{5.27}$$

where $W_{(1)}$ and $W_{(2)}$ denote the displacements of the wheel and axle, and the chassis, respectively i.e. $W_{(1)}$ and $W_{(2)}$ were same as W_1 and W_2. The parenthesis is included to differentiate the variables from their differential quadrature indices. Also the variables W_1 or $W_{(1)}$ and W_2 or $W_{(2)}$ are functions of time i.e. $W_1 \equiv W_1(\tau)$ and $W_2 \equiv W_2(\tau)$, and in other words, W_1 at $\tau = \tau_s$ is denoted by $W_{(1)s}$.

In the above relations, the reaction force at the point of contact $R(\tau)$ is given by

$$R(\tau) = \frac{2\kappa\kappa_{ws}}{1+\kappa_{ws}}\gamma_w^2\left(W_1 - W\big|_{\xi=\tau} - r(\tau)\right) \tag{5.28}$$

and the initial conditions for the above set of governing equations were given by,

$$w_j(\tau=0) = w_{j1} = 0 \text{ and } \dot{w}_j\big|_{\tau=0} = \sum_{k=1}^{n} A_{1k} w_{jk} = 0 \text{ for the beam,} \tag{5.29}$$

$$W_1(\tau=0) = 0 \text{ and } \sum_{k=1}^{n} A_{1k} W_{(1)k} = 0 \text{ for the unsprung mass, and} \tag{5.30}$$

$$W_2(\tau=0) = 0 \text{ and } \sum_{k=1}^{n} A_{1k} W_{(2)k} = 0 \text{ for the sprung mass.} \tag{5.31}$$

The system of equations, *Equations 5.25 – 5.27,* with the initial conditions, *Equations 5.29 – 5.31*, were solved similar to the moving mass model i.e. with the moving force first and then iterated with the updated vertical displacement, velocity and acceleration values of unsprung and sprung masses.

5.3 Discussion on VBI study results:

To facilitate the validation of results obtained from the DQM, some of the literature results on moving oscillator systems were taken as references, and the solution

characteristics were discussed and qualitatively compared in the following section i.e. no attempt was made to reproduce their results but the results were compared for the salient behavior of the dynamical vehicle-bridge system.

5.3.1 Comparison of DQM results using literature results:

5.3.1 (a) Validation of model using *Yang* and *Yau* VBI results:

Yang and Yau [60] recently introduced a condensation technique to develop a vehicle-bridge interaction element and compared the results with those for single mode solution of the sprung mass model given by *Biggs* [20]. The values of parameters used by *Yang and Yau* [60] were listed below and were used to qualitatively validate the DQM results with respect to the vehicle bridge interaction element method, or in general to assess the dynamical behavior of the vehicle-bridge system. The author also found an extraneous term in the *Equation 33* of *Yang* and *Yau* [60], mass ratio $\frac{M_v}{\mu L}$ term in $-\omega_v^2 \frac{M_v}{\mu L} Sin\frac{\pi ct}{L}$.

Data used for the analysis:

Beam's span length, $L = 25\,m$

Elasticity modulus for the beam, $E = 2.87\,GPa = 2.87 \times 10^9\ N/m^2$

Poisson's ratio for the beam, $\upsilon = 0.2$

Area moment of inertia, $I = 2.9\,m^4$

Beam's mass per unit length, $\mu = 2303\,kg/m$

Suspended mass, $M_v = 5750\,kg$

Suspension stiffness, $k_v = 1595\,kN/m$

Speed of the moving oscillator, $c = 100\,km/h \equiv 27.778\,m/s$

Natural frequency of the bridge (beam), $\omega_{(1)} = 30.02\,rad/s$

Natural frequency of the sprung mass, $\omega_v = 16.66\,rad/s$

The final governing equations were written in a normalized form so that only those parameters such as speed parameter, damping parameter, mass ratio, etc. were considered necessary to characterize the dynamic behavior of the vehicle-bridge system. Since these parameters were defined using independent variables such as span length, mass per unit length, natural frequency, etc., the effect of variations within independent variables on the dynamic behavior of the system is studied by suitably modifying the dependent parameters. The normalization procedure is useful to compare the dynamic behavior of different vehicle-bridge systems. The normalized or dimensionless parameters corresponding to the set of data presented above are given below:-

Speed parameter, $\alpha = \dfrac{\omega}{\omega_{(1)}} = 0.116$

Damping parameter, $\beta = \dfrac{\omega_b}{\omega_{(1)}} = 0$

Vehicle to Bridge Mass ratio, $\kappa = \dfrac{M_v}{\mu L} = 0.1$

In addition to the above dimensionless parameters, the dynamic displacement of the beam and masses were expressed as a fraction of the mid-span deflection of the beam under a static load of same magnitude acting at the center of the beam. The mid-span static

deflection for the *Euler* beam of the given geometry and specified load conditions was computed to be 0.00217464 m, and hence the actual measure of dynamic deflection under a moving load is obtained by multiplying the dimensionless deflection solved from the DQM with the mid-span static deflection.

The dynamic response characteristics of vehicle-bridge system modeled as a beam carrying a moving oscillator with the above parameters are presented in the *Figures 5.2 – 5.5*. *Figure 5.2* shows the absolute dynamic displacement of the beam obtained for moving force problem using analytical procedure compared with that obtained for moving oscillator system using DQM.

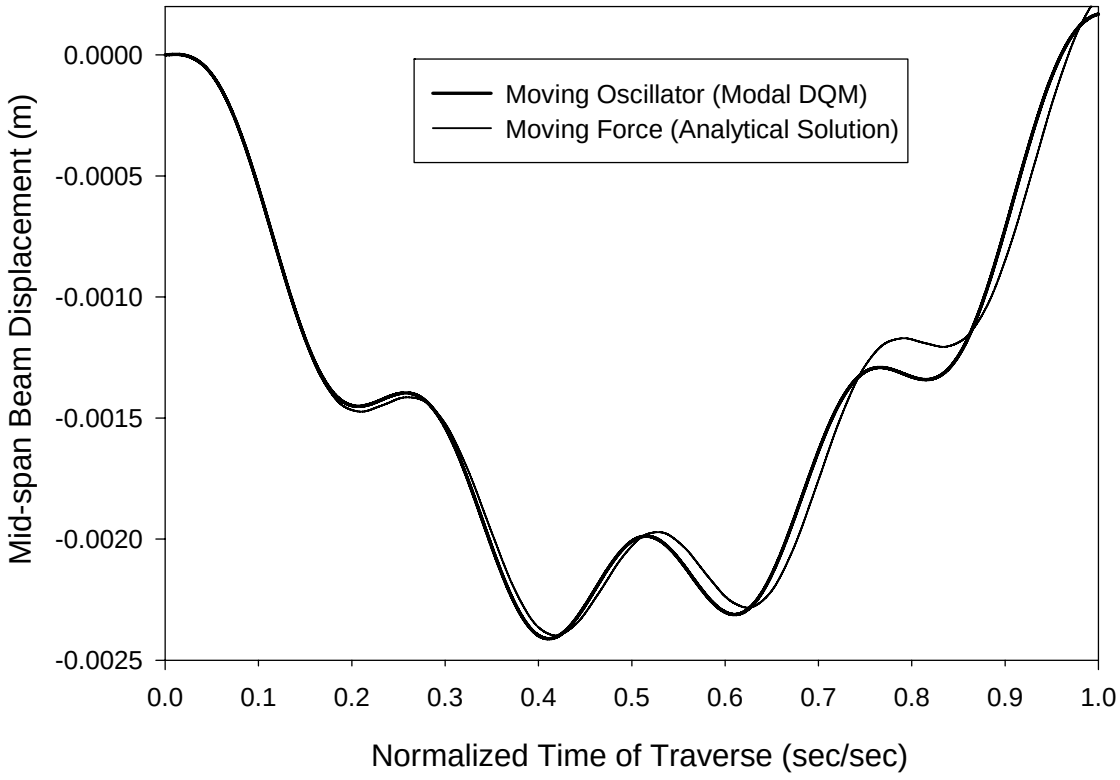

Figure 5.2: Mid-span beam (absolute) displacement for moving force and moving oscillator models ($\alpha = 0.116$, $\beta = 0$, $\kappa = 0.1$)

Figure 5.3 shows the normalized mid-span dynamic displacements of the beam obtained using moving force, moving mass and moving oscillator systems. The dynamic response obtained from the moving mass model suggested a time delay of the effect of mass on the dynamic response however no other significant differences existed among the three models for the given beam geometry and loading conditions.

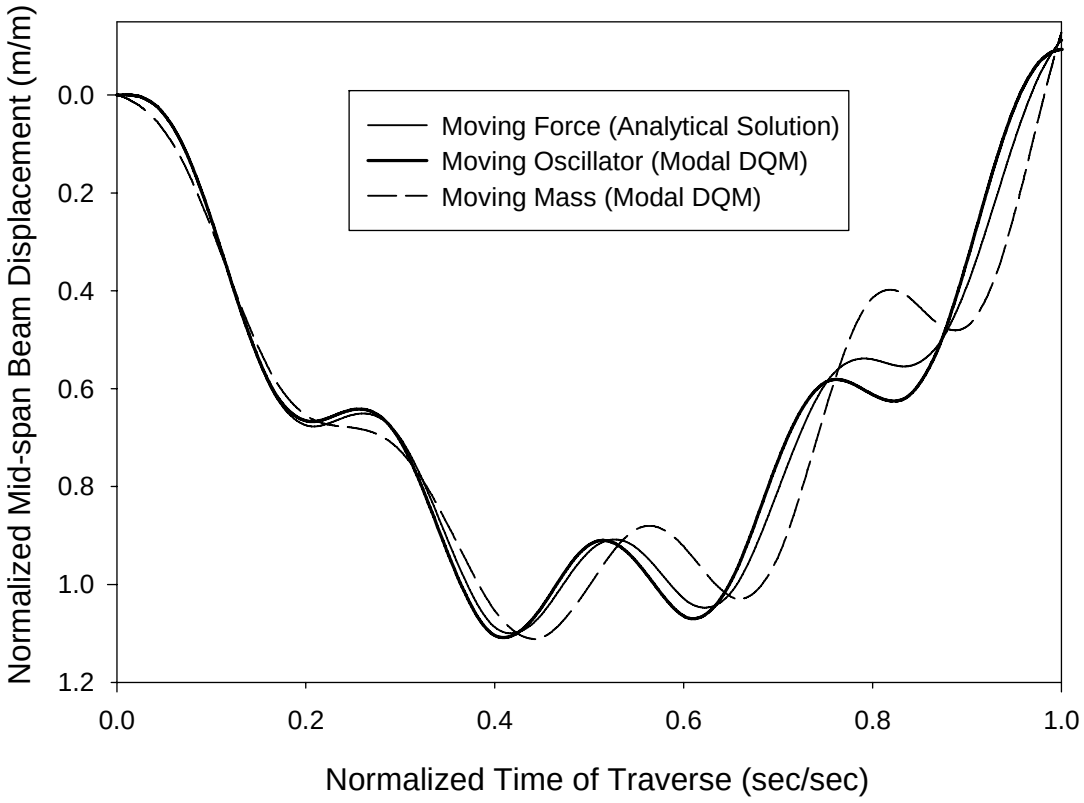

Figure 5.3: Mid-span beam dynamic response using moving force, moving mass and moving oscillator models ($\alpha = 0.116$, $\beta = 0$, $\kappa = 0.1$)

The displacements computed from solving the linear system of equations were then interpolated on space and time to enable easy computation of velocity and acceleration data. The computed vertical acceleration data at the mid-span beam and for the sprung

mass were shown in *Figures 5.4* and *5.6*, respectively. *Yang and Yau* [60] reported vertical acceleration data at the mid-span beam using analytical as well as their dynamic condensation technique. The acceleration data at mid-span beam for moving oscillator system obtained from the DQM matched with the analytical data reported by *Yang and Yau* but did not match the acceleration response at mid-span beam using *Yang and Yau*'s dynamic condensation technique.

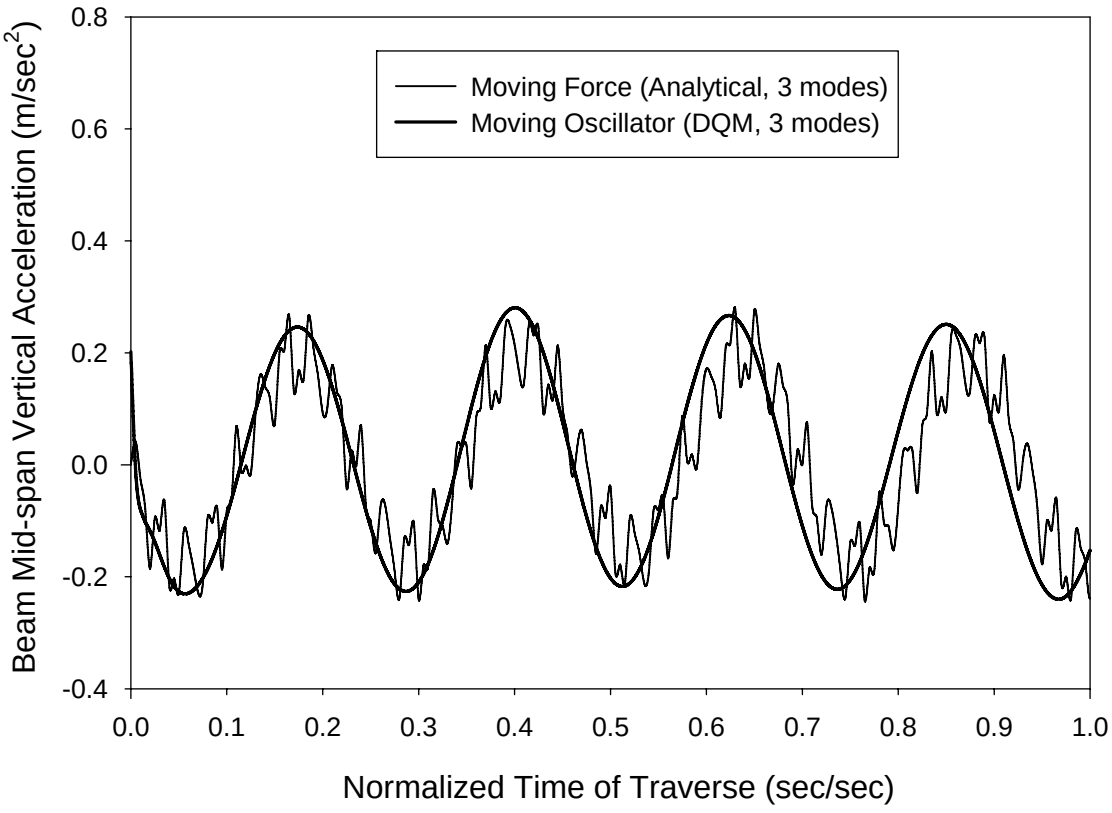

Figure 5.4: Mid-span beam (absolute) vertical acceleration response using moving force and oscillator models (α = 0.116, β = 0, κ = 0.1)

The sprung mass displacement data shown in the *Figure 5.5* suggested that for a smooth track, the sprung mass displaces to a maximum near the mid-span of the beam at which

point also the mid-span beam retracts from the point of maximum displacement. This was an expected behavior since no loss of contact between the vehicle and the bridge was assumed a priori. The displacement and the acceleration response of the sprung mass shown in *Figures 5.5* and *5.6*, respectively agreed well with the results reported in *Yang and Yau* [60]. *Figure 5.6* compares the acceleration data obtained for sprung mass by considering only a mode and up to 3 modes of significance for the beam.

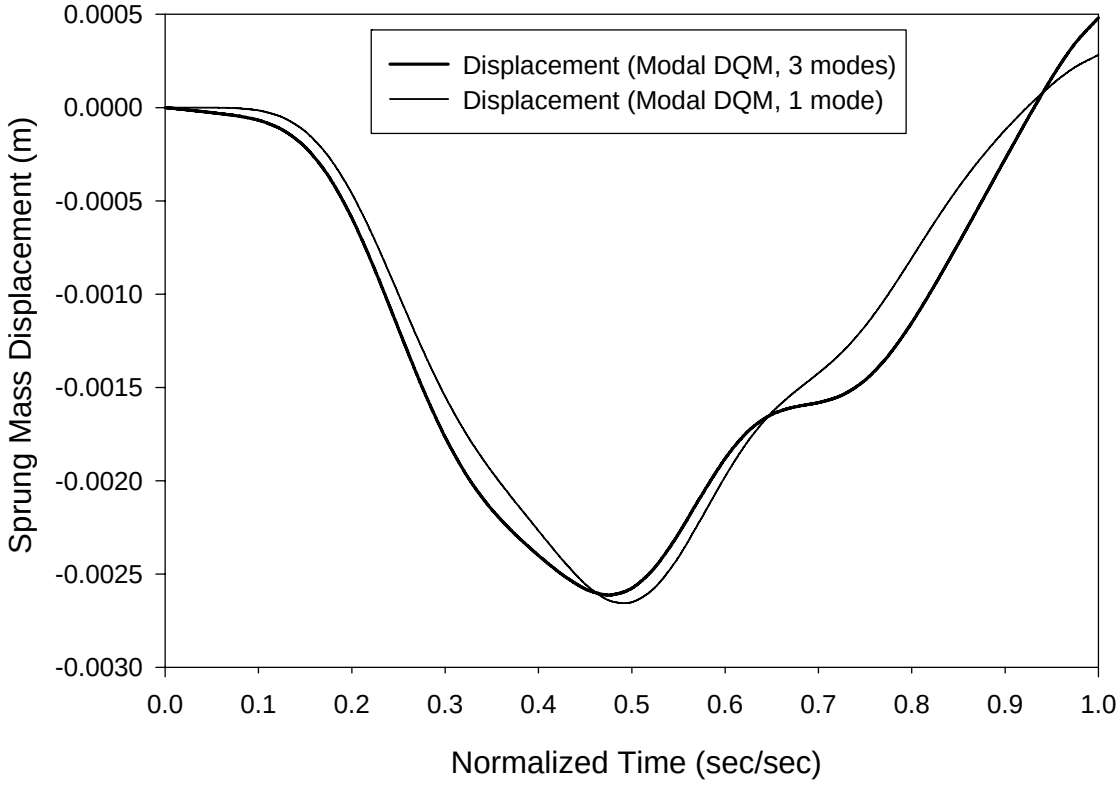

Figure 5.5: Sprung mass vertical (absolute) displacement response (1 mode vs. 3 modes solution)

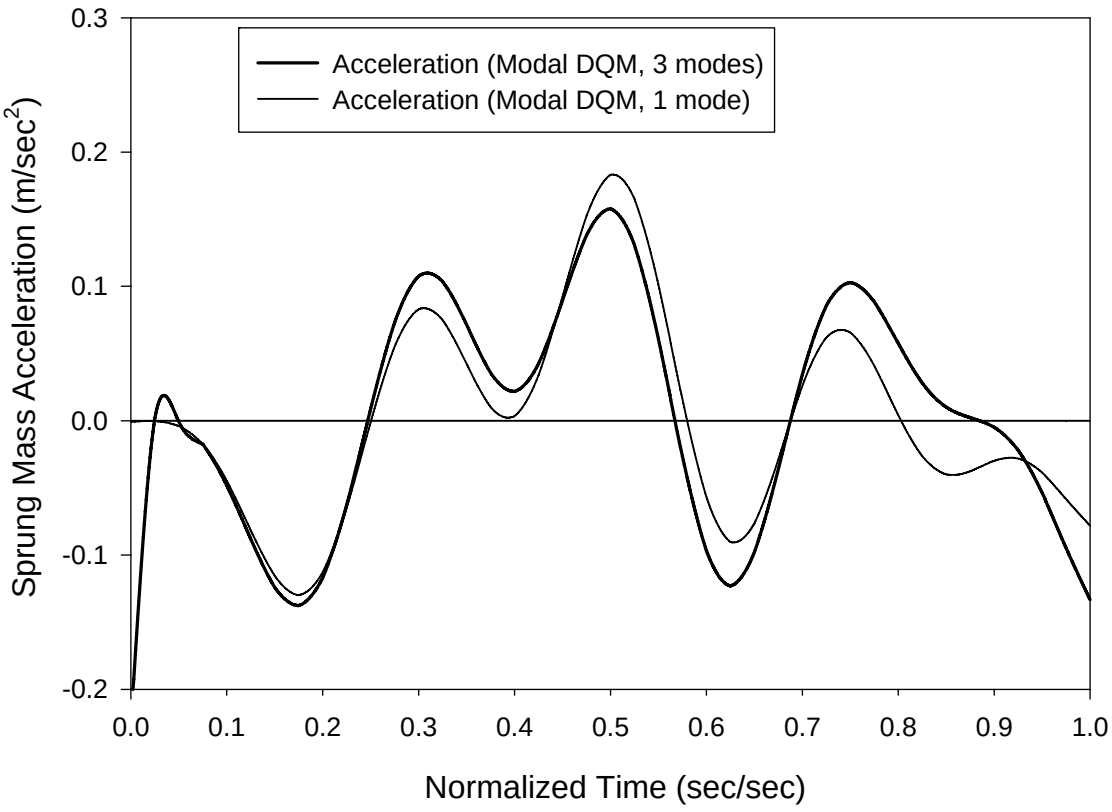

Figure 5.6: Sprung mass vertical (absolute) acceleration (1 Mode vs. 3 Modes solution)

The dynamic response of the beam at the point of action of moving load over the time of load traverse is shown in the *Figure 5.7*. The *Figures 5.2* and *5.7* showed similar maximum dynamic responses occurring at around the same time i.e. at the normalized time $\tau = 0.425$. The mid-span dynamic response of the beam was at the peak even before the dynamic response of the beam at the point of action of moving load reaches its maximum, and when the dynamic response at the point of action of load reaches the maximum, the mid-span dynamic response of the beam started to decrease, at the above mentioned beam parameters and load conditions. This characteristic grows stronger for increased speeds i.e., at increased speeds, the mid-span dynamic response reaches peak value well before the dynamic response at the point of action of load could reach its

maximum. The interactive force experienced by the wheel at the point of contact will also follow the same variation as the dynamic response of the beam at the point of action of moving load shown in the *Figure 5.7*. The deflected beam shape at instants of time i.e. at $1/5^{th}$, $2/5^{th}$, $3/5^{th}$ and $4/5^{th}$ of the total normalized time, is shown in the *Figure 5.8*.

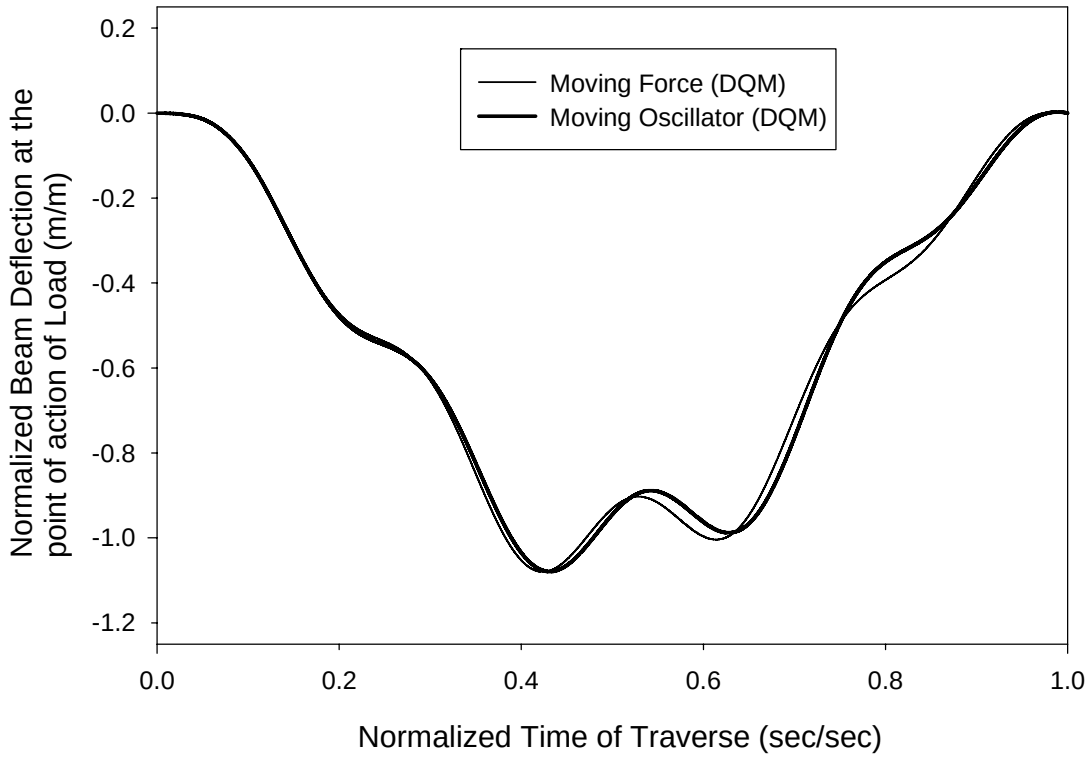

Figure 5.7: Dynamic beam response at the point of action of load for moving force and moving oscillator systems at $\alpha = 0.116$

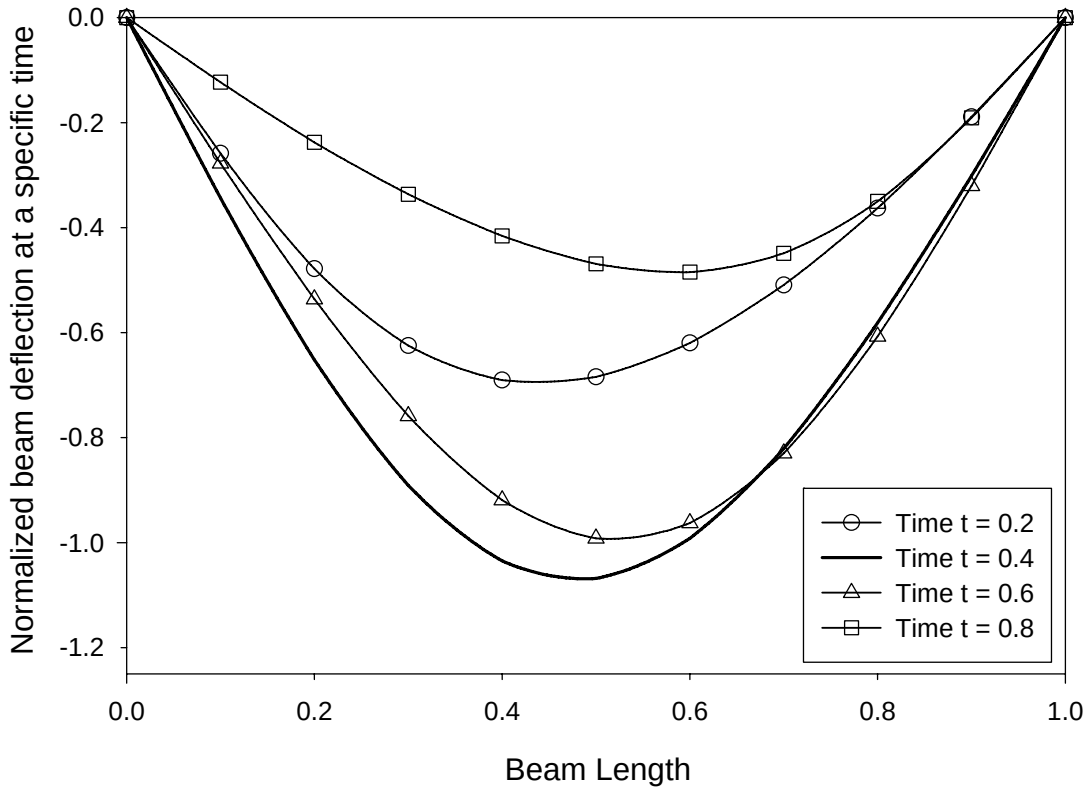

Figure 5.8: Deflected beam shape at specific instants of (normalized) time for moving oscillator

5.3.1 (b) Validation of model using *Green* and *Cebon* results:

Green and Cebon [58] studied the vehicle-bridge interaction and commented on the error involved in the computation of dynamic response of the bridge structure neglecting any possible vehicle-bridge interaction phenomena based on the speed parameter, frequency ratio, modal mass ratio, and vehicle and bridge damping ratio. *Green and Cebon* defined the error involved in computing dynamic response neglecting VBI as,

$$\varepsilon(t) = \frac{W(x_0,t) - W_{in}(x_0,t)}{\Delta_{st}} \tag{5.32}$$

where $W(x_0,t)$ is the iterated mid-span displacement solution i.e. dynamic response including vehicle-bridge interaction phenomenon, $W_{in}(x_0,t)$ is the initial mid-span displacement solution i.e. dynamic response considering only the moving force, and Δ_{st} is the mid-span static displacement. This definition is slightly different from the dynamic amplification factor but one could easily see that the error above is the difference in the amplification factors for moving oscillator and moving force problems discussed before.

They noted the heavy vehicles typically were able to generate higher bridge responses at low frequencies due to sprung mass bouncing and pitching motions. This characteristic was observed at some of the tests conducted at the four-post vehicle shaker structural test system at the OU's north campus facility, where resonance phenomenon is spotted at frequencies close to 2 *Hz* (for a vehicle weighing around 40 ton), however the test set up was limited to identify the lower frequencies of importance that resulted in higher vehicle response without having a knowledge on the impact of this effect over bridge structures, and also that only the front axle and intermediate axle were tested in the vehicle shaker system.

Green and Cebon [58] defined the modal mass ratio to be the ratio of twice the mass of the vehicle over the bridge mass whereas other literature works defined it to be the ratio of vehicle mass over the bridge mass. The author found slightly contradicting results for the dynamic response due to moving oscillator with those published by *Green and Cebon* [58] while *Yang and Yau* [60] results (and other literature results) were quite in agreement.

Green and Cebon [58] did not mention about the initial conditions for the sprung mass which could significantly affect the solution. The usual initial conditions were that both the lateral displacement and slope (speed) are zero i.e. sprung mass displacement due to its own weight is already taken into account, or to assume that the sprung mass is yet to take its equilibrium position in which case the displacement is given by $\overline{W_{20}} = \frac{P}{K}$ or in the normalized form, $W_{20} = \frac{1}{2\kappa}\left(\frac{1}{\gamma_s^2}\right)$.

While *Green and Cebon* concluded that at a frequency ratio of $\gamma = 1$, the dynamic response under moving point force ignoring *VBI* phenomenon seemed higher than that observed including *VBI*, the current study observed that both of the models i.e. with and without *VBI* produced same or similar maximum dynamic response but occurring at different times as shown in the *Figures 5.9* and *5.10*. The mid-span dynamic response in the case of moving oscillator system reached the peak value ahead of the moving force scenario. In fact, the response of the mid-span beam for the moving oscillator was found to be higher than that observed for moving force at increased speeds, $\alpha = 0.2$ shown in the *Figure 5.10*, which contradicts the results reported by *Green and Cebon*.

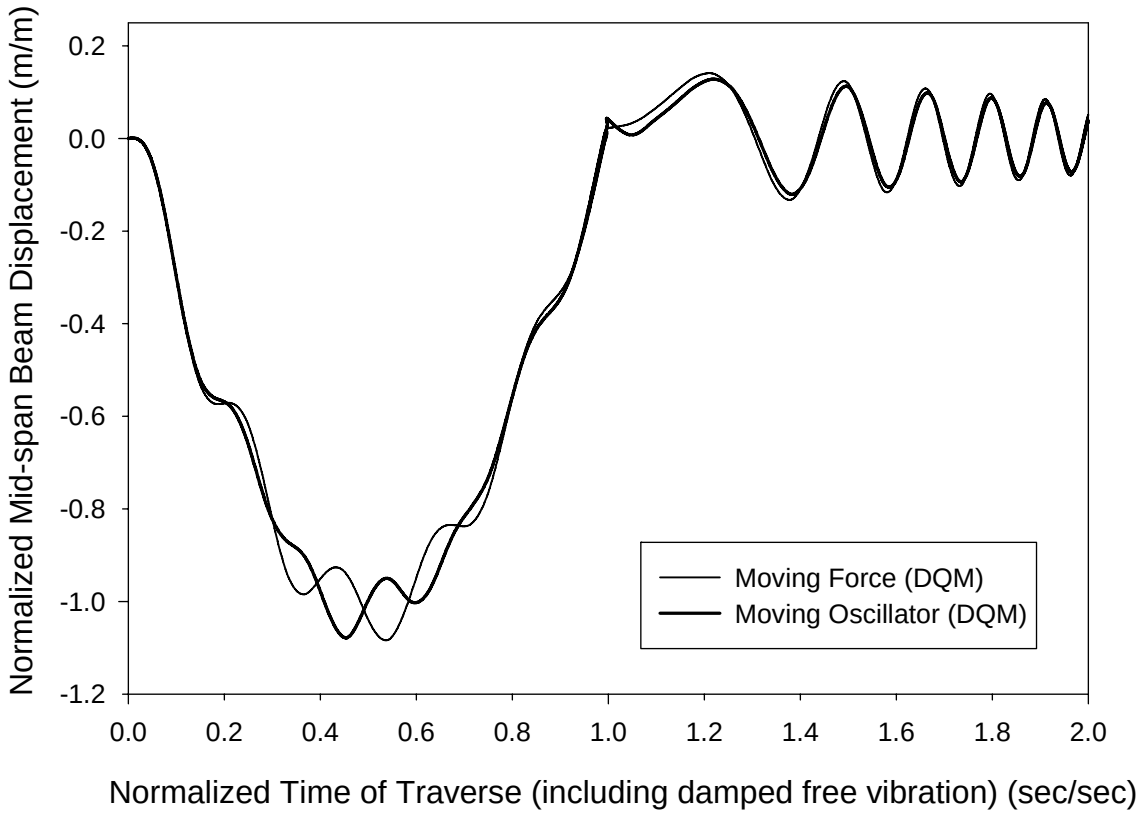

Figure 5.9: Dynamic beam response to moving point force and oscillator system

at $\alpha = 0.098$, $\gamma = 1$, $\kappa = 0.16$ and $\beta = 0.02$

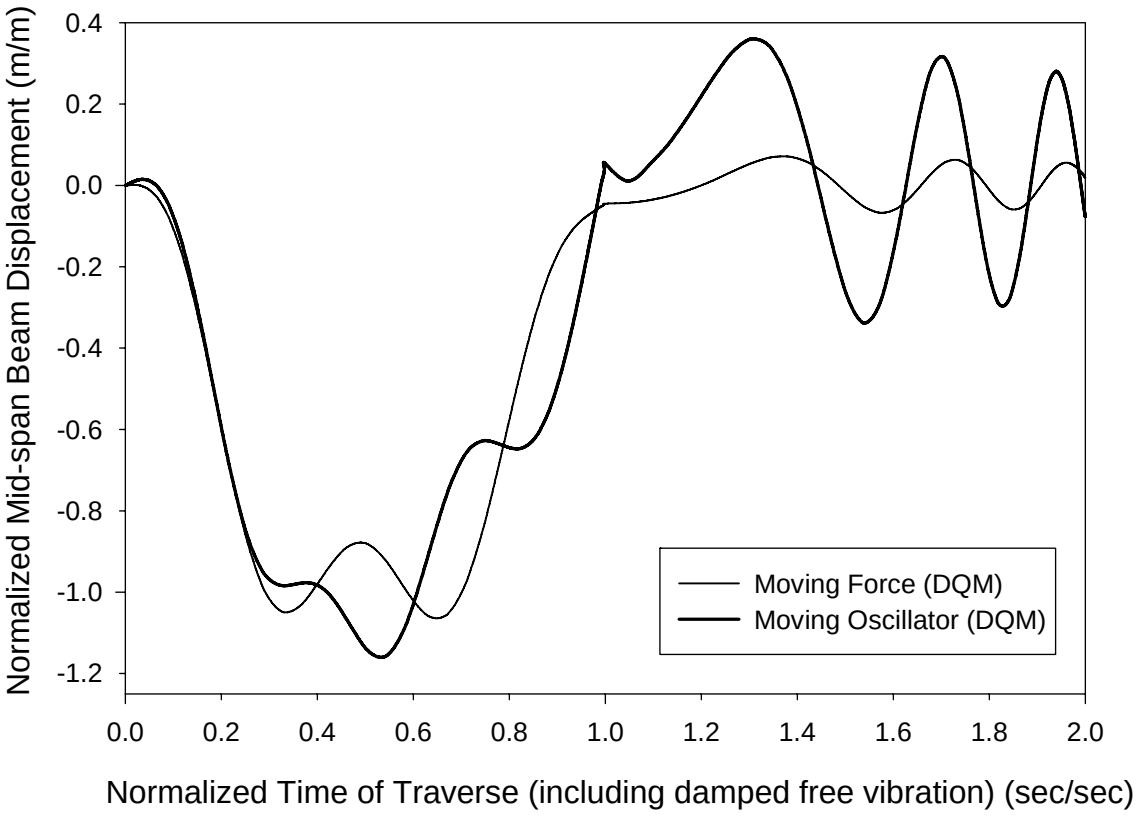

Figure 5.10: Dynamic beam response to moving point force and oscillator system at $\alpha = 0.196$, $\gamma = 1$, $\kappa = 0.16$ and $\beta = 0.02$

The deflected beam shapes for the above cases i.e. at $\alpha = 0.1$ and $\alpha = 0.2$ at a given instant of normalized time were shown in the *Figure 5.11* and *5.12*, respectively.

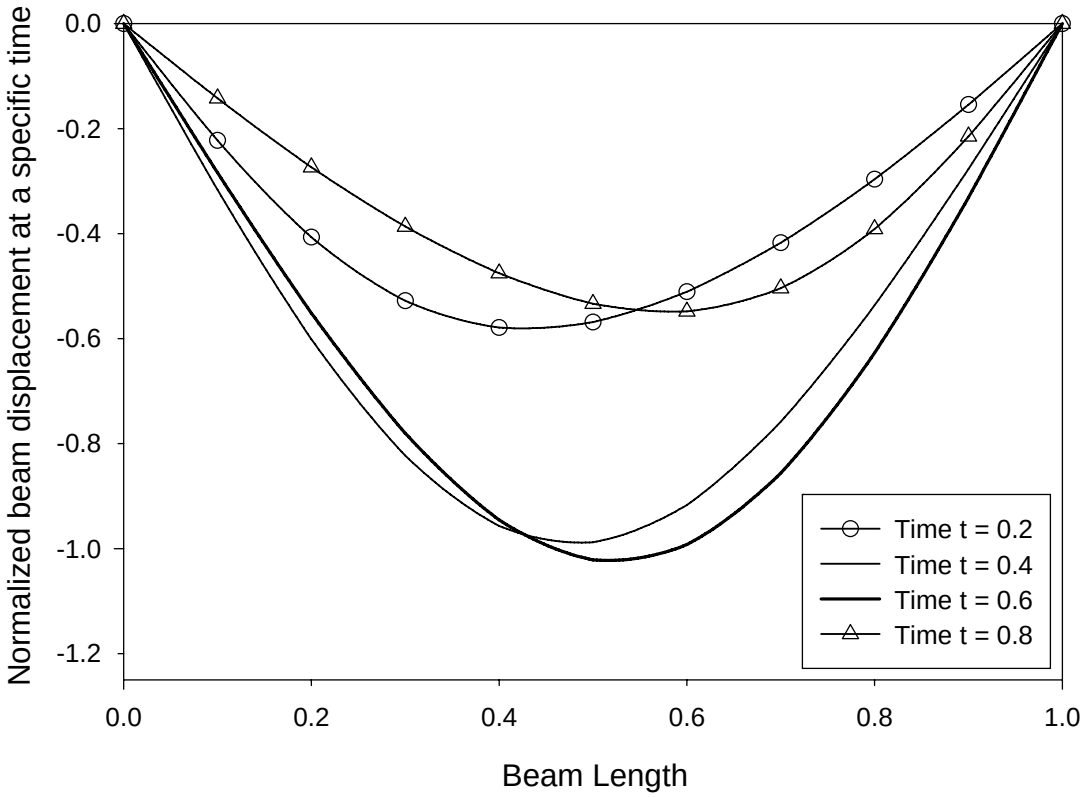

Figure 5.11: Deflected beam shape at specific instants of normalized time

for $\alpha = 0.098$, $\gamma = 1$, $\kappa = 0.16$ and $\beta = 0.02$

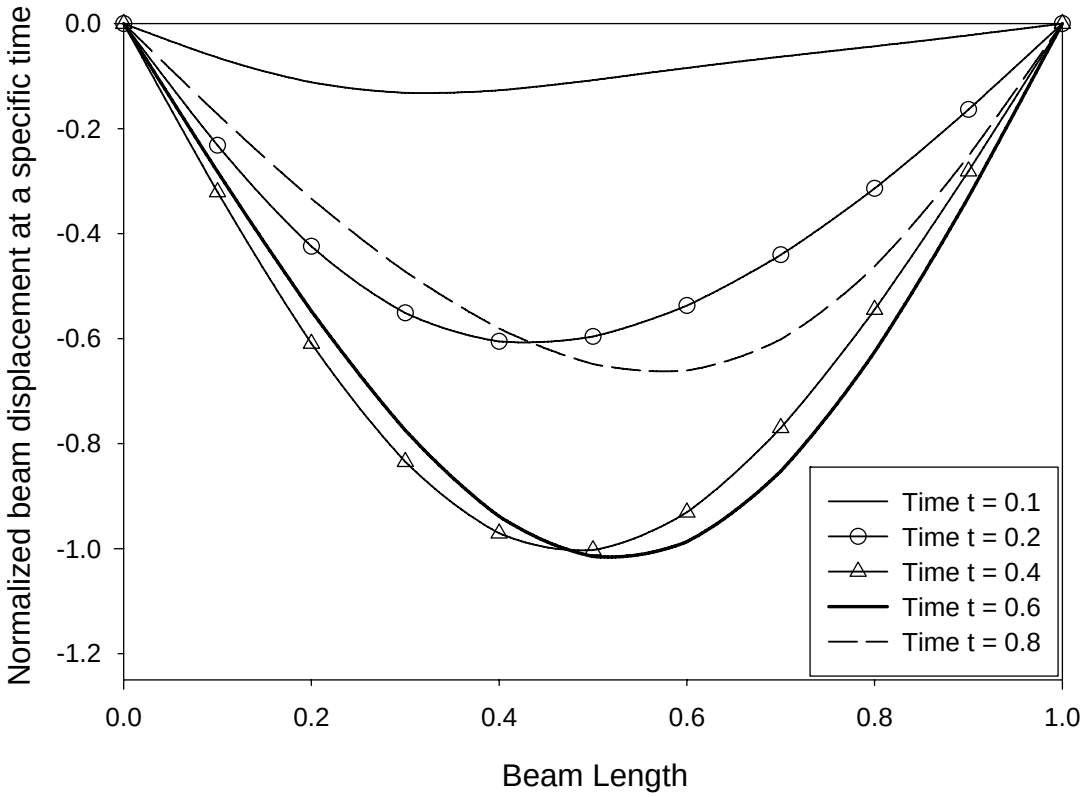

Figure 5.12: Deflected beam shape at specific instants of (normalized) time for $\alpha = 0.196$, $\gamma = 1$, $\kappa = 0.16$ and $\beta = 0.02$

The sprung mass displacement was found to increase with higher speeds as shown in the *Figure 5.13*. This follows directly from the fact that there is no loss of contact and more the beam displaces, the larger is the sprung mass displacement. The interaction (reaction) force between the oscillator and the beam is shown in the *Figure 5.14*. The *Figures 5.13* and *5.14* suggested that the sprung mass displaced to a maximum value when the interaction force also reached a maximum. The interaction force should always be non-negative to avoid loss of contact from the beam but it also should be sufficiently low so as to not to induce upward force on the moving oscillator.

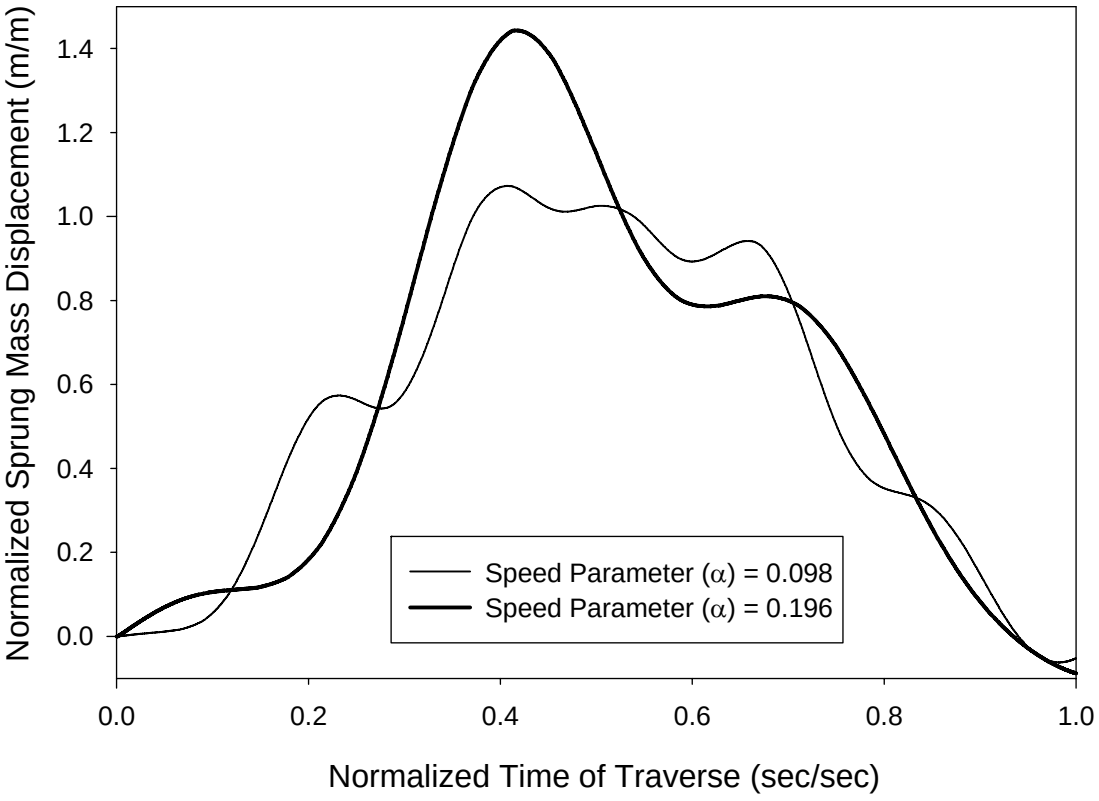

Figure 5.13: Sprung mass displacement response at $\kappa = 0.16$ and $\gamma = 1$

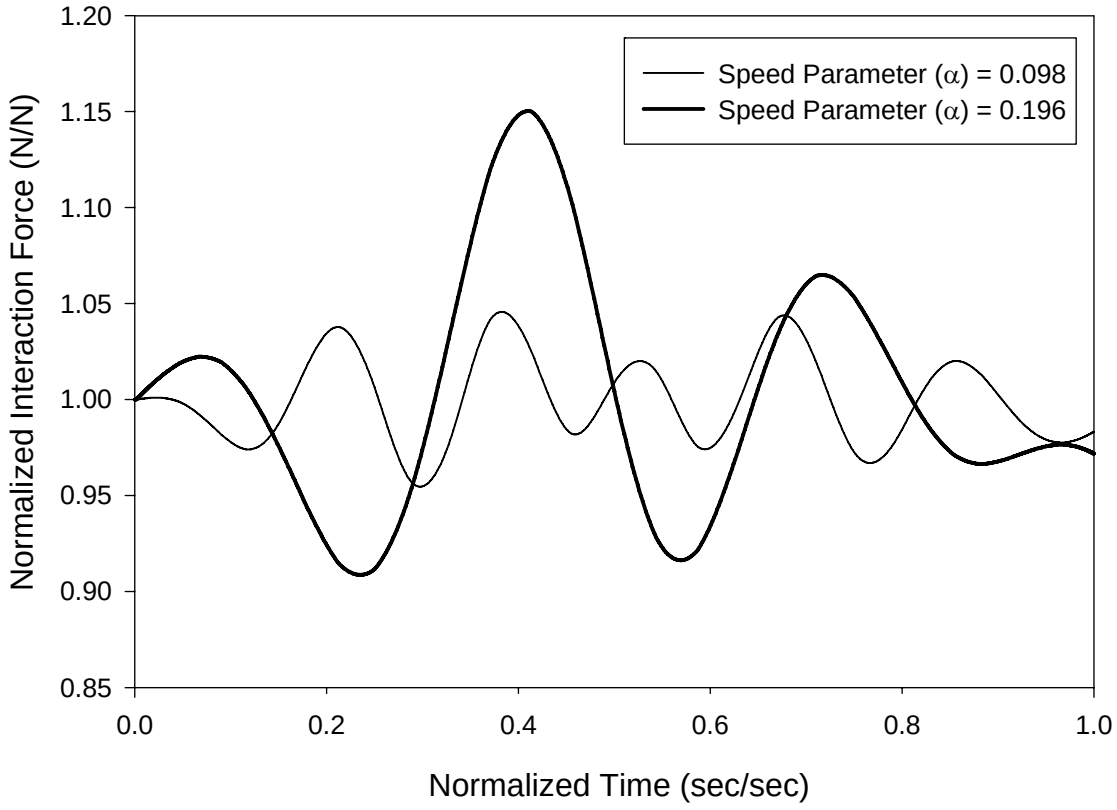

Figure 5.14: Vehicle Bridge Interaction force at κ = 0.16 and γ = 1

The *Mathematica* code for the moving oscillator can be modified to include variable stiffness surface for the bridge deck by redefining the constant stiffness parameter $K_{original}$, for example $K = K_{original}(1 + 0.3Cos[2\pi\tau])$ in accordance with input parameters presented in *Table 8.1* of [10]. Similarly, track irregularities can also be included as a sinusoidal function of space variable at the point of contact. Both the track stiffness variability and track waviness were not included in the current study.

5.3.2 Effect of Parameters on VBI:

The effect of speed parameter on the dynamic amplification factor obtained for moving force and moving oscillator system at a vehicle to bridge mass ratio $\kappa = 0.1$ is shown in

the *Figure 5.15*. For speed parameters $\alpha < 0.2$, dynamic response obtained from both the moving force and moving oscillator models seemed almost the same.

The moving force model predicted higher dynamic amplification factors for speed parameters $\alpha > 0.2$. This observation also agreed with the *Green and Cebon* [58] conclusions on the results obtained using the moving oscillator model. The effect of damping parameter on the dynamic amplification factor using moving oscillator is very similar to that obtained from moving force model.

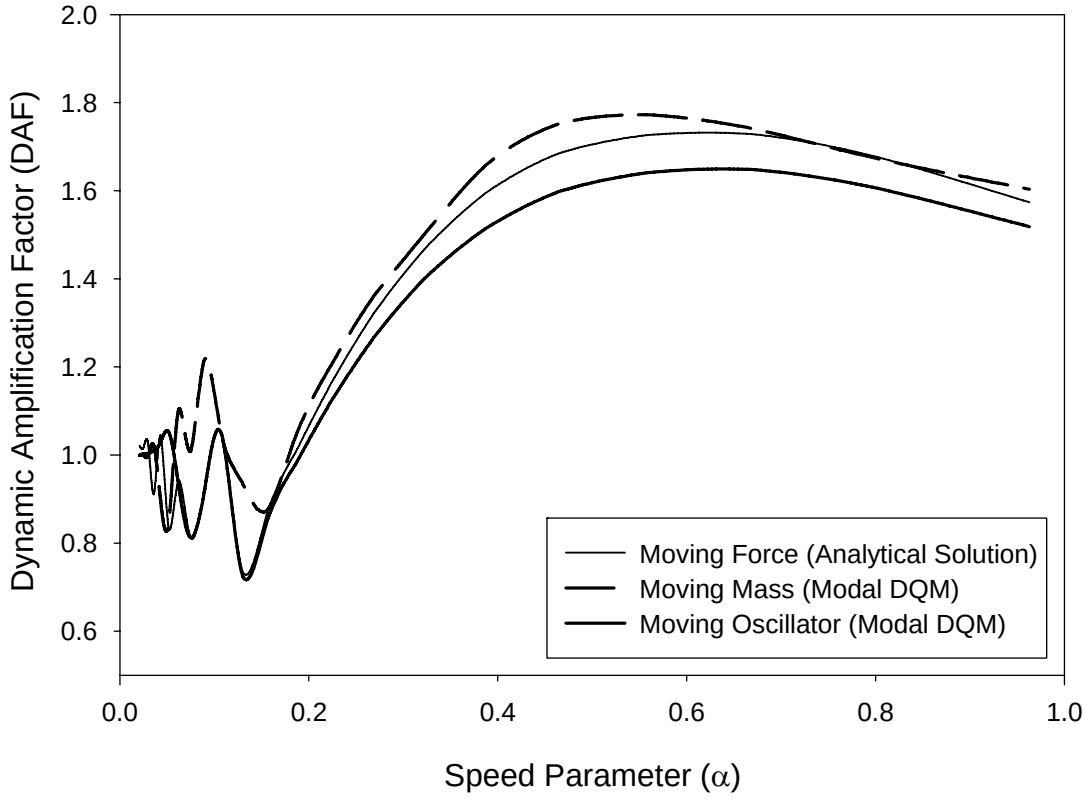

Figure 5.15: Effect of speed parameter on the dynamic amplification factor for moving force, moving mass and moving oscillator models

The *Figure 5.16* shows the variation in dynamic amplification factor over frequency ratio at different speed parameter values. However it did not show any resonance due to frequency match at $\gamma = 1$, rather the dynamic amplification decreases near $\gamma = 1$ implying that the oscillator absorbs energy at or near the resonance zone. *Green and Cebon* [58] noted that the resonance phenomenon occurred at $\gamma = 1$ while also concluded that the dynamic response of the bridge structure using moving oscillator model to be lower than that obtained from the moving force model. The *Figure 5.17* shows the effect of unsprung to sprung mass ratio on the dynamic amplification factor at $\alpha = 0.063, 0.125$ *and* 0.25. The dynamic response of the system increased with the increase in mass ratio at higher speed parameters.

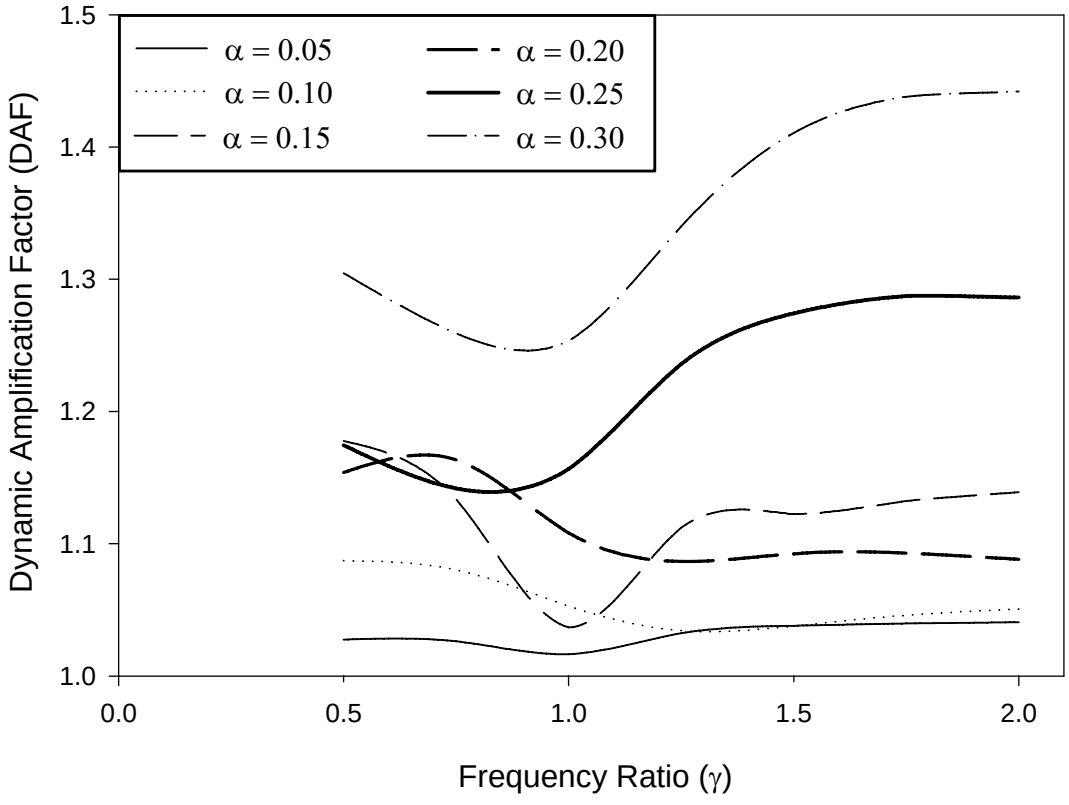

Figure 5.16: Effect of frequency ratio on the dynamic amplification factor at various speeds (n = 61)

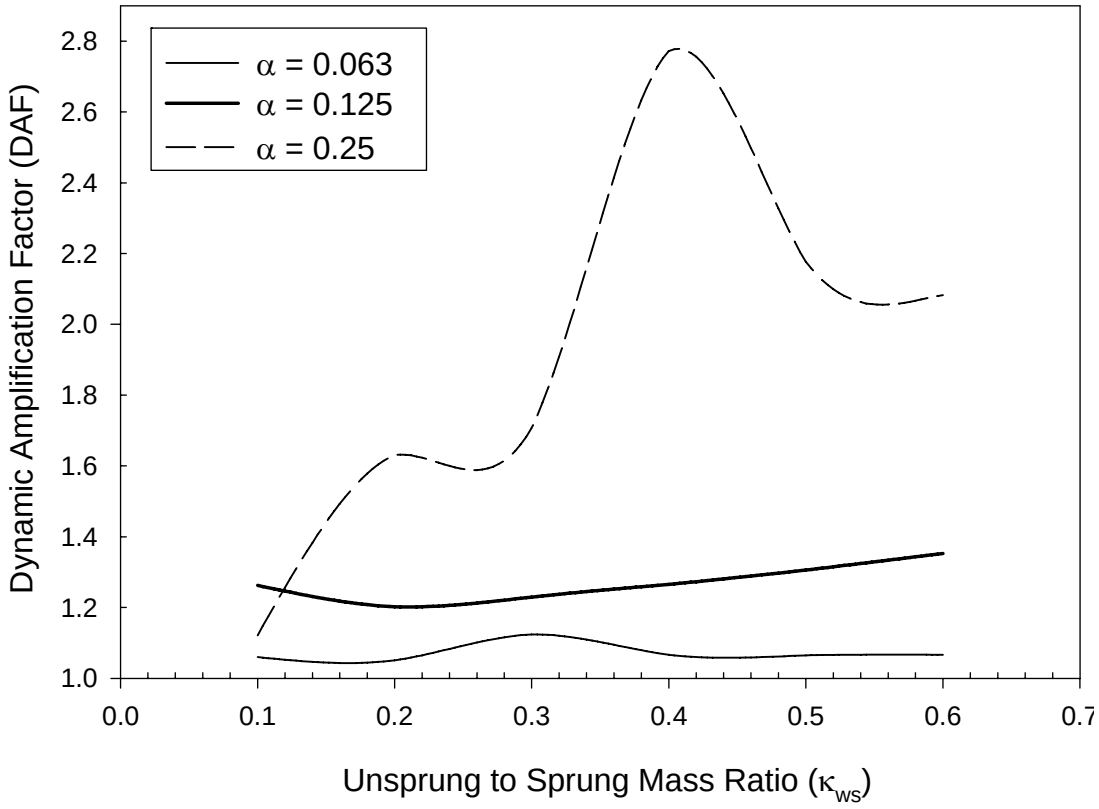

Figure 5.17: Effect of unsprung to sprung mass ratio on the dynamic amplification factor at different speeds

The dynamic behavior of a bridge-vehicle system using moving force, moving mass and moving oscillator models were discussed with respect to the dynamic amplification factors across the speed parameter range. The moving force model seemed conservative when compared to the moving oscillator model. The moving mass model produced the most conservative results among the three models used.

Chapter 6: Two Axle Moving Load System Using Oscillator Model

Introduction:

This chapter discusses the dynamic behavior of an idealized bridge structure modeled as an *Euler* beam subjected to a moving vehicular load represented by a two axle load system i.e. a half car model. The vehicle system is considered as four degrees of freedom system i.e. two unsprung masses representing front and rear wheel & axle loads with only vertical displacement degree of freedom, and one sprung mass representing vehicle chassis weight with one vertical displacement and one rotational degree of freedom as shown in the *Figure 6.1*. The sprung mass (chassis mass) is connected to the unsprung masses (wheel and axle mass) through linear springs and dashpot systems.

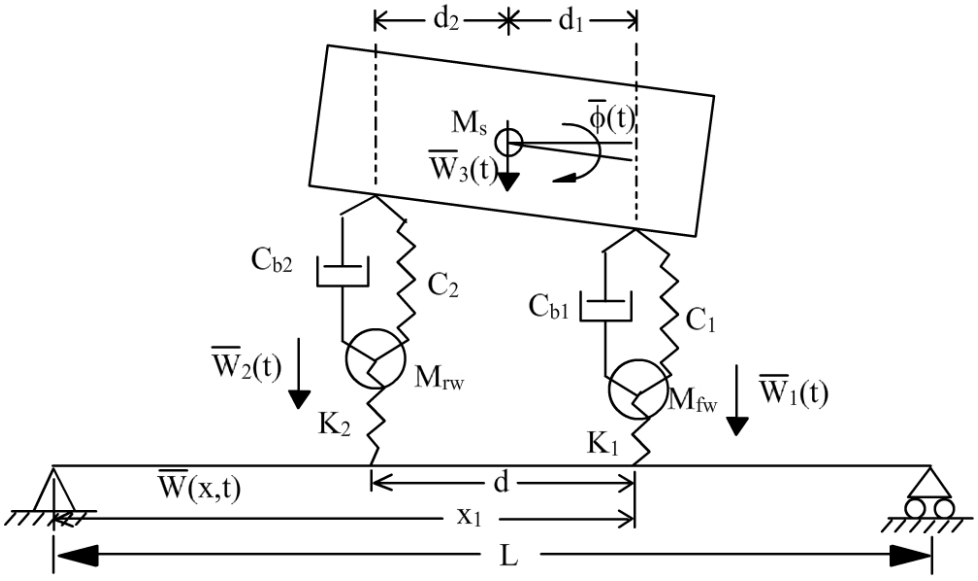

Figure 6.1: Beam under moving two axle load system

6.1 Model description and parameter definitions:

The front and rear wheel tires were assumed to carry a constant stiffness of K_1 and K_2, respectively and were separated by an axle spacing of d. The parameters d_1 and d_2 represent the distance from the center of gravity of sprung mass (chassis) to the front and rear axle load points, respectively. Other parameters used in the analysis were listed with their descriptions below.

Unsprung weight of vehicle (front wheels/axle) due to mass (M_{fw}), $P_{fw} = M_{fw}g$

Unsprung weight of vehicle (rear wheels/axle) due to mass (M_{rw}), $P_{rw} = M_{rw}g$

Sprung weight of vehicle (chassis) due to mass (M_s), $P_s = M_s g$

Total weight of the vehicle, $P = Mg = P_{fw} + P_{rw} + P_s = (M_{fw} + M_{rw} + M_s)g$

Spring constant of the suspension system at front axle = C_1

Spring constant of the suspension system at rear axle = C_2

Viscous damping coefficient of suspension system at front axle = C_{b1}

Viscous damping coefficient of suspension system at rear axle = C_{b2}

Natural frequency of the beam at j^{th} mode of vibration, $f_{(j)} = \frac{j^2\pi}{2L^2}\sqrt{\frac{EI}{\mu}}$

Sprung mass frequency at front wheel, $f_{s1} = \frac{1}{2\pi}\sqrt{\frac{C_1}{M}}$

Sprung mass frequency at rear wheel, $f_{s2} = \frac{1}{2\pi}\sqrt{\frac{C_2}{M}}$

Unsprung front axle mass frequency, $f_{fw} = \frac{1}{2\pi}\sqrt{\frac{K_1}{M}}$

Unsprung rear axle mass frequency, $f_{rw} = \frac{1}{2\pi}\sqrt{\frac{K_2}{M}}$

The damping ratio or the damping parameter (β) for the beam is defined as the ratio of frequency of damping for the beam to its natural frequency i.e. $\beta = \frac{\omega_b}{\omega_{(1)}}$, and the logarithmic damping decrements for the front and rear axle suspension systems are given by $\vartheta_1 = \frac{C_{b1}}{2M\ f_{s1}}$ and $\vartheta_2 = \frac{C_{b2}}{2M\ f_{s2}}$, respectively. Also the static mid-span deflection of the beam due to load *P* acting at the center of the beam is given by, $\Delta_{st} = \frac{PL^3}{48EI}$.

The lateral deflection of the beam at any location *x* and time *t* is represented by $\overline{W}(x,t)$ and that of front and rear unsprung masses by $\overline{W}_1(t)$ and $\overline{W}_2(t)$, respectively. Similarly the deflection of the sprung mass is represented by $\overline{W}_3(t)$, and the angle of clockwise rotation of the sprung mass about its center of gravity is given by $\overline{\phi}(t)$.

The forces experienced by the suspension springs due to stiffness C_1 and C_2 are given by $\overline{Z}_1(t) = C_1[\overline{W}_3(t) + d_1\overline{\phi}(t) - \overline{W}_1(t)]$ and $\overline{Z}_2(t) = C_2[\overline{W}_3(t) - d_2\overline{\phi}(t) - \overline{W}_2(t)]$, respectively. Similarly the damping forces associated with viscous damping coefficients C_{b1} and C_{b2} of the dashpots are given by, $\overline{Z}_{b1}(t) = C_{b1}[\dot{\overline{W}}_3(t) + d_1\dot{\overline{\phi}}(t) - \dot{\overline{W}}_1(t)]$ and $\overline{Z}_{b2}(t) = C_{b2}[\dot{\overline{W}}_3(t) - d_2\dot{\overline{\phi}}(t) - \dot{\overline{W}}_2(t)]$, respectively, where the dots indicate the time derivatives of the respective parameters.

Several dependent parameters were defined to normalize the resultant deflection parameters. The following relations for normalization of primary variables were practiced by several researchers including *Fryba* [10]. Assuming dimensionless space and time parameters, ξ and τ such that $\xi = x/L$ and $\tau = c\,t/L$, then the dimensionless primary deflection parameters as shown in *Equations* 6.1 – 6.5.

$$W(\xi,\tau) = \frac{\overline{W}(x,t)}{\Delta_{st}} \tag{6.1}$$

$$W_1(\tau) = \frac{\overline{W_1}(t)}{\Delta_{st}} \tag{6.2}$$

$$W_2(\tau) = \frac{\overline{W}_2(t)}{\Delta_{st}} \tag{6.3}$$

$$W_3(\tau) = \frac{\overline{W}_3(t)}{\Delta_{st}} \tag{6.4}$$

$$\phi(\tau) = \frac{\overline{\phi}(t)\,d}{\Delta_{st}} \tag{6.5}$$

A few derived dimensionless parameters were introduced to measure the effects of fundamental quantities such as speed and weight of the moving vehicle, weight of the

bridge, etc. on the vibration characteristics of a coupled bridge and vehicle system, and are listed below.

Vehicle to bridge mass ratio, $\kappa = \frac{P}{G}$

Front axle to vehicle mass ratio, $\kappa_1 = \frac{P_{fw}}{P}$

Rear axle to vehicle mass ratio, $\kappa_2 = \frac{P_{rw}}{P}$

Dimensionless inertia parameter, $\lambda = \frac{I_p}{M d^2}$, where I_p is the polar moment of inertia of sprung mass about its centroid and d is the axle spacing or separation distance.

Dimensionless speed parameter, $\alpha = \frac{\omega}{\omega_{(1)}} = \frac{c}{2 f_{(1)} L}$

Sprung frequency parameter at front wheel, $\gamma_{s1} = \frac{f_{s1}}{f_{(1)}} = \frac{\sqrt{C_1 / M}}{\omega_{(1)}}$

Sprung frequency parameter at rear wheel, $\gamma_{s2} = \frac{f_{s2}}{f_{(1)}} = \frac{\sqrt{C_2 / M}}{\omega_{(1)}}$

Unsprung frequency parameter at front wheel, $\gamma_{w1} = \dfrac{f_{fw}}{f_{(1)}} = \dfrac{\sqrt{K_1 / M}}{\omega_{(1)}}$

Unsprung frequency parameter at rear wheel, $\gamma_{w2} = \dfrac{f_{rw}}{f_{(1)}} = \dfrac{\sqrt{K_2 / M}}{\omega_{(1)}}$

The dimensionless terms associated with the spring forces of the front and rear suspension system are given by, $z_1(\tau) = \dfrac{\overline{Z}_1(t)}{C_1 \Delta_{st}} = W_3(\tau) + \dfrac{d_1}{d}\phi(\tau) - W_1(\tau)$ and $z_2(\tau) = \dfrac{\overline{Z}_2(t)}{C_2 \Delta_{st}} = W_3(\tau) - \dfrac{d_2}{d}\phi(\tau) - W_2(\tau)$, respectively and associated damping forces are given by $\dot{z}_1(\tau) = \dot{W}_3(\tau) + \dfrac{d_1}{d}\dot{\phi}(\tau) - \dot{W}_1(\tau)$ and $\dot{z}_2(\tau) = \dot{W}_3(\tau) - \dfrac{d_2}{d}\dot{\phi}(\tau) - \dot{W}_2(\tau)$, respectively.

6.2 Governing equations of motion for two axle load system:

6.2.1 Governing equations in dimensionless form:

The equations of motion governing the rotational and vertical displacements of the sprung mass in terms of the above defined dimensionless parameters are given by *Equations* 6.6 and 6.7, respectively.

$$\ddot{\phi}(\tau) = \frac{1}{\lambda\alpha^2}\left\{-\frac{\pi^2\gamma_{s1}^2 d_1}{d} z_1(\tau) - \frac{\alpha\vartheta_1\gamma_{s1} d_1}{d}\dot{z}_1(\tau) + \frac{\pi^2\gamma_{s2}^2 d_2}{d} z_2(\tau) + \frac{\alpha\vartheta_2\gamma_{s2} d_2}{d}\dot{z}_2(\tau)\right\} \tag{6.6}$$

$$\ddot{W}_3(\tau) = -\frac{1}{(1-\kappa_1-\kappa_2)\alpha^2}\left\{\pi^2\gamma_{s1}^2 z_1(\tau) + \alpha\vartheta_1\gamma_{s1}\dot{z}_1(\tau) + \pi^2\gamma_{s2}^2 z_2(\tau) + \alpha\vartheta_2\gamma_{s2}\dot{z}_2(\tau)\right\} \tag{6.7}$$

The governing equations of motion for the two unsprung masses are given by,

$$\ddot{W}_1(\tau) = \frac{24}{\pi^2\kappa_1\kappa\alpha^2}\left\{2Q_1 + \frac{\pi^4}{24}\kappa\gamma_{s1}^2 z_1(\tau) + \frac{\pi^2}{24}\kappa\alpha\vartheta_1\gamma_{s1}\dot{z}_1(\tau) - R_1(\tau)\right\} \tag{6.8}$$

$$\ddot{W}_2(\tau) = \frac{24}{\pi^2\kappa_2\kappa\alpha^2}\left\{2Q_2 + \frac{\pi^4}{24}\kappa\gamma_{s2}^2 z_2(\tau) + \frac{\pi^2}{24}\kappa\alpha\vartheta_2\gamma_{s2}\dot{z}_2(\tau) - R_2(\tau)\right\} \tag{6.9}$$

where $Q_1 = \frac{P_{fw} + P_s(d_2/d)}{P}$ and $Q_2 = \frac{P_{rw} + P_s(d_1/d)}{P}$ represent the dimensionless static axle loads, $R_1(\tau) = \frac{\pi^4\kappa\gamma_{w1}^2}{24}\left(W_1(\tau) - W(\xi_1,\tau)\right)$ and $R_2(\tau) = \frac{\pi^4\kappa\gamma_{w2}^2}{24}\left(W_2(\tau) - W(\xi_2,\tau)\right)$ represent the reaction forces experienced at the points of contact of front and rear axle loads.

The governing equation of motion for the beam is given by

$$\pi^2\alpha^2\frac{\partial^2 W}{\partial\tau^2} + 2\pi^3\alpha\beta\frac{\partial W}{\partial\tau} + \frac{\partial^4 W}{\partial\xi^4} = 48\left\{\varepsilon_1\delta(\xi-\xi_1)R_1(\tau) + \varepsilon_2\delta(\xi-\xi_2)R_2(\tau)\right\} \tag{6.10}$$

where $\varepsilon_1 = \begin{cases} 1 & \text{if } 0 < \xi_1 < 1 \\ 0 & \text{otherwise} \end{cases}$, and $\varepsilon_2 = \begin{cases} 1 & \text{if } \frac{d}{L} < \xi_2 < 1 + \frac{d}{L} \\ 0 & \text{otherwise} \end{cases}$

The governing differential equation of motion for the beam is further simplified as

$$\frac{\alpha^2}{\pi^2}\frac{d^2 w_j}{d\tau^2} + \frac{2\alpha\beta}{\pi}\frac{dw_j}{d\tau} + j^4 w_j = R_1(\tau) Sin\ j\pi\xi_1 + R_2(\tau) Sin\ j\pi\xi_2 \qquad (6.11)$$

using $W(\xi,\tau) = \sum_{j=1}^{n} w_j(\tau) Sin\ j\pi\xi$ where n is the number of modes of significance. The governing equation in the time coordinate system required only initial conditions since the spatial term was decoupled. Also, the initial conditions for the beam, i.e., $W(\xi,0) = 0$ and $\frac{\partial W(\xi,0)}{\partial\tau} = 0$ transforms to $w_j(\tau)\Big|_{\tau=0} = 0$ and $\left.\frac{dw_j(\tau)}{d\tau}\right|_{\tau=0} = 0$ for $j = 1, 2, ..., n$ at any arbitrary location of the beam.

Since the governing differential equations of beam, unsprung and sprung masses are of second order, two initial conditions are required as given by

$W(\xi,0) = 0$ and $\frac{1}{T}\frac{\partial W(\xi,0)}{\partial\tau} = 0$ for the beam,

$W_1(0) = W_{10}$ and $\frac{1}{T}\frac{dW_1(0)}{d\tau} = \dot{W}_{10}$ for the unsprung front axle/wheel load,

$W_2(0) = W_{20}$ and $\frac{1}{T}\frac{dW_2(0)}{d\tau} = \dot{W}_{20}$ for the unsprung front axle/wheel load,

$W_3(0) = W_{30}$ and $\frac{1}{T}\frac{dW_3(0)}{d\tau} = \dot{W}_{30}$ for the vertical movement, and

$\phi(0) = \phi_0$ and $\frac{1}{T}\frac{d\phi(0)}{d\tau} = \dot{\phi}_0$ for the rotational motion of sprung chassis load.

In the above descriptions, $T = L/c$ is the normalization factor for time, and some of the initial values to be input were shown with an additional subscript '0'.

6.2.2 DQ analog of the governing equations:

The DQ analog of the governing equation of motion for the beam in mode coordinates is given by

$$\frac{\alpha^2}{\pi^2}\sum_{k=1}^{N} B_{jk} w_{ik} + \frac{2\alpha\beta}{\pi}\sum_{k=1}^{N} A_{jk} w_{ik} + i^4 w_{ij}$$

$$= \begin{cases} R_{1j}\, Sin\ i\pi\tau_j & \text{for } 0 \le \tau_j \le \frac{d}{L} \\ R_{1j}\, Sin\ i\pi\tau_j \ + \ R_{2j}\, Sin\ i\pi\left(\tau_j - \frac{d}{L}\right) & \text{for } \frac{d}{L} < \tau_j < 1 \\ R_{2j}\, Sin\ i\pi\left(\tau_j - \frac{d}{L}\right) & \text{for } 1 \le \tau_j \le 1 + \frac{d}{L} \end{cases} \qquad (6.12)$$

The DQ analog of the equation governing the rotational and vertical motion of sprung mass are given by

$$\lambda\alpha^2\sum_{k=1}^{N}B_{jk}\varphi_k + \frac{\pi^2\gamma_{s1}^2 d_1}{d}z_{1j} + \frac{\alpha\vartheta_1\gamma_{s1}d_1}{d}\sum_{k=1}^{N}A_{jk}z_{1k} - \frac{\pi^2\gamma_{s2}^2 d_2}{d}z_{2j} - \frac{\alpha\vartheta_2\gamma_{s2}d_2}{d}\sum_{k=1}^{N}A_{jk}z_{2k} = 0 \tag{6.13}$$

where $z_{1j} = z_1(\tau_j)$ and $z_{2j} = z_2(\tau_j)$.

$$(1-\kappa_1-\kappa_2)\alpha^2\sum_{k=1}^{N}B_{jk}W_{3k} + \pi^2\gamma_{s1}^2 z_{1j} + \alpha\vartheta_1\gamma_{s1}\sum_{k=1}^{N}A_{jk}z_{1k} + \pi^2\gamma_{s2}^2 z_{2j} + \alpha\vartheta_2\gamma_{s2}\sum_{k=1}^{N}A_{jk}z_{2k} = 0 \tag{6.14}$$

where $W_{3j} = W_3(\tau_j)$.

The DQ analog governing the vertical motion of the unsprung masses are given by,

$$\frac{\pi^2\kappa_1\kappa\alpha^2}{24}\sum_{k=1}^{N}B_{jk}W_{1k} - 2Q_1 + \frac{\pi^4}{24}\kappa\gamma_{s1}^2 z_{1j} + \frac{\pi^2}{24}\kappa\alpha\vartheta_1\gamma_{s1}\sum_{k=1}^{N}A_{jk}z_{1k} - R_{1j} = 0 \tag{6.15}$$

where $W_{1j} = W_1(\tau_j)$.

$$\frac{\pi^2 \kappa_2 \kappa \alpha^2}{24} \sum_{k=1}^{N} B_{jk} W_{2k} - 2Q_2 + \frac{\pi^4}{24} \kappa \gamma_{s2}^2 z_{2j} + \frac{\pi^2}{24} \kappa \alpha \vartheta_2 \gamma_{s2} \sum_{k=1}^{N} A_{jk} z_{2k} - R_{2j} = 0 \tag{6.16}$$

where $W_{2j} = W_2(\tau_j)$.

In the above set of equations *Equations* 6.13-6.16, it should be further noted that the terms involving $z_1(\tau)$ and $z_2(\tau)$ included the definitions of appropriate DQ analogs i.e.

$z_{1j} = z_1(\tau_j) = W_{3j} + \frac{d_1}{d}\phi_j - W_{1j}$ and $z_{2j} = z_2(\tau_j) = W_{3j} - \frac{d_2}{d}\phi_j - W_{2j}$.

6.3 Discussion of Results:

The results obtained for a two axle load system using a moving two point force model and moving system of two connected oscillators cannot be effectively compared i.e. the parameters defining the dynamic characteristics of a two axle load oscillator system are many, and a slight change in the choice of these parameters could affect the comparison. For this reason, this section discusses the dynamic behavior of an *Euler* beam due to a two axle load system using moving force and moving oscillator models by fixing a set of parameters on the moving oscillator except the speed parameter and inter-load spacing parameter which are then varied to study the differences in the results obtained from the two models.

The beam and load parameters used in the preceding chapter “Chapter 4: Two point moving force system” were also used in this chapter with an additional set of parameters

characteristic of the oscillator model, and all the parameters used in the study were listed below: -

Length of the beam, $L = 25m$

Natural frequency of the beam, $\omega_{(1)} = 21.86\ rad/\sec$

Linear density of the beam, $\mu = 2289\ kg/m$

Front unsprung wheel/axle load, $P_{fw} = 2806.88\ N$

Rear unsprung wheel/axle load, $P_{rw} = 2806.88\ N$

Sprung vehicle chassis load, $P_s = 50523.95\ N$

Total vehicle load, $P = P_{fw} + P_{rw} + P_s = 56137.7\ N$

Vehicle mass to bridge mass ratio, $\kappa = 0.1$

Unsprung front wheel mass to vehicle mass ratio, $\kappa_1 = 0.05$

Unsprung rear wheel mass to vehicle mass ratio, $\kappa_2 = 0.05$

Speed parameter, $\alpha = 0.1$

Damping parameter, $\beta = 0.03$

Frequency of sprung mass w.r.t front wheel, $f_{s1} = 0.19\ Hz$

Frequency of sprung mass w.r.t rear wheel, $f_{s2} = 0.19\ Hz$

Frequency of unsprung front wheel mass, $f_{fw} = 0.957\ Hz$

Frequency of unsprung rear wheel mass, $f_{rw} = 0.957\ Hz$

Logarithmic damping decrement of the front and rear end dashpots, $\vartheta_1 = \vartheta_2 = 0.5$

Polar moment of inertia of sprung mass I_p is chosen such that the dimensionless inertia parameter $\lambda = \frac{I_p}{M d^2} = 0.2$, i.e. $I_p = 1144.5\, d^2$ where d is the axle spacing.

6.3.1 Effect of ILS on dynamic response:

As discussed in the *Chapter 4: Two point moving force system*, the dynamic response of the beam due to moving two axle oscillator decreased with increase in the ILS which is expected in view of the definition of the normalized dynamic deflection. The *Figures 6.2* and *6.3* show the dynamic responses of the beam obtained from moving force and moving oscillator models at $ILS = 0.1\ and\ 0.3$. Both the models, moving force and moving oscillator, yielded similar results with the moving oscillator model predicting slightly increased response.

The *Figure 6.4* compares the dynamic response obtained from the moving oscillator model at different ILS values. The maximum normalized dynamic deflection reduced from 1.07 at $ILS = 0.1$ to 0.852 at $ILS = 0.4$. However, as discussed before, this decrease is a result of the definition of the normalized dynamic deflection.

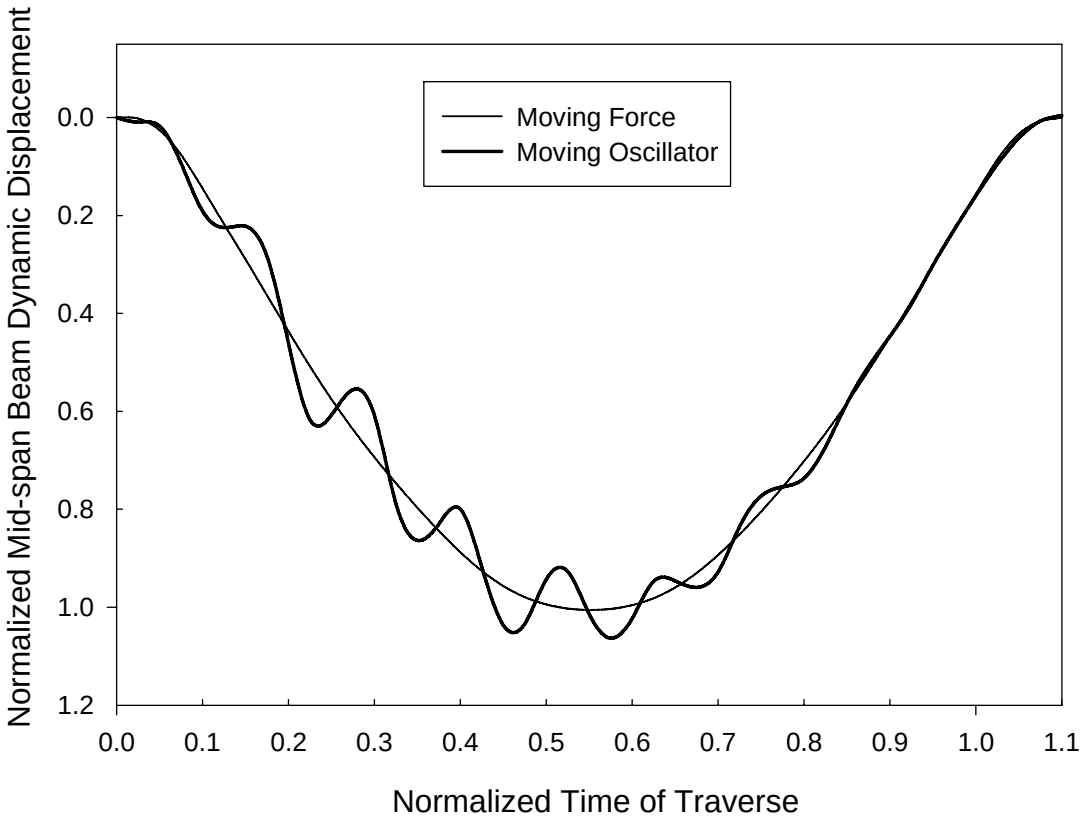

Figure 6.2: Dynamic response due to moving two axle load system using moving force and moving oscillator models (α = 0.1, κ = 0.1, β = 0.03, ILS = 0.1, $P_{fw} = P_{rw} = 2807\,N,\ P_s = 50524\,N$ **)**

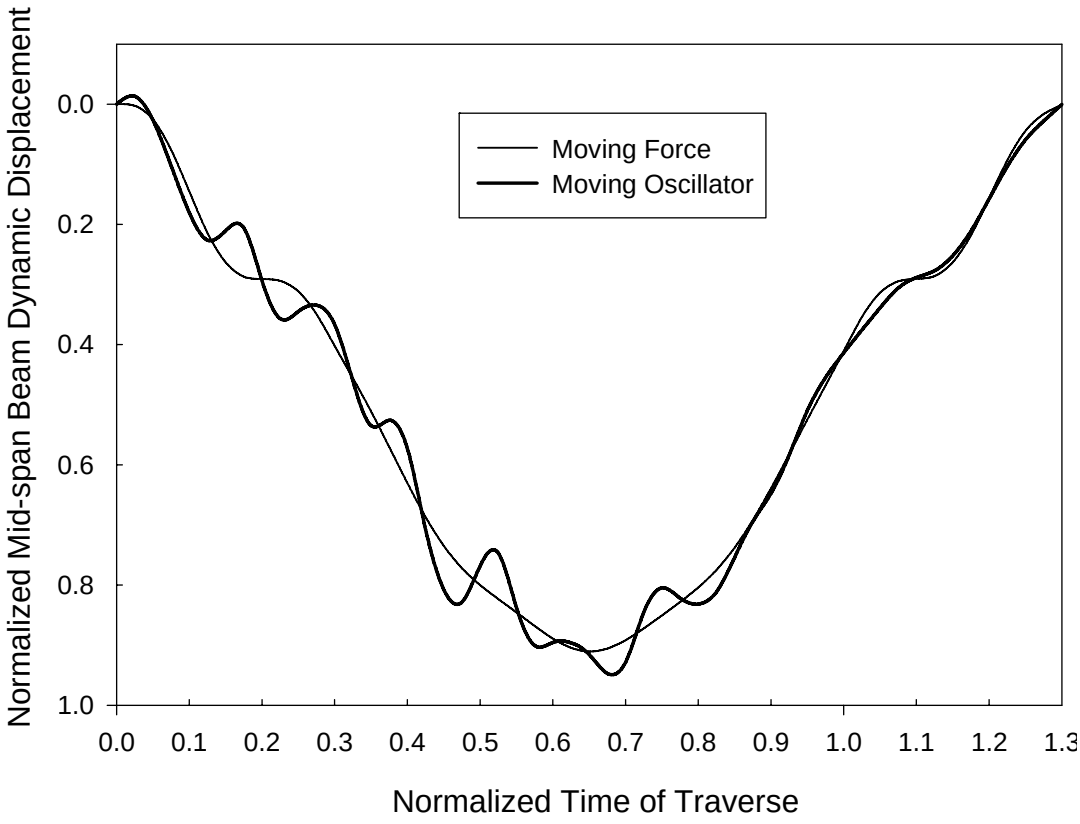

Figure 6.3: Dynamic response due to moving two axle load system using moving force and moving oscillator models (α = 0.1, κ = 0.1, β = 0.03, ILS = 0.3, $P_{fw} = P_{rw} = 2807\,N,\ P_s = 50524\,N$ **)**

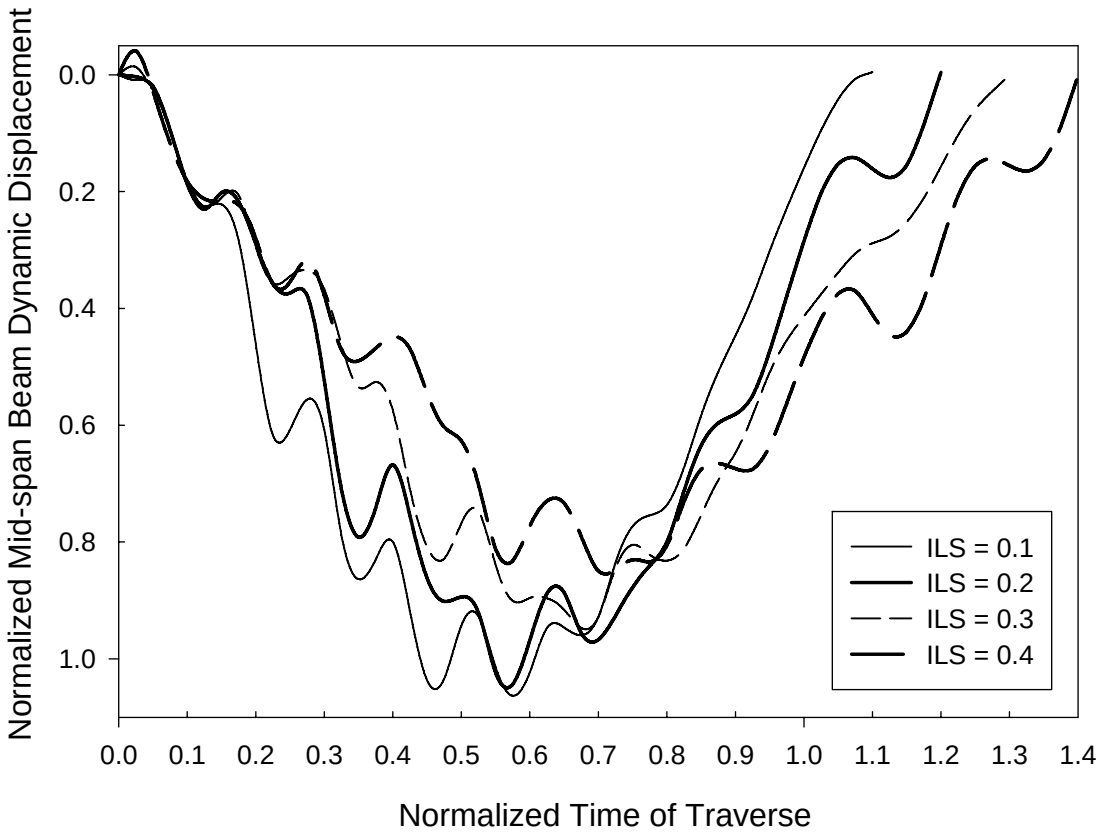

Figure 6.4: Effect of ILS on the beam dynamic response computed using moving oscillator model at $\alpha = 0.1$, $\beta = 0.03$ and $\kappa = 0.1$

6.3.2 Effect of speed parameter on dynamic response:

The *Figures 6.2* and *6.5* shows the dynamic response resulting from the increase of speed parameter from $\alpha = 0.1$ to $\alpha = 0.2$ at $ILS = 0.1$, other parameters being the same. The maximum normalized dynamic deflection of the beam predicted from the moving force model remained almost same and close to 1. However, the dynamic response computed from the moving oscillator model suggested that the increase in speed parameter resulted in the increased dynamic response of the beam.

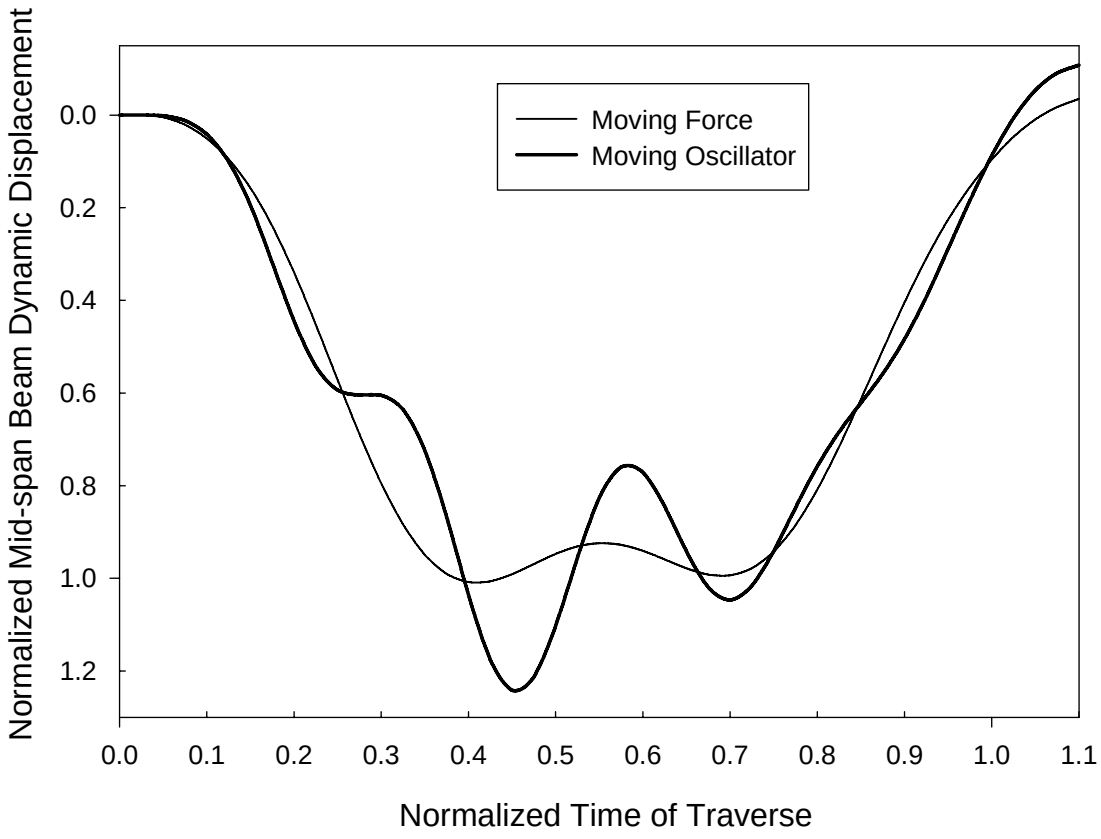

Figure 6.5: Dynamic response due to moving two axle load system using moving force and moving oscillator models (α = 0.2, κ = 0.1, β = 0.03, ILS = 0.1, $P_{fw} = P_{rw} = 2807\,N,\ P_s = 50524\,N$ **)**

The *Figure 6.6* shows the effect of speed parameter on the dynamic amplification factor obtained from moving force and moving oscillator models. The *Figure 6.7* gives a closer look at the low speed parameter range (which is typical of the highway vehicles).

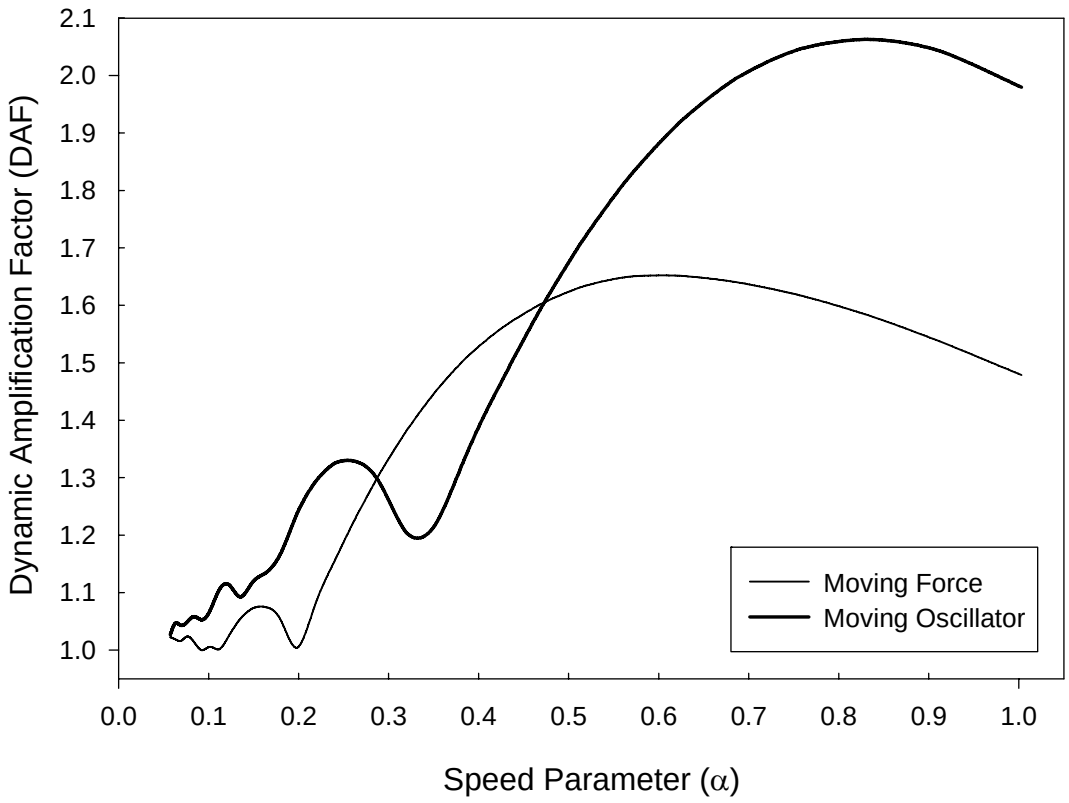

Figure 6.6: Effect of speed on the beam dynamic response due to two axle load system using moving force and moving oscillator models ($\beta = 0.03$, $\kappa = 0.1$, ILS = 0.1)

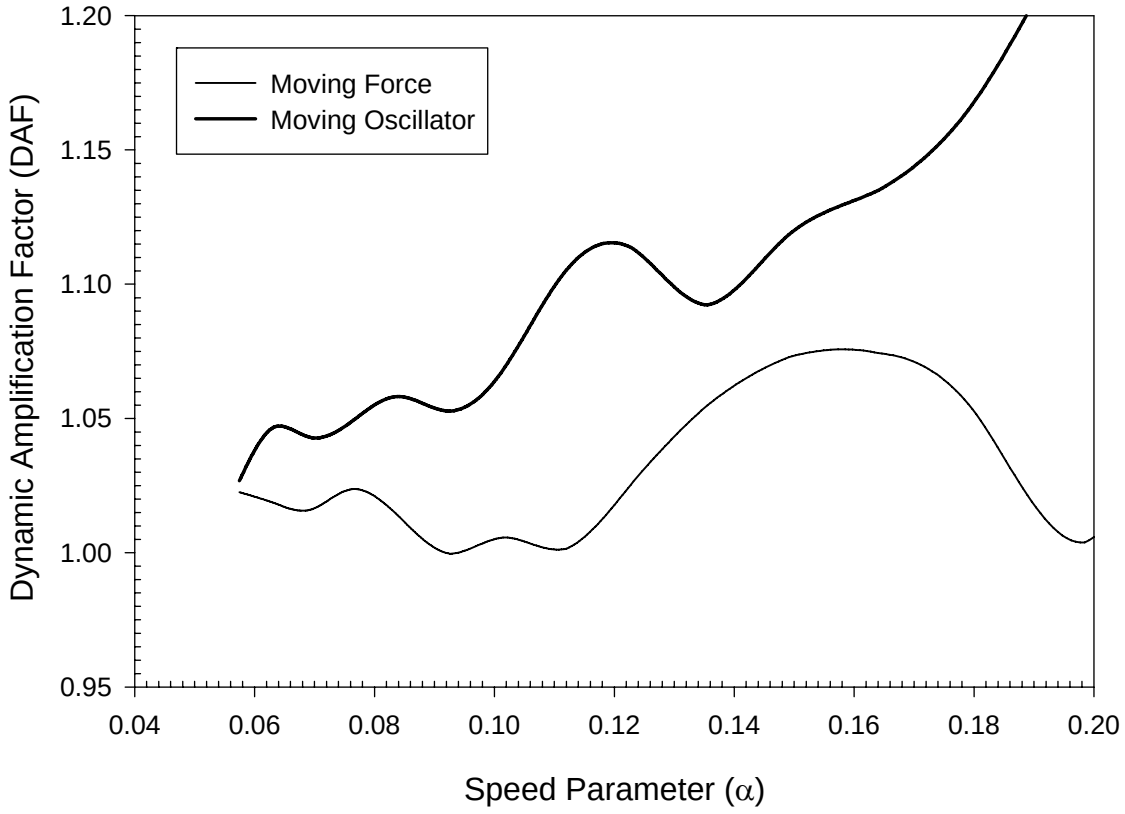

Figure 6.7: Effect of speed on the beam dynamic response due to two axle load system using moving force and moving oscillator models (β = 0.03, κ = 0.1, ILS = 0.1) – Closer look at the low speed parameter range

The dynamic response predicted from the moving oscillator model clearly exceeded the response computed from a moving force model. This behavior is observed for the mass ratio of $\kappa = 0.1$ which is usually a higher figure compared to the ratio of the mass of an actual highway vehicle to the bridge mass. The increased mass ratio is expected to bring more differences in the prediction of dynamic responses from both these models since the VBI phenomenon becomes significant.

The *Figures 6.8* and *6.9* compared the effect of speed parameter on the dynamic amplification factor for moving force and moving oscillator models at an increased axle spacing of $ILS = 0.2$. The differences seen in the dynamic responses obtained from the moving force and moving oscillator models decreased with the increase in the axle spacing. The *Figure 6.10* also suggested the same behavior i.e. the differences due to use of moving force and moving oscillator models becomes insignificant for vehicles with larger axle spacing.

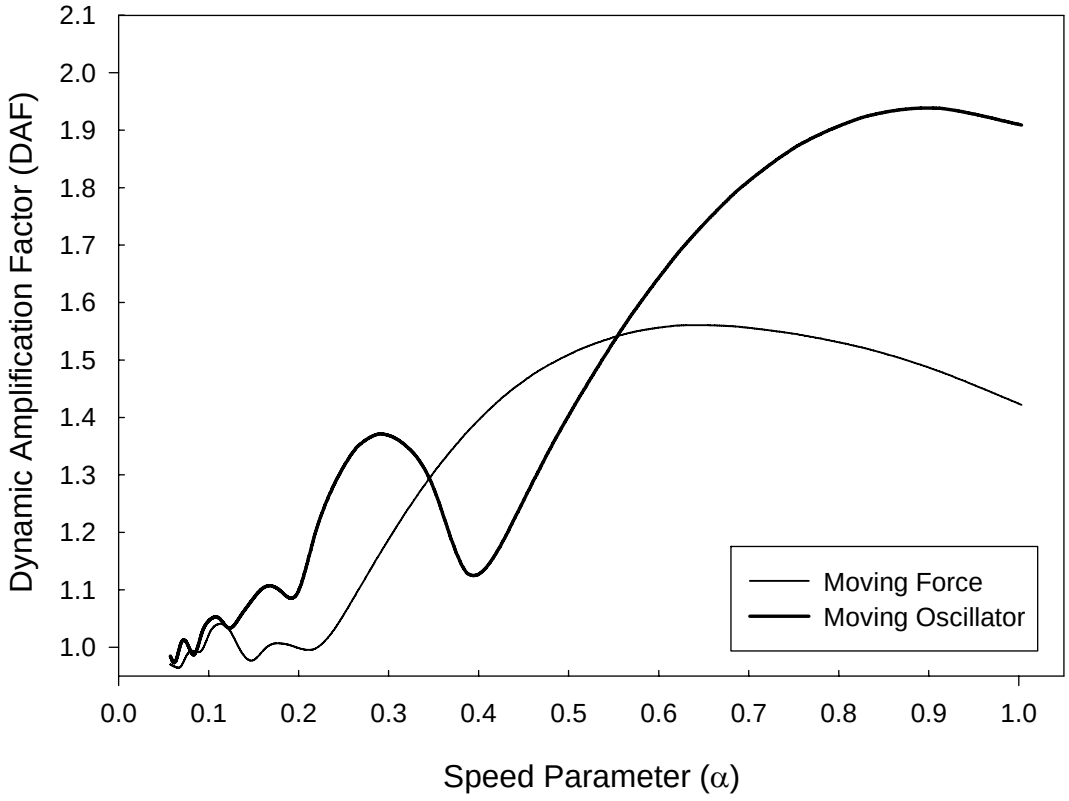

Figure 6.8: Effect of speed on the beam dynamic response due to two axle load system using moving force and moving oscillator models (β = 0.03, κ = 0.1, ILS = 0.2)

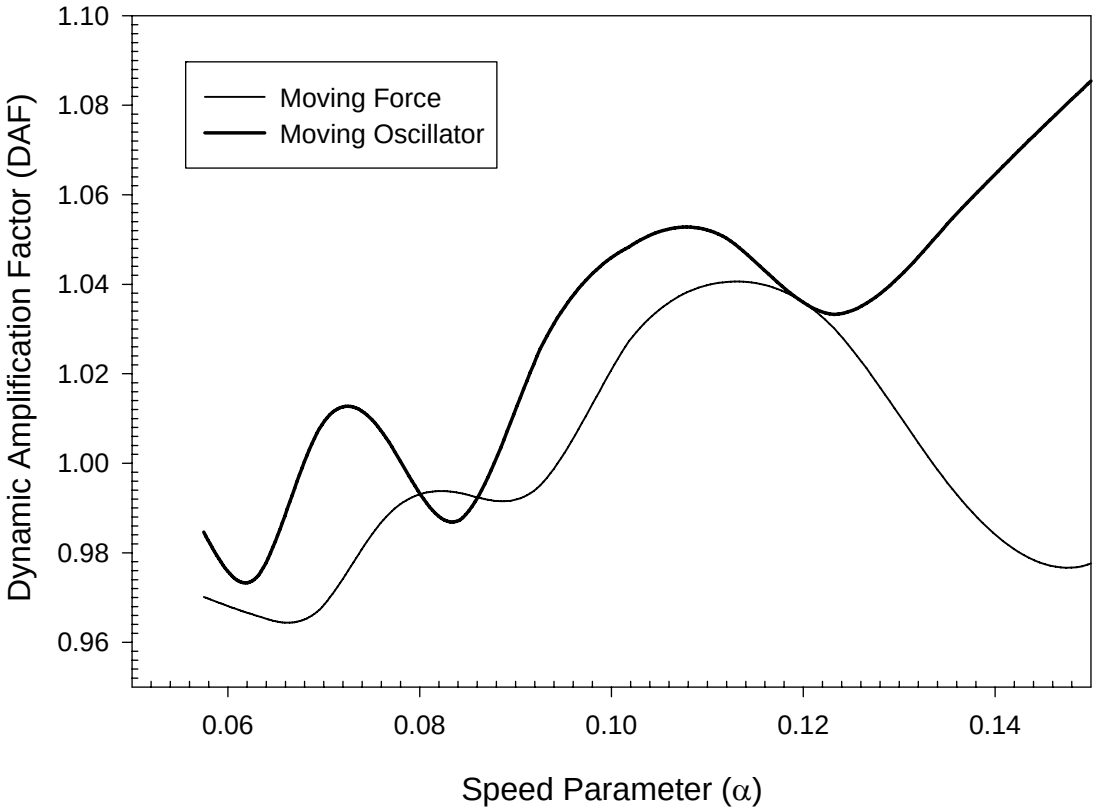

Figure 6.9: Effect of speed on the beam dynamic response due to two axle load system using moving force and moving oscillator models ($\beta = 0.03$, $\kappa = 0.1$, ILS = 0.2) – Closer look at the low speed parameter range

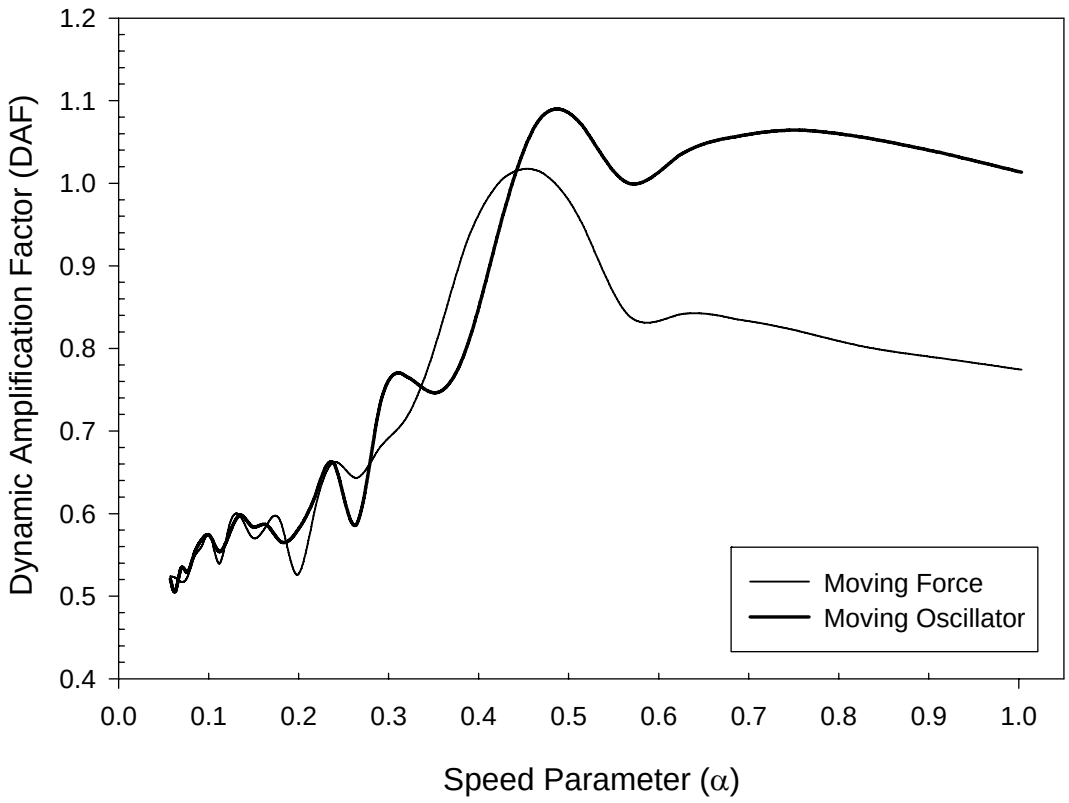

Figure 6.10: Effects of speed on the beam dynamic response due to two axle load system using moving force and moving oscillator models (β = 0.03, κ = 0.1, ILS = 0.8)

The *Figure 6.11* compared the effect of speed parameter on the dynamic amplification factor at different ILS values. As expected, the dynamic amplification factor decreased with the increase of axle spacing over the range of speed parameter.

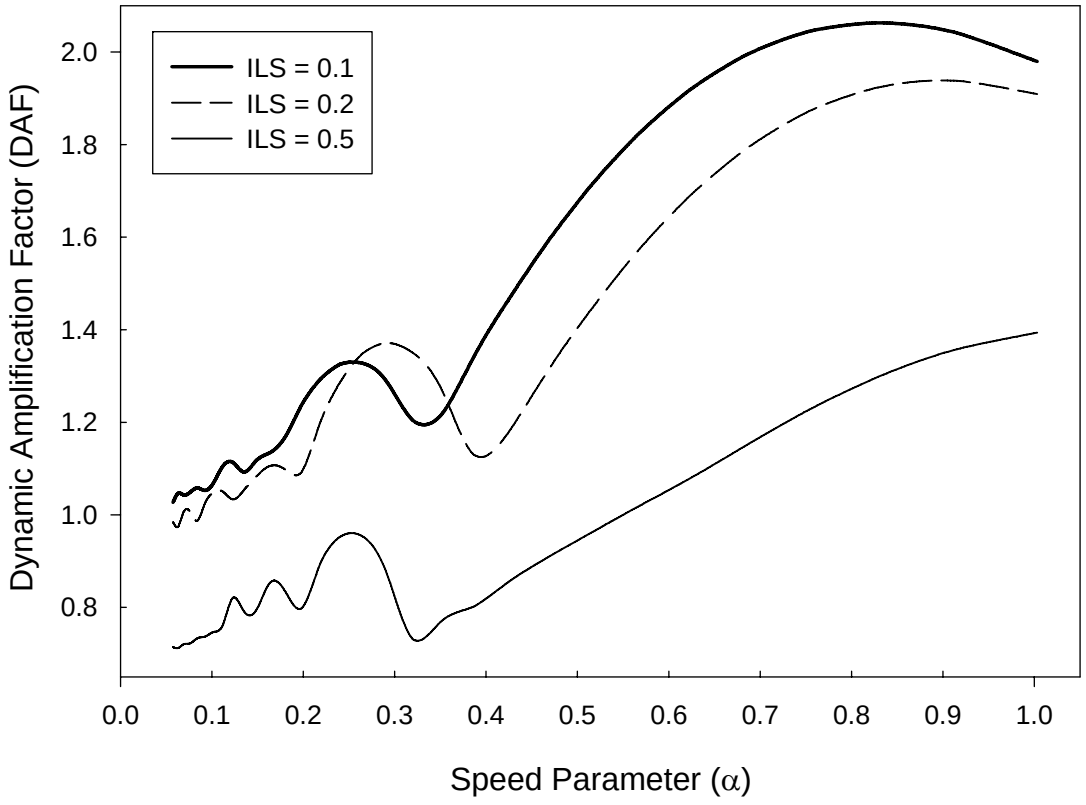

Figure 6.11: Dynamic amplification factor vs. speed parameter for a two axle load system using oscillator model at ILS = 0.1, 0.2 and 0.5 (β = 0.03 and κ = 0.1)

The dynamic response due to two axle load system using moving oscillator model was higher than that obtained using moving two point force model. This is a significant finding because in the case of single moving force and oscillator systems, the dynamic response due to moving oscillator was less that that obtained using moving point force.

Chapter 7: Kirchhoff-Love plates under moving loads

Introduction:

A vast majority of the published research on the moving load problems addressed the issue of ‘moving force-moving mass’ using beam models. The beam model and its formulation proved quite effective for introducing several new and different approaches to solve the same problem. Moreover the closed-form solutions and/or the analytical (numerically exact) solutions, if any, could be worked out easily for representative beam models including comparisons among different methods for their effectiveness i.e. ease of applicability and accuracy.

Beam model representation yields satisfactory results for higher aspect ratio bridge structures. Modern bridge structures are built with several lanes to diffuse traffic congestion, and it is likely their aspect ratios are low such that the bridge width is of the same order as its span length. Since the vehicular loads can no more thought to be always applied at the central line of bridge cross-section (which is the only possible case for beam models), plate models are necessary to account for transverse flexural and torsional modes of vibration. In this section, a simply supported (SS) rectangular isotropic *Kirchhoff* plate is used to demonstrate the application of DQM to solve for moving force problems.

7.1 Free vibration of isotropic plates:

A free vibration analysis is performed as discussed in the *Chapter 2 (Differential Quadrature Method)* to extract modal properties of the bridge. This chapter is focused on the application of the DQM to study the moving load problem, and for simplicity, the results are discussed for an isotropic plate assumed to be simply supported on all its sides i.e. SS-SS-SS-SS. The natural frequency of vibration for a simply supported plate obtained analytically by variable separable method is given by,

$$\omega_{mn} = \pi^2 \left(\frac{m^2}{L^2} + \frac{n^2}{b^2} \right) \sqrt{\frac{D}{\mu}} \tag{7.1}$$

where $D = Eh^3/12(1-\nu^2)$ is the flexural rigidity of the plate (with E and h being elastic modulus and thickness of the plate, respectively), $\mu = \rho h$ is the mass per unit area of the plate where ρ is the mass density of the plate, L and b being the plate length and width, respectively and m and n are mode numbers characterizing mode shapes along length and width, respectively and ω_{mn} is the natural frequency corresponding to the above modes, m and n. Some of the other methods to obtain modal properties include *Rayleigh* maximum energy principle, *Ritz* and *Galerkin* methods.

7.2 Moving force analysis using DQM:

The governing equation of a rectangular isotropic plate subjected to a moving point load P is given by

$$\frac{\mu}{T^2}\frac{\partial^2 W}{\partial \tau^2} + D\left(\frac{1}{L^4}\frac{\partial^4 W}{\partial x^4} + \frac{2}{L^2 b^2}\frac{\partial^4 W}{\partial x^2 \partial y^2} + \frac{1}{b^4}\frac{\partial^4 W}{\partial y^4}\right) = \delta(x - x_0)\,\delta(y - y_0)\,P \tag{7.2}$$

where $W = W(x, y, \tau)$ is the normalized transverse displacement of the plate, $\lambda = L/b$ is the plate aspect ratio, and $T = L/c$ is the total time of traverse for the load to cross the bridge at a speed c, $\tau = t/T$ is the normalized time and (x_0, y_0) is the point of action of the load with $x_0 = ct$ and y_0 is assumed to be the center of the plate width.

The variable separation principle is employed to decouple the spatial and temporal components of transverse displacement, and using the *Navier's* solution for a simply supported plate, the displacement function is assumed to be in the *Fourier* series i.e.

$$W = W(x, y, \tau) = \sum_{m=1}^{\infty}\sum_{n=1}^{\infty} w_{mn}(\tau)\ Sin\, m\pi x\ Sin\, n\pi y \tag{7.3}$$

where w is the time coordinate function, and m and n are the mode numbers.

The governing equation of motion, i.e., *Equation 7.2*, is then simplified from a partial differential equation (initial-boundary value problem) to an ordinary differential equation (initial value problem) as

$$\frac{1}{T^2}\frac{d^2 w_{mn}(\tau)}{d\tau^2}+\frac{D\pi^4}{\mu}\left(\frac{m^2}{L^2}+\frac{n^2}{b^2}\right)^2 w_{mn}(\tau)-\frac{4P}{\mu L b}Sin\, m\pi\tau\, Sin\frac{n\pi y_0}{b}=0 \qquad (7.4)$$

using the assumed displacement function. The time coordinate $w_{mn}(\tau)$, if assumed to be evaluated at a time $\tau=\tau_j$, then the governing equation in its equivalent DQ form is given by

$$\frac{1}{T^2}\sum_{k=1}^{N}B_{jk}^{(\tau)}w_{mn}(\tau_k)+\omega_{mn}^2\, w_{mn}(\tau_j)-\frac{4P}{\mu L b}Sin\, m\pi\tau_j\, Sin\frac{n\pi y_0}{b}=0 \qquad (7.5)$$

The governing equation for damped vibration of a plate structure in DQ form is given by

$$\frac{1}{T^2}\sum_{k=1}^{N}B_{jk}^{(\tau)}w_{mn}(\tau_k)+\frac{2\beta\omega_{11}}{T}\sum_{k=1}^{N}A_{jk}^{(\tau)}w_{mn}(\tau_k)+\omega_{mn}^2\, w_{mn}(\tau_j) -\frac{4P}{\mu L b}Sin\, m\pi\tau_j\, Sin\frac{n\pi y_0}{b}=0 \qquad (7.6)$$

The analytical displacement solution of an isotropic *Kirchhoff* SS-SS-SS-SS plate subjected to a moving constant force is given by

$$W(x,y,\tau)=\sum_{j=1}^{\infty}\sum_{k=1}^{\infty}\left\{\frac{4P}{\mu L b\left(\omega_{jk}^2-\omega_j^2\right)}Sin\, j\pi x\, Sin\, k\pi y\ \times Sin\frac{k\pi y_0}{b}\left(Sin\, j\pi\tau-\frac{\omega_j}{\omega_{jk}}Sin\frac{\omega_{jk}}{\omega_j}\tau\right)\right\} \qquad (7.7)$$

where $\omega_j=\frac{j\pi c}{L}$ is the driving frequency of the load.

7.3 Results and Discussion:

The normalized dynamic deflection computed using plate model was found to be slightly larger than that computed using beam model. The dynamic mid-span deflection in the speed parameter range [0-0.2] is 20% more than the static mid-span deflection. The maximum dynamic amplification was recorded around 1.81 at $\alpha \approx 0.43$. The dynamic amplification factor vs. speed parameter obtained from the analytical solution and the modal DQM using moving force model was shown in *Figure 7.1 and Figure 7.2*.

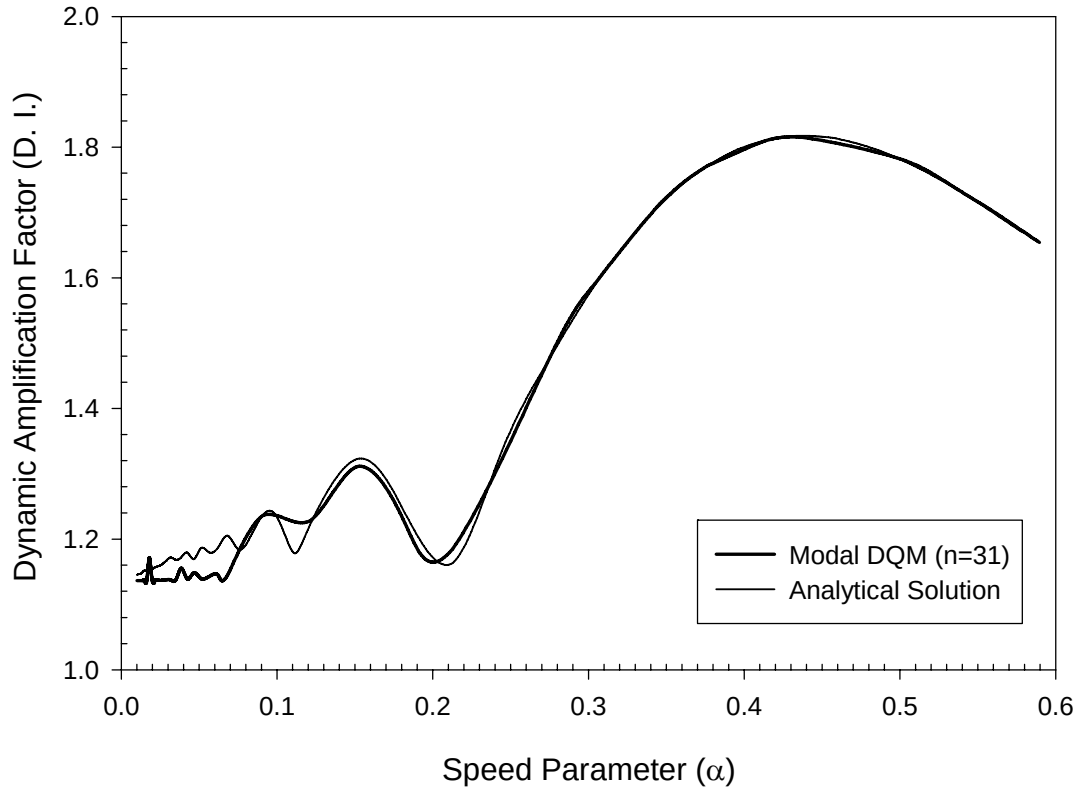

Figure 7.1: Dynamic amplification factor vs. speed parameter using analytical and modal DQM (n=31 nodes in temporal domain)

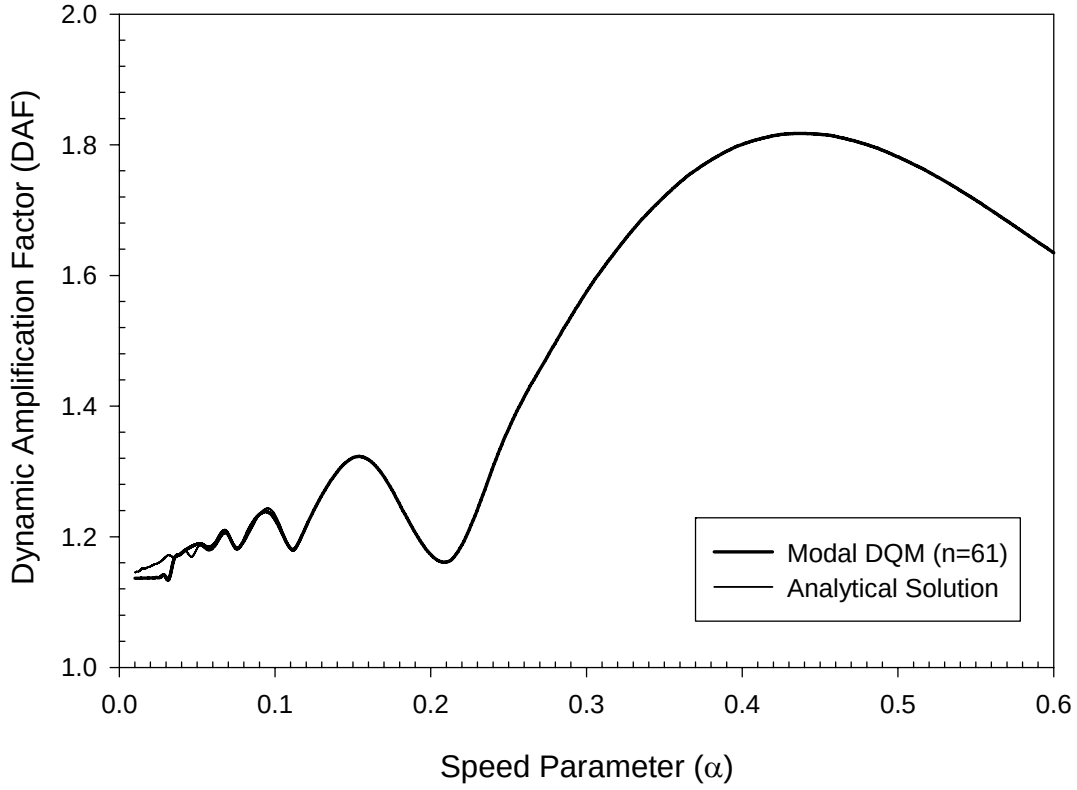

Figure 7.2: Dynamic amplification factor vs. speed parameter using analytical and modal DQM (n=61 nodes in temporal domain)

The dynamic response obtained from a moving mass model using DQ procedure showed sharp and abnormal increase in the DAF at certain values of speed parameter as shown in the *Figure 7.3*.

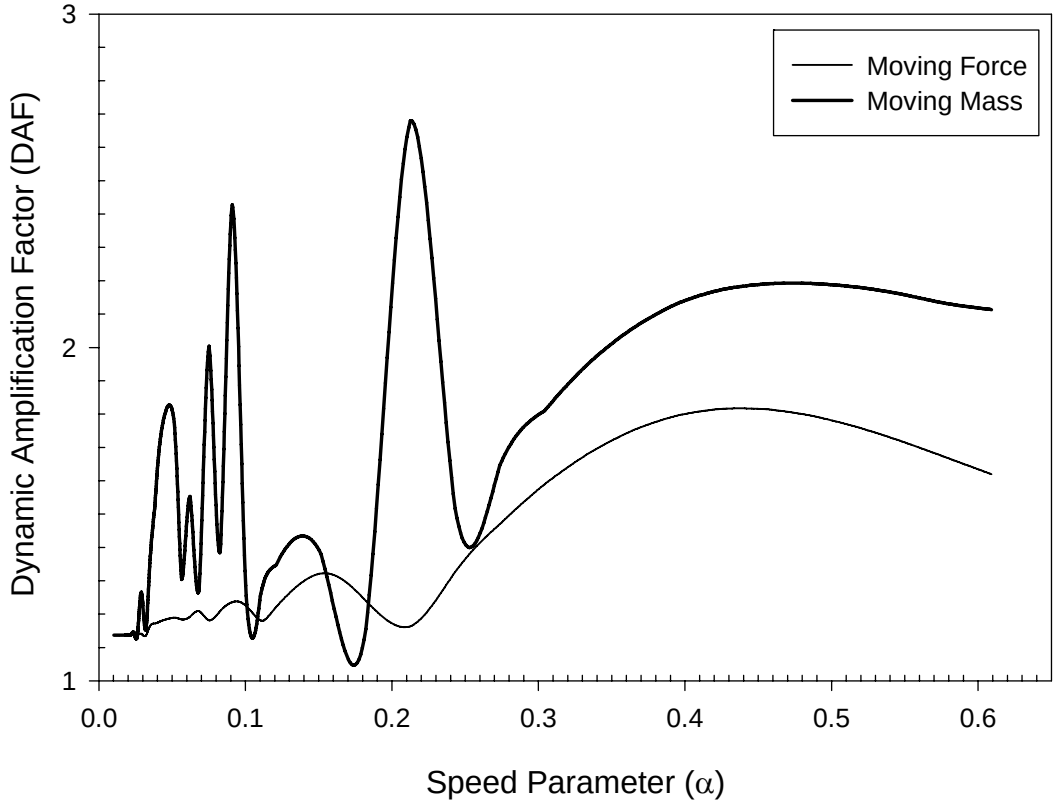

Figure 7.3: Dynamic amplification factor vs. speed parameter from moving force and moving mass models

In this chapter, the dynamic response of the bridge structure modeled using plate structures were studied with the DQM. However, the study is limited to the application of DQM to solve for dynamic response of a plate structure that is simply supported in all sides, and is also limited to the scope of moving force and moving mass models. The dynamic response obtained using moving mass model was higher than that obtained using moving force model.

Chapter 8: Conclusion

Introduction:

The present study successfully applied the *Differential Quadrature Method* (DQM) to study the dynamic behavior of idealized bridge structures under moving vehicular load based on three models, i.e., moving force, moving mass and moving oscillator models. The dissertation also discussed the effects of speed parameter (α) and damping parameter (β) on the dynamic behavior of bridge structures.

8.1 Results in brief:

1) The procedures for the application of DQM including the steps to calculate the weighting coefficients using different test functions, i.e., power polynomial, *Lagrange* and *Hermite-Fejér* type interpolating polynomials, were discussed in the *Chapter 2- Differential Quadrature Method*. The DQM was first applied to study free vibration problem as an introductory step using beam model, and confirmed the results with the frequencies obtained from analytical expression. An isotropic *Kirchhoff* plate with SS-F-SS-F boundary conditions was also modeled using DQ method and dimensionless natural frequencies obtained were in good agreement with *Bert and Malik* [103] and *Leissa* [115].
2) The DQ procedure was successfully implemented to study the dynamic behavior of beams and plates subjected to moving loads using power polynomials, *Lagrange, Hermite-Fejér*, and *Spline* type interpolation polynomials. However, the results and discussions were limited to the use of *Lagrange* type interpolation

polynomials as they were found to be easy and effective. The *Chebyshev* type interpolation polynomial was also used for moving force problem, and the study found the weighting coefficients obtained using the *Lagrange* interpolation scheme to be same as those obtained using the *Chebyshev* interpolation polynomials. However, the *Lagrange* interpolation based DQ scheme took less time than the *Chebyshev* interpolation based DQ scheme for higher number of grid points.

3) For a moving point force, the study applied both the space-time and modal DQ methods, and found the modal DQ procedure simple and effective. In the case of space-time DQM, the processing time increased with the increase in spatial nodes but with no appreciable increase in the solution accuracy.

    a. The dynamic response for an undamped vibration obtained from both the space-time and modal DQ procedures compared well the analytical results. The maximum error in the case of space-time DQM was about 3 % when the number of nodes used were 15 and 61 for spatial and temporal domains, respectively. The modal DQ procedure matched excellently with the analytical solution with only 31 temporal nodes.

    b. In the moving force analysis, the maximum dynamic amplification factor of 1.73 occurred at a speed parameter of about 0.62.

    c. The DAF vs. speed parameter plot showed a wavy pattern at low speed parameter (in the range 0-0.2). The bridge dynamic response in this low speed parameter range was lower than the static response. Actually this low speed parameter corresponds to pretty high highway speeds i.e. for a

highway bridge 25 *m* in length having a typical 5 *Hz* natural frequency, the speed parameter $\alpha = 0.2$ converts to about 50 *m/s* or 112 *mph*.

d. The oscillations in the DAF at low speed parameter range were missing for the damped case, and the dynamic amplification factor (in the low speed range) was close to unity i.e. has same effects of a static load.

e. In the low speed parameter range, the DQ procedure required more number of nodal points to yield satisfactory results. This behavior also suggested that there could be similar difficulties for other numerical procedures to study the dynamic response at low speed parameter range because some of the literature works (such as *Fryba* [10]) did not report the wavy pattern observed at low speed parameter range. The author speculates that *Fryba* could have used a marginally higher time increment for the direct time integration method.

f. The dynamic response of a damped bridge structure for different damping parameters at the low speed parameter range was similar. The differences in the dynamic response due to changes in the damping parameter show up when the speed parameter is greater than 0.2.

g. The dynamic response of the bridge structure subjected to a moving load using *Inglis* model i.e. mass effects of the moving loads were included by defining a lumped mass at the center of the beam - was found to be higher than that predicted from using either of a moving force or a moving mass model.

h. For the moving mass problem, the maximum dynamic amplification factor of 1.78 occurred at a speed parameter of about 0.54, i.e., at a lower speed than observed in a corresponding moving force system.

4) The dynamic behavior of idealized bridge structures subjected to moving two point load system (moving force model) was also studied with the modal DQ method. The study found that the bridge dynamic response due to a moving two point force system is less than that due to a moving point force system. The dynamic amplification factor is found to vary with the inter-load spacing (ILS). At $ILS = 0.1$, the dynamic amplification factor was close to unity for $\alpha < 0.2$. Moreover the oscillations in the dynamic amplification factor, found in the case of a moving point force system for $\alpha = 0 - 0.2$, were missing for the moving two point force system. The dynamic response decreased with the increase in the *ILS* which is actually due to the dynamic amplification definition for two point loads.

5) The VBI phenomenon was also studied using single moving oscillator system. The bridge dynamic response using moving oscillator model yielded similar results to that in moving force at low speeds and mass ratios. On the time scale, the bridge dynamic response obtained from the moving oscillator model precedes the dynamic response obtained from the moving force model. The study found *Green and Cebon* [58] results for bridge dynamic response slightly contradictory. The present study observed similar and/or higher bridge response predicted from moving oscillator model (compared to dynamic response predicted using a moving force model) at lower speed parameter range while *Cebon and Green* [58] concluded that the bridge response is higher in case of a moving force model i.e.

moving force model is conservative compared with the moving oscillator model – which defeats the purpose of importance attached to VBI studies. However, the present study results agreed with *Green and Cebon* conclusive remarks at higher speed parameter range i.e. amplification factors obtained from moving force model are higher than the amplification factors obtained using a moving oscillator model. A maximum dynamic amplification factor of 1.65 approx. was recorded at a speed parameter of $\alpha \approx 0.67$.

6) Results from the dynamic analysis of bridge structures subjected to two axle load system modeled using moving oscillator suggested that the differences between moving oscillator and moving force models vanish for vehicles with higher axle spacing. At lower axle spacing, the moving oscillator model predicted higher dynamic response than a moving force model. In general, the DAF decreased with the increase in the ILS.
7) The application of DQM to study the dynamic behavior of bridge structures using plate models was also discussed. While the application of DQM to model SS-F-SS-F looked simple, a few difficulties were encountered in the implementation of the algorithm using *Mathematica*.
    a. Initially the DQ method (based on the *Karami and Malekzadeh* [112] approach to implement boundary conditions) was applied to study the *Eigen* system involving an isotropic SS-F-SS-F plate, and dimensionless natural frequencies were obtained for different plate aspect ratios. The results obtained matched excellently with the published works of *Bert and Malik* [103] and *Leissa* [115]. It is important to note that with the *Karami*

and Malekzadeh [112] approach, very accurate results were obtained without having to manually incorporate the boundary conditions into the governing equations or use δ-technique as suggested by *Bert and Malik* [88, 103]. However, there were issues such as the excessive time to solve an *Eigen* system beyond 11 nodes in spatial domain (along length and width of the plate), and physical memory run out issue during the solution process in *Mathematica*. Highly accurate results were obtained even with 7 nodes in the spatial domain.

b. The DQM was also applied to study the dynamic behavior of plate structures subjected to a moving point force. An isotropic plate simply supported on all sides was considered to simplify the procedure, and make use of the *Navier* solution [116] to decouple the spatial components from the governing equation. The DAF obtained using the plate model was slightly larger than those computed with the beam model. The maximum DAF at the mid-span of the plate length was recorded to be 1.81 approx. at the vicinity of speed parameter $\alpha = 0.43$. In the low speed parameter range (actual vehicle speeds in state highways), the DAF was around 1.2 i.e. the mid-span dynamic deflection is 20% more than the static mid-span deflection for the same plate configuration. Also the DAF using a plate model in this low speed parameter range is higher than that predicted from an equivalent beam model. The DAF predicted from a moving mass model at low and high speed parameter exceeded a value of 2 i.e. twice the mid-span static deflection caused due to the same load.

8.2 Comments: Advantages and Limitations of DQM:

The applicability of the DQ procedure was discussed in depth in the *Chapter 2 – Differential Quadrature Method*. The study found the DQM as an effective numerical approximation technique because of its direct computation of coefficients, and easy implementation of the algorithm on the governing differential equations of the system and also because of its higher solution accuracy with only a fewer grid points.

In this study, the DQM is successfully employed on the continuous systems modeled as beams and plate elements. However certain modifications are required to enable the DQM to be able to study the discrete structures [106, 107]. Though the DQ procedure can be extended to analyze irregular domains and/or incorporate weak forms similar to finite element procedures [107, 125], the application of the DQ procedure to irregular domain problems is not extensively found as it is for a finite element code.

Another issue identified with the application of the DQM observed in this study is the convergence issue associated with the number of temporal nodes. Initially the study faced difficulties with the number of temporal node points because different number of nodal points yielded completely different results. Later it was found that the solution oscillated due to *Runge* phenomenon (covered in *Chapter 3 – Moving force-moving mass problem for beam models*) and the use of *Chebyshev-Lobatto* distribution eliminated the occurrence of oscillations. The study however conceded that there is no established method to relate the number of nodal points to the solution accuracy but the efficiency of

the method can be evaluated based on the convergence of solution with a certain error window. This is also true for other approximation procedures such as finite element procedure.

8.3 Concluding remarks:

Overall the study yielded a good understanding on the DQM and its application to transient dynamic problems, and on the vehicle-bridge interaction phenomenon. The difficulties involved in the application of the DQ procedure to dynamic analysis were discussed, and some alternative approaches were applied to resolve the problem such as implementation of *Lagrange* or *Hermite* interpolation schemes in lieu of monomial based polynomials, use of *Chebyshev-Lobatto* nodal distribution, etc.

The spline based polynomials were also successfully applied but were left out of the discussion in the thesis work. The study also excluded the surface roughness effects on the dynamic behavior of bridge structures for simplicity, and the surface roughness can be easily included by defining a profile representing the bump or pit which is then added to the bridge deflection variable so that the effective interactive forces between wheel and bridge can be recalculated.

The subject of dynamic behavior of bridge structures under moving vehicular loads is an interesting and assumes significance from the standpoint of design of bridge structures anticipating the magnitude of vehicular loads and their passing speeds. It will be interesting to study the dynamic behavior of cracked bridge structures under moving

loads and assessing the durability and damage tolerance of such cracked structures under varying and/or increased loads.

References

1) American Association of State Highway and Transportation Officials (AASHTO), "Standard specifications for highway bridges", 1997-2003, sixteenth edition.

2) Barker, R. M., and Puckett, J. A., "Design of Highway Bridges", John Wiley & Sons, 1997.

3) R. Willis, "Report of the Commissioners Appointed to Inquire into the Application of Iron to Railway Structures", Appendix B, Stationery Office, London, England, 1849. (Refer [2], page 4)

4) Stokes, George Gabriel, Sir, "Discussion of a differential equation relating to the breaking of railway bridges", Mathematical and physical papers, vol. 2 of 5, 2nd edition, reprinted 1966, originally printed as Transactions of Cambridge Philosophical Society, 1849.

5) Wright, D. T., and Green, R., "Highway bridge vibrations I: Review of previous studies", 1959, Queen's University, Kingston, Ontario.

6) Ting, E. C., Genin, J., and Ginsberg, J. H., "Dynamic interaction of bridge structures and vehicles", The Shock and Vibration Digest, 1975, v 7(11), pp. 61-69.

7) Huang, T., "Vibration of Bridges", Shock and Vibration Digest, 1976, v 8, pp. 61-76.

8) Venancio Filho, "Finite element analysis of structures under moving loads", Shock and Vibration Digest, 1978, v 10(8), pp. 27-35.

9) Inglis, C. E., "A mathematical treatise on vibration in railway bridges", The University Press, Cambridge, 1934.

10) Fryba, L., “Vibration of Solids and Structures under Moving Loads”, Thomas Telford Ltd., Third Edition, 1999.

11) Yang, Y.B., Yau, J. D., and Wu, Y. S., “Vehicle Bridge Interaction Dynamics: With Applications to High Speed Railways”, World Scientific Publishing Company, 2004.

12) Humar, J. L., “Dynamics of Structure”, Taylor and Francis, 2002, 2nd edition, p. 994.

13) Zimmermann, H., Die Schwingungen eines Trägers mit bewegter Last. Centralblatt der Bauverwaltung, 16 (1896), No. 23, 249-251; No. 23A, 257-260; No. 24, 264-266; No. 26, 288. (Refer [9], page 4)

14) Kryloff, A. N., Mathematical Collection of Papers of the Academy of Sciences, Vol. 61. (Matematicheskiĭ sbornik Akademii Nauk). Peterburg 1905. Kriloff A. N.: Über die erzwungenen Schwingungen von gleichförmigen elastischen Stäben. Mathematische Annalen, 61 (1905), 211. (Refer [9], page 4)

15) Timoshenko, S. P., Forced Vibration of Prismatic Bars (in Russian). Izvestiya Kievskogo politekhnicheskogo institute, 1908. Also in German: Erzwungene Schwingungen prismatischer Stäbe. Zeitsch.f.Mathematik u.Physik, 59 (1911), No. 2, 163-203. (Refer [9], page 4)

16) Saller, H., Einfluss bewegter Last auf Eisenbahnoberbau und Brücken. Kreidels Verlag, Berlin, 1921. (Refer [9], page 5)

17) Schallenkamp, A., Schwingungen von Trägern bei bewegten Lasten. Ingenieur-Archiv, 8 (1937), 182-198. (Refer [9], page 5)

18) Jeffcott, H. H., “On the vibration of beams under the action of moving loads”, Dublin Philosophical Magazine and Journal of Science, Edinburgh, v8 (48), 1929, pp. 66-97.

19) Hillerborg, A., “Dynamic influences of smoothly running loads on simply supported girders”, Inst. of Structural Engineering and Bridge Building of the Royal Inst. of Technology, Stockholm, 1951. (Refer [9], page 6)

20) Biggs, J. M., Suer, H. S., and Louw, J. M., “Vibration of simple-span highway bridges”, Journal of the Structural Division, ASCE Proceedings, 83(ST2), 1957, pp. 291-318.

21) Tung T. P., Goodman, L. E., Chen, Y. Y., Newmark, N. M., “Highway bridge impact problems, Highway Research Board Bulletin, 1956, No. 124, pp. 111-134.

22) Bolotin, V. V., “On the effect of a moving load on bridges (in Russian), Trudy Moskovskogo institute inzhenerov zheleznodorozhnogo transporta, Vol. 74, 1950, pp. 269-296. (Refer [9], page 5)

23) Kolousek, V., Dynamics of civil engineering structures, Part 1 – General Problems, second edition; Part II – Continuous beams and frame systems, second edition; Part III – Selected topics (in Czech.) SNTL, Prague, 1967, 1956, 1961. (Refer [9], page 5)

24) Filippov, A. P., Vibrations of mechanical systems (Kolebaniya mekhanicheskikh system), Naukova dumka, Kiev 1965. (Refer [9], page 6)

25) Bondar, N. G., “Dynamic calculations of beams subjected to a moving load (in Russian) Issledovaniya po teorii sooruzhenii, Vol. 6, Stroiizdat, Moscow, 1965. (Refer [9], page 6)

26) Wen, R. K., “Dynamic response of beams traversed by two-axle loads”, Journal of the Engineering Mechanics Division, ASCE, v86 (n EM5), 1960, pp. 91-111.

27) Walker, W. H., and Veletsos, A. S., “Response of simple span highway bridges to moving vehicles”, University of Illinois – Engineering Experiment Station – Bulletin, 1966, p. 69.

28) Fryba, L., “Impacts of two axle system traversing a beam”, International Journal of Solids and Structures, 1968, v4, pp. 1107-1123.

29) Stanisic, M. M., Hardin, J. C., and Lou, Y. C., “On the response of the plate to a multi-masses moving system”, Acta Mechanica, 1968, v5, pp. 37-53.

30) Steele, C. R., “The Timoshenko beam with a moving load”, Journal of Applied Mechanics, Trans. ASME, 1968, v35(90), pp. 481-488.

31) Veletsos, A. S., and Huang, T., “Analysis of dynamic response of highway bridges”, Journal of Engineering Mechanics Division, Proceedings of ASCE, 1970, v 96, EM 5, pp. 593-620.

32) Nelson, H. D., and Conover, R. A., “Dynamic stability of a beam carrying moving masses”, Journal of Applied Mechanics, 1971, v38, Series E, pp. 1003-1006.

33) Csagoly, P. F., Campbell, T. I., and Agarwal, A. C., “Bridge Vibration Analysis”, Ministry of Transportation and Communications, Report No. RR181, September, 1972.

34) Shepherd, R. and Aves, R. S., “Impact factors for simple concrete bridges”, Proceedings of Institution of Civil Engineering, Research and Theory, 1973, Paper 7548, 55, Part 2.

35) Ting, E. C., Genin, J., and Ginsberg, J. H., “A general algorithm for moving mass problems”, Journal of Sound and Vibration, v 33(1), 1974, pp. 49-58.

36) Stanisic, M. M., Euler, J. A., Montgomery, S. T., “On a theory concerning the dynamical behavior of structures carrying moving masses”,

37) Blejwas, T. E., Feng, C. C., and Ayre, R. S., “Dynamic interaction of moving vehicles and structures”, Journal of Sound and Vibration, 1979, v 67 (4), pp. 513-521.

38) Hamada, T. R., “Dynamic analysis of a beam under a moving force: a double Laplace transform solution”, Journal of Sound and Vibration, 1981, v74, pp. 221-233.

39) Mulcahy, N. L., “Bridge response with tractor-trailer vehicle loading”, Earthquake Engineering and Structural Dynamics, 1983, v 11, pp. 649-665.

40) Olsson, M., “Finite element, modal co-ordinate analysis of structures subjected to moving loads”, Journal of Sound and Vibration, v 99(1), 1985, pp. 1-12.

41) J. Palamas, O. Coussy, and Y. Bamberger, “Effects of surface irregularities upon the dynamic response of bridges under suspended moving loads”, Journal of Sound and Vibration, v99(2), 1985, pp. 235-245.

42) J. Hino, T. Yoshimura, and N. Ananthanarayana, “Vibration analysis of non-linear beams subjected to a moving load using the finite element method”, Journal of Sound and Vibration, v100(4), 1985, pp. 477-491.

43) Sadiku, S., and Leipholz, H. H. E., “On the dynamics of elastic systems with moving concentrated mass”, Ingenieur Archiv., 1987, v57, pp. 223-242.

44) Jong-Shyong Wu, Ming-Ling Lee, and Tser-Shyong Lai, "The dynamic analysis of a flat plate under a moving load by the finite element method", International Journal for Numerical Methods in Engineering, v24, 1987, pp. 743-762.

45) Geannakakes, G. N. and Wang, P. C., "Moving load analysis of arbitrarily shaped plates using the B_3-spline finite strip method", Journal of Sound and Vibration, 1990, v141 (1), pp. 127-142.

46) Seroj Mackertich, "Moving load on a Timoshenko beam", Journal of the Acoustical Society of America, 1990, v88(2), pp. 1175-1178.

47) Seroj Mackertich, "Response of a beam to a moving mass", Journal of the Acoustical Society of America, 1992, v 92(3), pp. 1766-1769.

48) Ahmed H. Kashif, "Dynamic response of highway bridges to moving vehicles", PhD Dissertation, 1992, Carleton University, Canada, 357 pages.

49) Nassif, H. H., "Live load spectra for bridge-road-vehicle system", University of Michigan, Department of Civil and Environmental Engineering, 1993, PhD dissertation, p. 250.

50) Nassif, H. H., and Nowak, A. S., "Dynamic load spectra for girder bridges", Journal of the Transportation Research Board, 1995, No. 1476, Transportation Research Board, National Research Council, pp. 69-83.

51) Green, M. F., and Cebon, D., "Dynamic response of highway bridges to heavy vehicle loads: Theory and experimental validation", Journal of Sound and Vibration, 1994, v 170 (1), pp. 51-78.

52) Paz, M., "Modified dynamic condensation method", Journal of Structural Engineering, 1989, v 115(1), pp. 234-238.

53) Yang, Y. B., and Lin, B. H., "Vehicle bridge interaction analysis by dynamic condensation method", Journal of Structural Engineering, 1995, v 121(11), pp. 1636-1643.

54) G. Michaltsos, D. Sophinopoulos and A. N. Kounadis, "The effect of a moving mass and other parameters on the dynamic response of a simply supported beam", v 191(3), 1996, pp. 357-362.

55) Ali Al-Sowaidi, "Dynamic interaction of bridge and moving loading", PhD Dissertation, 1996, Arizona State University, USA, 229 pages.

56) H. P. Lee, "Dynamic response of a beam with a moving mass" – Letters to the Editor, Journal of Sound and Vibration, v 191(2), 1996, pp. 289-294.

57) Yang, F., and Fonder, G. A., "An iterative solution method for dynamic response of bridge-vehicles systems", Earthquake Engineering and Structural Dynamics, 1996, v 25, pp. 195-215.

58) Green, M. F., and Cebon, D., "Dynamic interaction between heavy vehicles and highway bridges", Computers and Structures, 1997, v 62(2), pp. 253-264.

59) Xu, X., Xu, W., and Genin, J., "A non-linear moving mass problem", Journal of Sound and Vibration, 1997, v 204(3), pp. 495-504.

60) Y. B. Yang and J. D. Yau, "Vehicle-bridge interaction element for dynamic analysis", Journal of Structural Engineering, ASCE, 123(11), 1997, pp. 1512-1518.

61) Pesterev, A. V., and Bergman, L. A., "Response of elastic continuum carrying moving linear oscillator", Journal of Engineering Mechanics, 1997, v 123(8), pp. 878-884.

62) M. A. Foda, and Z. Abduljabbar, “A dynamic Green function formulation for the response of a beam structure to a moving mass”, Journal of Sound and Vibration, v 210(3), 1998, pp. 295-306.

63) Henchi, K., Fafard, M., Talbot, M., and Dhatt, G., “An efficient algorithm for dynamic analysis of bridges under moving vehicles using coupled modal and physical components approach”, Journal of Sound and Vibration, 1998, v 212(4), pp. 663-683.

64) Kai Deng, “Dynamic response of certain types of highway bridges to moving vehicles”, PhD Dissertation, 1998, University of Ottawa, Canada, 311 pages.

65) Tan, G. H., Brameld, G. H., and Thambiratnam, D. P., “Development of an analytical model for treating bridge-vehicle interaction”, Engineering Structures, 1998, v 20(1-2), pp. 54-61.

66) Marchesiello, S., Fasana, A., Garibaldi, L., and Piombo, B. A. D., “Dynamics of multi-span continuous straight bridges subject to multi-degrees of freedom moving vehicle excitation”, Journal of Sound and Vibration, v224(3), 1999, pp. 541-561.

67) Huan Zeng, “Vibration of discreetly stiffened skew plates and bridge/vehicle interaction analysis”, PhD ME dissertation, 2000, University of Oklahoma.

68) Yang, B., Tan, C. A., and Bergman, L. A., “Direct numerical procedure for solution of moving oscillator problems”, Journal of Engineering Mechanics, 2000, v 126(5), pp. 462-469.

69) Xin Qun, Zhu, “Vehicular load on bridge deck”, PhD dissertation, 2001, Department of Civil & Structural Engineering, The Hong Kong Polytechnic University, UMI# 3028819.

70) Keh-Yang Lee, “Alternative solution techniques for non-conservative linear dynamic systems”, PhD dissertation, 2002, Columbia University, UMI# 3048174.

71) Nassif, H. H., Liu, M., Ertekin, O., “Model validation for bridge-road-vehicle dynamic interaction system”, Journal of Bridge Engineering, 2003, v 8(2), pp. 112-120.

72) Nassif, H. H., and Liu, M., “Analytical modeling of bridge-road-vehicle dynamic interaction system”, Journal of Vibration and Control, 2004, v 10(2), pp. 215-241.

73) Cristiano Bilello, Lawrence A. Bergman, and Daniel Kuchma, “Experimental investigation of a small-scale bridge model under a moving mass”, Journal of Structural Engineering, 2004, Vol. 130, No. 5, pp. 799-804.

74) Law, S. S., Bu, J. Q., Zhu, X. Q., and Chan, S. L., “Vehicle axle loads identification using finite element method”, Engineering Structures, 2004, v 26, pp. 1143-1153.

75) Pinkaew, T., “Identification of vehicle axle loads from bridge responses using updated static component technique”, Engineering Structures, 2006, v 28, pp. 1599-1608.

76) Yang, Y. B., Lin, C. W., and Yau, J. D., “Extracting bridge frequencies from the dynamic response of a passing vehicle”, Journal of Sound and Vibration, 2004, v 272(), pp. 471-493.

77) Zhu, X. Q., and Law, S. S., “Damage detection in simply supported concrete bridge structure under moving vehicular loads”, Journal of Vibration and Acoustics, Transactions of the ASME, 2007, v 129, pp. 58-64.

78) Patten, W. N., Sack, R. L., and He, Q., “Controlled semi-active hydraulic vibration absorber for bridges”, Journal of Structural Engineering, 1996, v 122(2), pp. 187-192.

79) Patten, W. N., Sun, J., Li, G., Kuehn, J., and Song, G., “Field test of an intelligent stiffener for bridges at the I-35 Walnut Creek bridge”, Earthquake Engineering and Structural Dynamics, 1999, v 28, pp. 109-126.

80) Taheri, M. R., and Ting, E. C., “Dynamic response of plate to moving loads: Structural impedance method”, Computers and Structures, 1989, v 33(6), pp. 1379-1393.

81) Taheri, M. R., and Ting, E. C., “Dynamic response of plates to moving loads: Finite element method”, 1990, v 34(3), pp. 509-521.

82) Zeng, H., and Bert, C. W., “A differential quadrature analysis of vibration for rectangular stiffened plates”, Journal of Sound and Vibration, 2001, v 241(2), pp. 247-252.

83) Abdel-Rohman, M., Quintana, V. H., and Leipholtz, H. H., “Optimal control of civil engineering structures”, Journal of Engineering Mechanics, 1980, v 106(1), pp. 57-73.

84) Lin, Y. H., and Trethewey, M. W., “Active vibration suppression of beam structures subjected to moving loads: A feasibility study using finite elements”, Journal of Sound and Vibration, 1993, v 166(3), pp. 383-395.

85) Zhou, D., DeBrunner, V., DeBrunner, L. S., Baldwin, J. D., Ta, M., Fuller, J., Wang, Y., Wang, P., Hohenberger, T., Pelot, S., Zuniga, L., "Semi-active control algorithms for a smart shock absorber", IEEE Intelligent Vehicles Symposium, 2005, pp. 813-818.

86) Hamming, R. W., "Numerical methods for scientists and engineers", 1973, McGraw Hill, New York.

87) Bellman, R., and Casti, J., Differential quadrature and long-term integration", Journal of Mathematical Analysis and Applications", 1971, v34, pp. 235-238.

88) Bert, C. W., and Moinuddin Malik, "Differential quadrature method in computational mechanics: A review", Applied Mechanics Review, 1996, Vol. 49, No. 1, ASME.

89) Shu, Chang, "Differential quadrature and its application in engineering", Textbook, 2000, Springer Publications, ISBN 1852332093.

90) Wu, T. Y., Liu, G. R., and Wang, Y. Y., "Application of the generalized differential quadrature rule to initial-boundary value problems", Journal of Sound and Vibration, 2003, v 264(4), pp. 883-891.

91) Bellman, R., Kashef, B. G., and Casti, J., "Differential Quadrature: a technique for the rapid solution of nonlinear partial differential equations", Journal of Computational Physics, 1972, v10(1), pp. 40-52.

92) Mingle, J. O., "The method of differential quadrature for transient nonlinear diffusion", Journal of Mathematical Analysis and Applications, 1977, v60 (3), pp. 559-569.

93) Civan, F., “Solution of transport phenomena type models by the method of differential quadrature”, PhD dissertation, 1978, University of Oklahoma.

94) Civan, F., and Sliepcevich, C. M., “Application of differential quadrature to transport processes”, Journal of Mathematical Analysis and Applications, 1983, v93 (1), pp. 206-221.

95) Jang, S. K., “Application of differential quadrature to the analysis of structural components”, PhD dissertation, 1987, University of Oklahoma.

96) Jang, S. K., Striz, A. G., and Bert, C. W., “Two new approximate methods for analyzing free vibration of structural components”, AIAA Journal, 1988, v 26(5), pp. 612-618.

97) Quan, J. R., and Chang, C. T., “New insights in solving distributed system equations by the quadrature method – I: Analysis”, Computers and Chemical Engineering, 1989, v 13(7), pp. 779-788.

98) Quan, J. R., and Chang, C. T., “New insights in solving distributed system equations by the quadrature method – II: Numerical Experiments”, Computers and Chemical Engineering, 1989, v 13(9), pp. 1017-24.

99) Björck, A., and Pereyra, V., “Solution of Vandermonde system of equations”, Mathematics of Computation, 24, 893-903.

100) Shu, C., and Richards, B. E., “Application of generalized differential quadrature to solve two-dimensional incompressible Navier-Stokes equations”, International Journal of Numerical Methods Fluids, 15, pp. 791-798.

101) Striz, A. G., Chen, W., and Bert, C. W., “Static analysis of structures by the quadrature element method (QEM)”, International Journal of Solids and Structures, 1994, v 31(20), pp. 2807-2818.

102) Wang, X., Bert, C. W., and Striz, A. G., “Static and free vibration analysis of beams and plates by differential quadrature method”, Acta Mechanica, 1994, v 102(1-4), pp. 11-24.

103) Malik, M., and Bert, C. W., “Implementing multiple boundary conditions in the DQ solution of higher-order PDE’s: application to free vibration of plates”, International Journal for Numerical Methods in Engineering, 1996, v 39(7), pp. 1237-1258.

104) Wang, X., Gu, H., and Liu, B., “On buckling analysis of beams and frame structures by the differential quadrature element method”, Proceedings of Engineering Mechanics, 1996, v 1, pp. 382-385.

105) Wang, X., and Gu, H., “Static analysis of frame structures by the differential quadrature element method”, International Journal for Numerical methods in Engineering, 1997, v 40(4), pp. 759-772.

106) Chen, Chang-New, “Analysis of frame problems by DQEM using EDQ”, ASME Dynamic Systems and Control Division Publication, 1999, v 67, pp. 671-678.

107) Chen, Chang-New, “Generalization of differential quadrature discretization”, Numerical Algorithms, 1999, v 22(2), pp. 167-182.

108) Wu, T. Y. and Liu, G. R., “Differential quadrature as a numerical method to solve differential equations”, Computational Mechanics, 1999, v 24(3), pp. 197-205.

109) Chen, W. L., Striz, A. G., and Bert, C.W., "High-accuracy plane stress and plate elements in the quadrature element method", International Journal of Solids and Structures, 2000, v 37(4), pp. 627-647.

110) Wu, T. Y., Liu, G. R. and Wang, Y. Y., "Application of the generalized differential quadrature rule to initial-boundary value problems", Journal of Sound and Vibration, 2003, v 264(4), pp. 883-891.

111) Shu, C., Yao, Q. and Yeo, K. S., "Block-marching in time with DQ discretization: an efficient method for time dependent problems", Computer Methods in Applied Mechanics and Engineering, 2002, v 191(41-42), pp. 4587-4597.

112) Karami, G. and Malekzadeh, P., "Application of a new differential quadrature methodology for free vibration analysis of plates", International Journal for Numerical Methods in Engineering, 2003, v 56, pp. 847-868.

113) Wu, T. Y. and Liu, G. R., "The generalized differential quadrature rule for initial-value differential equations", Journal of Sound and Vibration, 2000, v 233(2), pp. 195-213.

114) Wang, X., Liu, F., Wang, X. and Gan, L., "New approaches in application of differential quadrature method to fourth-order differential equations", Communications in Numerical Methods in Engineering, 2005, v 21(2), pp. 61-71.

115) Leissa, A. W., "The free vibration of rectangular plates", Journal of Sound and Vibration, 1973, v 31, pp. 267-293.

116) Rao, S. S., "Vibration of continuous systems", John Wiley & Sons, Inc., 2007, ISBN-13 978-0-471-77171-5, pp. 317-322.

117) C. J. Chen, W. Liu, and S. M. Chern, “Vibration analysis of stiffened plates”, Computers and Structures, 1994, v 50(4), pp. 471-480.

118) Striz, A. G., Wang, X., and Bert, C. W., “Harmonic differential quadrature method and application to analysis of structural components”, Acta Mech, 1995, v111, pp. 85-94.

119) Qiang Guo and Hongzhi Zhong, “Non-linear vibration analysis of beams by a spline-based differential quadrature method”, Journal of Sound and Vibration, v269, 2004, pp. 413-420.

120) Hongzhi Zhong, “Spline-based differential quadrature for fourth order differential equations and its application to Kirchhoff plates”, Applied Mathematical Modelling, 2004, v28, pp. 353-366.

121) Newmark, N. M., “A method of computation for structural dynamics”, ASCE, Journal of Engineering Mechanics Division, 1959, Vol. 85, No. EM3.

122) Gu, Y., Chen, B., Zhang, H. and Guan, Z., “Precise time-integration method with dimensional expanding for structural dynamic equations”, AIAA Journal, 2001, v 39(12), pp. 2394-2399.

123) Visweswara Rao, G., “Linear dynamics of an elastic beam under moving loads”, Journal of Vibration and Acoustics, Transactions of ASME, 2000, v 122(3), pp. 281-289.

124) Brady, S. P. and O’Brien, E. J., “Effect of vehicle velocity on the dynamic amplification of two vehicles crossing a simply supported bridge”, Journal of Bridge Engineering, ASCE, 2006, v 11(2), pp. 250-256.

125) Karami, G. and Malekzadeh, P., “A new differential quadrature methodology for beam analysis and the associated DQEM”, Computer Methods in Applied Mechanics and Engineering, 2002, v 191, pp. 3509-3526.

126) Zienkiewicz, O. C., Wood, W. L., and Hine, N. W., “A unified set of single step algorithms, part 1: general formulation and applications”, International Journal for Numerical Methods in Engineering, 1984, v 20, pp. 1529-1552.

127) Joe D. Hoffman, “Numerical methods for engineers and scientists”, CRC Press, 2001, ISBN: 9780824704438.

Appendix A

Nomenclature and Abbreviations

Symbol	Description
AASHTO	American Association of State Highway and Transportation Officials
DAF	Dynamic Amplification Factor
DQM	Differential Quadrature Method
QEM	Quadrature Element Method
EDQEM	Extended DQEM
GDQM, GDQEM	Generalized DQM, Generalized DQEM
IVBS	Intelligent Vehicle Bridge System
VBI	Vehicle Bridge Interaction
c	Speed of the moving load
D	Flexural rigidity of plate
E	Young's modulus
I	Area moment of inertia
L	Length of beam
M, N	Number of grid points in spatial and temporal domains, respectively
M_v	Representative mass of moving load
P	Magnitude of moving load
T	Time factor (ratio of distance traversed by load to time taken)
$\overline{W}(x,t),\ W(\xi,\tau)$	Absolute, Normalized lateral bridge displacement
α	Speed parameter

Symbol	Description
β	Damping parameter
$\delta(\cdot)$	Dirac Delta distribution function
ρ	Mass density of plate
κ	Vehicle to bridge mass ratio
$\kappa^{(x)}$, $\kappa^{(y)}$	Factor of bending moment or second derivative of the displacement w.r.t x and y, respectively
ξ	Normalized space variable
μ	Linear density (mass per unit length) of beam (or) Area density (mass per unit area) of plate
λ	Aspect ratio of plate
ω	Driving frequency of load
$\omega_{(1)}$	Natural frequency of bridge (beam)
ω_b	Frequency of damping for bridge vibration
τ	Normalized time variable
$w(t)$	Time coordinate function
Ω	Dimensionless natural frequency of vibration of plate